Understanding the pharmacological consequence of functional P2Y$_1$- P2Y$_{12}$ heterodimerisation

Mohammed Safar BScPharm MSc

Glasgow, UK
November, 2020

Mohammed Safar BScPharm MSc

Understanding the pharmacological consequence of functional P2Y$_1$- P2Y$_{12}$ heterodimerisation

A thesis submitted in the fulfilment of the requirements for the degree of Doctor of Philosophy.

Supervision: Dr Charles Kennedy
                 Dr Margaret Rose Cunningham

Glasgow, UK
November, 2020

This thesis is the result of the author's original research. It has been composed by the author and had not been previously submitted for examination which has led to the award of a degree.

The copyright of this thesis belongs to the author under the terms of the United Kingdom Copyright Acts as qualified by University of Strathclyde Regulation 3.50. Due acknowledgement must always be made of the use of any material contained in, or derived from, this thesis.

Signed:

Date: **01/11/2020**

ABSTRACT

G protein-coupled receptors (GPCRs) are a superfamily of transmembrane proteins that are responsible for transducing extracellular stimuli into intracellular responses. GPCRs are essential to a wide variety of distinct pathophysiologies and behaviours and represent approximately 34% of FDA-approved, human drug targets. In recent years the classical concept that GPCRs are monomeric membrane receptors has been challenged by a growing number of reports indicating that they can form dimers and higher-order functional oligomers. Furthermore, this has been demonstrated to affect receptor trafficking, ligand sensitivity, desensitization, and downstream effector response. Thus, an understanding of GPCR oligomerisation is vital to understand receptor dynamics.

The $P2Y_1$ and $P2Y_{12}$ receptors belong to the class A family of GPCRs and are widely expressed throughout the body. There is growing evidence that purinergic receptors also exist as oligomers. Previously, the Kennedy lab proposed the formation of a constitutive heterodimer between coexpressed human $P2Y_1$ and $P2Y_{12}$ receptors, based on functional responses. Evidence of a physical interaction between the two receptor subtypes was, however, lacking. The aim of this project was, therefore, to use a variety of experimental techniques to determine if $P2Y_1$ and $P2Y_{12}$ receptors interact physically to form dimers and how this affected receptor function.

In this study, tSA201 cells were transfected with $hP2Y_1$ and $hP2Y_{12}$ receptors containing a haemagglutinin (HA) or fluorescent protein (FP) tag. Transfection efficiency was first optimised for all receptor constructs and experimental conditions. Fluorescence microscopy then showed that both receptors localised at the cell plasma membrane and in close proximity to each other. By quantification the receptors on the cell surface, it is found that $P2Y_1$ receptors expressed more on the cell surface in compare to $P2Y_{12}$ receptors. Interestingly, $hP2Y_{12}$ receptor surface expression decreased when coexpressed with the $hP2Y_1$ receptor. The $hP2Y_1$ and $hP2Y_{12}$ receptor agonist, ADP, induced internalisation of both receptors when they were expressed on their own, but not when they were coexpressed. Physical interaction between $hP2Y_1$ and $hP2Y_{12}$ receptors was investigated using co-immunoprecipitation (co-IP), proximity ligation assay (PLA) and fluorescence lifetime imaging microscopy Förster resonance energy transfer (FLIM-

FRET). These experiments demonstrated that $P2Y_1$ and $P2Y_{12}$ receptors formed a dimer that localised to the cell plasma membrane and the distance between both receptors decreases with AR-C69931MX addition. Moreover, in this study, the $P2Y_1$-$P2Y_{12}$ dimer was found natively in BV-2 microglial cells. Also, AR-C69931MX demolished the calcium-induced by ADP in BV-2 cells, which is a similar finding noticed by Kennedy lab but in the recombinant system.

These findings reveal $P2Y_1$ and $P2Y_{12}$ receptor heterodimerisation with implications upon receptor internalisation and signalling in recombinant and endogenous receptor cell models. The next step requires further understanding of how these events might influence the pharmacology of both receptors and their function in normal physiology and disease.

PUBLICATIONS

Research Articles

Xiao, D., Sapermsap, N., **Safar, M**., Cunningham, M. R., Chen, Y. & Li, D. D. (2021). *On synthetic instrument response functions of time-correlated single-photon counting based fluorescence lifetime imaging analysis.* Frontiers in Physics, section Optics and Photonics. Manuscript ID: 635645. (published article)

Li, Y., Sapermsap, N., Chen, Y., **Safar, M.**, Cunningham, M. R., Tian, J., Li, D. D. (2020). *Investigations on average fluorescence lifetimes for visualising multi-exponential decays*. Frontiers in Physics, section Optics and Photonics. Manuscript ID: 576862. (published article)

Abstracts published

Safar, M. A., Wood, R., Cunningham, M. R., & Kennedy, C. (2019). P2Y1 and P2Y12 receptor heterodimerisation: from recombinant systems to native detection. *British Journal of Pharmacology*, *176*(16), 3049. https://doi.org/10.1111/bph.14681

Safar, M. (2018). *Evidence that human P2Y1 and P2Y12 receptors form heterodimers*. Proceedings of the British Pharmacological Society. pA2online 20(1). Abstract 015P http://www.pA2online.org/abstracts/Vol20Issue1abst015P

McMullen, CJ., McCluskey, C., Kim, SJ., Laovitthayanggoon, S., MacDonald, M., **Safar, M**., ... Currie, S. (2018). Anti-cancer tyrosine kinase inhibitors increase oxidative stress in primary cardiac fibroblasts. *Heart*, *104*(S4). https://doi.org/10.1136/heartintjnl-2018-SCF22

Oral Presentations

Safar, M. A. A., Wood, R. A., Tate, R., Cunningham, M. R. & Kennedy, C. (2019). *Native detection for P2Y1 and P2Y12 receptor heterodimerisation*. Cellular Basis of Disease (CBD) group seminar, University of Strathclyde, Glasgow, UK.

Safar, M. A. A., Wood, R. A., Tate, R., Cunningham, M. R. & Kennedy, C. (2018). *P2Y1 and P2Y12 receptor heterodimerisation: from recombinant systems to native detection*. Pharmacology 2018, QEII Centre, London, UK.

Safar, M. A. A., Wood, R. A., Tate, R., Cunningham, M. R. & Kennedy, C. (2018). *P2Y1 and P2Y12 receptor heterodimerisation: from recombinant systems to native detection*. BPS-MPGPCR 2018, Monash University, Parkville Campus, Melbourne, Australia.

Safar, M. A. A., Tate, R., Cunningham, M. R. & Kennedy, C. (2017). *Different methods to detect P2Y1 and P2Y12 dimerisation*. Cardiovascular and Metabolic Diseases (CVMD) research group seminar. University of Strathclyde, Glasgow, UK.

Safar, M., Cunningham, M. R. & Kennedy, C. (2016). *P2Y1 and P2Y12 dimerisation*. New Medicines Fundamental Group (NMFG) internal seminar, University of Strathclyde, Glasgow, UK.

Poster Presentations

Safar, M. A. A., Tate, R., Natakorn, S., Li, D. D., Cunningham, M. R. & Kennedy, C. (2020). *The functional relevance of P2Y1 and P2Y12 receptor heterodimerization.* Pharmacology 2020, online.

Safar, M., Tate, R., Natakorn, S., Li, D. D., Cunningham, M. R. & Kennedy, C. (2020). *Interrogating purinergic P2Y1 and P2Y12 heterodimerisation.* The 3rd European Research Network on Signal Transduction (ERNEST) Meeting, online.

Safar, M. A. A., Wood, R. A., Cunningham, M. R. & Kennedy, C. (2018). *Heterodimerisation of purinergic GPCRs.* Molecular Neuropharmacology in Health and Wellbeing: Exploring new targets for drug discovery, University of Strathclyde Technology and Innovation Centre, Glasgow, UK.

Safar, M. (2018). *Evidence that human P2Y1 and P2Y12 receptors form heterodimers.* Poster session presented at Pharmacology Futures 2018, Edinburgh, United Kingdom. Published meeting abstract.

Safar, M. (2018). *Evidence that human P2Y1 and P2Y12 receptors form heterodimers.* University of Strathclyde Research Day, University of Strathclyde, Glasgow, UK.

Safar, M. A. A., Wood, R. A., Tate, R., Cunningham, M. R. & Kennedy, C. (2018). *The influence of P2Y ligands on P2Y1 and P2Y12 dimer.* BPS-MPGPCR 2018 - Monash University, Parkville Campus, Melbourne, Australia

ACKNOWLEDGEMENTS

I give glory to Allah, the Exalted for giving me the opportunity to get to this stage of my studies and career. Firstly, I would like to thank Charles for giving me the opportunity to work in this project and for his continual support and guidance throughout the project. Then I would like to thank my mentor, Margaret, for giving me the wonderful opportunity to be part of her lab and develop as a scientist under her excellent guidance. Her incredible enthusiasm, wealth of knowledge and excitement in science is inspiring and motivating, and I feel privileged to have been her student. Due to her patience, discussions, criticisms and questions, she immensely brought out the best in me.

I would like to thank my collaborator Dr David Li, for developing the tool that helped me analyse my FLIM-FRET images and for all the support. Also, Yok who worked hard in imaging my FLIM-FRET samples. I would also like to show my appreciation to my colleagues at the Cunningham lab for creating such a vibrant and motivating environment in which to do my research. All of the other students and members of staff that I've met throughout my PhD also deserve thanks for the encouraging words and enjoyable times I have had with them in SIPBS.

I would like to thank my friends in Glasgow and Saudi for their love, care, support, encouragement and guidance. Also, I would like to thank Gemma for being there for me and helped me through the most challenging moments.

Thanks to my parents, Samira and Adnan Safar, for loving me, nurturing me, encouraging me and supporting me with their non-judgemental guidance, and sorry for being so far from you all these years. Thanks to my sisters Ohud and Rasha for giving the opportunity to be here in the UK in the first place, and to my other sisters Wafa and Abrar and lovely brother Fahad for supporting my parents and me. Last but not least, special thanks to my sister Roaa who passed away of TNBC in 2019. The person who helped me throughout my life. I hope you can forgive me as I haven't been there when you left us. This thesis is dedicated to your soul, I love you.

ABBREVIATIONS

AC	Adenylyl cyclase
ADP	Adenosine diphosphate
AFM	Atomic force microscopy
AGS	Activators of G protein signalling
ANOVA	Analysis of variance
APS	Ammonium persulfate
Asn	Asparagine
AT	Angiotensin receptor
ATP	Adenosine triphosphate
AUC	Area under the curve
BiFC	Bimolecular fluorescence complementation
BLAST	Basic Local Alignment Search Tool
BLT1	Leukotriene receptor B4
BRET	Bioluminescent resonant energy transfer
BSA	Bovine serum albumin
C-	Carboxyl terminus
Ca^{+2}	Calcium
cAMP	Cyclic adenosine monophosphate
CB	Cannabinoid receptor
cDNA	Complementary deoxyribonucleic acid
CFA	Complete Freund's adjuvant
CFP	Cyan fluorescent protein
CHO	Chinese hamster ovary
CNS	Central nervous system
Co-IP	Co-immunoprecipitation
COPII	Coat protein complex II
CYP450	Cytochrome P450
Cys	Cysteine
DAG	Diacylglycerol

DAPI	4',6-diamidino-2-phenylindole
DMEM	Dulbecco's Modified Eagle's medium
DMSO	Dimethyl sulfoxide
DNA	Deoxyribonucleic acid
DOR	δ-Opioid receptor
DRG	Dorsal root ganglia
DRY	Glu/Asp-Arg-Tyr
DTT	Dithiothreitol
EBI	European Bioinformatics Institute
ECACC	European Collection of Authenticated Cell Cultures
ECL	Enhanced chemiluminescence
EDTA	Ethylenediaminetetraacetic acid
EL	Extracellular loops
ER	Endoplasmic Reticulum
ERAD	ER-associated degradation
ERGIC	ER-Golgi intermediate complex
ERK	Extracellular signal-regulated kinase
HEK293	Human embryonic kidney 293
HEPES	(4-(2-hydroxyethyl)-1-piperazineethanesulfonic acid)
HMC3	The human microglial clone 3
FBS	Fetal Bovine Serum
FDA	Food and Drug Administration
FLIM	Fluorescence Lifetime Imaging Microscopy
FP	Fluorescent protein
FRAP	Fluorescence recovery after photobleaching
FRET	Fluorescence resonance energy transfer
FSHR	Follicle-stimulating hormone receptor
GABA	Ƴ-aminobutyric acid
GDP	Guanosine diphosphate
GIRK	G protein-regulated inwardly rectifying potassium channels
GFP	Green fluorescent protein

GPCR	G protein-coupled receptor
Gt	Transducin G protein
GRK	G protein-coupled receptor kinase
Grp78	78 kDa glucose-regulated protein
GTP	Guanosine triphosphate
HA	Haemagglutinin
HEK293	Human embryonic kidney cells 293
H8	Helix 8
IC$_{50}$	Half maximal inhibiting concentration
IL	Intracellular loops
IP	Immunoprecipitation
IP$_3$	Inositol 1, 4, 5- triphosphate
K$_{2P}$	Two-pore potassium channels
KDa	Kilodalton
KOR	κ-Opioid receptor
LDS	Lithium dodecyl sulphate
LTB$_4$	Leukotriene B$_4$
MAPK	Mitogen-activated protein kinase
MAPKK	MAP kinase kinases
MAPKKK	MAP kinase kinase kinases
mGlu	Metabotropic glutamate
MOC	Manders' overlap coefficient
MOR	μ-Opioid receptor
MR	Muscarinic receptor
mRNA	Messenger ribonucleic acid
N-	Extracellular amino terminus
NHERF-1	Na$^+$-H$^+$ Exchanger Regulatory factor-1
NPXXY	Asn-Pro-X-X-Tyr
NTPDases	Ecto-nucleoside triphosphate diphosphohydrolases
PCC	Pearson correlation coefficient
PDZ	Postsynaptic Density 95/disc large/Zonula occludens-1

PEI	Polyethylenimine
PI3-K	Phosphatidylinositol-4,5-bisphosphate3-kinase
PIP$_2$	Phosphatidylinositol- 4, 5-biphosphate
PKA	Protein kinase A
PKC	Protein kinase C
PLA	Proximity Ligation Assay
PLC	Phospholipase C
PLC$_\beta$	Phospholipase C-β
PLL	Poly-L-lysine
PTX	Pertussis toxin
PVDF	Polyvinylidene difluoride
RER	Rough endoplasmic reticulum
RET	Resonant energy transfer
RCA	Rolling circle amplification
RGS	Regulators of G protein signalling
Rho- GEFs	Rho guanine nucleotide exchange factors
RNA	Ribonucleic acid
SDS	Sodium dodecyl sulphate
SDS-PAGE	Sodium dodecyl sulphate polyacrylamide gel electrophoresis
SEM	Standard error of the mean
SIM	Structured illumination microscopy
SPAD	Single-Photon Avalanche Diode
STED	Stimulated emission depletion microscopy
TCSPC	time-correlated single-photon counting
TEMED	Tetramethylethylenediamine
TIRFM	Total internal reflection fluorescence microscopy
TM	Trans-membrane
TPR1	Topless-related 1
TRPM8	Transient receptor potential melastatin 8
TRPV	Transient receptor potential cation channel subfamily V
tSA201	Temperature sensitive antigen 201

UDP	Uridine diphosphate
UT	Untransfected
UTP	Uridine triphosphate
V2R	V2 vasopressin receptor
VFT	Venus fly trap
WT	Wild type
YFP	Yellow fluorescent protein
α-AR	α-adrenergic receptor
α-Tub	α-Tubulin
β-AR	β-adrenergic receptor

LIST OF CONTENTS

Chapter Five - Expression, dimerisation and functional characterization of endogenous $P2Y_1$ and $P2Y_{12}$ receptors...*168*

Chapter Six – General Discussion..*206*

References *219*

LIST OF FIGURES

Chapter one – General Introduction

_____

Chapter two - Materials and Methods

_____

Chapter Three - Transfection Efficiency, Surface Expression and Functional Characterisation of Recombinant P2Y$_1$ and P2Y$_{12}$ Receptors

_____

Chapter Four - Investigating heterodimer formation between P2Y$_1$ and P2Y$_{12}$ receptors

_____

Chapter Five - Expression, dimerization and functional characterisation of endogenous P2Y$_1$ and P2Y$_{12}$ receptors

LIST OF TABLES

Chapter One

General Introduction

1   G Protein-coupled receptors

1.1   Introduction

The G protein-coupled receptors (GPCRs) superfamily are a vast and diverse family of plasma membrane proteins, which play an essential role in cellular communication between the extra- and intracellular milieus across the plasma membrane. It consists of approximately 800 receptors in the human genome (Lin, 2013; Canals et al., 2019), which are linked to the signalling transduction pathways that regulate various critical cellular processes in all cells in the body (Lagerstrom and Schioth, 2008).   GPCRs regulate numerous physiological systems and disease states, such as gastrointestinal disorders, cancer, pain, cardiovascular disorders, and conditions of the central nervous system (Milligan and McGrath, 2009; Hauser et al., 2017). Approximately 70% of GPCRs have identified ligands and the remainder are classed as orphan GPCRs (Hu et al., 2017). Unsurprisingly, 34% of FDA approved drugs are targeted at GPCRs (Syu et al., 2019).

1.2   GPCRs Classification

Based on sequence homology and the endogenous ligands binding, the most widely used classification system of GPCRs comprises six groups (A to F) (Waldhoer et al. 2005; Cherezov et al., 2007). This covers all GPCRs, but not all classes are found in humans. Mammalian GPCRs are divided into four classes which are class A (rhodopsin-like receptor family), class B (secretin receptor family), class C (family of metabotropic glutamate receptors) (Emami-Nemini et al., 2013) and class F (frizzled/smoothened). Class D (fungal mating receptors) and E (cyclic adenosine monophosphate (cAMP) receptors) are not found in vertebrates.

1.3   GPCRs structure

GPCRs share a standard core structure consisting of a single polypeptide chain that has an extracellular amino (N-) terminus, an intracellular carboxyl (C-) terminus and which crosses the plasma membrane seven times. Each TM domain is an α-helix formed of 25-30 amino acid residues with a high degree of hydrophobicity, and they are linked by three intracellular loops (IL1-3) and three extracellular loops (EL1-3) (Perez and Karnik, 2005). Different types of GPCRs show sequence variations and

differences in the length and the function of N-terminal, C-terminal domains and the intracellular loops (Wheatley et al., 2012). The N-terminus is located in the extracellular region of the GPCR, and its organisation influenced by disulphide bond formation between the extracellular cysteine (Cys) residues that create an internal scaffold within the receptor structure (Naranjo et al., 2015). The C-terminus is frequently palmitoylated for attaching the receptor to the membrane, within the family Cys residue (Gahbauer and Bockmann, 2016).

The tertiary GPCR structure was first demonstrated in 2000 by crystallizing bovine rhodopsin from mixed micelles (Palczewski et al., 2000), which was considered as a structural template for other GPCRs (Filipek et al., 2003). In 2007, the second GPCR structure was obtained when the crystal structure of the β_2-adrenergic receptor (β_2-AR) was resolved (Cherezov et al., 2007; Rasmussen et al., 2007) (**Figure 1.1**). The figure demonstrates the inactivated (PDB ID code 3SN6) and the activated (PDB ID code 1GP2) conformations. The inactive state of the receptor is shown binding to an "open out" G protein, whereas, the active state is binding to a "closed-in" G protein (Alhadeff et al., 2018).
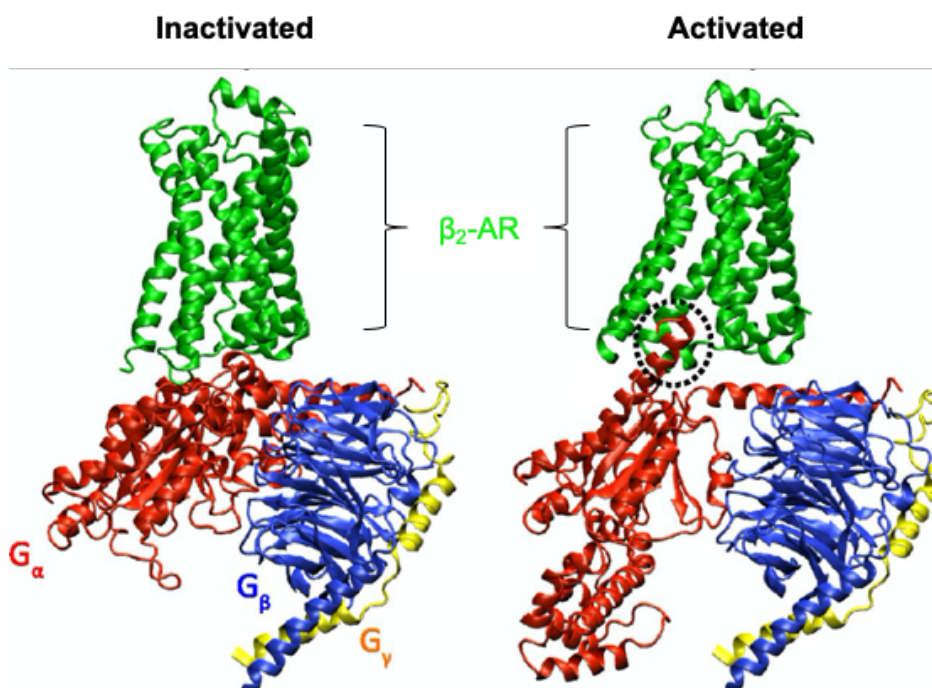
Figure 1.1: Visual representation of β_2-AR
Crystal structure of inactivated (left) and activated (right) β_2-AR. The receptor is shown in green, and the G protein α- (red), β- (blue), and γ- (yellow) subunits are shown. The inactivated β_2-AR shows an open-out G protein while the activated β_2-AR shows a closed-in G protein. Figure was adapted from (Alhadeff et al., 2018).

There are now over 180 known comprehensive structures of individual GPCRs (Gacasan et al., 2017), with more than 150 of these structures co-crystallized with ligands. These crystal structure are including the muscarinic M2 (Haga et al., 2012) and M3 (Kruse et al., 2012) receptors, µ-opioid receptor (MOR) (Manglik et al., 2012), δ-opioid receptor (DOR) (Granier et al., 2012), κ-opioid receptor (KOR) (Wu et al., 2012), the nociceptin receptor (Thompson et al., 2012), the dopamine receptor D_3 (Chien et al., 2010), the adenosine A_{2A} receptor (Jaakola et al., 2008) the $P2Y_1$ receptor (Zhang et al., 2014) and the $P2Y_{12}$ receptor (Zhang et al., 2015).

In class A GPCRs, their crystal structures with their G proteins revealed conformational changes in the TM bundle of GPCRs known as helix 8 (H8) (Weis and Kobilka, 2018). H8 is located immediately after the end of the 7th TM domain, which has been reported to be involved in various cellular processes, such as G-protein coupling (Ernst et al., 2000), receptor expression (Tetsuka et al., 2004), activation (Delos Santos et al., 2006) and internalisation (Aratake et al., 2012) (**Figure 1.2**). In addition, interactions with the palmitoylated cysteines of H8 localise GPCRs in certain regions of the cell membrane, namely in lipid rafts (Chini and Parenti, 2009).
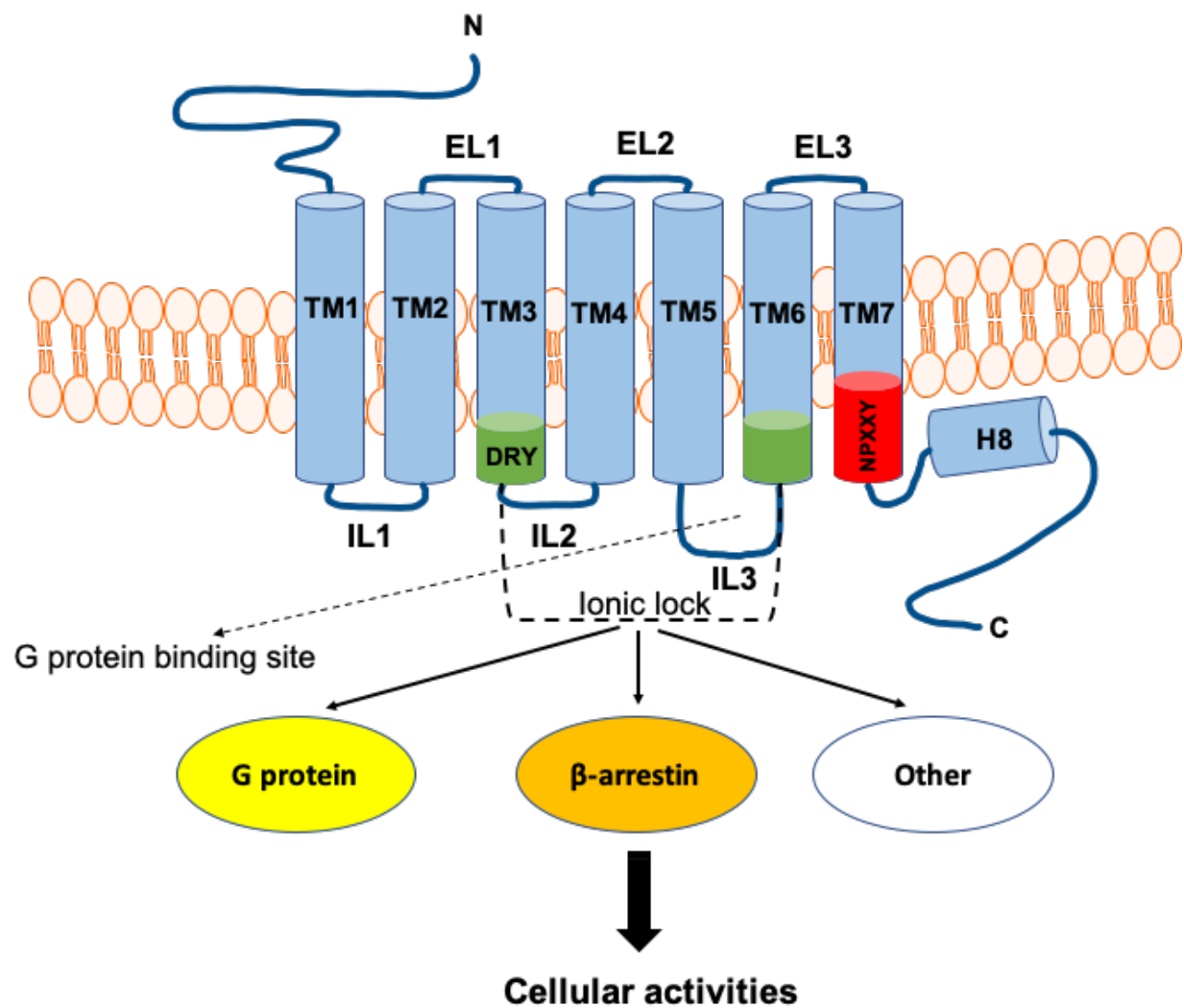
Figure 1.2: Illustration of the seven transmembrane-spanning GPCRs.
The figure shows the positions of some of the conserved structural features of the class A GPCRs, such as the DRY and NPXXY motifs. The dotted line indicates the two domains (in green) involved in the ionic interactions known as the ionic lock. The figure also illustrates the canonical G-protein-dependent and more recently described G-protein-independent signalling modes involving β-arrestin and other signalling effectors. TM =transmembrane domains, H8 = helix 8, IL = intracellular loop; EL = extracellular loop.

GPCRs in this class share regions of residues conserved across the subfamily that involve a Glu/Asp-Arg-Tyr (DRY) motif on the intracellular side of TM3 (Rovati et al., 2007) and a Asn-Pro-X-X-Tyr (NPXXY) motif on the intracellular side of TM7 (Urizar et al., 2005), that are thought to stabilize different conformational states of the receptor (Schoneberg et al., 1999; Audet and Bouvier, 2012) (**Figure 1.2**). The DRY motif also contributes to the activation of the receptor (Audet and Bouvier, 2012; Zhou et al., 2019). From previous structural models, it was noted that there was a polar interaction between an arginine located at the bottom of TM3 and a glutamate on TM6 (Audet and Bouvier, 2012; Zhou et al., 2019). This was named the "ionic lock" and it contributes to receptor stabilization in its inactive state (Audet and Bouvier, 2012; Zhou et al., 2019). The helical rearrangements that occur during GPCR activation also correlate with the breaking of the ionic lock within the DRY motif upon ligand binding and the formation of interactions within the NPXXY motif once the receptor is in an active conformation (Rasmussen et al., 2011, Kruse et al., 2013, Huang et al., 2015).

Ligand binding for most class A receptors takes place within a cavity formed between the TM regions, which causes specific structural rearrangements from the inactive-state. The crystal structures of activated class A receptors has shown a rotation of TM6 by 6-14 Å away from the helical bundle (Rasmussen et al., 2011, Kruse et al., 2013, Huang et al., 2015). The rearrangement of the intracellular helix leads to the formation of a crevice surrounded by TM3, TM5 and TM7, which functions as the G protein, and possibly β-arrestin, binding site (Liang et al., 2017) **(Figure 1.2)**.

The active state structure of the β_1 adrenergic receptor (β_1-AR) and molecular dynamics simulations infer that residues of TM3, TM5, TM6 and TM7 located within the helical bundle play a role in transmitting the signal of ligand binding into the conserved intracellular rearrangements (Latorraca et al., 2017). This finding could be applied on other receptors; however, the conformational changes and the pharmacology of employed ligands might vary from one receptor to another.

1.4   GPCR signaling

GPCRs are activated by a wide range of extracellular stimuli and activate signalling pathways that lead to transduction of a diverse range of cellular activities (Masuho et al., 2015; Civelli et al., 2013). GPCRs induce signals via activation of associated guanine nucleotide-binding proteins (G proteins). G proteins are heterotrimeric proteins that are formed of three subunits: α, β and γ (Lambright et al., 1996). The activation of the GPCRs triggers the exchange of guanosine diphosphate (GDP) to guanosine triphosphate (GTP) in the cleft between the GTPase and α-helical domain of Gα (Dror et al., 2015). In the inactive conformation, GDP-bound Gα subunits bind tightly to the Gβγ heterodimer. GPCRs activation leads to conformational changes, causing association with heterotrimeric G proteins, which causes the exchange of GDP for GTP binding to Gα. This induces dissociation of the Gα subunit from the Gβγ dimer, resulting in two functional subunits (Gα and Gβγ) that interact independently and with different downstream effectors (Bondar and Lazar, 2014; Syrovatkina et al., 2016). Intrinsic GTPase activity of Gα terminates Gα subunit signalling by hydrolysing the bound GTP to GDP. Reassociation of Gα-GDP with Gβγ terminates signalling (Syrovatkina et al., 2016).

Four major classes of Gα subunits are recognized based on downstream GPCR signalling events (Neves et al., 2002) and these are summarised below (**Table 1.1**; Syrovatkina et al., 2016). The $G\alpha_s$ subunit stimulates AC activity, leading to formation of cAMP from ATP. Four molecules of cAMP bind to and activate cAMP-dependent protein kinase, also known as protein kinase A (PKA) (Wehbi and Tasken, 2016). The activation of PKA leads to the phosphorylation of downstream target proteins, by removing a phosphate from ATP, and adding it to specific serine and/or threonine residues (Ardito et al., 2017). On the other hand, the activation of $G\alpha_{i/o}$ subunit leads to the inhibition of AC activity, which in turn leads to a lowering of cAMP levels and so less stimulation of PKA. The $G\alpha_{q/11}$ subunits activate PLC_β, which in turn cleaves plasma membrane phosphatidylinositol- 4, 5-bisphosphate (PIP_2) to the second messengers inositol 1,4,5-phosphate (IP_3) and diacylglycerol (DAG). IP_3 binds to IP_3 receptors in the endoplasmic reticulum (ER) to release Ca^{2+} into the cytosol, while DAG remains bound to the membrane and activates protein kinase C (PKC), leading to protein phosphorylation (Griner and Kazanietz, 2007; Lipp and Reither, 2011). The $G\alpha_{12/13}$ subunits activate Rho guanine nucleotide exchange factors (Rho-

GEFs) that lead to activation of the small cytosolic Rho-GTPase. Rho-GTPase can activate several proteins, for example, Rho-kinase, that are responsible for the regulation of actin cytoskeletal remodelling in cells (Spiering and Hodgson, 2011).

Table 1.1: Gα subunits and their effectors

Gα subunit	Well-defined G-protein effectors	Other G-protein-interacting proteins
Gα$_s$, Gα$_{olf}$	Adenylate cyclase (+)	Tubulin, Src tyrosine kinase, axin
Gα$_o$, Gα$_{i1-3}$, Gα$_{t1,2}$, Gα$_g$, Gα$_z$	Adenylate cyclase (-), cGMP phosphodiesterase (+)	Rap1Gapll, Src tyrosine kinase, nuclebindin 2, Tubulin, Pins, PcP1, LGN, GRIN1, Eya2, Pcp1
Gα$_q$, Gα$_{11}$, Gα$_{14}$, Gα$_{15/16}$	Phospholipase C-β (+), p63RhoGEF	GRK2, actin, tubulin, PI3K, TPR1, Btk tyrosine kinase, Phospholipase C, TRPM8
Gα$_{12}$, Gα$_{13}$	P115RhoGEF, leukemia-associated RhoGEF, and PDZ-RhoGEF	Gap1, rasGap, BtK tyrosine kinase, Radixin, Hax-1, Cadherins, α-SNAP, P120caterin, Integrin αlllbβ3

Table adapted from (Syrovatkina et al., 2016)

The Gβγ subunits act independently from Gα and activate a range of effectors across different signal transduction pathways (Sadja et al., 2003), including G protein receptor kinase 2 (GRK2) (Evron et al., 2012), N-type calcium channels (Brown and Sihra, 2008), PLC$_β$ (Lin and Smrcka, 2011), G protein-regulated inwardly rectifying potassium channels (GIRK) (Luscher and Slesinger, 2010) and AC isoforms (Sunahara and Taussig, 2002).

Accessory proteins can also regulate G protein activity. For example, activators of G protein signalling (AGS) facilitate the exchange rate of GDP for GTP (Bernard et al., 2001), while regulators of G protein signalling (RGS) act by accelerating the rate of GTP hydrolysis by the Gα subunit, and therefore regulate the duration of G protein activation (Traynor and Neubig, 2005).

Other factors that can regulate GPCR signalling include desensitization and internalisation (Dupre et al., 2012). When activated, GRKs phosphorylate various serine and threonine residues in the receptor C terminal tail and/or intracellular loops (Tobin et al., 2008), which increases the affinity of the receptor for the binding of arrestin adaptor proteins. The arrestin family contains four members, two visual arrestins (arrestin 1 and 4), which bind to photoreceptors, such as rhodopsin (Gurevich

and Benovic, 1993) and two non-visual arrestins (arrestin 2 and 3), also known as β-arrestin 1 and β-arrestin 2, respectively (Lefkowitz and Shenoy, 2005; Nisar et al., 2012). The term "β-arrestins" was given to arrestin (2 and 3) because they were initially identified as regulators of β_2-AR (Lohse et al., 1990), then later known as a regulator of non-photoreceptor GPCR desensitization (DeWire et al., 2007). Historically, investigations have shown that β-arrestins can impact GPCRs internalisation via facilitating clathrin-mediated endocytosis (Goodman et al., 1996). β-arrestins can also activate specific mitogen-activated protein kinase (MAPK) signalling cascades upon receptor internalisation (Calebiro et al., 2010; Mundell and Benovic, 2000). However, activation of some GPCRs does not seem to trigger β-arrestin signalling, which might indicate that β-arrestins undergo some conformational changes upon interaction with a GPCR (Cahill et al., 2017). The vasopressin type 2 receptor can form a complex with β-arrestin and G_s, which does not seem to activate the G protein after being internalised by β-arrestin (Cahill et al., 2017).

1.5   GPCR maturation and transport to the cell surface

The expression of GPCRs at the plasma membrane is essential for extracellular stimuli to be able to initiate intracellular responses. The ER is where GPCRs are synthesized, folded into their tertiary functional structure, and assembled (Sauvageau et al., 2014). Following folding, receptors leave the ER in coat protein complex II (COPII)-coated vesicles to be transported to the plasma membrane via the ER-Golgi intermediate complex (ERGIC), the Golgi apparatus, and the trans-Golgi network (Sauvageau et al., 2014). During this process, GPCRs may undergo post-translational modifications, such as glycosylation and palmitoylation, which lead to them becoming functional receptors (Carrington et al., 2018). In the ER, N-glycosylation of asparagine residues begins, rendering the extracellular portions of GPCR more hydrophilic (Wang et al., 2020). In addition, this can also affect receptor maturation, receptor oligomerisation, ligand affinity, G protein-coupling, intracellular trafficking and receptor degradation (Tao and Conn, 2014). Further modifications that can take place in the ER include cleavage of existing signal sequences from the N terminal and the formation of disulphide bonds between Cys residues, which stabilizes the receptor structure (Wang et al., 2020). These processes are controlled via one or more chaperones (Tao and Conn, 2014). During transport through the Golgi apparatus to

the plasma membrane, final processing such as O-glycosylation, palmitoylation, phosphorylation, and sulfation (Dong et al., 2007; Park et al., 2017) may take place; all of which modulate GPCR function.

Glycosylation and its role in exporting GPCR to the cell surface

Protein glycosylation is the attachment of sugar moieties to polypeptides (Moradi et al., 2016) and more than half of all mammalian proteins are glycosylated (Apweiler et al., 1999; Zafar et al., 2011). There are five main types of glycosylation depending upon different carbohydrate structures, but the most important are N- and O-linked glycosylation (Ohtsubo et al., 2006; Zafar et al., 2011). N-linked glycosylation is the most common post-translational modification of GPCRs and occurs in the rough ER (RER) (Moradi et al., 2016). This process involves the attachment of a high-mannose oligosaccharide structure to selected asparagine (Asn) residues in the polypeptide backbone (Moradi et al., 2016). N-linked glycosylation plays an essential role in modulating GPCR surface expression and varies among GPCRs. For example, N-linked glycosylation is required for angiotensin (AT1) receptor and follicle-stimulating hormone receptor (FSHR) cell surface expression. Receptor transport to the plasma membrane was abolished by mutation of the glycosylation sites, leading to an accumulation of mutated receptors in the perinuclear region (Davis et al., 1995; Jayadev et al., 1999). Likewise, mutation of N-linked glycosylation sites in the β_2-AR is accompanied by a marked reduction in plasma membrane expression (Rands et al., 1990). In contrast, it was reported that the N-linked glycosylation plays no role in α_1-AR, H_2 histamine receptor and muscarinic M2 receptor expression at the cell surface (Fukushima et al., 1995, Sawutz et al., 1987).

Interestingly, a recent study demonstrated a role for N-glycosylation in receptor dimerisation, with mutation of key Asn residues resulting in decreased β_2-AR homodimer formation (Li et al., 2017). The β_1-AR is N-glycosylated on Asn-15, and the mutation of this residue enhances α_{2A}-AR and β_1-AR heterodimerisation. Also blocking glycosylation has differential effects on β_1-AR homo- versus heterodimerisation (Xu et al., 2003).

1.6   GPCR oligomerisation

1.6.1   The concept of oligomerisation

In the past, it was thought that GPCRs functioned as monomeric entities that coupled with G proteins on a 1:1 stoichiometric basis to trigger physiological effects (Kuhn et al., 1981; Milligan, 2004; Albizu et al., 2010). This theory has since been revised in light of evidence that suggests that GPCRs can interact with each other to form dimeric or oligomeric complexes, with the potential to couple to one or more type of G protein (**Figure 1.3**) (Ferré et al., 2009; Kamal et al., 2011; Ferré et al., 2014).The dimer theory started in 1980's, as the existence of GPCR mosaics and a direct interaction of two receptors with each other was proposed by two laboratories at the Karolinska Institute in Stockholm and the National Institute for Research in London (Agnati et al., 1980, 1982; Birdsall, 1982). This was consistent with a previous study, Limbird et al., (1975), which demonstrated negatively cooperative site-site interactions among β-ARs. Likewise, Sokolovsky and collaborators suggested that muscarinic receptors exist in interconvertible dimer and tetramer forms by using a photoaffinity labelling approach (Avissar et al., 1983). It was assumed that two G proteins bound per GPCR dimer, a 2:2 stoichiometric basis (**Figure 1.3**). However, the crystal structure for rhodopsin, a class A GPCR, showed that the receptor dimer associated with one transducin (Gt) G protein molecule, i.e. a 2:1 stoichiometric basis (**Figure 1.3**) (Giraldo and Ciruela, 2013).
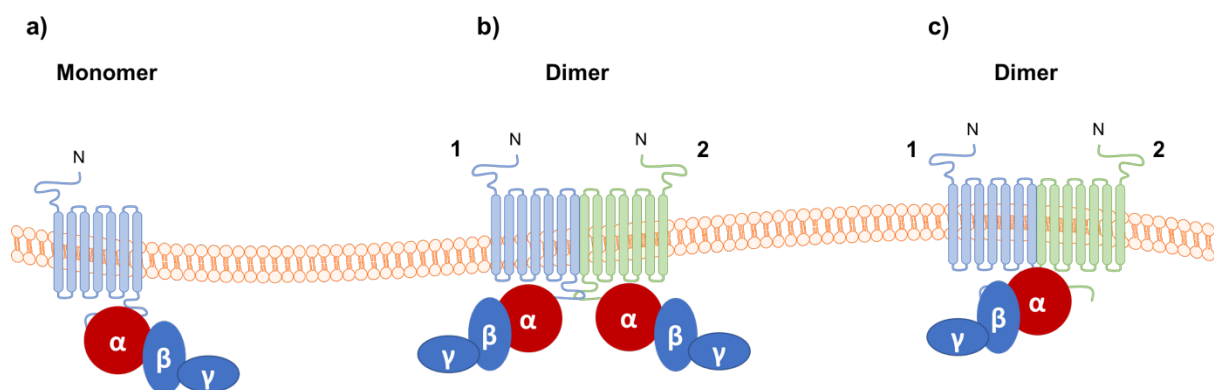
Figure 1.3: Possible stoichiometric models of G protein coupling to receptors.
(a) The simplest possible model a monomeric receptor coupled to a heterotrimeric G protein (1:1). **(b)** Two G protein each coupled to a protomer within a dimer complex (2:2). **(c)** A single G protein-coupled to both protomers of a dimer complex (2:1)*. Figure was adapted from (*Kamal et al., 2011).

GPCRs can assemble into dimer or as larger "oligomer" complexes in their native environment (Moller et al., 2018), with dimers being either homo- or heterodimers. A homodimer is formed from the interaction of two receptors of the same type, while a heterodimer is a complex comprised of two different receptors (**Figure 1.4**) (Ferré et al., 2009). In some cases, more than two receptors interact with each other to form an oligomer (Vischer et al., 2011) (**Figure 1.4**), such as the α_{2A}-AR and β_1-AR heterodimer (Xu et al., 2003). According to Felce et al. (2017), around 20% of class A GPCR members can form dimers, with essential roles for dimerisation in cell signalling. For example, Baneres and Parello (2003) found that one G protein binds to a leukotriene receptor B4 (BLT1) dimer and is important for BLT1 signalling. In most of class C GPCRs, such as the Υ-aminobutyric acid (GABA$_B$) receptor (Agnati et al. 2003), it has been conclusively demonstrated that dimerisation is essential for normal receptor function and expression (Pin et al., 2007).
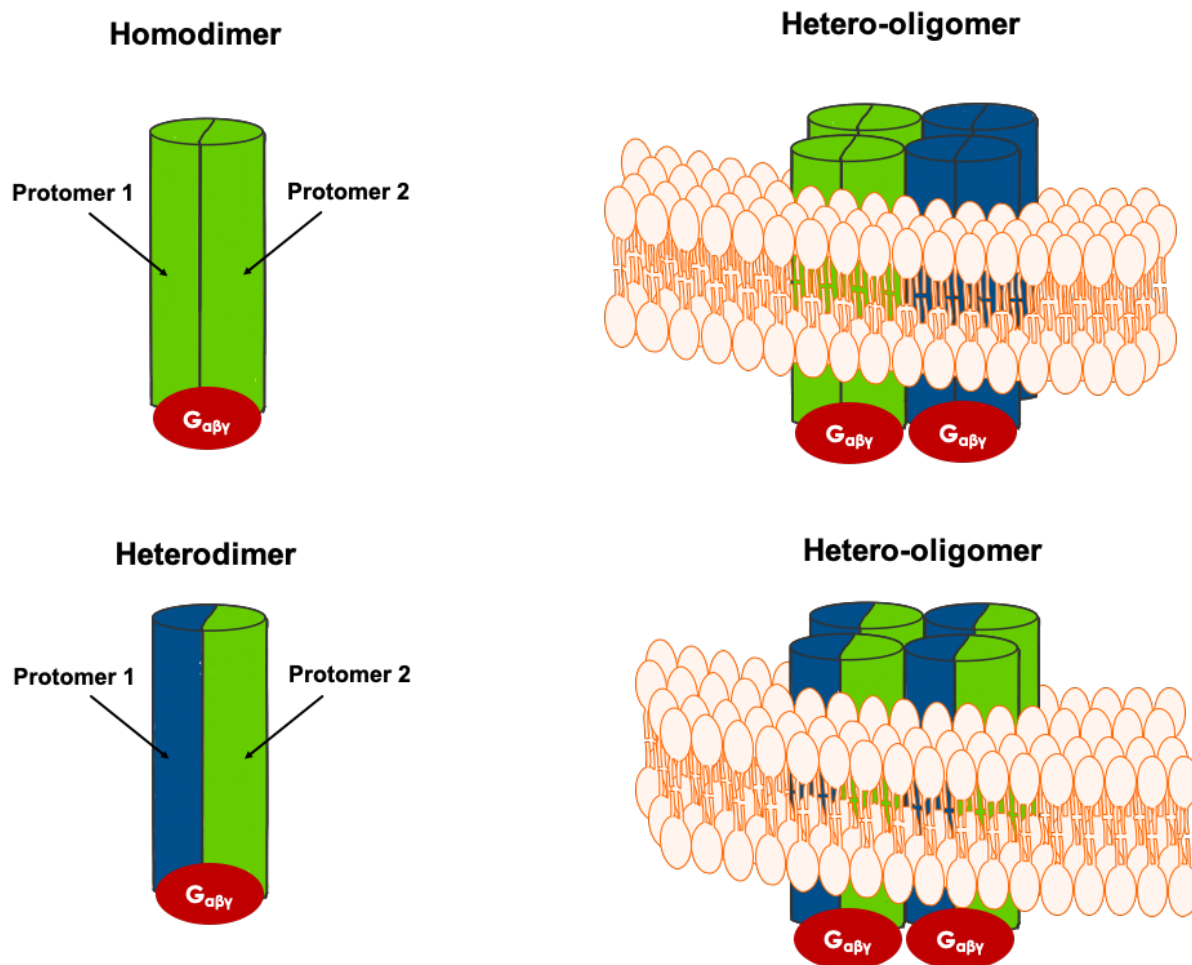
Figure 1.4: Hypothetical structure of G protein-coupled receptor homo- and heterodimers on the plasma membrane.
The schematic representation shows the homodimer and heterodimer formation between GPCRs. Also, in assumption of dimers are the building block of a hetero-oligomer, then two possible models of assembly can be hypothesized. *Figure was simplified and adapted from* (Maggio et al., 2007)

As the number of identified tertiary structures of GPCRs continues to grow, more computational approaches have emerged with the capability of predicting and modelling GPCR dimer interfaces (Meng et al., 2014; Townsend-Nicholson et al., 2019). Computational modelling offers unique insights into the structural features of GPCRs that may be important for dimer formation, however it does not entirely replace the need for experimental validation that employ more traditional methods cell-based systems (Guo et al., 2017), many of which are outlined in **Section 1.6.2.**

1.6.2   Common methods to detect GPCR dimerisation

An increasing number of approaches have been developed with the aim of investigating GPCR dimerisation. These range from the traditional biochemical methods, such as co-immunoprecipitation (Co-IP) with western blotting, to the more sophisticated biophysical and imaging-based approaches of Förster Resonance Energy Transfer (FRET) and Proximity Ligation Assay (PLA). Each of the techniques have their limitations in interpretation, therefore they are rarely conducted in isolation. Instead many are used in combination to experimentally support dimer detection (Guo et al., 2017). Many of the techniques relevant to this thesis are described below.

1.6.2.1   Co-IP

Co-IP is probably one of the earliest techniques used to detect dimer formation (Hebert et al., 1996) and is a classical approach that remains in routine use in protein-protein interactions studies (Harrison and van der Graaf, 2006). It has been used to detect many oligomers, including β_2-AR (Hebert et al., 1996), DOR (Cvejic and Devi, 1997) and mGluR5 (Fiala et al., 2011) receptors and relies upon using epitope tagged GPCRs and appropriate antibodies to study GPCR quaternary structure following recombinant expression in cells. Typical epitope tags used for this technique include human influenza hemagglutinin (HA), Myc and FLAG (Zhao et al., 2013; DeCaprio and Kohl, 2019). Cells are usually transfected with different tagged GPCRs, then lysed and harvested followed by pull-down of the GPCR of interest before being probed by Western blot analysis for proteins of interest. A positive result is not a definitive indication that the GPCRs "directly" interact with one another. The involvement of other proteins in GPCR complexes cannot be ruled out and may depend upon the lysis buffer used. The stringency of the lysis buffer to release the protein of interest from its insoluble membrane environment may cause artificial protein–protein associations or abolish existing associations and therefore requires careful optimisation. Another challenge of this technique is the inability to reliably detect oligomers in native systems due to the need for specific and high-affinity antibodies for GPCRs (Milligan and Bouvier, 2005). Therefore, recombinant over-expression systems with tagged GPCRs are typically used. It is therefore prudent to use a combination of approaches to circumvent any issues related to misinterpretation due to potential false positives

associated with lysis conditions. Current complementary techniques to Co-IP are those that rely upon imaging protein interactions.

1.6.2.2   *Colocalisation*

Colocalisation is commonly measured as a first step indicator of overlapping protein expression. This technique uses fluorescence microscopy to compare the spatial distributions of multiple fluorescent labels to establish if two labelled proteins colocalise at the same location. Measuring colocalisation relies upon pixel-based measurements that include two fundamental strategies (Adler and Parmryd, 2013). One approach measures the pixel overlap, while the other measures statistical correlation, where the relationships between the relative intensities of each pixel are considered. The correlation measurements are Pearson correlation coefficient (PCC), Manders' overlap coefficient (MOC) and Manders' coefficients (M1, M2). The most popular correlation (and the one that have been used in this study) is PCC, which was first used for colocalisation analysis in fluorescence microscopy by Manders et al. (1992). The value range for PCC is (-1 to 1) where 1 represents perfect correlation, -1 perfect anti- correlation and 0 no correlation **(Figure 1.5).** The PCC is an excellent indicator of (linear) correlation and presence of colocalisation. The measurement of protein colocalisation is often misunderstood or poorly implemented due to the physical limits of the spatial resolution of conventional fluorescence microscopy techniques. While often used to infer interaction between overlapping expressing proteins, this technique is inappropriate for determining the existence of direct protein-protein interaction (Adler and Parmryd, 2010). Even super-resolution techniques, such as structured illumination microscopy (SIM) (Gustafsson, 2000) and stimulated emission depletion microscopy (STED) (Hell and Wichmann, 1994) are unsuitable for determining the interactions between proteins. Many often follow up colocalisation analysis with more sensitive biophysical methods, such as FRET microscopy to quantify interactions between proteins (Sekar and Periasamy, 2003).
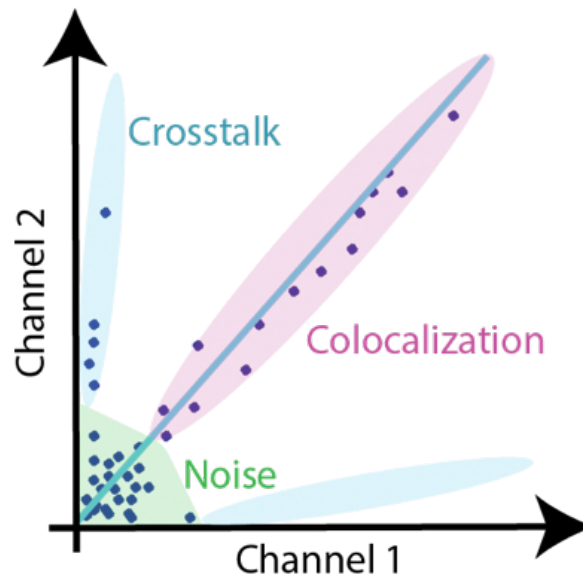
Figure 1.5: Colocalisation visualisation.

Interpretation of a joint histogram. Well correlated pixels are centred around a linear fit (pink). Note the gradient of the fit will only by equal to one if the intensity distribution of both fluorophores is the same. Background noise (green) will be centred around the origin. If crosstalk is present it will appear as a linear distribution of points near the X- or Y-axis (blue). Figure adapted from (Bolte and Cordelieres, 2006).

1.6.2.3 FRET

The most common technique utilized to test dimer formation has been FRET. It was developed in the late 1940s (Förster, 1948) and is based on a physical phenomenon in which energy transfers from an excited fluorescent protein (FP, donor) to another (acceptor) in a non-radiative (dipole–dipole) manner (Cardullo, 2007). It is essential for the donor and acceptor to be in a close proximity (<10 nm) and for there to be an overlap between the emission spectrum of the donor molecule and the excitation spectrum of the acceptor molecule (Fernandez-Duenas et al., 2012) (**Figure 1.6**). A classical fluorophore pair for FRET experiments is cyan fluorescent protein (CFP) and yellow fluorescent protein (YFP), which is the fluorophore pair that was used in this study. Both CFP and YFP are variants of green fluorescent protein (GFP) from the crystal jelly *Aequorea victoria* (Maier-Peuschel et al., 2010; Alvarez-Curto et al., 2011). In order to study GPCR dimerisation, the GPCRs of interest are tagged with the different GFP variants (e.g. GPCR1-CFP and GPCR2-YFP), with energy transfer from the donor to acceptor indicating interaction between the GPCR pair (Day and Davidson, 2009; Piston and Kremers, 2007). This technique has been used to

investigate a variety of GPCR dimers, such as mGluR, which function as homodimers (Pin et al., 2005), and α_{1B}-AR that exists as oligomers (Lopez-Gimenez et al., 2007).
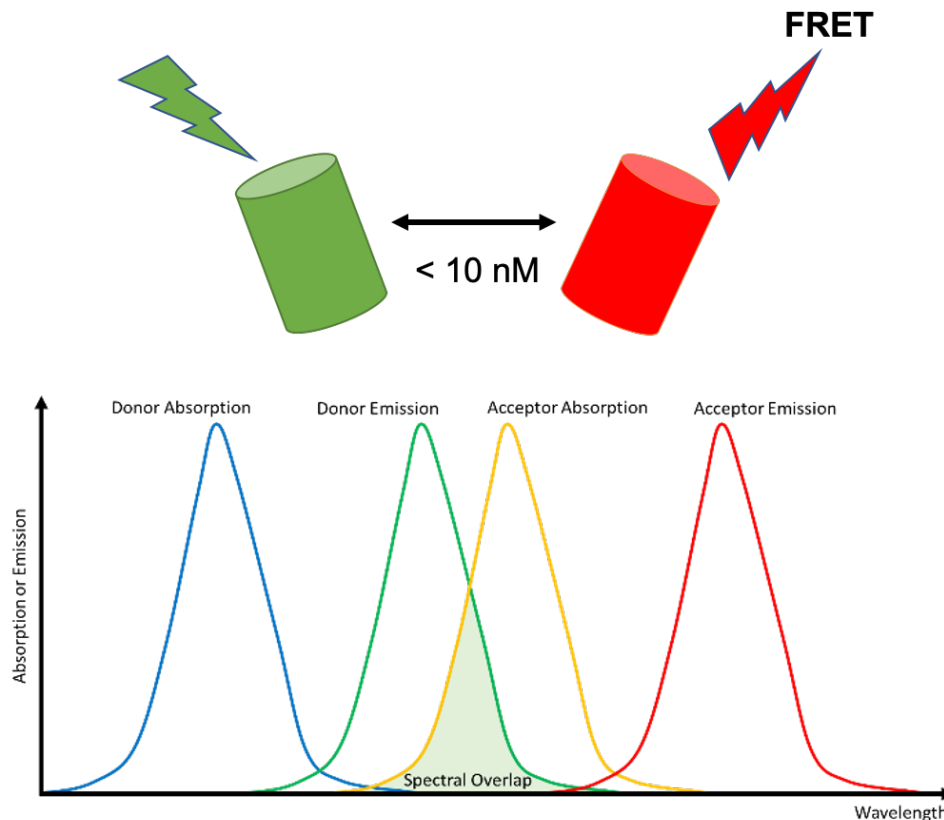
Figure 1.6: Principle of FRET.

Spectral overlap of excitation (Ex) and emission (Em) wavelengths of donor and acceptor fluorophores that results in FRET. FRET efficiency is highest when the donor and acceptor molecules are within 10 nm of each other and their dipoles are at a parallel orientation.

One of the limitations of conventional FRET is the direct dependence on the stoichiometry of the donor and acceptor proteins, as FRET efficiency would increase if more acceptor protein was present than the acceptor protein in the cell, which could easily happen during the transfection process (Krause et al., 2013). The other limitation is that GFP variants (CFP and YFP) are large proteins (27kDa) that may affect normal receptor function or disrupt interactions (Piston and Kremers, 2007). Moreover, other factors might also influence accuracy, for example spectral bleed-through due to collisional FRET or fluorophore photobleaching (Kirber et al., 2007). Over the years, advances in the approaches to FRET imaging have led to its use in

combination with other imaging methods, including super-resolution microscopy, total internal reflection fluorescence microscopy (TIRFM) and Fluorescence Lifetime Imaging Microscopy (FLIM). FLIM offers a solution to some limitations of FRET imaging and can be used in combination with FRET to detect interactions with higher accuracy (Ishikawa-Ankerhold et al., 2012). This is discussed below.

1.6.2.4 FLIM/FLIM-FRET

FLIM is a method used to quantify FRET and is based on measuring the reduction in the fluorescence lifetime of the donor fluorophore only, which is different from intensity-based FRET measurements as it dependent on both the acceptor and the donor. FLIM-FRET depend on the donor fluorescence lifetime, and excited fluorophore population will decay faster when FRET offers more way to lose energy (**Figure 1.7**). The figure shows that the lifetime of the donor is unchanged when there is no FRET, however, when there is FRET, the donor passes excitation energy to the acceptor, and its lifetime decreases. Measurements of the donor lifetime makes is less prone to cross-talk compared to intensity-based measurements.
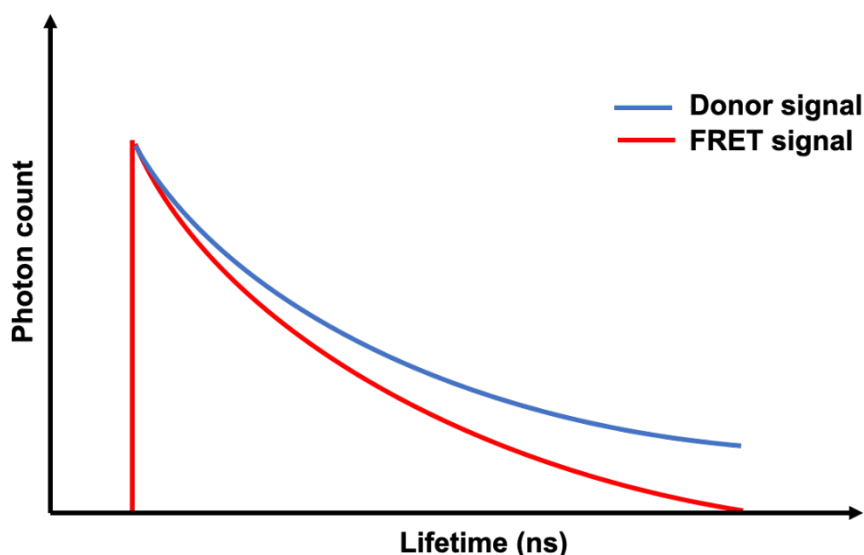
Figure 1.7: FLIM-FRET lifetime response.

Simulated fluorescent lifetime readings from a FRET pair. Due to the acceptor absorbing photons during FRET, the decrease in the lifetime of donor signal (red) is shown compared to when imaged alone (blue).

FLIM allows for the calculation of both the FRET efficiency and the distance between the two fluorophores. The sample is allocated into pixels then illuminated by either single- or multi-photon excitation and scanned pixel-by-pixel in scanning FLIM. Alternatively, wide-field FLIM can be carried out using a camera-based Single-Photon Avalanche Diode (SPAD) array. The scanning FLIM used in this project was two-photon excitation together with a time-correlated single-photon counting (TCSPC) module, which helped determine the fluorescence lifetime for the donor with and without the acceptor. Both FRET and FLIM-FRET still use tagged receptors, so therefore cannot be easily applied to native tissues (Cottet et al., 2011). Other methods exist that have been used in GPCR cell biology systems to study the interaction between native proteins endogenously expressed in primary cells (Guo et al., 2017).

1.6.2.5   *In situ PLA*

PLA is a suitable and sensitive assay to detect direct protein-protein interactions (Soderberg et al., 2008). The principle of PLA relies on the distance between two protomers being small enough (<40 nm) to generate a signal (Alam, 2018). Through the use of selective primary antibodies directed against the proteins of interest (**Figure 1.8a**), oligonucleotide-conjugated secondary antibodies are added (**Figure 1.8b**) and if the proteins are within the <40 nm proximity, a closed circle will form between the two oligonucleotides (**Figure 1.8c**). This is followed by ligation of the oligonucleotides and subsequent rolling circle amplification (RCA), leading to a DNA structure that can be detected by the labelled oligonucleotides (**Figure 1.8d**) and readily visualised under the microscope**.**
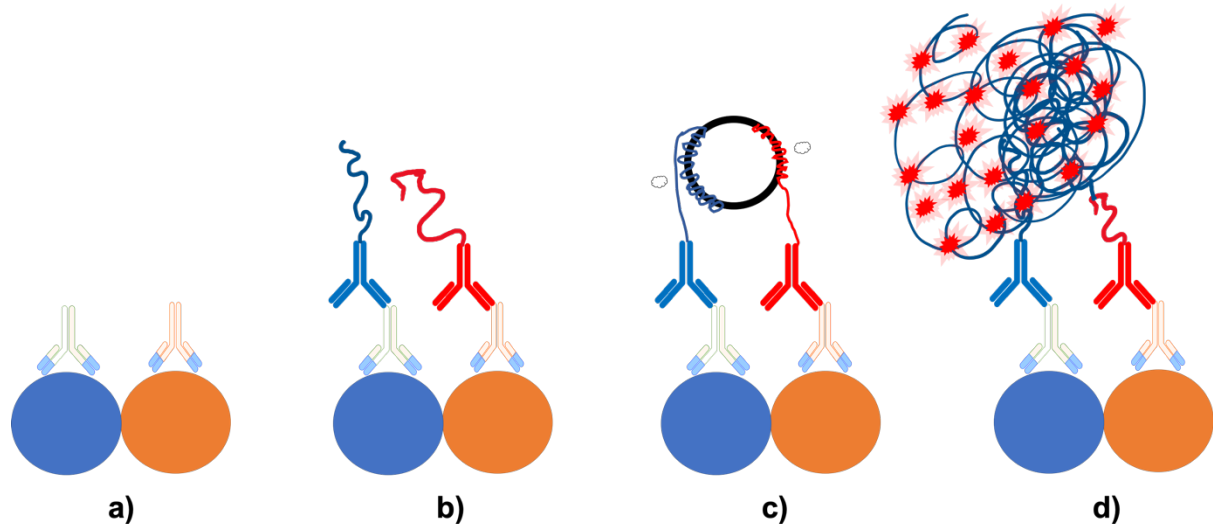
Figure 1.8: The principle of proximity ligation assay.

a) The primary antibodies bind to their target protein. b) The oligonucleotide-conjugated secondary antibodies bind to the primary antibodies. c) Ligase and oligonucleotides hybridize the PLA probes and make a closed circle. d) Polymerase uses the circle as a template for rolling circle amplification (RCA). Fluorescently labelled oligonucleotides hybridize with the RCA product.

In 2002, PLA was used for specific and sensitive measurement of proteins in solution (Fredriksson et al., 2002). It was then used to measure and visualise proteins interactions and post-translational modifications in cells and tissue sections (Soderberg et al., 2008). In 2009, PLA was used along with flow cytometry readout for extracellular protein detection and interaction (Leuchowius et al., 2009). More recently, PLA was developed for the detection with high specificity, and without genetic manipulation of complexes of multiple proteins (Greenwood et al., 2015), particularly interactions of native proteins expressed in cells and tissues. Examples include characterisation of the D_2-A_{2A} dimer in the striatum (Trifilieff et al., 2011) and cannabinoid CB1 and CB2 receptors in the rat brain pineal gland (Callen et al., 2012).

The main advantage of PLA is the detection of endogenous protein interactions in cells and tissues, along with the ability visualise individual signals that enable the relative quantification of proteins (Weibrecht et al., 2010, Alam, 2018). This does, however, rely upon the availability of selective antibodies to target native proteins (Weibrecht et al., 2010). The method of chemical fixation of the specimen may also influence the availability of the antigen by changing or destroying its structure

(Raykova et al., 2016). This method generally places focus upon protein interaction on fixed specimens, however there has to be an appreciation that GPCR dimerisation is a dynamic process that may require additional considerations when it comes to the methods used to detect them.

1.6.3   GPCR Oligomerisation Boundaries

Dimerisation mechanisms differs between GPCR classes. Class C receptors contain a unique and extended N-terminal domain, known as a Venus flytrap (VFT) domain, that influences properties of these receptors, such as ligand binding (Chun et al., 2012), whereas the TM domains in Class A receptors play an essential role in ligand binding (Chun et al., 2012). Class C receptor dimerisation occurs because of covalent binding between the protomers (El Moustaine et al., 2012), whereas Class A and B receptors express as transient, rather than stable, dimers at the cell surface (Milligan et al., 2019). Different TM domains have been identified as critical players at the GPCR dimer interface. Using interfering synthetic TM mimetic peptides, TM6 of Class A GPCRs has been proven to be important for BLT1 and β_2-AR dimers (Granier et al., 2004). Other approaches, such as atomic force microscopy (AFM) in mouse rhodopsin, found dimer formation via TM4-TM5 interactions (Fotiadis et al., 2004). High resolution crystal structure analysis of the β_1-AR showed that TM1-TM2-C terminus and TM4-TM5 interfaces are responsible for stabilizing the β_1-AR homodimer (Huang et al., 2013). Also, the TM5 domain is required in homodimerisation of serotonin 5-HT$_{2C}$ dopamine D$_2$ and muscarinic M3 receptors. (Ferre et al., 2014). Moreover, a recent study indicates that the interaction between TM4 and TM5 stabilizes the heterodimer formed by adenosine A$_{2A}$ and D$_2$ receptors (Borroto-Escuela et al., 2018). In contrast, crystal structure analysis of the chemokine receptor CXCR4 and MOR suggests that the homodimer interface of these receptors involves both TM5 and TM6 domains (Wu et al., 2010; Manglik et al. 2012). From these examples, it is clear that a number of different GPCR dimerisation interfaces exist, each with their own specific receptor regions that are essential for dimerisation.

1.6.4   Effects of GPCR dimerisation on receptor function

Dimerisation has the ability to influence a GPCR at various stages throughout its life cycle, such as receptor maturation, ligand binding, signalling or changing G-protein selectivity and internalisation (Terrillon and Bouvier, 2004; Bohme and Beck-Sickinger, 2009; Hanlon and Andrew, 2015). Understanding the role of dimerisation in GPCR function could be important in the development of new therapeutic targets.

1.6.4.1   Trafficking and surface expression

One of the first functional characterizations of GPCR dimerisation was described for the Class C GPCR, $GABA_B$ receptors. When the first isoform of $GABA_B$ ($GABA_{B(1)}$) receptor was cloned and then expressed in a cell line, it was found to have substantially lower affinity for agonists compared to native receptors (Kaupmann et al., 1997). This was latterly found to be due to its inability to be expressed on the cell surface (Couve et al., 1998). Subsequently, a second $GABA_B$ receptor isoform was cloned ($GABA_{B(2)}$) and it was discovered that both isoforms need to exist for a functional $GABA_B$ receptor to be expressed **Figure 1.9** (Jones et al., 1998; White et al., 1998). Later work identified the mechanism of this phenomenon as the dimerisation between both isoforms, which resulted in the effective masking of a C-terminal RXR ER retention motif present on the $GABA_{B(1)}$ receptor (Margeta-Mitrovic et al., 2000).
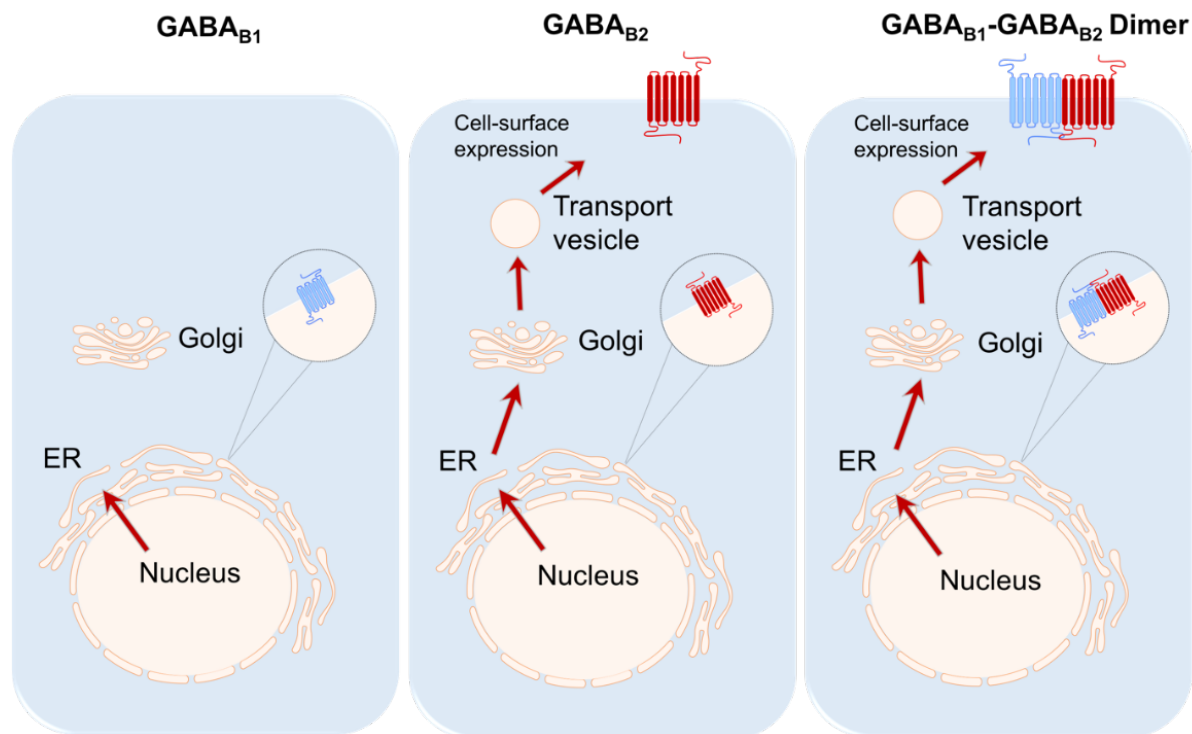
Figure 1.9: Role of heterodimerisation in GABA$_B$ receptor trafficking.
When GABA$_{B1}$ receptor is expressed alone, it retains as an immature protein in the ER and never reaches the cell surface. By contrast, the GABA$_{B2}$ isoform is transported normally to the plasma membrane but is unable to bind GABA and thus to signal. When coexpressed, the two receptors are properly processed and transported to the cell surface as a stable dimer, where they act as a functional metabotropic GABA$_B$ receptor.

Class A receptors can exist as monomers, dimers and oligomers at the cell surface (Dijkman et al., 2018). Whilst several studies indicate that the impact of dimerisation on receptor trafficking and function could be limited to Class C receptors (Pioszak et al., 2010; Vischer et al., 2015), it is intriguing that dimerisation of 5HT$_{2c}$ receptor takes place in the ER and Golgi apparatus during receptor maturation, showing that dimerisation can influence Class A receptor trafficking as well, although, further investigation is needed to study the functional receptor at the cell surface (Herrick-Davis et al., 2006).

1.6.4.2   Ligand pharmacology

It has been established for some dimer pairs that dimerisation alters their ligand binding affinity (Milligan, 2009), and receptor transactivation (Szymanska et al., 2018). The KOR was shown to dimerise with the DOR (Ramsay et al., 2002). This dimer demonstrated no significant binding affinity for selective agonists for either receptor. However, incubation with specific ligands to one of the subtypes synergistically increased the binding affinity of agonists for the other. The KOR selective agonist was six-fold more potent in cells coexpressing the KOR and DOR when compared to cells expressing only the KOR (Waldhoer et al., 2005). Dimerisation of KOR and DOR was supported by bioluminescent resonant energy transfer (BRET) analysis (Ramsay et al., 2002). Heterodimerisation between MOR and DOR has also been shown using co-immunoprecipitation (George et al., 2000; Gomes et al., 2000) and BRET (Gomes at al., 2004), and similar effects of dimerisation on ligand binding features to KOR-DOR heterodimers were seen (Gomes at al., 2004; Gomes at al., 2011). Further research has demonstrated heterodimers between KOR and MOR via both co-immunoprecipitation and BRET (Wang et al., 2005; Chakrabarti et al., 2010). In these studies, KOR-MOR opioid dimers appear to have similar affinity as KOR for KOR-selective agonists, whereas the binding affinity for MOR agonists was reduced compared to MOR alone. Interestingly, binding of the KOR-selective agonists appears to increase MOR agonist binding affinity, but not vice versa (Wang et al., 2005).

1.6.4.3   Dimerisation-dependent changes to G protein coupling

Dimerisation can also change the signal transduction pathways used by GPCRs. For example, dopamine D_1 receptors couple to G_s and D_2 receptors couple to $G_{i/o}$, and act via AC and the cAMP second messenger system (Beaulieu and Gainetdinov, 2011). Nonetheless, several studies indicated that a D_1-like receptor stimulates intracellular Ca^{2+} release in brain striatal tissue (Undie et al., 1994; Pacheco and Jope, 1997; Jin et al., 2003; Tang and Bezprozvanny, 2004). This was unaffected by pertussis toxin (PTX), a potent $G_{i/o}$ inhibitor (Mangmool and Kurose, 2011), but was blocked by an anti-$G_{q/11}$ monoclonal antibody (Pacheco and Jope, 1997). Later, it was demonstrated that this release of intracellular Ca^{2+} only happened when D_1 and D_2 receptors were coexpressed, and can be blocked by inhibiting PLC, indicating the

possible formation of a D_1-D_2 dimer that couples to $G_{q/11}$ **Figure 1.10**. (Lee et al., 2004; Rashid et al., 2007). Formation of a D_1-D_2 heterodimer was indicated by co-immunoprecipitation (Lee et al., 2004) and resonance energy transfer (RET) (So et al., 2005) in native striatal tissue (Rashid et al., 2007).
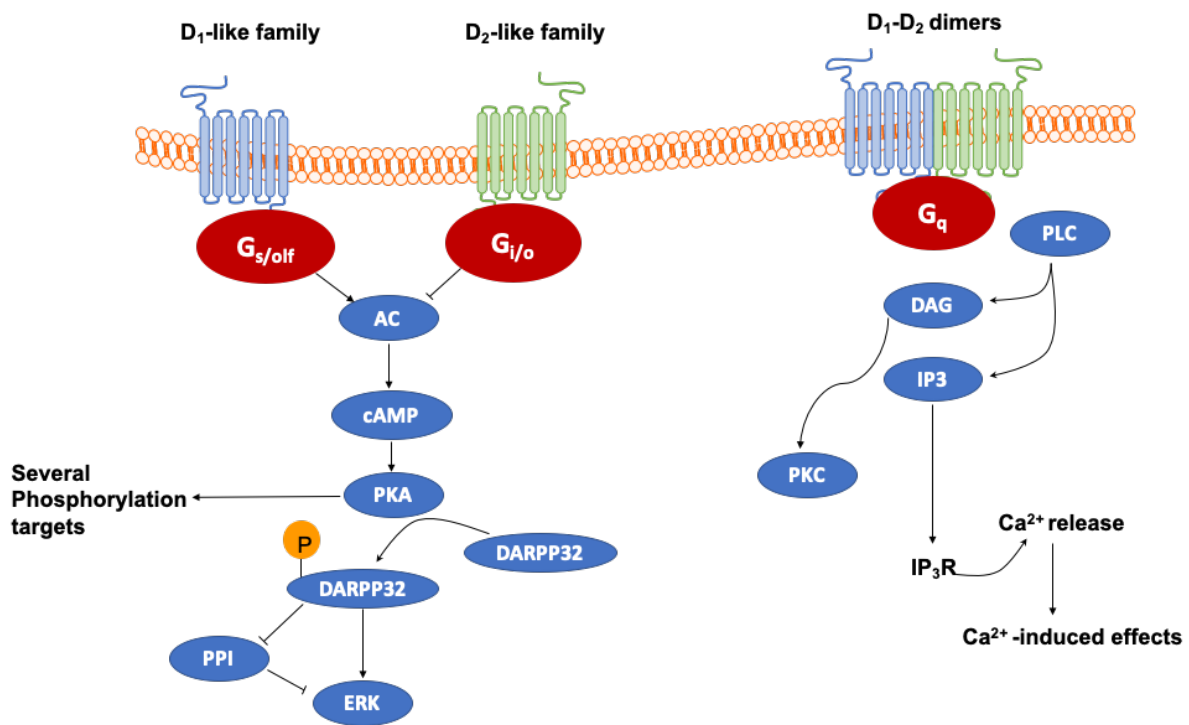
Figure 1.10: Impact of dimerisation on dopamine receptors signalling.
Intracellular signalling pathways activated by D_1- and D_2-like receptors families. $G_{s/olf}$, $G_{i/o}$, G_q, $G_{\beta\gamma}$, G proteins; AC, adenylyl cyclase; cAMP, 3′-5′-cyclic adenosine monophosphate; DARPP32, cyclic AMP-regulated phosphoprotein, 32 kDa; PPI, protein-phosphatase 1; ERK, extracellular signal-regulated kinase protein kinase; PLC, phospholipase C; DAG, diacylglycerol; PKC, protein kinase C; IP_3, inositol trisphosphate; IP_3R, inositol trisphosphate receptor; Ca^{2+}, calcium.

Another example of dimer-dependent alterations to G protein coupling is that between the AT1 receptor, which couples to G_i protein, and the α_{2C}-AR, which is coupled to G_q. By co-activating both receptors with their own selective ligands, the dimer coupled to G_s protein (Bellot et al., 2015). Heterodimer formation was confirmed by using BRET (Bellot et al., 2015). Further examples include melatonin MT1 and MT2 receptors, which are coupled to G_i proteins. Inhibiting G_i proteins or PKA did not impact dimer activity. However, inhibition of PKC decreased the effect of exogenous melatonin on photoreceptors, while activation of PKC mimicked the effects of melatonin, which confirmed that MT1-MT2 dimer was coupled to G_q protein (Baba et al., 2013).

1.6.4.4   Receptor internalisation

When the $P2Y_{11}$ receptor is expressed on its own in HEK293 cells it does not undergo agonist-induced endocytosis, but does so when the $P2Y_1$ receptor is coexpressed (Ecke et al., 2008; Dreisig and Kornum, 2016). In addition, agonist and antagonist action was altered by the formation of the heterodimer. For example, NF157, which is a selective $P2Y_{11}$ receptor antagonist, was unable to inhibit activation of the heterodimer (Ecke et al., 2008; Dreisig and Kornum, 2016). On the other hand, MRS2179, a selective $P2Y_1$ receptor antagonist, inhibited $P2Y_{11}$ activity induced by the $P2Y_{11}$ receptor agonist, Bz-ATP (Ecke et al., 2008; Dreisig and Kornum, 2016). Thus, the dimerisation between both $P2Y_1$ and $P2Y_{11}$ impacts receptor internalisation and activity.

2 Purinergic receptors

2.1 Introduction

Endogenous purine nucleosides and nucleotides act at purinergic receptors to produce their physiological and pharmacological effects. The characteristics of these receptors were first described in 1978, when Burnstock proposed that they could be divided into two types according to agonist and antagonist selectivity (see Burnstock, 2018). P1 receptors are activated by adenosine and antagonized by methylxanthines, such as theophlline, whilst P2 receptors are activated by adenosine 5'-triphosphate (ATP) and adenosine diphosphate (ADP) and unaffected by methylxanthines. Subsequently, P1 receptors subtypes, A_1, A_{2A}, A_{2B} and A_3, were cloned and found to be GPCRs (**Figure 1.11**), (Ralevic & Burnstock, 1998). In 1985, the P2 receptors were subdivided into the P2X and P2Y subtypes based on their pharmacological profiles (Burnstock & Kennedy, 1985). In the early 1990's cloning studies confirmed this subdivision and showed that they have different structures, pharmacological properties and signal transduction mechanisms (**Figure 1.11**) (Burnstock, 2007).
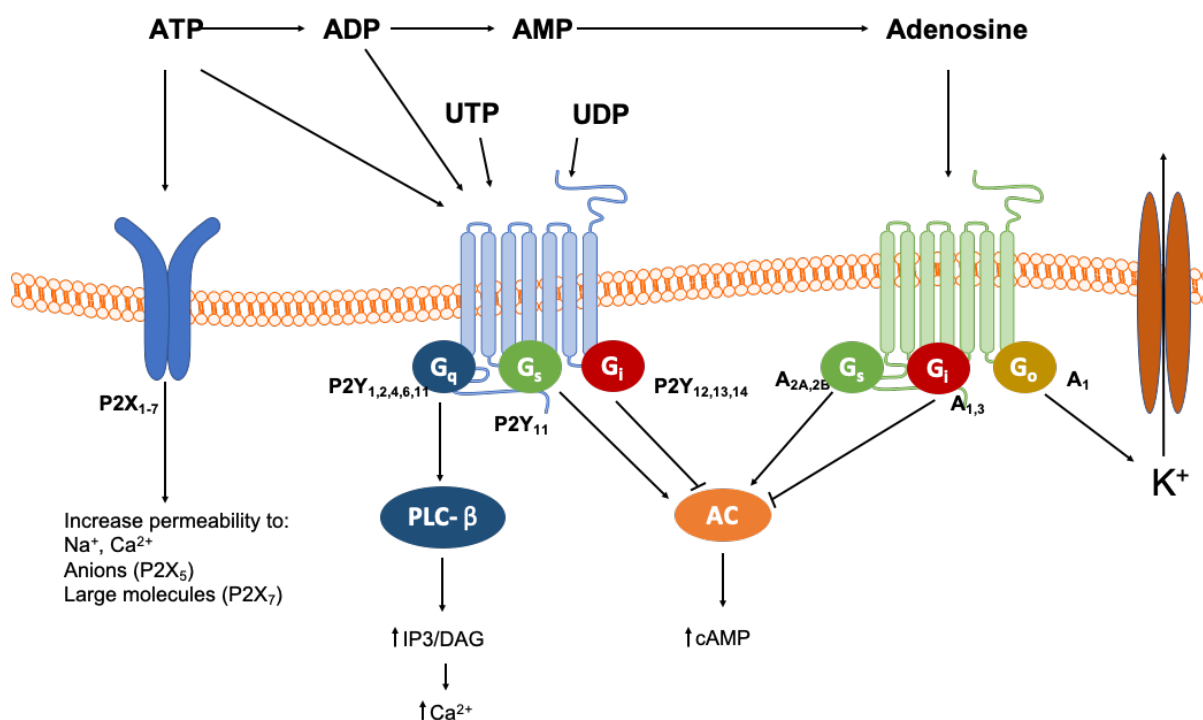
Figure 1.11: Purinoceptor signalling.
Relationship of nucleotides, nucleotide metabolism and activity of P2X, P2Y and adenosine receptors. ATP activates P2X receptors, ATP, ADP, UTP and UDP activate P2Y receptors, and adenosine activates adenosine receptors. P2Y receptors are coupled to G_q, leading to intracellular Ca^{2+} release, and G_s or G_i, which modulate cAMP levels. Adenosine receptors are coupled to G_s or G_i as well as, G_o, which is can activate K^+ channels. Figure was adapted from Ham and Evans, (2012); Kaebisch et al., (2015).

2.2   P2X receptors

P2X receptors are ligand-gated cation channels that are widely expressed throughout the body. Seven subtypes have been cloned, all of which respond to ATP, but not ADP, uridine 5'-triphosphate (UTP), uridine-5'-diphosphate (UDP) or UDP-glucose (Burnstock, 2004). The P2X1-7 receptors have 30% to 50% sequence identity at the amino acid level (Burnstock, 2006) and form homo- or heteromeric receptors (Khakh et al. 2001; Kennedy et al. 2013), apart from P2X7 receptors, which do not form heterodimers (Burnstock, 2006), and P2X6 receptors, which do not form a functional homomer (Burnstock, 2006). These receptors have been proposed to be involved in many of roles, such as cardiovascular disease (Kennedy et al. 2013), kidney disease (Birch et al., 2013), osteoporosis (Lenertz et al., 2015) and cancer pain (Franceschini and Adinolfi, 2014).

2.3   P2Y receptors

Metabotropic P2Y receptors are members of the rhodopsin-like, Class A family of GPCRs (Abbracchio et al., 2006). In humans, eight subtypes (P2Y$_{1, 2, 4, 6, 11, 12, 13, 14}$) have been cloned and they couple to heterotrimeric G proteins (**Figure 1.11**). P2Y receptors can be divided regarding their selectivity to G proteins. P2Y$_1$, P2Y$_2$, P2Y$_4$, P2Y$_6$ and P2Y$_{11}$ receptors couple with G$_{q/11}$, which activates the PLC$_\beta$ pathway and mobilization of intracellular Ca^{2+} (as noted in **section 1.3**). P2Y$_{11}$ receptors can also couple to G$_s$ (Abbracchio et al., 2006; Burnstock, 2006), which is associated with the stimulation of AC, whilst, P2Y$_{12}$, P2Y$_{13}$ and P2Y$_{14}$ receptors couple to G$_{i/o}$, which inhibits AC activity. P2Y receptors can also modulate cellular activities via other signalling pathways, for instance, G$_{q/11}$ also stimulates the p63RhoGEF guanine nucleotide exchange factor that acts on downstream Rho targets (Lutz et al., 2005).

In some cases, certain P2Y receptor subtypes have been reported to couple to other G proteins. For example, when stimulated by high concentrations of ADP, overexpressed P2Y$_{13}$ receptors, couple to G$_s$ (Marteau et al., 2003). P2Y receptors respond strongly to the endogenous nucleotides, ATP, ADP, UTP, UDP and UDP-glucose, with different pharmacological profiles (**Figure 1.12**). P2Y$_1$, P2Y$_{11}$, P2Y$_{12}$ and P2Y$_{13}$ receptors prefer adenine nucleotides, with ADP being the most potent at P2Y$_1$, P2Y$_{12}$ and P2Y$_{13}$ receptors, whereas ATP is more potent than ADP at P2Y$_{11}$ receptors. P2Y$_2$ and P2Y$_4$ receptors prefer triphosphate nucleotides, with ATP and UTP being potent agonists, while ADP and UDP are inactive. P2Y$_6$ receptors prefer uridine nucleotides, but UDP is more potent than UTP. The P2Y$_{14}$ receptors prefer uridine nucleotides, with UDP and UDP-glucose being agonists (Kennedy et al., 2013).

The gaps in the numbering sequence are because some of the proposed subtypes, p2y5, p2y7 and p2y10, were subsequently found to have no fuctional responsiveness to nucleotides, or because they are non-mammalian orthologues of one of the known mammalian subtypes. For example, p2y3 may be a chicken orthologue of P2Y$_6$ receptors, while p2y8 and tp2y may be *Xenopus laevis* and turkey orthologues of P2Y$_4$ receptors (Abbracchio et al., 2006; Burnstock, 2014). Phylogenetic analysis of the relationships amoung mammalian P2Y receptors indicates two subgroups (Jacobson et al., 2002). The first contains P2Y$_{1,2,4,6,11}$ receptors and they have 29 - 46% sequence homology similarity, while the other subgroup contains P2Y$_{12,13,14}$ receptors, which have 21 - 48% homology in common

(Abbracchio et al., 2006). The human $P2Y_1$ and $P2Y_{12}$ receptors, which are the focus of this thesis,have only 9% identical amino acid residues in common (von Kugelgen and Hoffmann, 2016).

2.3.1   P2Y receptor structure

TM6 and TM7 of P2Y receptors contain specific amino acid motifs that are considered to be important for the binding of extracellular nucleotides (Erb et al., 1995; Boeynaems et al., 2012). All have the TM6 H-X-X-R/K motif that is essential for agonist activity (Erb et al., 1995; Conigrave et al., 1998; Boeynaems et al., 2012). However, the motifs in TM7 vary between the two phylogenetic subgroups, as the $P2Y_{1,2,4,6,11}$ subgroup has a Q/K-X-X-R motif, while the $P2Y_{12,13,14}$ subgroup has a K-E-X-X-L motif (Abbracchio et al., 2006; Boeynaems et al., 2012), which is not specific for P2Y receptors, as it is also found in GPR87 receptors (Boeynaems et al., 2012). This difference might impact on the ligand binding profile and affinity for these receptors (Abbracchio et al., 2006).

Studying receptor crystal structure provides much greater depth in our understanding of receptor ligand binding and activation. The only crystal structures available at present are of the human $P2Y_1$ and $P2Y_{12}$ receptors (**Figure 1.12**) (Zhang et al., 2014a,b, 2015). It is notable that both subtypes crystallized as homodimers. Both also contain disulphide bridges that stabilize the receptor structure. Two are formed in the $P2Y_1$ receptor, one connecting the N-terminus (Cys42) to extracellular end of TM7 (Cys296), which is a critical region for receptor activation and the connecting TM3 (Cys124) to the second extracellular loop (Cys202) and this is thought to be critical for proper receptor trafficking to the cell surface (Hoffmann et al., 1999; Moro et al., 1999; Zhang et al., 2015). On the other hand, the $P2Y_{12}$ receptor only has one disulphide bond that links the N-terminus (Cys17) with TM7 (Cys270) (Zhang et al., 2014b), which are important sites for receptor expression (Mansour et al., 2020). Other cysteines, (Cys97) and (Cys175), do not form disulphide bridges, but are able to interact with the thiol moieties of drug metabolites, such as clopidogrel and prasugrel (Savi et al., 2006; Algaier et al., 2008; Ding et al., 2009).

The crystal structures also provided detailed insight into the sites where drugs bind (**Figure 1.12**). To date, the orthosteric agonist binding site has only been reported for the P2Y$_{12}$ receptor (Zhang et al., 2014a), and comprises residues in helices III, IV, V, VI and VII and also ECL2 and the N terminus. The non-nucleotide, reversible P2Y$_{12}$ antagonist, AZD1283, binds to a distinct site, formed by helices III–VII, that partially overlaps the orthosteric agonist binding site (Zhang et al., 2014b). Other crystal structures for human P2Y$_{12}$ receptor binding to ticagrelor have also been modelled (Paoletta et al., 2015). The P2Y$_1$ receptor has two distinct antagonist-binding sites (Zhang et al., 2015). The first is a pocket comprising residues mainly from the N terminus, ECL2 and helices VI and VII that serves as a binding site for the nucleotide antagonist MRS2500 (Zhang et al., 2015). The other is on the external receptor interface with the lipid bilayer, comprising residues within helices I, II and III and ECL1, and acts as a binding site for the allosteric, non-nucleotide modulator, BPTU.
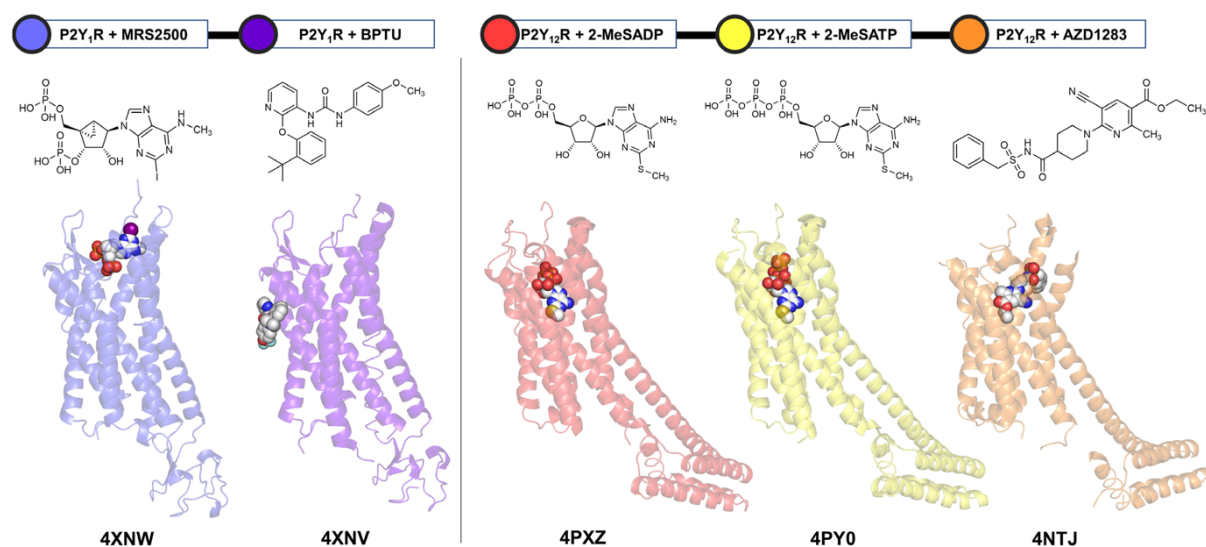
Figure 1.12: Published crystal structures of P2Y$_1$ and P2Y$_{12}$ receptors.
On the left, crystal structures of P2Y$_1$ receptors binding to MRS2500 and BPTU. On the right, crystal structure of P2Y$_{12}$ receptors binding to 2-MeSADP, 2-MeSATP and AZD1283. The PDB-ID shown at the bottom. Figure was adapted from Neumann et al., (2020).

2.3.2   P2Y receptor antagonists

P2Y receptors are potential drug targets for numerous conditions, but unfortunately for the majority of the subtypes, this has not translated into clinically-used drugs, due to a lack of sub-type selective ligands (Jacobson et al., 2009). P2Y receptor ligands are listed in **Table 1.2 and 1.3**) along with their EC_{50}/IC_{50} values and potential therapeutic targets. The $P2Y_1$ and $P2Y_{12}$ receptors play a key role in platelet activation and aggregation, whereas the $P2Y_1$ antagonists are at the preclinical stage (Gasecka et al., 2020). However, the $P2Y_{12}$ antagonists are the most effective treatment strategy, nowadays, to prevent stent thrombosis after percutaneous coronary intervention (Gasecka et al., 2020). Of particular relevance to this thesis, MRS2500 and MRS2179 are competitive $P2Y_1$ receptor antagonists, that bind reversibly to the active site of the receptor, leading to inhibition of receptor activation (Baurand et al., 2001; Cattaneo et al., 2004), with half maximal inhibiting concentration values (IC_{50}) of 0.23µM (Baurand et al., 2001) and 1nM (Cattaneo et al., 2004), for MRS2179 and MRS2500, respectively.

The most widely used $P2Y_{12}$ antagonist and one of the world's best-selling drugs in recent years is the pro-drug clopidogrel (Plavix), which is metabolised to produce a $P2Y_{12}$ antagonist (Debnath et al., 2010; Raju et al., 2008). Interestingly, it is less effective in some patients who express hepatic cytochrome P450 (CYP450) polymorphisms, as it relies on these isoenzymes to convert it to its active metabolite (O'Conner et al., 2011). Other $P2Y_{12}$ receptors antagonists that act directly at $P2Y_{12}$ receptors are ticagrelor (Brilinta) and cangrelor (Kengrexal), which is also known as its developmental name ARC-69931MX (O'Conner et al., 2011). Cangrelor has a high selectivity for the $P2Y_{12}$ receptor, and this, coupled with its high potency has led its frequent use for testing the presence of functional $P2Y_{12}$ receptor expression (Suzuki et al., 2011).

Table 1.2: P2Y receptors (coupled to Gq or Gs) agonists, antagonists and therapeutic pathways

Receptor	Agonist	pEC_{50}	Cross reactivity	Synthetic antagonist	pIC_{50}	Cross reactivity	Potential therapeutic targets
$P2Y_1$	ADP 2-MeSADP ADP-β-S MRS2365	5.09 8.2 7 9.4	$P2Y_{12}$ $P2Y_{12, 13}$ $P2Y_{12, 13}$ None	MRS2298 MRS2496 MRS2179 MRS2279 MRS2500	7.2 5.8 6.4 8.1 9	None None None None None	Antagonists can prevent cytokine/chemokine-induced damage following ischemia in mice, agonists can induce axonal elongation in neurons and modulation of pain sensation, antagonists can reduce anxiolytic behavior in rats
$P2Y_2$	UTP PSB-1114 INS37217 MRS2698	7.2 6.8 6.7 8.1	$P2Y_4$ None $P2Y_4$ None	AR-C118925	7.2	None	Agonists can increase the migration of glial cells through $P2Y_2$ receptor/integrin interactions, proliferation of glial cells, non- amyloidogenic APP processing in neurons, and the uptake and degradation of neurotoxic forms of A1-42 by microglial cells
$P2Y_4$	UTP	6.2	$P2Y_2$	PSB-1699	6.4	None	Receptor activation can inhibit presynaptic glutamate release, modulate blood-brain barrier function, and inhibit K^+ currents in rat myocytes
$P2Y_6$	UDP INS48823 MRS2782 MRS2693	6.2 6.9 6.4 7.8	$P2Y_{14}$ None $P2Y_{14}$ None	MRS2578	7.4	None	Receptor activation can increase phagocytic activity of microglia and regulate repair mechanisms in response to CNS injury
$P2Y_{11}$	AR-C67085 ATP-γ-S	8.5 4.6	$P2Y_{12}$ $P2Y_{2,4}$	NF340 NF157	7.7 7.3	None P2X1,2,3	Receptor activation delays pathogen- or inflammation-induced apoptosis in neutrophils, inhibits TLR signalling and modulates cytokine release

Table adapted from Weisman et al., (2012); Jacobson et al., (2020).

Table 1.3: P2Y receptors (coupled to Gi) agonists, antagonists and therapeutic pathways

Receptor	Agonist	pEC_{50}	Cross reactivity	Synthetic/native antagonist	pIC_{50}	Cross reactivity	Potential therapeutic Pathways
$P2Y_{12}$				ACT246475	9	None	Receptor antagonists are in widespread clinical use as inhibitors of platelet aggregation, and $P2Y_{12}$ receptor activation can regulate glial cell migration and increase cell proliferation
	ADP	7.22	$P2Y_{1,13}$	AR-C67085	8.2	$P2Y_{11}$	
	2-MeSADP	8.3	$P2Y_{1,13}$	AR-C69931MX	9.4	$P2Y_{13}$	
	ADP-β-S	6.7	$P2Y_{1,13}$	AZD6140	7.9	None	
				AZD1283	7.5	None	
				elinogrel	7.6	None	
$P2Y_{13}$	ADP	7.9	$P2Y_{1,12}$	MRS2211	6	None	Receptor activation enhances glycine transport in the synaptic cleft, and promotes cell survival through a PI3K/Akt-dependent mechanism
	2-MeSADP	7.7	$P2Y_{1,12}$				
$P2Y_{14}$	UDP	6.8	$P2Y_6$				Receptor activation can modulate inflammatory responses through chemokine and cytokine production, and may play a role in muscle contraction
	UDP-glucose	6.4	$P2Y_2$	MRS4478	6.5	None	
	MRS2690	7.3	None				

Table adapted from Weisman et al., (2012); Jacobson et al., (2020).

2.3.3   P2Y receptor regulation

As discussed in **section 1.3**, β-arrestins play an important role in internalisation and desensitization of GPCRs. The interaction between $P2Y_{1,2,4,6,11,12}$ receptors and β-arrestin was studied in transfected HEK-293 cells using FRET analysis to measure β-arrestin translocation to the plasma membrane in response to receptor activation (Hoffmann et al., 2008). All six of these P2Y receptor subtypes interacted to some degree with β-arrestin 2, while the $P2Y_2$ and $P2Y_4$ receptors interacted with both β-arrestin 1 and β-arrestin 2. It has also been reported that the $P2Y_2$ receptor couples differently to β-arrestins depending on whether ATP or UTP is used as an agonist. Activation by ATP leads to a strong interaction with β-arrestin 1 and a weak interaction with β-arrestin 2, while activation by UTP causes a strong interaction with both β-arrestin 1 and β-arrestin 2 (Velazquez et al., 2000).

A differential effect on the duration of ERK1/2 activation initiated by different $P2Y_2$ receptor agonists has also been seen, as ATP caused sustained ERK1/2 activation, whereas the activation induced by UTP was transient (Hoffmann et al., 2008). Many studies indicate that the duration of ERK1/2 activation is essential for determining cell fate, which suggests that the $P2Y_2$ receptor may regulate different cell fates, depending on the agonist present (Ebisuya et al., 2005). Hardy et al. (2005) showed that suppression of GRK2 and GRK6 with siRNA cause desensitization of the $P2Y_{12}$ receptor, whereas desensitization of $P2Y_1$ receptor was mainly dependent on PKC. A study conducted in retinal glial cells found that native P2Y receptors, of undefined subtype, were desensitized by ATP and re-sensitized by growth factors, such as EGF, PDGF and NGF, through activation of PI3K and protein phosphatases, but not PKC, Src kinases, or ERK1/2 (Weick et al., 2005).

2.3.4   P2Y receptor homo- and heterodimers

Most P2Y receptor subtypes have been shown to form homodimers and/or heterodimers with other P2Y subtypes and even non-P2Y receptors. Choi et al., (2008) reported that $hP2Y_1$ receptors form homodimers after expressing them at high levels in the HEK-293 cell line and this was confirmed when the receptor was crystallized (Zhang et al., 2015). Interestingly, Choi et al., (2008) also found that the number of

dimers detected decreased with agonist stimulation. Both $P2Y_1$ and $P2Y_2$ receptors heterodimerise with adenosine A_1 receptors (Yoshioka et al., 2001; Suzuki et al., 2006). The dimerisation of A_1 and $P2Y_1$ receptors increased the binding affinity of $P2Y_1$ ligands, but decreased that of A_1 ligands, and changed the pharmacological profile of activation of of G_i and G_q (Yoshioka et al., 2001). In contrast, dimerisation of A_1 and $P2Y_2$ receptors had no effect on ligand binding for both type of receptors, but did change the pharmacological profile of coupling to G_q and G_i (Suzuki et al., 2006).

D'Amrosi et al., (2006) reported the homodimerisation of $P2Y_4$ receptors by using co-immunoprecipitation of transfected SH-SY5Y cells with Myc-P2Y4 receptors. Subsequently, the same group found that the $P2Y_4$ receptor exists mostly as homodimers and homo-oligomers (D'Amrosi et al., 2007). The same study indicated that $P2Y_6$ receptors can also form homodimers, as well as heterodimers with $P2Y_4$ receptors in transfected and native cells. After agonist stimulation, $P2Y_6$ receptors formed homodimers only. Savi et al., (2006) reported that $P2Y_{12}$ receptors exist as homo-oligomers, which was confirmed when the receptor was crystallized (Zhang et al., 2014a,b) and proposed that the active metabolite of clopidogrel, which is $P2Y_{12}$ receptor antagonist, interferes with this homodimerisation, reducing it to the monomer form (Savi et al., 2006). Interestingly, the $P2Y_{12}$ receptor can also form a heterodimer with the PAR4 receptor (Khan et al., 2014; Smith et al., 2017).

$P2Y_{11}$ receptors do not undergo agonist-induced internalisation, but when coexpressed with $P2Y_1$ receptors they form heterodimers, which do internalise when activated by ATP (Ecke et al., 2008). This was inhibited by the $P2Y_1$ antagonist, MRS2179, but not by the $P2Y_{11}$ antagonist, NF157. The Kennedy group at Strathclyde University suggested that $P2Y_1$ also forms heterodimers with $P2Y_{12}$ receptors to modulate the activity of two-pore potassium channels (K_{2P}) in tSA201 cells (Shrestha et al., 2010). This is the initial basis for the experiments that will be reported in this thesis.

3   Chronic Pain

3.1   Introduction

Pain can be classified in a number of ways, but a basic, initial subdivision is into two main categories, acute and chronic. Acute pain is generally a rapid response that alerts the body to an ongoing noxious stimulus, with the aim of inducing an immediate response to minimize physical harm. It is mediated by nociceptors and usually described as nociceptive or inflammatory pain (St John Smith, 2018). On the other hand, chronic pain is a severe pain that last over a period of at least several months, beyond the expected time of wound healing. It serves no biologic purpose, but is instead a disease state itself. Again, it can be classified in a number of ways, but a common subdivision is inflammatory and neuropathic pain (Voscopoulos and Lema, 2010; St John Smith, 2018).

3.2   Chronic Inflammatory Pain

Inflammatory pain is caused by activation and sensitization of the nociceptive pathway by a variety of pro-inflammatory mediators released at the site of tissue inflammation (Scholz and Woolf, 2002; Treede et al., 2015). Tissue damage leads to the release of "inflammatory soup" which contains signalling molecules like serotonin, histamine, glutamate, calcitonin-gene related peptide (CGRP), bradykinin, eicosinoids prostaglandins, tumor necrosis factor α (TNF-α), interleukin 1β (IL-1β), ATP, adenosine, substance P, thromboxanes, leukotrienes, endocannabinoids, nerve growth factor (NGF), extracellular proteases, and protons (Basbaum et al., 2009). This leads to sensitisation of peripheral and central components of the nociceptive signalling pathway via one or more of cell surface receptors, ion channels and transcription factors (Hucho and Levine, 2007; Basbaum et al., 2009; Latremoliere and Woolf, 2009; Deval et al., 2010; Schaible et al., 2010; Ji et al., 2014).

The animal model most commonly used to study inflammatory pain is the complete Freund's adjuvant (CFA) model, in which a solution of inactivated mycobacteria is injected subcutaneously into the dorsal plantar surface of the hind paw in rodents. This causes immune cell recruitment and an inflammatory response, with associated edema and sensitization of the paw to mechanical and thermal stimulii (Billiau and Matthys, 2001; Gauldie et al., 2004; Lin et al., 2007; Barrot, 2012; Li et al.,

2013). CFA is used to model chronic inflammatory pain conditions because a single dose generates hypersensitivity that peaks at three days post-injection and lasts as long as two weeks (Ren and Dubner, 1999).

3.3　Chronic Neuropathic Pain

Neuropathic pain can arise from damage to the neurons in the peripheral and central nervous systems from a primary lesion or disease in the somatosensory nervous system and includes peripheral neuropathies, such as those due to diabetic complications, compression neuropathies, phantom limb pain, central pain, for example pain that develops after a stroke or spinal cord injury and postherpetic neuralgia, which isperipheral nerve damage following acute herpes zoster infection (shingles) (Scholz and Woolf, 2002; Treede et al., 2015; British National Formulary, 2020). Neuronal damage leads to one or more of the following changes; peripheral and central sensitization, ectopic activity and impaired inhibitory modulation, which leads to characteristic symptoms of tingling (also described as pins and needles or prickling), burning and shooting pains in the affected area (Xu et al., 2016).

Several animal models of neuropathic pain have been developed that involve damaging the sciatic nerve, which carries efferent and afferent neurons to the hind paw, or its associated spinal nerves. The first was the chronic constriction injury (CCI) model in which a ligature is tied loosely around the sciatic nerve (Bennett and Xie, 1988). This was modified in the partial nerve ligation model, such that about 50% of the sciatic nerve is tightly ligated (Seltzer et al., 1990). In both models, some sciatic neurones are damaged, but the remainder are left intact, which maintains signalling to and from the hind paw. An alternative adaptation is to ligate the tibial and peroneal branches of the sciatic nerve, but to leave the sural branch intact (Decosterd and Woolf, 2000). A major advantage of this model is that it allows for neighboring injured and uninjured nociceptive neurones to be studied. Finally, Kim and Chung, (1992) introduced tight ligation of the 5th and 6th lumbar spinal nerves of the sciatic nerve, close to the dorsal root ganglion (DRG), but leaving its L4 spinal nerve intact. Again, allows for neighboring injured and uninjured nociceptive neurones to be studied.

3.4   Management of Chronic Pain

According to the British Pain Society (2016), it is estimated that 43% of the population experience chronic pain at some point, which produces a substantial reduction in the overall quality of life, via negative impacts on their physical and psychological well-being. It is a serious public health issue, due to the economic burden and the pressure placed on the healthcare system. In general, acute pain can be managed successfully through the use of paracetamol, non-steroidal anti-inflammatory drugs (NSAIDs) and opioids (Yawn et al., 2014), but the management of chronic pain tends to be more difficult. Inflammatory pain may respond to paracetamol and NSAIDs, but can require administration of opioids, which is associated with the issues, such as tolerance and the risk of developing dependence on long-term use (Chou et al., 2009; Painter and Crofford, 2013; Wilson and Nelson, 2015). Neuropathic pain can be reduced in some people by off-label treatments, including the tricyclic antidepressants, desipramine, amitriptyline and imipramine and the anti-epileptic drugs pregabalin and gabapentin, but the efficacy can be variable (British National Formulary, 2020). Opioids can be more effective, but as noted above, have issues of their own. Thus, even with vigorous management, chronic inflammatory and neuropathic pain can persist such that further treatment is required.

It is clear that effective treatment of chronic pain requires the development of more potent and selective analgesics, with fewer side-effects. In the last 10-15 years a number of novel potential therapeutic targets have been identified and studied, including capsaicin-sensitive $TRPV_1$ receptors, voltage-dependent Na^+ and Ca^{2+} channels, CB1 and CB2 cannabinoid receptors, P2X3, P2X4 and P2X7 receptors and, as will be discussed in more detail below, P2Y receptors (Yekkirala et al., 2017).

3.5   P2Y receptors in pain

P2Y receptors are potential therapeutic targets for treating chronic pain, as all P2Y subtypes, apart from the $P2Y_{11}$ receptor, are expressed in sensory neurons and many are also expressed in satellite and microglial cells that have implicated in the development and maintenance of chronic pain (Burnstock, 2013; Magni and Ceruti, 2019). Furthermore, endogenous nucleotides, but particularly ATP, are released from damaged cells and during inflammation and ATP can be dephosphorylated by ecto-

nucleoside triphosphate diphosphohydrolases (NTPDases) to produce ADP (Robson et al., 2006; Zimmermann et al., 2012). Consequently, the role of P2Y receptors in mediating pain has been studied in a variety of animal models.

P2Y$_1$ receptors appear to play a role in the perception of noxious heat through an interaction with the TRPV$_1$ receptors (Kwon et al., 2014). In this study, the thermal pain threshold was raised after stimulation of P2Y$_1$ receptors with low doses of the selective P2Y$_1$ agonist, MRS2365, though there was no effect at higher doses (Malin and Molliver, 2010). In addition, induction of peripheral inflammatory sensitization by CFA was inhibited after P2Y$_1$ inhibition or knockout (Malin and Molliver, 2010). P2Y$_1$ receptors are similarly pro-nociceptive in formalin-induced inflammatory pain, as MRS2365 produced a noxious response, which was prevented by the P2Y$_1$ receptor antagonist, MRS2500, indicating a pronociceptive role for P2Y$_1$ receptors (Barragán-Iglesias et al., 2015).

It was reported that chronic inflammatory pain induced by CFA was associated with upregulation of P2Y$_2$ receptor mRNA expression in mouse DRG (Zhu et al., 2015). In the hot plate test, activation of P2Y$_2$ and/or P2Y$_4$ receptors by UTP increased the pain threshold (Andó et al., 2010). Moreover, it appears that P2Y$_2$ receptors also interact with TRPV$_1$ receptors their activation potentiated the noxious response to TRPV$_1$ stimulation (Moriyama et al., 2003).

Due to the lack of selective ligands for P2Y$_4$ and P2Y$_6$ receptors, the roles of these receptors in pain are not clear. The administration of UTP or UDP is linked with a rise in pain threshold during the hotplate test (Andó et al., 2010), and both P2Y$_4$ and P2Y$_6$ activation decreases the transmission of pain signals at the spinal cord level (Okada et al., 2002). Barragán-Iglesias et al., (2015) proposed that peripheral P2Y$_6$ receptors are upregulated by formalin administration and contribute to the associated pain. Before formalin injection, P2Y$_6$ receptor activation by UDP and PSB0474 (endogenous and synthetic P2Y$_6$ receptor agonists, respectively), increased pain, which was evaluated by flinching behaviour. Furthermore, this was inhibited by MRS2578, selective P2Y$_6$ receptor antagonist. Thus, the authors suggested that antagonising P2Y$_6$ receptors might be a good strategy to treat peripheral inflammatory pain.

In neuropathic pain, P2Y receptors also appear to be potential drug targets, as the selective agonist for $P2Y_1$ receptors, MRS2365, reversed mechanical allodynia associated with surgery. Furthermore, the $P2Y_2$ and $P2Y_4$ agonist, UTP, has an anti-nociceptive action, although this effect was minor (Andó et al., 2010). In numerous studies, $P2Y_{12}$ selective antagonists produce anti-allodynic effects and decrease neuropathic pain development (Tozaki-Saitoh et al., 2008; Andó et al., 2010; Horváth et al., 2014). In rodent models (rats and mice), there is a correlation between the time-dependence of central and peripheral $P2Y_{12}$ mRNA expression and central sensitisation development for both neuropathic and inflammatory pain, which can be prevented by $P2Y_{12}$ selective receptor antagonists, such as clopidogrel and cangrelor, or receptor knockout (Tozaki-Saitoh et al., 2008; Horváth et al., 2014).

Malin and Molliver (2010) suggested that $P2Y_{12}$, $P2Y_{13}$ and $P2Y_{14}$ receptors have an inhibitory effect on inflammatory and nociceptive pain signalling and that when $P2Y_1$ receptors are blocked or knocked out, inflammatory hyperalgesia is reduced. So, the integration of these opposing signals can adjust nociceptor sensitivity (**Figure 1.13**). On the contrary, the expression levels of $P2Y_{12}$ are upregulated in hyperalgesic states (Horváth et al., 2014). Also, in rodent models, $P2Y_{12}$-selective antagonists are anti-nociceptive in many types of pain like neuropathic, acute and inflammatory pain, with $P2Y_{12}$ receptor knockout mice showing a similar decrease in the response to noxious stimulii (Andó et al., 2010; Horváth et al., 2014).
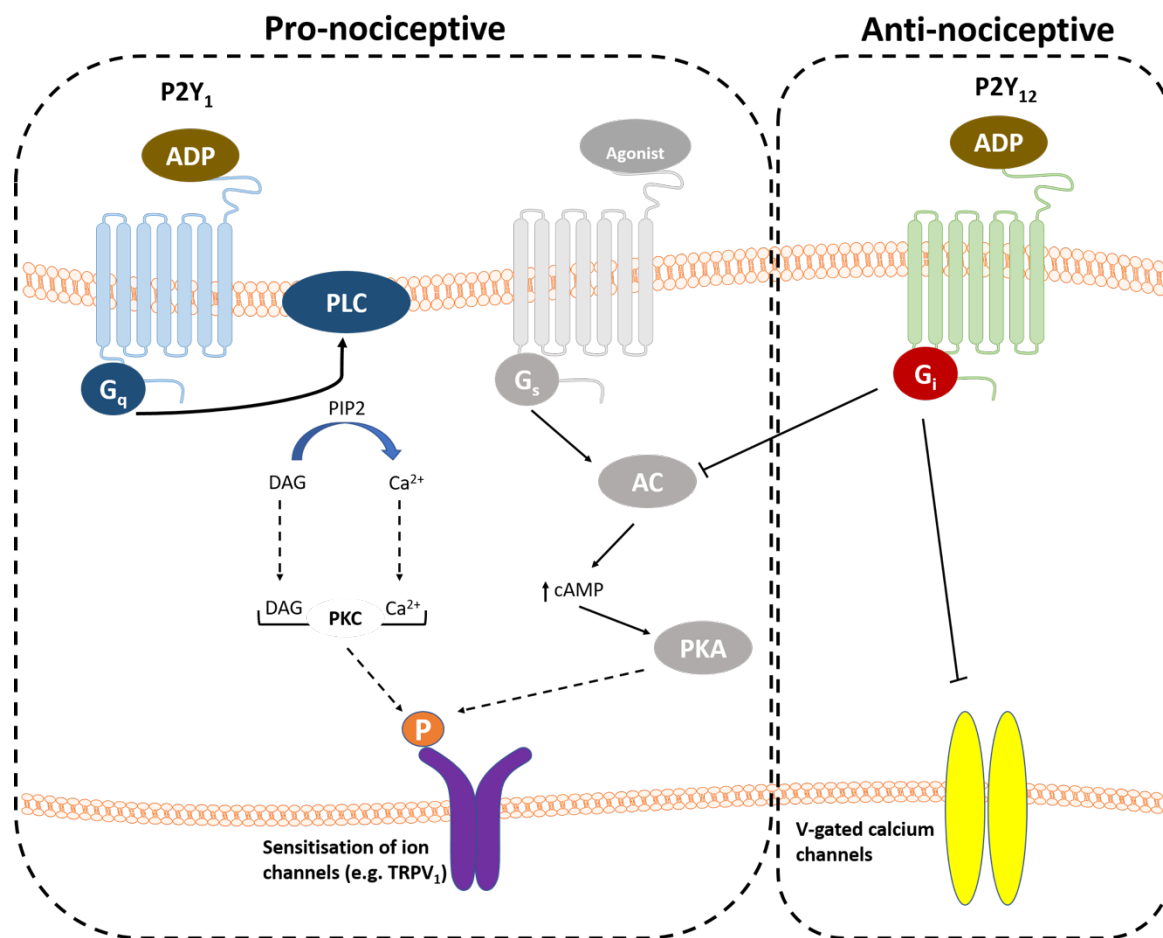
Figure 1.13: Purinergic P2Y$_1$ and P2Y$_{12}$ receptor signaling.

Activation of the pro-nociceptive P2Y$_1$ G$_q$-coupled receptor and the G$_{i/o}$-coupled anti-nociceptive P2Y$_{12}$ receptor with ADP. Protein kinase C (PKC), which is a key downstream effector for P2Y$_1$ receptors signaling is that modulates proteins by phosphorylation. P2Y$_{12}$ receptor stop cAMP production which block activation of protein kinase A (PKA), the downstream effector for G$_s$-coupled signaling. Similar to PKC, PKA has been showed to alter key proteins involved in inflammation by phosphorylation.

4 Aims

Although we have some knowledge and understanding of individual characteristics of $P2Y_1$ and $P2Y_{12}$ receptors, including signalling mechanisms and membrane trafficking, however, the communication and interaction between these two subtypes are somewhat unknown. Thus, the driving motive behind this study was to provide a better understanding of the properties of the coexpressed receptors, as these can often differ from those of individual receptor subtypes and offers novel avenues for the development of new therapeutic agents. Indeed, it has already been proposed that $P2Y_1$ and $P2Y_{12}$ receptors interact and modulate the activity of K_{2P} channels and that this could lead to the discovery of a new drug target in the chronic pain field (Shrestha et al., 2010).

Specifically, the aims of this study were to:

- Characterise the cellular expression and localisation of coexpressed recombinant $P2Y_1$ and $P2Y_{12}$ receptors using a variety of techniques, and determine the effects of ADP on expression and internalisation.
- Determine if there is a physical interaction between coexpressed $P2Y_1$ and $P2Y_{12}$ receptors, and whether this is modified by $P2Y_1$ and $P2Y_{12}$ agonists and antagonists.
- Determine if native $P2Y_1$ and $P2Y_{12}$ receptors dimerise and how this might be modified by $P2Y_1$ and $P2Y_{12}$ agonists and antagonists.

Chapter Two

Materials and Method

1   Materials

1.1   General reagents

All reagents used were of the highest commercial grade possible and solutions were prepared in deionized water, unless otherwise stated.

Sigma-Aldrich Co Ltd (Poole, Dorset, UK)

Bovine Serum Albumin (BSA)

Phosphate buffered saline (PBS) tablets

Poly-L-lysine solution, 0.1 % (w/v) in H_2O

cOmplete™ Protease Inhibitor Cocktail

Triton x100

Thermo Fisher Scientific UK Ltd (Leicestershire, UK)

Pierce™ BCA Protein Assay Kit

1.2   Tagged plasmid DNA constructs

The cDNAs encoding HA-hP2Y$_1$ and HA-hP2Y$_{12}$ receptors were a gift from Professors T.K. Harden and R.A. Nicholas, (University of North Carolina, Chapel Hill, NC, USA). To generate fluorescent tagged constructs, the HA tag was removed from the N-terminal and the receptors then cloned into pEYFP and pECFP at the C-terminal (BD Biosciences Clontech) to generate P2Y$_1$-eYFP and P2Y$_{12}$-eCFP. These procedures were carried out by Dr. Roth Tate (University of Strathclyde, Glasgow, UK).

1.3   Reagents for molecular biology and cellular transfection

Integrated DNA Technologies (Leuven, Belgium)

All primers, RNA free water

Polysciences Inc., (Warrington, UK)

Polyethylenimine (PEI), (Linear MW~25,000, 23966)

QIAGEN (West Sussex, UK)

Qiagen Endofree Plasmid maxi kit

Sigma-Aldrich Co Ltd (Poole, Dorset, UK)

Amplification Grade DNAse I kit

RNA isolation kit

Thermo Fisher Scientific UK Ltd (Leicestershire, UK)

Applied Biosystems SYBR Green Master Mix

Applied Biosystems High Capacity Reverse Transcription Kit

1.4   Tissue culture consumables

BioSera Ltd (Heathfield, East Sussex, UK)

Fetal Bovine Serum (FBS)

Corning B.V (Buckinghamshire, UK)

All tissue culture flasks, 10cm dishes, (6, 12 and 24) well plates, graduated pipettes and falcon tubes

Sigma-Aldrich Co Ltd (Poole, Dorset, UK)

Dimethyl sulfoxide (DMSO) and ethanol.

Thermo Fisher Scientific UK Ltd (Leicestershire, UK)

GibcoTM Penicillin-Streptomycin

GibcoTM Dulbecco's Modified Eagle Medium (DMEM)

GibcoTM TrypLE™ Express Enzyme (1X)

Pre-stained SDS-PAGE Molecular Weight Marker

1.5   Reagents for immunoprecipitation

Merck (Darmstadt, Germany)

Calbiochem Protein G Plus/Protein A Agarose Suspension

Sigma-Aldrich Co Ltd (Poole, Dorset, UK)

Monoclonal Anti-HA−Agarose antibody produced in mouse

1.6   Reagents for Western blotting

Bio-Rad Laboratories (Hertfordshire, UK)

Bio-Rad Mini PROTEAN IIITM electrophoresis system

GE Healthcare Ltd (Buckinghamshire, UK)

AmershamTM Hybond™ -ECL nitrocellulose membrane

Santa Cruz Biotechnology, Inc (Heidelberg, Germany)

UltraCruz® Autoradiography Film

Sigma-Aldrich Co Ltd (Poole, Dorset, UK)

Acrylamide, Ammonium Persulfate (APS), Glycerol, Glycine, methanol, Sodium
Chloride, N,N,N',N'-tetramethylenediamine (TEMED), TWEEN-20, p-coumeric acid,
Luminol, Trizma Base and Dithiothreitol (DTT), 2-Mercaptoethanol

Thermo Fisher Scientific UK Ltd (Leicestershire, UK)

Sodium dodecyl sulphate (SDS)
NuPAGE LDS sample buffer (4x)

Whatmann (Kent, UK)

17 CHR Chromatography Paper

1.7   Reagents for surface expression

Bio-Rad Laboratories (Hertfordshire, UK)

Alkaline phosphate kit

Thermo Fisher Scientific UK Ltd (Leicestershire, UK)

Pierce cell surface protein isolation kit

1.8   Microscopy

Becker & Hickl GmbH, Berlin, Germany

Time-Correlated Single Photon Counting (TCSPC) module (SPC-830)

Carl Zeiss Ltd (Cambridge, UK)

LSM510 microscope

Coherent UK Ltd, Newnham, UK

Femtosecond Ti:Sapphire two-photon laser (Chameleon, Coherent)

Leica Microsystems (Milton Keynes, UK)

Leica Confocal SP8 microscope

Merck (Darmstadt, Germany)

Mowiol

VWR International Ltd (Leicestershire, UK)

No. 0, (0.09-0.13 mm thick), circular glass 13 or 22 mm diameter coverslips. 0.8-1.0mm thick glass microscopy slides

Thermo Fisher Scientific UK Ltd (Leicestershire, UK)

4',6-diamidino-2-phenylindole (DAPI)

Rhodamine phalloidin

Sigma-Aldrich Co Ltd (Poole, Dorset, UK)

Duolink™ In Situ Detection Reagents Orange

1.9   Antibodies

Abcam plc. (Cambridge, UK)

Anti-GAPDH (ab8245)

Membrane Fraction WB Cocktail (ab140365)

Alomone Labs Ltd (Jerusalem, Israel)

Anti-P2Y$_{12}$ Receptor Antibody (APR-012)

BioLegend (San Diego, CA, USA)

Anti-HA.11 Epitope Tag Antibody (Previously Covance catalog# MMS-101R)

Chromotek (Planegg, Germany)

GFP antibody (3H9)

Invitrogen Ltd (Paisley, UK)

Alexa Fluor 555 goat anti-rabbit IgG (A21428)

Alexa Fluor 488 goat anti-rabbit IgG (A11008)

Alexa Fluor 555 goat anti-mouse IgG (A21422)

Alexa Fluor 488 goat anti-mouse IgG (A11001)

Jackson ImmunoResearch Laboratories Inc. (PA, USA)

Donkey Anti-Mouse IgG (H+L) (AB_2340770)

Goat Anti-Rabbit IgG (H+L) (AB_2307391)

Texas Red® dye-conjugated AffiniPure donkey anti-mouse IgG (715-075-150)

Laboratory Chemicals Alpha Laboratories Ltd (Hampshire, UK)

Microglia Marker - Iba1 Antibody (019-19741)

R&D systems (Wiesbaden, Germany)

Goat Anti-Rat IgG HRP-conjugated Antibody (HAF005)

Santa Cruz Biotechnology, Inc (Heidelberg, Germany)

P2Y$_1$ Antibody (E-1) (sc-377324)

Sigma-Aldrich Co Ltd (Poole, Dorset, UK)

Anti-α-Tubulin (T5168)

Alkaline Phosphatase goat Anti-Mouse IgG (whole molecule) antibody (A9316)

1.10 Ligands

Abcam plc. (Cambridge, UK)

MRS2179, $P2Y_1$ antagonist (ab120414)

Sigma-Aldrich Co Ltd (Poole, Dorset, UK)

Adenosine 5′-diphosphate (ADP)

Tocris Bioscience (Abingdon, UK)

MRS2365, $P2Y_1$ agonist

BPTU, $P2Y_1$ allosteric antagonist

AR-C69931 tetrasodium salt, highly potent $P2Y_{12}$ antagonist

1.11 Calcium Imaging

Abcam plc. (Cambridge, UK)

Cal-520, AM (ab171868)

Molecular Devices (UK) Ltd

FlexStation 3 Multi-Mode Microplate Reader, Wokingham,UK

PerkinElmer (UK) Ltd, Beaconfield, UK

LS-50B luminance/spectrophotometer

Sigma-Aldrich Co Ltd (Poole, Dorset, UK)

Corning™ 96 Well Black Polystyrene Microplate

2   Methods

2.1   Plasmid propagation

2.1.1   Transform the plasmid into NEB 10-beta competent E. coli

Competent cells were thawed on ice and 50 μL transferred into a transformation tube with 3 μL of plasmid DNA (HA-hP2Y$_1$, HA-hP2Y$_{12}$, hP2Y$_1$-eYFP and hP2Y$_{12}$-eCFP receptors). The mixture was incubated on ice for 30 minutes, heated-shocked at 42 °C for 30 seconds, then returned immediately to ice for 5 minutes. 950 μL of room temperature super optimal broth with Catabolite repression (S.O.C) medium was added to the mixture, which was then incubated at 37°C on a shaker for 60 minutes. 50 μL of each dilution was spread onto the pre-warmed selection 10 cm plates containing sterile Luria Broth (LB) Agar mix (1% (w/v) Tryptone, 0.5% (w/v) yeast Extract, 1% (w/v) NaCl, 1.5% (w/v) Agar containing 100μg/mL ampicillin or 50 μg/mL of kanamycin. The competent cells incubated with hP2Y$_1$-eYFP or hP2Y$_{12}$-eCFP plasmid were spread onto kanamycin agar plates, while the competent cells incubated with HA-hP2Y$_1$ or HA-hP2Y$_{12}$ plasmid were spread onto ampicillin agar plates. The plates were inverted and incubated overnight at 37°C to allow for colony formation.

2.1.2   Maxi preparation of plasmid DNA from E. coli

To produce larger amounts of purified, transfection grade plasmid-DNA, large-scale plasmid preparation was set up using the QIAGEN Hi-Speed Plasmid Maxi Kit. Firstly, a single colony was aseptically picked and used to inoculate 5mL of sterile LB broth (1% (w/v) tryptone, 0.5% (w/v) yeast extract, 1% (w/v) NaCl) in a 30mL universal tube containing ampicillin or kanamycin (as described above). The culture was then incubated at 37°C whilst shaking at 200 rpm for 9 hours. Once the culture became turbid, it was transferred to a sterile 1L conical flask containing 250mL of antibiotic supplemented LB broth. The culture was incubated by shaking for 16 hours at 37°C before being harvested by centrifugation at 6000 x g for 15 minutes at 4°C. Pelleted cells were resuspended in 10 mL of Buffer P1 before the addition of 10 mL of Buffer P2. Cells were mixed gently by inverting and incubated at room temperature for 5min. To the lysed cells, 10 mL of chilled Buffer P3 was added, and the mixture was allowed to separate into two distinct layers. The lysate was poured into the barrel of the

QIAfilter Cartridge and incubated at room temperature for 10 minutes. An additional 5 minutes was required to allow for HA-hP2Y$_1$ preparations to clarify. During this incubation step 10mL QBT Buffer was added to a QIAgen HiSpeed tip and allowed to equilibrate with the tip by gravity flow. The clarified filtrate in the QIAfilter Cartridge was added to the QIAgen HiSpeed tip and allowed to pass through the column by gravity flow. The tip was washed with 60 mL of Buffer QC, and DNA eluted following addition of 15 mL of Buffer QF to the column. The DNA in the flow through was collected into a sterile tube and precipitated with the addition of 10.5 mL of isopropanol followed by incubation at room temperature for 5 minutes after mixing. The DNA/isopropanol mix was filtered through a QIAprecipitator and then washed with 2 mL of 70% ethanol (EtOH). DNA was eluted from the QIAprecipitator following the addition of 0.5 mL Elution Buffer (Buffer TE) to the precipitator with a syringe. The concentration and purity of the DNA in the flow through was determined by Nanodrop 2000c spectrophotometer (Thermo Fisher Scientific).

2.2 Cell lines

2.2.1 tSA201 cells

tSA201 is a transformed human kidney (European Collection of Authenticated Cell Cultures [ECACC] 96121229) cell line that is derived from HEK293 cells. They stably express a simian virus 40 (SV40) temperature-sensitive T antigen. The cell line has been used in a variety of functional expression assays and has been reported to produce high levels of recombinant proteins (Thomas and Smart, 2005). Transfection efficiency in these cells decreases with increased passage number, therefore frozen cell stocks were prepared as a reserve for the duration of the project.

2.2.2 BV-2 cells

BV-2 cells (a murine microglial cell) were generated by immortalizing primary mouse microglia and were a kind gift from Dr Hui-Rong Jiang, University of Strathclyde. These cells possess functional and phenotypic properties common to primary microglia, including phagocytic ability, secretion of pro-inflammatory cytokines and expression of surface receptors and antigens. They have been used extensively

as an *in vitro* model to study microglial function, immune responses, and the role of microglia in neurodegenerative diseases (Timmerman et al., 2018).

2.2.3 HMC3 cells

The human microglial clone 3 cell line (HMC3) was established in 1995, through SV40-dependent immortalization of human embryonic microglial cells. It has been recently authenticated by the American Type Culture Collection (ATCC®) and distributed under the name of HMC3 (ATCC®CRL-3304). The HMC3 cells have been used in many research studies, two of which also indicated by ATCC® as reference articles. However, a more accurate literature revision suggests that clone 3 was initially distributed under the name of CHME3 (Dello Russo et al., 2018).

2.3 Cell Culture

All cell culture was carried out in a Class II laminar flow hood under aseptic conditions.

2.3.1 Recovery of cryopreserved cells

Cells were stored in liquid nitrogen in 1 mL of freezing mix (FCS + 10% DMSO) in cryogenic vials (E3110-6112, StarLab). Cells were defrosted and transferred to a centrifuge tube and recovered in Dulbecco's Modified Eagles medium (DMEM) supplemented with 100U/mL penicillin, 100 **μ**g/mL streptomycin and 10% (v/v) FBS prior to centrifugation at 1000 rpm for 5 minutes at room temperature. The supernatant was removed and fresh modified DMEM was added to the cell pellet. The cells were dispersed by gentle mixing by pipette and transferred to a new T75 flask and incubated at 37°C in a 5% CO_2 humidified atmosphere in modified DMEM until full recovery. Media was replaced with fresh modified DMEM 24 hours after recovery from liquid nitrogen to ensure that residual DMSO was removed.

2.3.2   Cell passaging

Cells were grown in Corning T25 or T75 flasks to 70 - 90% confluence prior to passage for experimentation. For cell dissociation, cells were washed twice with serum-free DMEM before being incubated at 37°C with versene solution (0.48 mM EDTA in phosphate buffered saline (PBS)) for tSA201 cells or TrypLE for microglial cells. Detached cells were collected in modified DMEM and centrifuged at 1000 rpm for 5 minutes at room temperature. The cell pellet was resuspended in fresh DMEM, and either added to a fresh flask for continuous growth or seeded for further experimentation. Cells were maintained in a 5% CO_2 humidified atmosphere at 37°C until used.

2.3.3   Coverslip preparation

13 mm coverslips (Thermo Scientific) were autoclaved and placed in 12 or 24 well plates. 0.01% poly-L-lysine (PLL) solution (Sigma-Aldrich) was added to each coverslip and left in the tissue culture hood for 30 minutes for effective coating. The coverslips were then washed in PBS to remove excess PLL solution and left to dry in the tissue culture hood before refrigeration or use.

2.4   Cell Transfection

2.4.1   Transient transfection using polyethylenimine (PEI)

Cells were transfected with the following plasmids; HA-hP2Y$_1$, HA-hP2Y$_{12}$, hP2Y$_1$-eYFP, hP2Y$_{12}$-eCFP, yellow fluorescent protein (YFP) and cyan fluorescent protein (CFP) using PEI (linear, MW-2500 from Polysciences Inc). **Table 2.1** presents the DNA/PEI transfection conditions used for different tissue culture formats. Briefly, cells in modified DMEM were seeded into a culture dish and transfected once 50% - 60% confluence was reached. Transfection grade plasmid DNA and PEI (1mg/mL stock) were incubated at room temperature separately in modified DMEM for 5 minutes and then the tube contents were combined and incubated at room temperature for 20 minutes. The PEI-DNA complex was then added dropwise to the

cells and placed back into the incubator with 5% CO_2 humidified atmosphere at 37°C for 24 hours. Media was replaced and cells were left to recover for a further 24 hours prior to experimentation.

Table 2.1: DNA amount, PEI amount and transfection conditions used in this project.

Tissue Culture Dish format	DNA Quantity (μg) in 250 μL DMEM		PEI (μL) in 250 μL DMEM	
	Solo transfection	Cotransfection	Solo transfection	Cotransfection
60mm dish	2.0	2 each plasmid	11.4	22.8
6 well plate	2.0	2 each plasmid	11.4	22.8
12 well plate	1.0	1 each plasmid	5.7	11.4
24 well plate	0.5	0.5 each plasmid	2.85	5.7

2.5   Ca^{2+} Flux Imaging

2.5.1   Cal-520 AM Fluorescent Dye Preparation

Cal-520 AM fluorescent dye (Abcam) was diluted from a frozen stock (1 mM in DMSO) to 5 μM in 1.5 mL HEPES-Krebs buffer (122mM NaCl, 5 mM KCl, 10 mM HEPES, 0.5 mM KH_2PO_4, 0.5 mM NaH_2PO_4, 1 mM $MgCl_2$, 11 mM glucose, 1.8 mM $CaCl_2$, pH 7.3) containing 0.05% F-127 Pluronic acid (Thermo Fisher Scientific).

2.5.2   Ca^{2+} flux Imaging of Transfected Tagged Receptor Constructs with the Perkin-Elmer LS-50 Luminance-spectrophotometer

Cells were grown on PLL coated coverslips prior to incubation with Cal-520 dye (above) for 1 hour at 37°C. The coverslips containing Cal-520 loaded cells were washed twice with HEPES-Krebs buffer and placed in a plastic cuvette, which in turn was placed in the recording chamber of a LS-50 Luminance-spectrophotometer (Perkin-Elmer). The cells were continuously superfused with HEPES buffer at 4 mL per minute gravity flow. Fluorescence was recorded at a 10Hz sampling frequency

with 490±10 nM excitation and 525±10 nM emission using Perkin-Elmer FL Winlab V4.00.02 software.

2.5.2.1 Confirmation of functional expression of tagged $P2Y_1$ and $P2Y_{12}$ receptors

The aim of the initial experiments was to determine if the tagged $P2Y_1$ and $P2Y_{12}$ receptor plasmids were functionally expressed when transfected in tSA201 cells. First, the ability of the $P2Y_1$ agonist, ADP, to evoke a rise in intracellular Ca^{2+} levels in cells transfected with tagged $P2Y_1$ receptors was studied. After recording the baseline signal for 30 seconds, 10 µM ADP (Sigma-Aldrich) was applied in the superfusate for 1 minute, twice at 15 minute intervals to confirm the integrity of the cells. ADP log concentration-response curves (10nM - 10µM) were then constructed. The lower concentrations were added to the cells for 2 minutes at 10 minute intervals, while the higher concentrations, 1 µM ADP and above, were added for 1 minute at 15 minute intervals. Previous studies in the Kennedy lab found that ADP elicited reproducible responses when applied using this protocol (Kennedy, unpublished data). The peak amplitude in the rise of fluorescence evoked at each concentration of ADP was measured and normalized as a percentage of the response to the final 10 µM ADP addition. The Hill equation was then fitted to the data in GraphPad Prism 6 and $logEC_{50}$, Hill slope and E_{max} calculated.

Functional expression of tagged $P2Y_{12}$ receptor plasmids was investigated using the selective $hP2Y_{12}$ receptor antagonist, AR-C69931MX (Cangrelor), as previous studies in the lab showed that it inhibits the rise in Ca^{2+} evoked by ADP in tSA201 cells only when $P2Y_{12}$ receptors are expressed (Kennedy, unpublished data). First, 10 µM ADP was applied in the superfusate for 1 minute, twice at 15 minute intervals to confirm the integrity of the cells. 300nM ADP was then applied 3 times at 10 minute intervals to ensure that the responses were reproducible, Cells were then incubated with AR-C69931MX (1 µM) for 5 minutes, prior to addition of 300 nM ADP plus 1 µM AR-C69931MX. Cells were then superfused with drug-free buffer for 10 minutes and ADP (300 nM) then reapplied to determine if the effects of AR-C69931MX were reversible on washout. The peak amplitude in the rise of fluorescence evoked at each concentration of ADP was measured and normalized as a percentage of the response to 10 µM ADP.

2.5.3 Ca^{2+} Flux Imaging with the Molecular Devices FlexStation 3 Platereader

BV-2 or HMC3 cells were seeded into clear bottomed, black walled 96 well polystyrene microplate (Corning, Sigma Aldridge) at a low density and left to grow until confluent. First, cells were incubated with Cal-520 dye for 2 hours, as previously described. Residual extracellular dye was then removed by washing with HEPES-Krebbs buffer, 80 µL of HEPES-Krebs was added to each well and the plate was loaded into the reading chamber of a Molecular Devices FlexStation 3 Multi-Mode Microplate Reader. The assay was performed using SoftMax Pro 5, set at excitation λ = 490nm and emission λ = 525nm, to report averaged reads every 3 seconds, apply 40 µL of respective agonist to the wells in the lane 17 seconds into each read and finish recording after 300 seconds; the photomultiplier tube sensitivity was set as "high". The automated microfluidics and dispensing system was loaded with ADP and MRS2365 at 3x the concentrations being tested, along with a buffer only, control well for each lane. Changes in Ca^{2+} levels were measured in response to ADP (10 nM-3 mM) and MRS2365 (0.3 nM-30 µM), which were prepared in buffer with the plate reader programmed to apply the loaded concentrations of each to 2 adjacent lanes of the plate for duplicate reads. After the assay had finished the data were automatically transferred to an Excel file, to be presented as maximum – minimum/min, then analysed in GraphPad Prism 8, where the data was normalised and the "log(agonist) vs. response -- variable slope" equation fitted. All other equation parameters were fitted automatically up to the maximal response.

2.5.3.1 Effect of P2Y$_1$ and P2Y$_{12}$ antagonists on BV-2 cells response

The concentration-response curve was repeated for both ADP and MRS2365, in the absence and presence of AR-C69931MX (1 µM). In the final step prior to inserting the plate into the plate reader, cells were incubated with the AR-C69931MX. The agonists were prepared with a buffer that contained the antagonist to avoid a change in the antagonist concentration upon the addition of the agonist.

2.6   Fluorescence microscopy

2.6.1   Direct Immunofluorescence

tSA201 cells were grown to 60% confluence on 13mm glass coverslips located in 12 or 24 well plates. Coverslips were coated with PLL (outlined in **section 2.3.3**), however, microglial cells do not require this step due to their ability to adhere on the coverslip. tSA201 cells were transiently transfected with eYFP or eCFP proteins, or a fluorescent tagged plasmid as outlined in **section 2.4.1**. 48 hours later the cells were washed 3 times gently with PBS followed by fixation with ice cold methanol for 10 minutes at room temperature. The cells were washed a further 3 times with PBS and then incubated at room temperature in the dark for 5 minutes with PBS containing the specific fluorescent nuclear marker 4',6- diamidino-2-phenylindole (DAPI) (500nM) **Table 2.2**. The cells were again washed 3 times with PBS, and the coverslips were mounted on to glass microscope slides with Mowiol. The microscope slides were then stored in the dark at room temperature overnight to allow the coverslips to dry, then stored at $4^{o}C$ for later use. Cells were visualised using a Leica confocal microscope at x63 magnification with an oil-immersion lens. Images were edited via ImageJ for background correction.

2.6.2   Indirect Immunofluorescence

To view expression of HA-tagged $hP2Y_1$ and $hP2Y_{12}$ receptors, cells were transfected and fixed as outlined in the previous section. However, to view β-actin staining via rhodamine phalloidin cells were fixed by incubation in 3.7% formaldehyde solution for 10 minutes then permeabilized in 0.1% Triton-X-100/PSA for 5 minutes with 2 PSA washes in between. Next, all cells were washed twice with PBS and then blocked with 2% BSA in PBS for an hour at room temperature. After blocking, the coverslips were incubated with one of the selected primary antibodies overnight (**Table 2.3**). The cells were then washed twice in PBS then blocked in 2% BSA in PBS for 15 minutes. After that, the coverslips were placed cell side down onto 100 µL of secondary antibody selected from **Table 2.4,** and incubated for 2 hours at room temperature. The cells were then washed twice with PBS, as before, followed by incubation at room temperature in the dark for 5 minutes with PBS containing DAPI (500nM) (**Table 2.2**). The cells were washed once with PBS to remove residual DAPI,

and the coverslips were mounted on to glass microscope slides with Mowiol. The microscope slides were stored and processed as outlined in the previous section.

2.6.3   Proximity Ligation Assay (in situ PLA) or (PLA)

In situ PLAs were used to identify the physical interaction between $P2Y_1$ and $P2Y_{12}$ receptors. Cells were seeded in 12-well plates containing 13 mm diameter glass coverslips. For tSA201 cells, cotransfection was carred out as outline in **section 2.4.1** with HA-tagged receptor and the other receptor tagged with fluorescence protein. Cell fixation and permeabilization was done using ice cold methanol for 10 minutes at room temperature. The cells then washed twice with PBS and blocked with 2% BSA in PBS for an hour at room temperature. Following that, the coverslips were incubated with one of the selected primary antibodies overnight (**Table 2.3**)**.** PLAs were performed as per the Duolink™ *In Situ* PLA protocol from (Sigma-Aldrich) using the Duolink *In Situ* range of detection reagents (orange), wash buffers and PLA probe kits. All incubation steps were carried out in a humidity chamber 37 °C. Briefly, the coverslips were then incubated in rabbit PLUS and mouse MINUS Duolink PLA probes used at a dilution of 1:5 in Duolink Antibody Diluent at 37 °C for 1 hour. Following this incubation period, the coverslips were washed twice in Duolink wash buffer A for 5 min then incubated in 40 µL 5X Duolink ligation buffer (1:5) containing 1 U ligase at 37°C for 30 min. Following that, coverslips were washed twice in buffer A for 5 min and incubated in 40 µL 5X Duolink amplification buffer (1:5) containing 0.5 U polymerase at 37 °C for 100 min. The samples were covered with foil to protect the photosensitive reaction from light at all following steps. Coverslips were washed in Duolink wash buffer B for 10 min at room temperature followed with a final wash in 0.01X buffer B for 1 min. DAPI staining was done as usual by incubating the coverslips at room temperature in the dark for 5 minutes with PBS containing 500nM of DAPI (**Table 2.2**). The cells were washed 3 times with PBS, and the coverslips were mounted on to glass microscope slides with Mowiol. The microscope slides were then stored in the dark at room temperature overnight to allow the coverslips to dry, then stored at 4°C for later use. Cells were visualised using a Leica confocal microscop at x63 magnification with an oil-immersion lens. Images were processed via ImageJ for background correction.

Table 2.2: List of immunofluorescence stains

Name	Conc.	Dilution	Ref No.
DAPI (Sigma)	1mM aliquots	1/2000 in PBS	D-9542
Rhodamine phalloidin (ThermoFisher)	300U	1/40 in PBS	R415

Table 2.3: Primary antibody information including their target, species and concentrations.

Target	Species	Primary Antibody	Dilution	Ref No.
HA tag	Mouse	HA antibody (BioLegend)	1:1000 in 0.2% BSA/PBS	MMS-101R
P2Y$_1$ receptor	Mouse	Anti-P2Y$_1$ (Santa-Cruz Biotechnology)	1:100 in 0.2% BSA/PBS	sc-377324
GFP tag	Rabbit	EGFP antibody (Clontech, Takara)	1:100 in 0.2% BSA/PBS	632592
P2Y$_{12}$ receptor	Rabbit	Anti-P2Y12 (Alomone Labs)	1:100 in 0.2% BSA/PBS	APR-012
Iba1	Rabbit	Anti-Iba1 (Laboratory Chemicals Alpha Laboratories Ltd)	1:100 in 0.2% BSA/PBS	019-19741

Table 2.4: Secondary antibody information including their species and concentrations.

Secondary Antibody	Species	Dilution	Ref No.
Dye-conjugated AffiniPure donkey (Texas Red®)	Mouse	1:100 in 0.2% BSA/PBS	715-075-150
Alexa Flour 555 goat (Invitrogen®)	Mouse	1:100 in 0.2% BSA/PBS	A21422
Alexa Flour 555 goat (Invitrogen®)	Rabbit	1:100 in 0.2% BSA/PBS	A21428
Alexa Flour 488 goat (Invitrogen®)	Mouse	1:100 in 0.2% BSA/PBS	A11001
Alexa Flour 488 goat (Invitrogen®)	Rabbit	1:100 in 0.2% BSA/PBS	A11008

2.6.4   Fluorescence-lifetime imaging microscopy (FLIM)

tSA201 cells were grown to 60% confluence on 13mm glass coverslips in 24 well plates as previous. The cells were transfected with hP2Y$_{12}$-eCFP or cotransfected with hP2Y$_{12}$-eCFP and eYFP or hP2Y$_{12}$-eCFP and hP2Y$_1$-eYFP). 48 hours later, the cells were washed once gently with PBS, followed by fixation with ice cold methanol for 10 minutes at room temperature,then washed 3 times with PBS before being were mounted on to glass microscope slides with Mowiol. The microscope slides were then stored in the dark at room temperature overnight to allow the coverslips to dry, then stored at 4°C for later use.

Cells were imaged on LSM510 (Cral Zeiss) equipped with a Time-Correlated Single Photon Counting (TCSPC) module (SPC-830, Becker & Hickl GmbH), to determine the fluorescence lifetime and FRET. In TCSPC, one measures the time between sample excitation by a pulsed laser and the arrival of the emitted photon at the detector (**Figure 2.1**). The sample is allocated into 256x256 pixels and scanned pixel by pixel by a femtosecond Ti:Sapphire two-photon laser (Chameleon, Coherent) at 800 nm, as a two-photon excitation source to reduce cellular damage. The excitation/sampling rate was 80 MHz, with illuminating duration less than 200 fs. The emitted fluorescence signal was collected through a 63x water-immersion objective lens (N.A. = 1.0), a 480-520 nm bandpass filter, and transferred into a photomultiplier (PMT) detector. The FLIM scanning was done in a dark room protected from light, and the data were collected over an exposure of up to 15 minutes.

The fluorescence lifetimes of the donor without acceptor (τ_D) and with acceptor (τ_{DA}) and was obtained from images by software developed by Dr David Li (University of Strathclyde). The FRET efficiency (E) was calculated using the following equation (Bajar et al., 2016):

$$E = 1 - (\tau DA/\tau D)$$

Also, the distance between donor and acceptor (r) was calculated using the following equation (Dacres et al., 2010):

$$r^6 = \frac{R_0^6}{E} - R_0^6$$

R_0 is the critical distance (Förster distance) defined by quantum yield and extinction coefficient of donor and acceptor, which is 4.9 nm for eCFP/eYFP pair (Patterson et al., 2000).
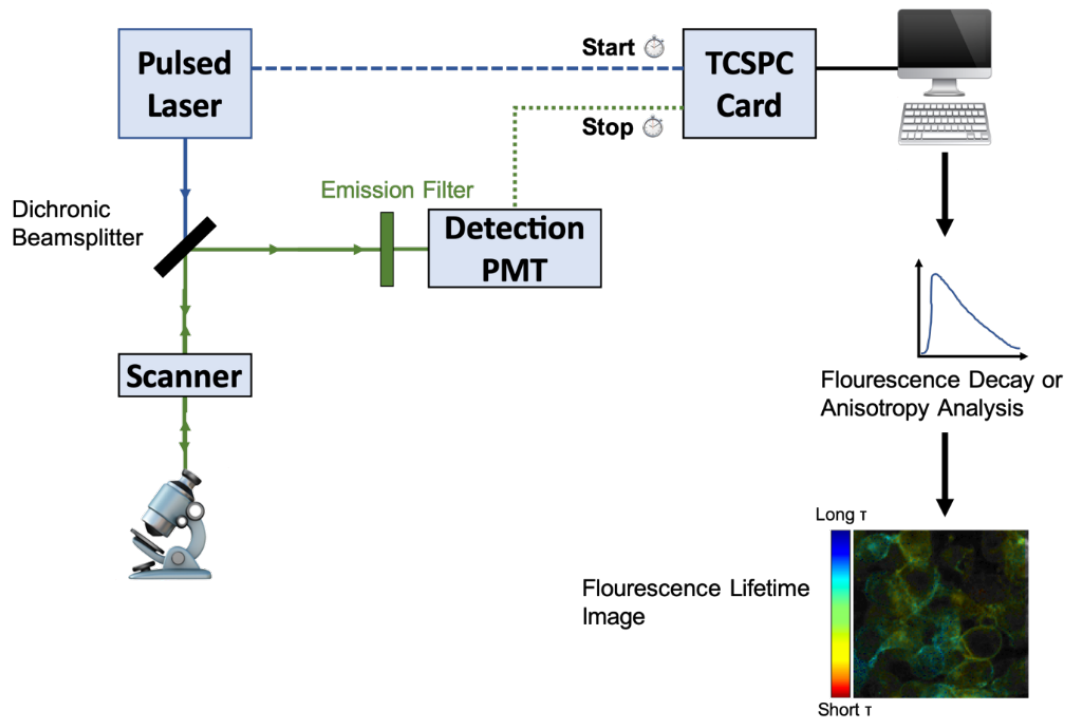
Figure 2.1: Schematic diagram of TCSPC-based scanning FLIM
The specimen is excited by the pulsed light source. A trigger pulse synchronized with the pulsed laser is used to start a time-correlated single-photon counting (TCSPC) module. The fluorescence emitted by the specimen is detected by a photo-multiplier tube (PMT), then used to stop the TCSPC. The output from the TCSPC will be proportional to the time difference between the start and stop pulses and is generated by the computer as a histogram. After repeating this process numerous times, the histogram will represent the fluorescence decay curve, which help us calculate the fluorescence lifetime.

2.7   Surface ELISA Method and internalisation

All ELISAs were performed as described in Mundell et al., (2010), however the protocol was modified according to the lab equipment. Briefly, cells were seeded in 24-well plate, and transfected at 70% confluence. Medium on the cells was replaced with prewarmed media (37°C) 24 hours later. For the ligand-induced internalisation experiments only, the media bathing the cells was replaced with prewarmed media

(37°C) 48 hours later and the cells incubated at 37°C for 15 minutes. Then the ligand was added. Ror example, ADP 10μM, was added at intervals to give incubation times (60 min, 30 min, 15 min, 5 min and 0 min). After that for both internalisation and surface expression ELISA experiments, the media was removed and the cells were washed gently by TBS then fixed by addition of 3.7% formaldehyde for 5 min. Cells were washed three times with TBS then blocked by incubatiion with 1%BSA in TBS for 45 min at room temperature. Cells were then bathed with 0.1%BSA in TBS containing (1:1000) of the primary antibody (Anti-HA) (BioLegend) then incubated for an hour at room temperature. Cells were washed 3 times with TBS and after the final wash they were blocked with blocking solution for 15 min at room temperature. The blocking solution was replaced with 0.1%BSA in TBS containing (1:1000) of the secondary antibody (alkaline phosphatase goat Anti-Mouse IgG (whole molecule) antibody) (Sigma-Aldrich) then incubated for an hour at room temperature. Cells were washed 4 times with TBS and prepared for development. Developing solution was prepared from the alkaline phosphate kit by combining *p*-nitrophenyl phosphate tablets, 5X diethanolamine buffer and double-distilled H_2O in a ratio of one tablet: 1 mL: 4 mL (e.g. for 2 X 24-well plates, use three tablets: 3 mL: 12 mL). After removing the final TBS wash from cells, the developing solution was added to each well and incubated at 37°C until the colour changed (deeper yellow colour). 100μl of the solution was then transferred from each well to the wells of a 96-well plate, along with 100μl of 0.4M NaOH to terminate the reaction. Samples were placed on a FlexStation 3 Multi-Mode Microplate Reader and their absorbance at 405 nm measured. Untransfected cells were used to determine the background value.

2.8   Lysing Cells

After 48 hours of growth and reaching confluence, cells were typically harvested by removing media, washing once in cold PBS and scraping cells in lysis buffer (50 mM Tris-HCl pH 7.4, 1% Triton-X-100 plus Roche Mini Protease Inhibitor cocktail 1 tablet/10 mL added on the day of the experiment). The amount of lysis buffer used depended on dish or well size, for example; 500 μl of lysis buffer was used for 60mm dishes, while 250 μl was usedfor 6 well plates and 75 μl for 24 well plates. Cell scrapings were mixed using a syringe and transferred into 1.5 mL microfuge tubes. The tubes were rotated for an hour at 4°C, then spun at 10.000 rpm at 4°C for 10

minutes to pellet any cellular debris that had not lysed. Lysated cells were stored at -20 $^{\circ}$C for later use. For whole cell lysate (WCL) samples, 2X NuPage- lithium dodecyl sulphate (LDS) sample buffer (Thermo Fisher Scientific) plus 50 mM dithiothreitol (DTT) were added onto lysated cells in a 1:1 ratio, and heated to 95°C for 2 minutes then stored in a cold place for later use.

2.8.1 Protein determination using BCA assay

Numerous methods are available to estimate the total protein concentration. In the following experiments, the amount of protein in the cells was determined using the Pierce BCA protein assay kit, with BSA as a standard as described in the manufacturer manual. This method is based on a reduction of Cu^{2+} to Cu^{1+} in alkaline environment. In the first step, copper ions chelate in an alkaline medium containing sodium potassium tartrate, with peptides that have three or more amino acid residues, forming a light blue coloured complex. In the second step, two bicinchoninic acid (BCA) molecules react with one reduced cuprous-cation formed in the first step, and create a strong purple coloured, BCA-copper complex. The purple colour absorbs visible light, which is measured with a microplate reader (FlexStation 3 Multi-Mode Microplate Reader) at a wavelength of 562 nm. A standard curve was plotted with the absorbance value as the dependent variable (y-axis) and concentration of BSA as the independent variable (x-axis) and the equation $y = ax + b$ fitted to the data. Solving for x, by inserting the sample's absorbance value, determined the protein concentration of the sample.

2.8.2 Immunoprecipitation (IP)

tSA201 cells were seeded in 60mm dishes and transfected with receptors tagged with an HA tag, as outlined in **section 2.4.1**. For co-IP experiments, cells were cotransfected with an HA-tagged receptor and the other receptor tagged with fluorescence protein. WCL were prepared by taking 50 µl of the lysated cells, which was then pre-cleared with Calbiochem Protein G Plus/Protein A Agarose Suspension (Merck Millipore) that had been prepared by adding 20 µl of beads to new tubes and washed twice with lysis buffer before the supernatants were removed to leave the washed pellet. 300 µl of each WCL was added to a tube of beads and left to rotate end over end at 4°C for at least 6 minutes before being pelleted by centrifugation and the pre-cleared supernatants transferred into new tubes.

20 µl per sample of the respective agarose immunoprecipitation beads (anti-HA-agarose produced in mouse (Sigma-Aldrich) for HA immunoprecipitation and GFP-Trap (ChromoTek) for GFP) were washed twice with lysis buffer to remove any residual storage buffer. The supernatants were then removed and 300 µl of each pre-cleared lysate added. Tubes were sealed and rotated at 40 rpm at 4°C overnight, followed by centrifugation at 5,000 rpm at 4°C for 5 minutes. Pellet were washed 3 times by adding 300 uL of lysis buffer and centrifuging at 5,000 rpm for 3 minutes at 4°C and supernatant discarded each time, to remove any un-bound protein before being pelleted by centrifugation and removed. For the GFP IP only, 30 µl was removed from each to separate tubes and 30 µl 2XNuPage-LDS sample buffer plus 50 mM DTT added to elute the IP complexes. These samples were then boiled at 95°C for 2 minutes to denature the protein. For HA IP, the HA-tagged proteins were eluted with 30 to 40 µl of 200 µg/mL HA-Peptide (Sigma-Aldrich) that was added to the washed bead-lysate complexes, gently vortexed and then left at room temperature for 20 minutes, lightly vortexing every 3 minutes. The tubes were then centrifuged at 5000 rpm for 5 minutes and the supernatants (IP samples) were carefully transferred to new tubes. Both the IP samples and the leftover beads (HA-peptide controls) then had 2X NuPage-LDS sample buffer plus 50 nM DTT added at the same volume as the HA-peptide and were subsequently boiled at 95°C for 2 minutes to denature the protein.

2.8.3   Cell membrane protein isolation

Membrane proteins were isolated according to the Pierce cell surface protein isolation kit (Thermo Fisher Scientific). Transfected tSA201 cells at 90-95% confluence were prepared for biotinylation. Sulfo-NHS-SS-Biotin in PBS solution was added onto the cells, followed by incubation for 30 minutes at 4°C. After quenching the reaction, cells were transferred into tubes, TBS buffer added and and the samples centrifuged at 1000rpm. Pellet were washed with TBS buffer and centrifuged at 1000rpm. After discarding the supernatant, the pellet was dissolved in lysis buffer and incubatied on ice for half an hour with gentle vortexing every 3 minutes. Following that, samples were centrifuged at 10000g for 2 mixtures at 4 °C. 10% of the lysate was transferred to a new tube and used at the WCL sample.

Biotin labeled proteins were isolated via incubation for 1 hour at room temperature with Agarose then centrifugation at 1000g for 1 min. 50 µl of labelled

lysate was used as the intracellular sample. The pellet was washed with lysis buffer 4 times by centrifugation and discarding the supernatant each time. The pellet was eluted by NuPAGE sample buffer containing 50mM DTT and boiled at 95°C for 5 minutes.

2.9   Western blotting

2.9.1   Sodium Dodecyl Sulphate-Polyacrylamide Gel Electrophoresis (SDS-PAGE)

The Biorad Mini-Protean Tetra system was used for Western blotting. In order to separate proteins based upon their molecular size, 15-20 μl of sample per lane were separated by 8.5% resolving gels (30% [w/v] acrylamide solution, 0.8% [w/v] bis-acrylamide in 380 mM Tris-HCL pH 8.8, 0.10% [w/v] sodium dodecyl sulphate [SDS]). 0.02% (w/v) ammonium persulphate (APS) and 0.02% (v/v) N, N, N', N'-Tetramethylethylenediamine (TEMED) were added to these components to polymerise the gel. Gels were poured into pre-made gel chambers with 1mm thickness and 100% isopropanol used to ensure level setting and give an indication of when the gel had set. After setting, the isopropanol was washed out with distilled water and exogenous liquid gently drawn out with filter paper. 4% stacking gels were composed of 30% [w/v] acrylamide solution, 0.8% [w/v] bis-acrylamide diluted in 123 mM tris-HCl pH 6.6, 0.01% [w/v] SDS, 0.1% [w/v] APS and 0.07% [v/v] TEMED. Gels were poured and over the polymerised resolving gel, well-forming combs were immediately added and 1.0 mm 10 or 15 well comb (Biorad) inserted gently between the plates, then the gel was left to polymerise. After polymerisation, combs were removed and the polyacrylamide gel was washed twice with deionised water, then the wells were filled with running buffer (25 mM Tris base, 192 mM glycine and 3.5 mM SDS). Samples were heated to 80°C for 2 minutes, centrifuged at 13,000 rpm for 1 minute, and loaded with a Hamilton micro-syringe, along with a lane of pre-stained protein standards ladder (Thermo Fisher Scientific). The chamber between the plates was topped up with running buffer before running the electrophoresis at 120 V until the bromophenol blue tracking dye had run off the bottom of the gel, which took around 110 minutes.

2.9.2 Electrophoretic Transfer of Protein to Membrane

The proteins in gels were subsequently transferred to polyvinylidene difluoride (PVDF) membranes or nitrocellulose membranes using the Biorad Mini Trans-blot system. PVDF membranes were activated by soaking in 100% methanol until translucent, while nitrocellulose membranes were soaked in transfer buffer (12M Tris, 19mM glycine, 20% (v/v) methanol). All components for the transfer were soaked in ice cold transfer buffer and each transfer cassette arranged with the bottom side of the cassette down, followed by two sponge pads, two pieces of Whatman 3MM paper, the gel, the activated membrane, 1 mm filter paper and 1 mm sponge. The cassette was closed and inserted into the BIO-Rad Mini Trans-Blot^{TM} tank along with a cooling bath of frozen transfer buffer and the chamber filled to the level of the cassette clip with blotting buffer. The power supply was set to run at 280 mA for 110 minutes.

2.9.3 Immunological Detection of Protein

Following transfer of the proteins to the membrane, the cassette was removed, the membrane extracted and left to block in 3% (w/v) BSA diluted in TBS-T buffer (150mM NaCl, 20mM Tris (pH 7.5), 0.1% (v/v) Tween-20) on an orbital shaker at room temperature for at least 2 hours. The primary antibody in 0.3% (w/v) BSA diluted in TBS-T buffer was then applied, either by heat sealing the membrane in a plastic liner (to minimise the excessive use of antibody) with the antibody or by adding the antibody directly to the membrane's container. Preferably, the antibody was left to bind overnight (>12 hours) at room temperature on an orbital shaker. The primary antibodies that were used are detailed in **Table 2.5**.

Table 2.5: Primary antibody used for western blotting.

Antibody	Supplier	Species	Dilution
Anti-αGFP	Chromotek	Rat	1:1000
Anti-HA	BioLegend	Mouse	1:10,000/1:60,000/1:100,000
Anti-α-tubulin	Sigma-Aldrich	Mouse	1:60,000
Membrane Fraction Cocktail	Abcam	Rabbit	1:750

After the primary antibody had been applied for sufficiently long, the membranes were washed in TBS-T buffer 4 times at 5 minutes intervals; horseradish peroxidase (HRP) conjugated secondary antibody (**Table 2.6**) for the respective species of the primary antibody, was applied in 0.3% (w/v) BSA for at least 90 minutes at room temperature on an orbital shaker before another 4 washes were undertaken. Enhanced chemiluminescence (ECL) was then used for detection: ECL-1 (100 mM Tris-HCL pH 8.5. 2.5 mM luminol, 1.15 mM coumaric acid) and ECL-2 (100 mM Tris-HCL pH 8.5, 0.064% [v/v] H_2O_2) were applied to the membrane on a 1:1 basis to activate the conjugated HRP. The membranes were then placed in an exposure cassette beneath plastic wrap, and under safelight conditions exposed on UltraCruz autoradiography film (Santa Cruz Biotechnology), which was processed in a Kodak M-35M X-OMAT processor.

Table 2.6: Horseradish peroxidase (HRP) conjugated secondary antibodies

Antibody	Supplier	Dilution
Anti-Rat IgG	R&D systems	1:2000
Anti-Mouse IgG	Jackson ImmunoResearch Laboratories, INC.	1:60000
Secondary AB Cocktail	Abcam	1:2000

When membrane fraction WB cocktail ab140365 (Abcam) was used, membranes were blocked in 5% milk (diluted in 20Nm Tris-HCL, 0.1% Tween-20) as the protocol suggested. And both antibodies (primary and secondary) were added to 5% milk. Membranes were washed using this new formula provided by the product's protocol.

2.9.4   Membrane Stripping and Reprobing:

The blot was stripped, in order to re-probe the PVDF membranes, with 15 mL of stripping buffer (100 mM β-mercaptoethanol, 2% sodium dodecyl sulphate, 62.5 mM Tris-HCl, pH 6.7) at 60°C on a shaker (Stuart Science Equipment). Following the incubation period, the stripping buffer was discarded and membranes were rinsed in TBS-T buffer (pH = 7.5) 4 times at 5 minutes intervals to remove residual stripping

buffer. Final step, immunological detection of protein was carried out as described in **section 2.9.3**.

2.9.5   Scanning and Editing

The film was then scanned for a minimum of 300 d.p.i on a HP Deskjet 2540 and adjustments to the image's global brightness, contrast and density were made in ImageJ.

2.10 Molecular biology techniques

2.10.1 RNA extraction

Total RNA was isolated using a GenElute Mammalian Total RNA Kit (Sigma) according to the manufacturer's protocol. Cells were firstly lysed by adding 250 µl of lysis solution containing 1% (v/v) of 2-mercaptoethanol (2-ME), which is required to fully inactivate RNases. Cell lysates then were transferred into a blue filtration column placed in a 2 mL receiving tube and centrifuged at 16,000 ×g for 2 minutes. An equal volume of 70% ethanol solution (250 µl) was added to the filtrate and thoroughly mixed. Next the mixture was transferred into a GenElute Binding Column (colourless insert with a red o-ring) placed in a 2-mL receiving tube and centrifuged at 16,000 ×g for 15 seconds. Afterwards, flow-through was discarded, the column was washed once with 500 µl of Wash solution 1 and centrifuged at at 16,000 ×g for 15 seconds. The binding column was placed in a fresh 2-mL receiving tube and washed twice with 500 µl of Wash solution 2 containing ethanol, and centrifuged at 16,000 ×g for 15 seconds. Finally, total RNA was eluted from the column by placing the binding column in a fresh 2 mL receiving tube and adding 50 µl of RNase-free (elution solution) into the binding column. The RNA concentration was quantified using a Nanodrop 2000c spectrophotometer (Thermo Fisher Scientific) and the sample then stored at -80ºC until used.

2.10.2 DNase treatment of total RNA

Prior to cDNA synthesis, the RNA sample was diluted to a concentration of 100 ng/µL. Residual plasmid or genomic DNA was removed from RNA samples using the Amplification Grade DNAse I kit (AMPD1, Sigma-Aldrich) according to manufacturer's instructions. In brief, 1 µg (10 µL from 100 ng/µL) of total RNA was incubated with 1.25 µL DNAse and 1.25 µl of reaction buffer in 10 µl reaction mixture for 10 minutes at room temperature. Then DNAse was inactivated by the addition 1.25 µL of stop solution (EDTA), followed by incubation at 70°C for 10 minutes. Samples were then stored on ice until the next step.

2.10.3 Single-stranded DNA synthesis

The High Capacity Reverse Transcription Kit was used to generate cDNA. The reverse transcription kit (Applied Biosystems by Thermo Fisher Scientific) contains reagents that when combined form a 2X reverse transcription (RT) master mix (**Table 2.7**).

Table 2.7: High Capacity Reverse Transcription Master Mix components

Component	Volume/Reaction (µL)	
	Samples (RT)	-RT
10X RT Buffer	2.0	2.0
25X dNTP Mix (100 mM)	0.8	0.8
10X RT Random Primers	2.0	2.0
MultiScribe™ Reverse Transcriptase (RT)	1.0	-
Nuclease-free water	0.45	1.45
Total per Reaction	6.25	6.25

13.75 µL of RNA was mixed with 6.25 µL of master mix. The sample were pipetted up and down two times and placed in a thermocycler with temperatures set as follows: 25°C for 10 min, 37°C for 120 min and 85°C for 5 min. The complementary DNA (cDNA) generated was stored at -20°C until further use.

2.10.4 Quantitative reverse transcription PCR (qRT-PCR)

qRT-PCR was performed on cDNA samples to determine the expression of P2Y$_1$ and P2Y$_{12}$ receptor expression, using GAPDH for human cells and β-actin for mouse cells, as reference genes to normalise cDNA values. One target was run per PCR run to maximize plate efficiency and conserve reagents. All assays utilized SYBR Green Master Mix and entailed a 20 µL reaction volume consisting of 10 µl of SYBR Select Master Mix (Applied Biosystems by Thermo Fisher Scientific), 1.2 µL of 150 nM each primer and 1 µL of 100ng cDNA, with molecular grade water comprising any remaining reaction volume. Primers used were obtained from Integrated DNA Technologies and can be found in Supporting Information, **Table 2.8,** along with primer concentrations. Each assay run all applicable extraction blanks and a negative control of molecular grade water, with each sample plated in duplicate, pipetted into the 96 well qPCR optical plate, and sealed with optical adhesive film. qPCR optical plates were centrifuged at 500 x g for 1 min to collect reaction product and remove bubbles introduced by pipetting. All assays were performed under thermal cycling conditions for the qRT-PCR presented in the **Table 2.9,** using StepOne Plus (Applied Biosystems).

Table 2.8: Primers information

Gene name	Sequence (5' -3')	Exon Location	Ref Number	Assay Name
Human P2RY12	Primer1: GCTGCATTTCTTGTTGGTTAC Primer2: AATACCAGATGCCACTCTGC	2 - 3	NM_176876	Hs.PT.58.39733142
Mouse P2ry12	Primer1: GAGAAGGTGGTATTGGCTGAG Primer2: CCAGTCTGCAAGTTCCACTAAC	3 - 4	NM_027571	Mm.PT.58.43542033
Human P2RY1	Primer1: GTAACAGCCCAGAATCAGCA Primer2: CCACCTCAGACGAGTACCT	1 - 1	NM_002563	Hs.PT.58.24915313
Mouse P2ry1	Primer1: TGGTCAATAGAGTGTTGCTTCT Primer2: TCAAGCAGAATGGAGACACG	1 - 2	NM_008772	Mm.PT.58.33326673
Human GAPDH	Primer1: TGTAGTTGAGGTCAATGAAGGG Primer2: ACATCGCTCAGACACCATG	2 – 3	NM_002046	Hs.PT.39a.22214836
Mouse Actin	Primer1: GATTACTGCTCTGGCTCCTAG Primer2: GACTCATCGTACTCCTGCTTG	5 – 6	NM_007393	Mm.PT.39a.22214843.g

Table 2.9: PCR cyclic parameters for SYBR Green qRT-PCR.

Stages	Number of cycles	Temperature	Time
Holding stage	1	50 ºC	2 minutes
		95 ºC	2 minutes
Cycling Stage	40	95 ºC	15 seconds
		55 ºC	15 seconds
		72 ºC	1 minutes
Melting curve stage	Melting curve was recorded for each cycle.	95 ºC	15 seconds
		60 ºC	1 minutes

2.11 Statistical Analysis

All statistics were calculated using GraphPad Prism version 8. Datasets were analysed for statistical significance by using either a one- or two-way analysis of variance (ANOVA) or an unpaired t test, as appropriate. P values <0.05* and P<0.0001**** were considered significant and means ± standard errors of the mean (SEM) are shown in all figures

Chapter Three

Transfection Efficiency, Surface Expression and Functional Characterization of Recombinant P2Y$_1$ and P2Y$_{12}$ Receptors

1   Introduction

P2Y$_1$ receptors are thought to be widely distributed throughout the body, including in the heart, blood vessels, neural tissue, platelets, smooth muscle cells, the ovaries, testis and prostate gland (Abbracchio et al., 2006), whilst P2Y$_{12}$ receptors appear to have a more restricted distribution, including in platelets, subregions of the brain (Hollopeter et al., 2001) and microglial cells (Haynes et al., 2006). This can be difficult to confirm, however, due to issues related to the selectivity of commercially available antibodies, which are notoriously poor (Michel et al., 2009). Thus, the detection of endogenous P2Y receptors and the ability to visualise native dimers remains a challenge.

Recombinant DNA technology is an important approach that has made GPCR dimer detection possible, albeit using over-expressed epitope-tagged receptors (Khan et al., 2016). For the work carried out in this thesis, epitope tagging of recombinant P2Y$_1$ and P2Y$_{12}$ receptors was used to reliably track receptor expression using fluorescent microscopy, immunoprecipitation and western blotting. An advantage of the tags used in this study is the lack of cross-reactivity between the antibodies directed towards the tags (Costa et al., 2014). Functional characterization of tagged receptors was performed to ensure that the incorporation of the epitope tag did not alter receptor activity. Key features of P2Y$_1$ and P2Y$_{12}$ receptor expression and activity are well known and detailed below.

P2Y$_1$ receptors are coupled to Gq heterotrimeric G proteins, which induce phospholipase C (PLC) activity and subsequent cleavage of PIP$_2$ into IP$_3$/DAG to release intracellular Ca^{2+} from internal stores. Ca^{2+} flux assays are widely used for functional characterization of Gq-coupled GPCRs in response to known agonists and antagonists, making it a robust signalling assay for this investigation. P2Y$_{12}$ receptors couple to Gi family members, the alpha subunit of which inhibits adenylyl cyclase to control the production of cAMP. Interestingly, AR-C69931MX (cangrelor), which is a selective P2Y$_{12}$ antagonist, inhibits the rise of Ca^{2+} evoked by ADP in tSA201 cells (Kennedy, unpublished observations) and it is proposed that these effects are due to an interaction between P2Y$_1$ and P2Y$_{12}$ receptors, which is the focus of this thesis.

P2Y$_1$ and P2Y$_{12}$ receptors are typically expressed and localised at the plasma membrane (Rabani et al., 2018). Any changes to surface localisation impact receptor activity. Post-translational modification of GPCRs, such as N-linked glycosylation has been shown to play an essential role in the delivery of specific proteins and dimers to the cell surface. Previous studies have demonstrated that the P2Y$_{12}$ receptor protein sequence contains two potential N-linked glycosylation sites; however, these sites have been shown to not be important for P2Y$_{12}$ receptor surface expression (Zhong et al., 2004). The role of glycosylation in P2Y$_1$ receptor localisation remains unknown. Glycosylation can alter the dimerisation properties of GPCRs (Li et al., 2017), therefore this will be explored in this chapter.

Whilst the formation of functional P2Y$_1$ and P2Y$_{12}$ heterodimers remains to be confirmed, both P2Y$_1$ and P2Y$_{12}$ receptors can form homodimers, oligomers (Choi et al., 2008; Zhang et al., 2014a, b, 2015) and heterodimers with other GPCRs, such as proteinase-activated receptor 4 (PAR4) (Ribeiro-Filho et al., 2016; Smith et al., 2017). P2Y$_{12}$ oligomer expression in lipid rafts is essential for receptor activity (Norambuena et al., 2008). Disruption of critical disulphide bonds by reducing agents, such as DTT, can decrease P2Y$_{12}$ oligomer expression and partition receptors out of raft domains as monomers and dimers (Savi et al., 2006). Similar reducing conditions do not impact P2Y$_1$ receptor oligomer expression (Wang et al., 2003). The differences reported between P2Y$_1$ and P2Y$_{12}$ receptor activity will form the basis of experimental optimisation and characterization of the recombinant receptors generated for this thesis.

The experiments carried out in this chapter aimed to optimise conditions for functional expression of all recombinant epitope-tagged P2Y$_1$ and P2Y$_{12}$ receptors in tSA201 cells. Focus was placed upon determining transfection efficiency for each tagged receptor when expressed in isolation. These experiments enabled clear determination of the unique receptor protein expression patterns and confirmation of the subcellular localisation for each receptor. Ca^{2+} flux assays were used to determine functional expression and confirm interaction between the tagged P2Y$_1$ and P2Y$_{12}$ receptors, thus supporting previous observations with AR-C69931MX.

The impact of cotransfecting tagged $P2Y_1$ and $P2Y_{12}$ receptors in tSA201 cells was investigated to assess changes in transfection efficiency, receptor expression pattern and quantify colocalisation between each tagged receptor pair. ELISA was carried out to assess the surface levels of each extracellular epitope tagged receptor and to detect if surface expression was impacted when receptors were expressed in isolation compared to being coexpressed together. Cell surface biotinylation was further used to identify if this approach was sensitive enough to distinguish specific protein bands for each receptor population (i.e. discrimination between surface receptor bands vs intracellular receptor bands). The role of N-linked glygosylation and disulphide bonding upon $P2Y_1$ and $P2Y_{12}$ receptor expression and localisation was investigated pharmacologically using tunicamycin and increasing concentrations of DTT respectively. These experiments were then compared to receptor-coexpression cell models. Lastly, receptor internalisation to ADP was quantified using the established surface ELISA. This was carried out in single and cotransfected cell systems to identify if coexpression impacted $P2Y_1$ and $P2Y_{12}$ receptor internalisation, which has been previously implicated in $P2Y_{12}$-PAR4 heterodimers.

2 Results

2.1 Optimising recombinant hP2Y$_1$ and hP2Y$_{12}$ receptor expression in transiently transfected tSA201 cells

Recombinant P2Y$_1$ and P2Y$_{12}$ receptors were designed to express an HA (N-terminus) or CFP/YFP (C-terminus) tag, as follows; HA-hP2Y$_1$, HA-hP2Y$_{12}$, hP2Y$_1$-eYFP and hP2Y$_{12}$-eCFP receptors. Initial experiments investigated the cellular localisation and transfection efficiency of these plasmids in tSA201 cells by visualising their expression using confocal microscopy and quantifying expression using western blot and densitometry analysis. Following transfection with three different amounts of each plasmid (0.5, 1.0 and 1.5 µg), imaging of the fluorescence emitted by the eYFP tag of hP2Y$_1$-eYFP receptor showed that the receptor was localised mainly at the plasma membrane, with minimal intracellular clustering (**Figure 3.1a**). To identify the HA tag in cells transfected with HA-hP2Y$_1$ receptor, indirect immunostaining was carried out using a Texas red conjugated secondary antibody. Again, expression was predominantly at the plasma membrane, with low intracellular localisation (**Figure 3.2a**).

Next, protein expression was assessed using western blotting, and samples were prepare in the presence of 50mM DTT. The predicted molecular weights of monomeric hP2Y$_1$-eYFP and HA-hP2Y$_1$ receptors are 68.4 kilodaltons (kDa) and 43.2 kDa respectively. When the increasing amounts of hP2Y$_1$-eYFP plasmid were transfected into tSA201 cells, three prominent bands were detected in all blots (**Figure 3.1b** upper panel). The lowest molecular weight band resolved between 55 and 72 kDa, coinciding with the predicted molecular weight for monomeric hP2Y$_1$-eYFP (68.4 kDa). A second band was detected between 72-95 kDa, however the protein size of this band is too small to represent hP2Y$_1$-eYFP homodimers, but may be a post-translationally modified form of the hP2Y$_1$ receptor. A high molecular weight band was expressed as a "smear" which resolved between 130 and 250 kDa, thus representing hP2Y$_1$-eYFP oligomers. Quantification of these bands indicates that increasing the concentration of hP2Y$_1$-eYFP DNA transfected resulted in a concentration-dependent decrease in protein expression of all bands (**Figure 3.1c**). α-Tubulin expression (55 kDa) was similar across each lane and was used for normalization to obtain the relative quantitation shown.

When tSA201 cells were transfected with increasing amounts of HA-hP2Y$_1$ receptor plasmid, three prominent bands were again detected in all blots (**Figure 3.2b, upper panel**). However, the molecular weight of these bands was different from above, reflecting the smaller size of the HA epitope tag fused to the hP2Y$_1$ receptor. The lowest molecular weight protein expressed was an abundant band resolving at ~40 kDa, which coincided closely with the predicted protein size for monomeric HA-hP2Y$_1$ receptors (43.2 kDa). A second protein band migrated as an abundant "smear" which resolved between ~52-72 kDa. This protein band is too small to be HA-hP2Y$_1$ receptor homodimers, but may represent a post-translational modified form of the HA-hP2Y$_1$ receptor. The third band was the largest protein (>80 kDa), but was less abundant than the other two bands. Based on the predicted molecular weight of HA-hP2Y$_1$ receptor homodimer (~86 kDa), this band may represent homodimerisation of the receptor. Similar to hP2Y$_1$-eYFP expression data, protein expression appeared to decrease as more HA-hP2Y$_1$ plasmid was used (**Figure 3.2c**). α-Tubulin expression (55 kDa) was similar in each lane.

Important differences between the hP2Y$_1$-eYFP and HA-hP2Y$_1$ receptor plasmids were identified. Unlike the hP2Y$_1$-eYFP expression studies, the high molecular weight band >100 kDa, potentially representing hP2Y$_1$ oligomers, was not detected in cells transfected with HA-hP2Y$_1$ receptor. Conversely, the potential dimer band expressed in HA-hP2Y$_1$ receptor studies was not expressed in the hP2Y$_1$-eYFP experiments. One similarity across both sets of experiments was the expression of a protein band that may be a potential post-translationally modified form of hP2Y$_1$ receptor. This will be investigated further in this chapter.

These data highlight an important difference between the different epitope tagging strategies for the hP2Y$_1$ receptor, which provides insights into the different protein expression signatures of hP2Y$_1$ receptor monomers, dimers and oligomers between both constructs when analysed by western blot. Experiments were then carried out to identify if these differences were observed for the corresponding epitope-tagged hP2Y$_{12}$ receptor plasmids.
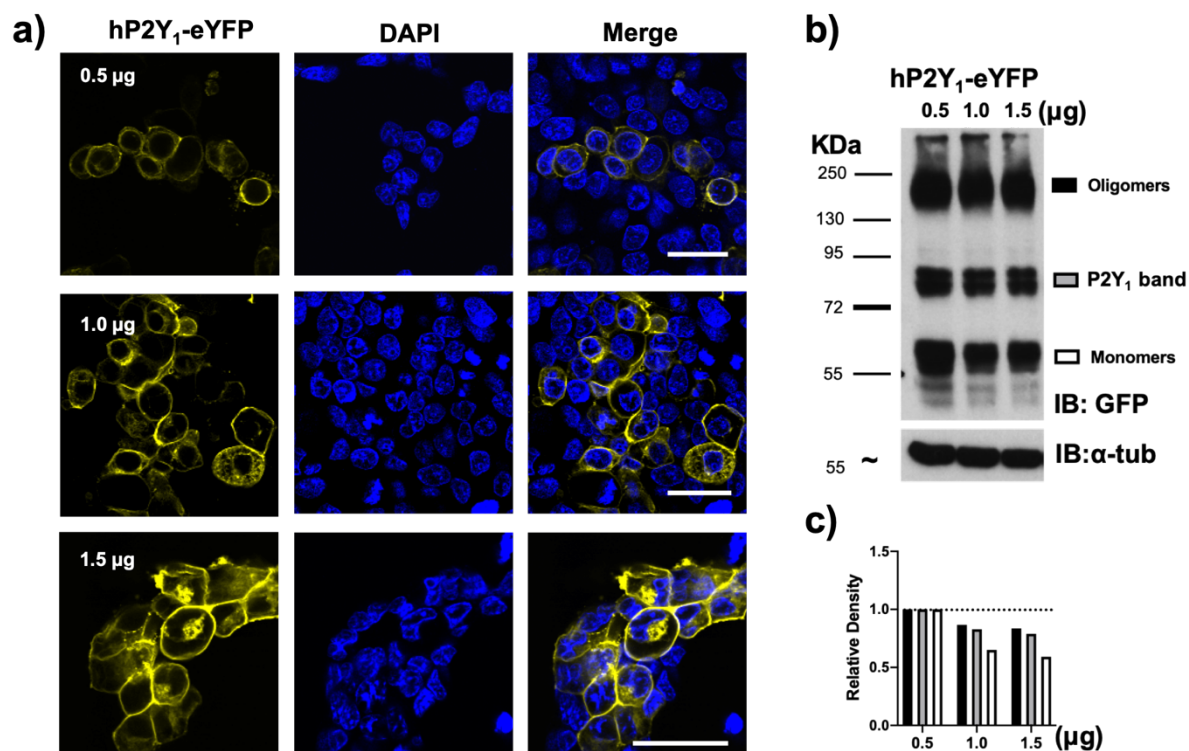
Figure 3.1: Direct fluorescence of the YFP tag of hP2Y₁-eYFP receptors expressed in tSA201 cells.

a) Representative images of fixed tSA201 cells 48 hours after transfection with 0.5 (top row) 1.0 (middle row) and 1.5 µg (bottom row) hP2Y₁-eYFP receptor plasmid are shown. The images show hP2Y₁-eYFP fluorescence (left-hand column) nuclear staining by DAPI (middle column) and overlay of both (right-hand column) and were visualised at 63x (oil) magnification using confocal microscopy (scale bar = 30 µm). **b, upper panel)** A western blot of whole cell lysates of tSA201 cells prepared 48 hours after transfection with 0.5 (left-hand lane), 1.0 (middle lane) and 1.5 µg (right-hand lane) hP2Y₁-eYFP receptor plasmid and probed with an anti-GFP antibody is shown. Molecular weight markers are shown on the left. **b, lower panel)** α-Tubulin (α-tub) was used to confirm equal loading of samples. **c)** The relative density of each group of bands, measured by densiometric analysis is shown. Data are representative of three **(a)** and one **(b,c)** experiments.
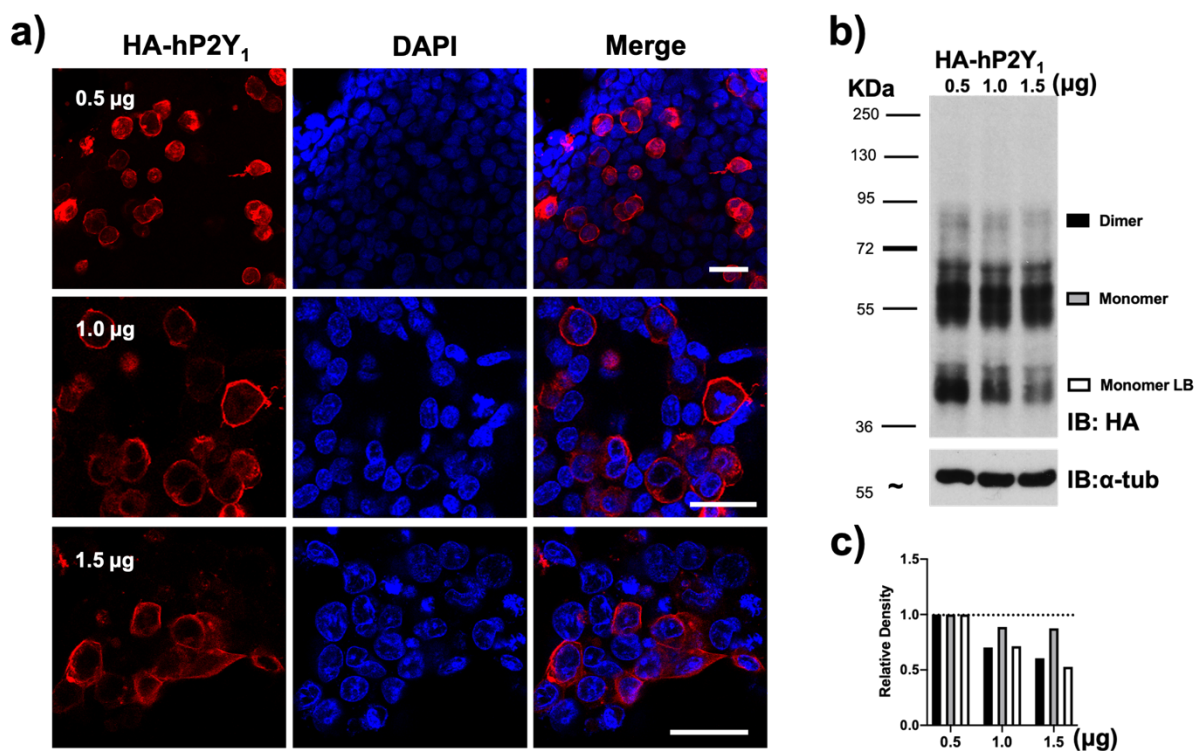
Figure 3.2: Indirect immunofluorescence of HA tag for hP2Y$_1$ receptors expressed in tSA201 cells.

   a) Representative images of fixed tSA201 cells 48 hours after transfection with 0.5 (top row) 1.0 (middle row) and 1.5 µg (bottom row) HA-hP2Y$_1$ receptor plasmid are shown. The images show Texas red filter setting to detect HA tag for HA-hP2Y$_1$ receptor (left-hand column) nuclear staining by DAPI (middle column) and overlay of both (right-hand column) and were visualised at 63x (oil) magnification using confocal microscopy (scale bar = 30 µm). **b, upper panel)** A western blot of whole cell lysates of tSA201 cells prepared 48 hours after transfection with 0.5 (left-hand lane), 1.0 (middle lane) and 1.5 µg (right-hand lane) HA-hP2Y$_1$ receptor plasmid and probed with an anti-HA antibody is shown. Molecular weight markers are shown on the left. **b, lower panel)** α-Tubulin (α-tub) was used to confirm equal loading of samples. **c)** The relative density of each band, as measured by densiometric analysis is shown. Data are representative of three **(a)** and one **(b,c)** experiments.

Next, tSA201 cells were transfected with the three different amounts of the $P2Y_{12}$ receptor plasmids. Imaging of the fluorescence emitted by the eCFP tag of $hP2Y_{12}$-eCFP receptor (**Figure 3.3a**) showed that the receptor was localised mainly at the plasma membrane, with minimal intracellular clustering. Likewise, the HA-$hP2Y_{12}$ receptor (**Figure 3.4a**), predominantly expressed at the plasma membrane, with low intracellular localisation. No change in the surface localisation was visualised for either tagged receptor upon increasing concentrations of DNA transfected. These localisation profiles resemble those presented above for tagged $P2Y_1$ receptors.

Next, protein expression was assessed using western blotting. The predicted molecular weights of monomeric $hP2Y_{12}$-eCFP and HA-$hP2Y_{12}$ receptors are 70.3 and 40.5 kDa respectively. As shown in **Figure 3.3b** upper panel, two $hP2Y_{12}$-eCFP receptor bands were detected in all three lanes. The lowest molecular weight protein band was visible at low expression level between the 55 and 72 kDa molecular weight markers, whilst a much more abundant protein band migrated between 72-95 kDa. This band coincides with the predicted molecular weight of monomeric $hP2Y_{12}$-eCFP receptors (70.3 kDa), whilst the other band is too small to represent receptor monomer expression. Quantification of the abundant monomeric band indicated that the concentration of $hP2Y_{12}$-eCFP receptor DNA transfected did not impact protein expression levels. α-Tubulin expression was similar in each lane, indicating equal protein loading across samples.

The same experiments were carried out to assess HA-$hP2Y_{12}$ receptor expression with increasing amounts of plasmid transfected into tSA201 cells. As shown in **Figure 3.4b, upper panel,** two clear HA-$hP2Y_{12}$ receptor protein bands were again seen in all transfected samples. The lowest molecular weight band was detected as a ~40 kDa protein, which coincided with the predicted molecular weight of monomeric HA-$hP2Y_{12}$ receptors (40.5 kDa). The second and most abundant protein detected migrated as a "smear" between ~45-72 kDa. The molecular weight of this band is too small to represent HA-$hP2Y_{12}$ receptor homodimers, but may reflect a post-translationally modified form of the $P2Y_{12}$ receptor. Band quantification showed that expression of the 45-72 kDa HA-$hP2Y_{12}$ receptor 'smear' remained the same across all concentrations of DNA transfected, however a concentration-dependent decrease in the proposed ~40 kDa monomeric HA-$hP2Y_{12}$ receptor band (monomer LB) was observed (**Figure 3.4c**). α-Tubulin expression was similar in each lane at 55 kDa.

Whilst the same number of protein bands were detected for both epitope-tagged $hP2Y_{12}$ receptors, important differences in their abundance were identified in the blotting experiments. Interestingly, only monomeric or potential post-translationally modified forms of $hP2Y_{12}$ receptor was resolved under these conditions, with no expression of homodimer or oligomeric complexes detected for either construct. The differences in protein expression band profiles will be investigated in more detail later in the chapter.
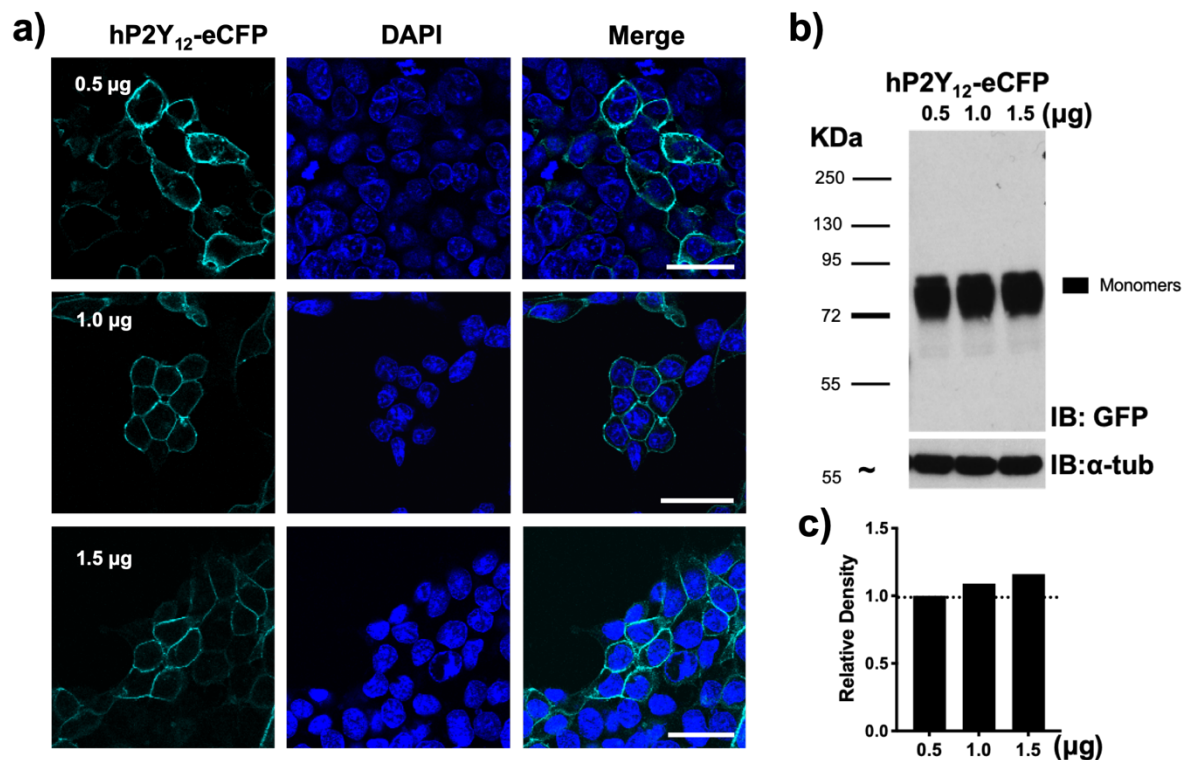
Figure 3.3: Direct fluorescence of the CFP tag for hP2Y$_{12}$ receptors expressed in tSA201 cells.

　　a) Representative images of fixed tSA201 cells 48 hours after transfection with 0.5 (top row) 1.0 (middle row) and 1.5 μg (bottom row) hP2Y$_{12}$-eCFP receptor plasmid are shown. The images show hP2Y$_{12}$-eCFP fluorescence (left-hand column) nuclear staining by DAPI (middle column) and overlay of both (right-hand column) and were visualised at 63x (oil) magnification using confocal microscopy (scale bar = 30 μm). **b, upper panel)** A western blot of whole cell lysates of tSA201 cells prepared 48 hours after transfection with 0.5 (left-hand lane), 1.0 (middle lane) and 1.5 μg (right-hand lane) hP2Y$_{12}$-eCFP receptor plasmid and probed with an anti-GFP antibody is shown. Molecular weight markers are shown on the left. **b, lower panel)** α-Tubulin (α-tub) was used to confirm equal loading of samples. **c)** The relative density of each band, as measured by densiometric analysis is shown. Data are representative of three **(a)** and one **(b,c)** experiments.
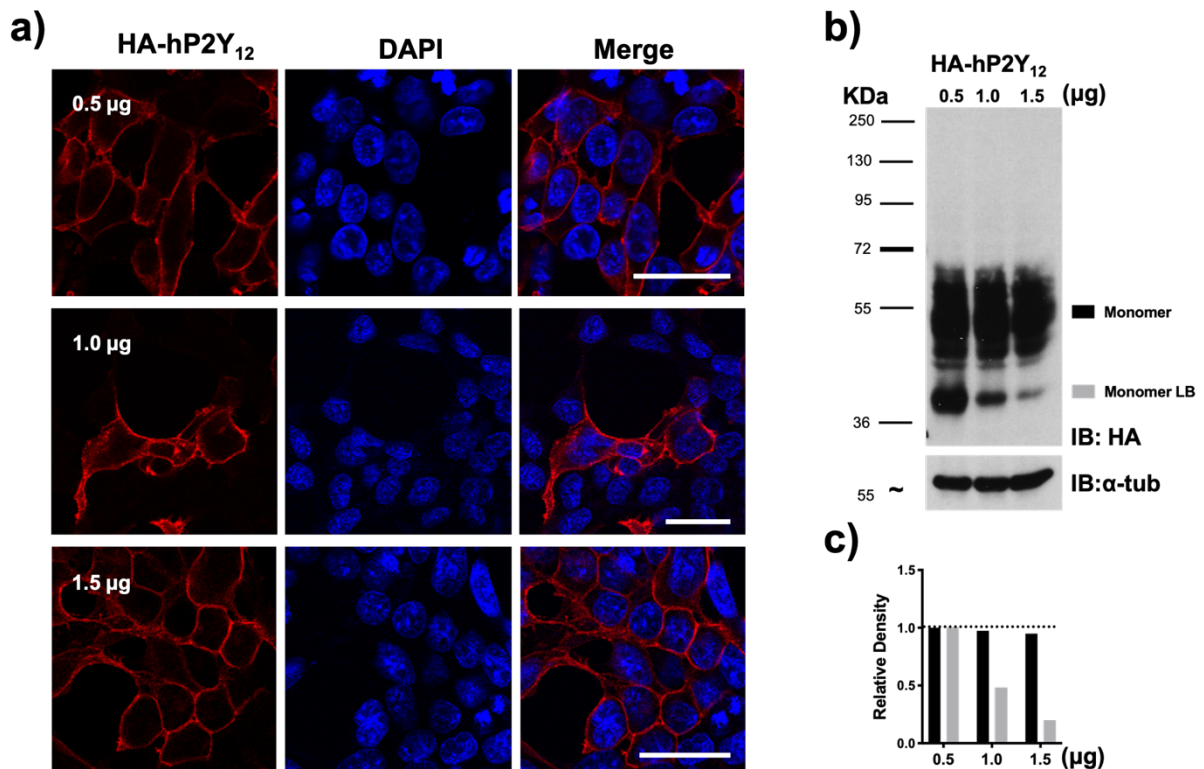
Figure 3.4: Indirect immunofluorescence of HA tag for hP2Y$_{12}$ receptors expressed in tSA201 cells.

a) Representative images of fixed tSA201 cells 48 hours after transfection with 0.5 (top row) 1.0 (middle row) and 1.5 µg (bottom row) HA-hP2Y$_{12}$ receptor plasmid are shown. The images show Texas red filter setting to detect HA tag for HA-hP2Y$_{12}$ receptor (left-hand column) nuclear staining by DAPI (middle column) and overlay of both (right-hand column) and were visualised at 63x (oil) magnification using confocal microscopy (scale bar = 30 µm). **b, upper panel)** A western blot of whole cell lysates of tSA201 cells prepared 48 hours after transfection with 0.5 (left-hand lane), 1.0 (middle lane) and 1.5 µg (right-hand lane) HA-hP2Y$_{12}$ receptor plasmid and probed with an anti-HA antibody is shown. Molecular weight markers are shown on the left. **b, lower panel)** α-Tubulin (α-tub) was used to confirm equal loading of samples. **c)** The relative density of each band, as measured by densiometric analysis is shown. Data are representative of three **(a)** and one **(b,c)** experiments.

Finally, the transfection efficiency for each plasmid was determined by counting the number of tSA201 cells with a fluorescence signal, with DAPI nuclear staining as a marker for the total cell population. **Figure 3.5a** shows that between 22.5 and 25.8% of cells were transfected following incubation with 0.5, 1.0 or 1.5 μg of the $hP2Y_1$-eYFP receptor, and there was no significant difference in the percentage of cells transfected. Cells incubated with the $HA-hP2Y_1$ receptor showed transfection efficiency of between 18.2 and 37.9%, with no significant differences between the three amounts of DNA (**Figure 3.5b**).

Next, the transfection efficiency for $P2Y_{12}$ receptor expressing cells was determined. **Figure 3.5c** shows that between 31.2 and 44.2% of cells were transfected with 0.5, 1.0 or 1.5 μg of the $hP2Y_{12}$-eCFP receptor, and there was no significant difference in the percentage of cells transfected. Cells transfected with $HA-hP2Y_{12}$ receptor showed transfection efficiency between 22.4 and 37.6%, again with no significant difference w between the three values (**Figure 3.5d**). Finally, there was no significant difference in transfection efficiency between the four plasmids. Based on these data, 1 μg of plasmid was used in subsequent experiments.
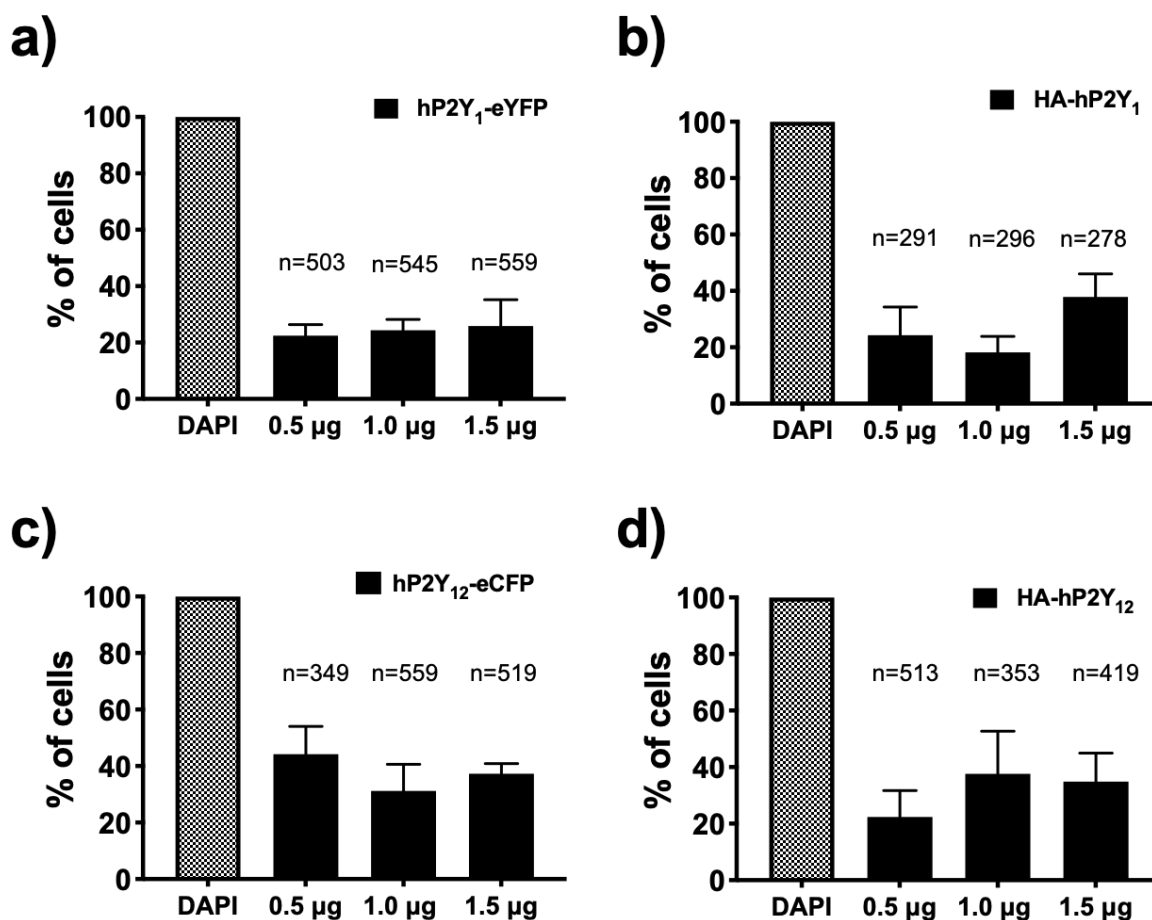
Figure 3.5: Transfection efficiency of tSA201 cells transiently expressing P2Y$_1$-eYFP, HA-hP2Y$_1$, hP2Y$_{12}$-eCFP or HA-hP2Y$_{12}$ receptor cDNA.

The bars show the percentage of tSA201 cells expressing **a)** hP2Y$_1$-eYFP, **b)** HA-hP2Y$_1$, **c)** hP2Y$_{12}$-eCFP and **d)** HA-hP2Y$_{12}$ receptors 48 hours after transfection with 0.5, 1.0 or 1.5µg cDNA. Vertical lines indicated s.e.m. The values were derived by calculating the percentage of DAPI positive cells in a field that also showed P2Y receptor expression, as indicated by FP fluorescence or HA indirect immunofluorescence, as appropriate. Each bar is the mean (± s.e.m) obtained from three separate transfections (n = total number of cells).

2.2 Functional expression of P2Y$_1$ and P2Y$_{12}$ receptors

Having demonstrated that each of the plasmids could be expressed in tSA201 cells and were largely located in the plasma membrane, the next set of experiments investigated whether the tagged receptors were functional, using a well-established fluorescent dye-based Ca^{2+} flux bioassay.

HA-P2Y$_1$ and hP2Y$_1$-eYFP receptors Ca^{2+} mobilization

tSA201 cells express endogenous ADP-responsive P2Y receptors, which is shown in **Figure 3.6a,** where ADP 10 µM (but not 10 nM) evoked a transient increase in intracellular Ca^{2+}. Representative traces show that when cells were transfected with either HA-hP2Y$_1$ (**Figure 3.6b**) or hP2Y$_1$-eYFP (**Figure 3.6c**), intracellular Ca^{2+} levels increase in response to ADP at 10 µM and 10 nM, thus indicating functional expression of these receptors.

Concentration-response curves were generated using a larger concentration range of ADP (**Figure 3.6d**). In untransfected (UT) tSA201 cells, ADP (10 nM-10 µM) evoked a concentration-dependent rise in cytoplasmic Ca^{2+}, with an EC$_{50}$ of 381 nM (95 % cl. 310 – 478 nM), Hill slope of 1.44 ± 0.17 and an E$_{max}$ of 99.0 ± 03.12% of the response to ADP (10 µM) (n=4). When tSA201 cells were transfected with hP2Y$_1$-eYFP or HA-hP2Y$_1$, ADP (300 pM - 10 µM) similarly evoked a concentration-dependent rise in cytoplasmic Ca^{2+}. Interestingly, in both cases, the concentration-responses curves were shifted to the left compared with that in UT cells and the curves were shallower, with low concentrations of ADP that were ineffective in UT cells, now effective **(Figure 3.6d**, blue and orange curves). For hP2Y$_1$-eYFP receptors the EC$_{50}$ was 204 nM (95 % cl. 103 – 586 nM), Hill slope was 0.42 ± 0.04 and E$_{max}$ was 112 ± 7.9% of the response to ADP (10 µM) (n=7). Cells expressing HA-hP2Y$_1$ receptors resulted in an EC$_{50}$ for ADP of 60 nM (95 % cl. 39 –102 nM), Hill slope of 0.47 ± 0.04 and E$_{max}$ of 99.9 ± 3.9% of the response to ADP (10 µM) (n=11).

The changes in EC$_{50}$ value between HA-hP2Y$_1$ and hP2Y$_1$-eYFP receptors were not significantly different from one another, however, the EC$_{50}$ for ADP in HA-hP2Y$_1$ expressing cells was significantly different from responses in untransfected cells (0.0001). The Hill slopes derived from ADP curves generated from cells

expressing HA-hP2Y$_1$ or hP2Y$_1$-eYFP were significantly lower than that in UT cells (P<0.05). Finally, there was no difference in the E$_{max}$ values in all 3 cases. Thus, both of the tagged hP2Y$_1$ receptors were functionally expressed in the tSA201 cells following transfection.
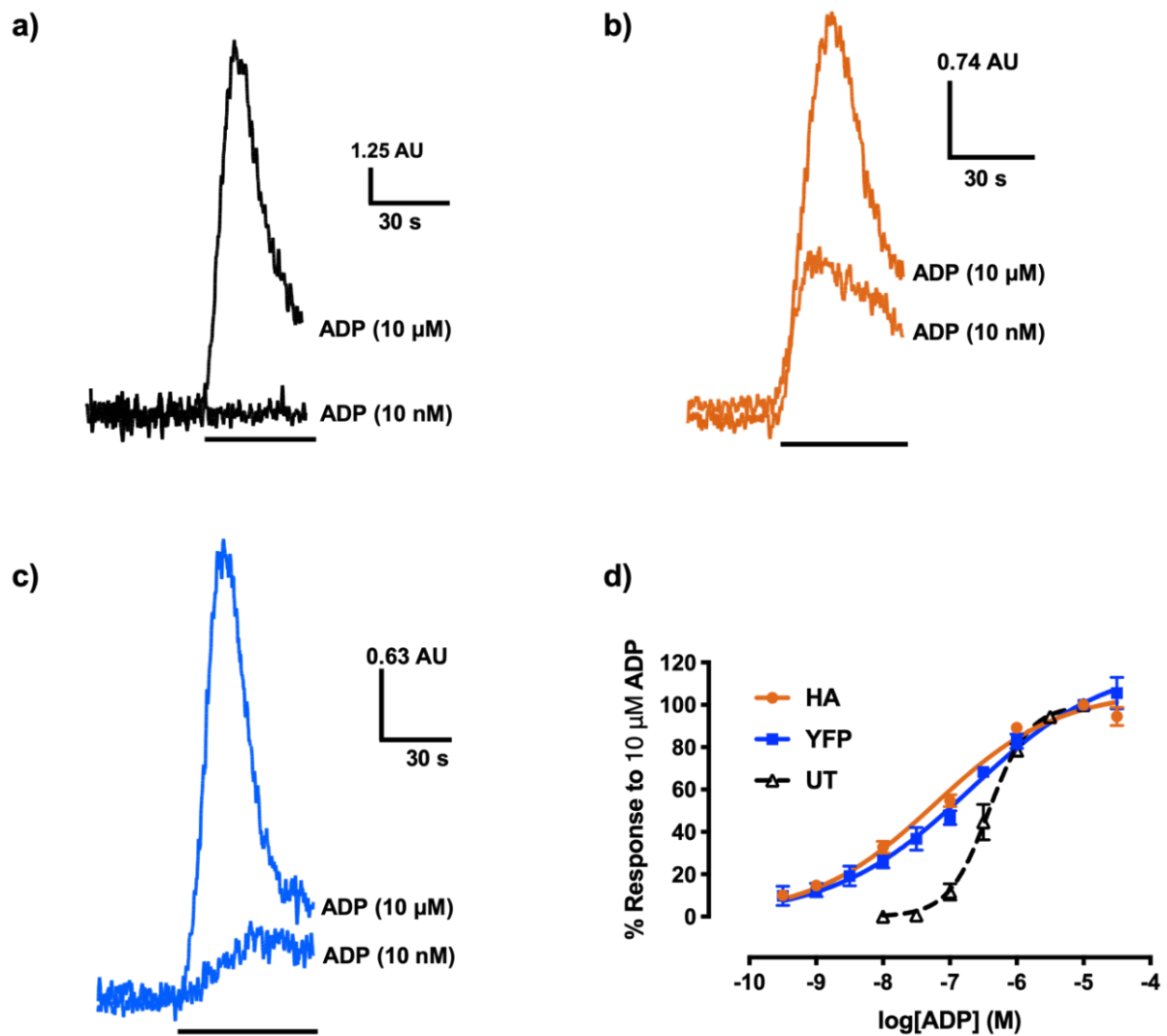
Figure 3.6: The effect of ADP on intracellular Ca^{2+} levels in untransfected tSA201 cells and cells transfected with HA-hP2Y$_1$ or hP2Y$_1$-eYFP receptor cDNA.
The superimposed traces show changes in Cal-520 fluorescence evoked by superfusion of cells with ADP (10 nM and 10 µM), as indicated by the horizontal bar in **a)** untransfected (UT), **b)** HA-hP2Y$_1$ receptor-expressing and **c)** hP2Y$_1$-eYFP receptor-expressing tSA201 cells. **d)** The mean (± s.e.m) peak amplitude of responses evoked by ADP are shown (n=4 for UT, n=11 for HA-hP2Y$_1$ receptors, n=7 for hP2Y$_1$-eYFP receptors). Responses are expressed as percent of the response to ADP (10 µM).

Effect of AR-C69931MX on HA-P2Y$_{12}$ and hP2Y$_{12}$-eCFP receptor expressing cells

Previous experiments in the Kennedy lab have shown that the highly selective P2Y$_{12}$ antagonist, AR-C69931MX, inhibits ADP-induced rises in intracellular Ca^{2+} in tSA201 cells expressing recombinant hP2Y$_{12}$ receptors, but not in UT cells (Kennedy, unpublished observations). Therefore, AR-C69931MX was used to determine functional expression of HA-hP2Y$_{12}$ and hP2Y$_{12}$-eCFP receptors.

AR-C69931MX (1 µM) had no effect on intracellular Ca^{2+} on its own (data not shown), but in cells transfected with HA-hP2Y$_{12}$ (**Figure 3.7a,c**) or hP2Y$_{12}$-eCFP (**Figure 3.7b,d**) it inhibited ADP (300 nM)-induced rises in intracellular Ca^{2+} by 67.8 ± 5.3%, (n=5, P<0.05) and 68 ± 6.6 % (n=5, P<0.05) respectively. Furthermore, inhibition was fully reversed after washout of AR-C69931MX. Thus, both of the tagged hP2Y$_{12}$ receptors were functionally expressed in the tSA201 cells following transfection.
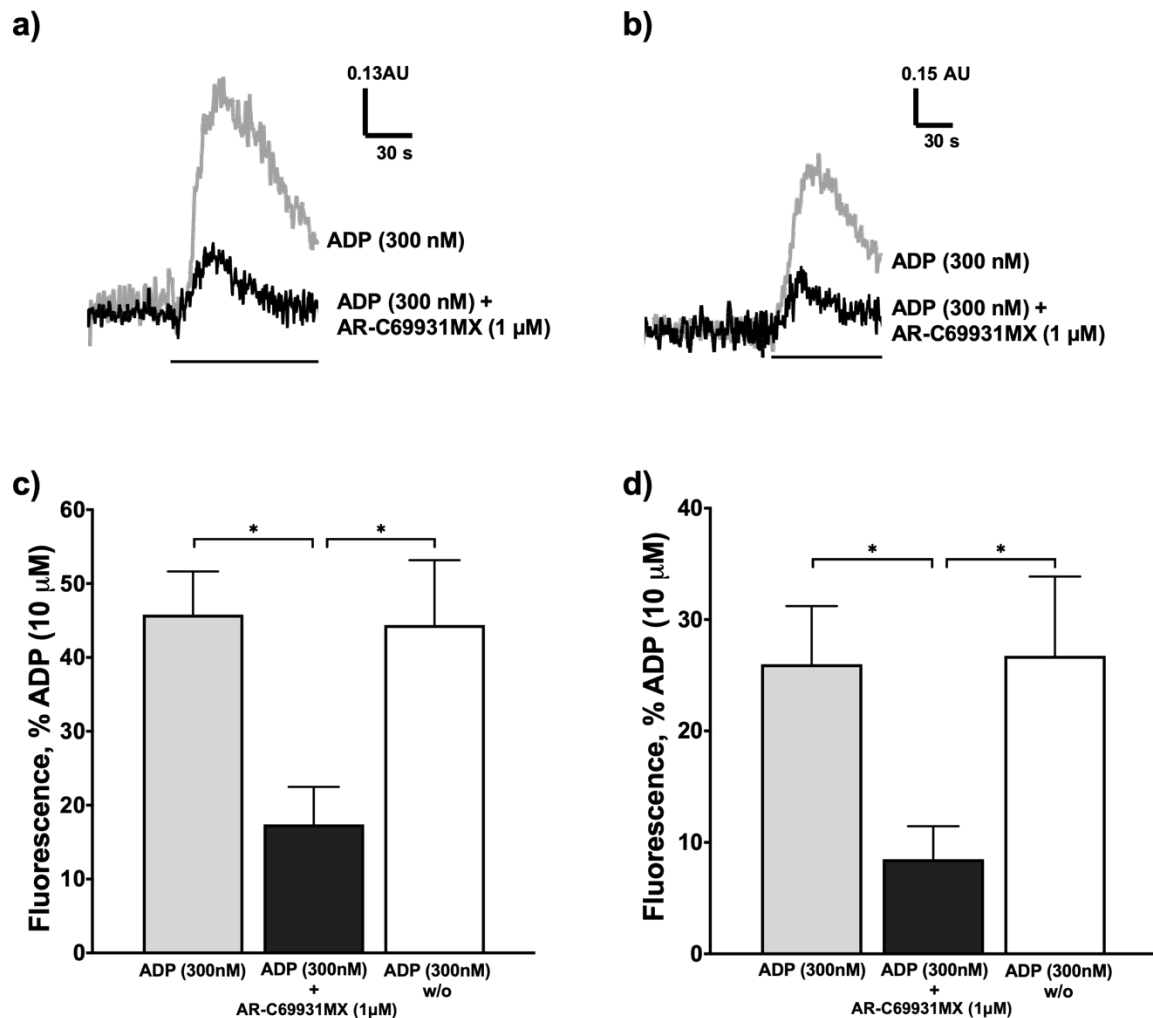
Figure 3.7: The effect of ADP and AR-C69931MX on intracellular Ca^{2+} levels in tSA201 cells transfected with HA-hP2Y$_{12}$ or hP2Y$_{12}$-eCFP receptor cDNA.

The superimposed traces show changes in Cal-520 fluorescence evoked by superfusion of cells with ADP (300 nM), as indicated by the horizontal bar in tSA201 cells expressing **a)** HA-hP2Y$_{12}$ and **b)** hP2Y$_{12}$-eCFP receptors in the absence and presence of AR-C69931MX (1 µM). The mean peak amplitude of responses evoked by ADP (300 nM) in the absence, presence and after washout of AR-C69931MX (1 µM) in tSA201 cells expressing **c)** HA-hP2Y$_{12}$ and **d)** hP2Y$_{12}$-eCFP receptors are shown (mean ± s.e.m). *$P<0.05$ between the two sets of data indicated by the horizontal bars.

2.3   P2Y$_1$ and P2Y$_{12}$ receptors cotransfection in tSA201 cells

Thus far, the expression of hP2Y$_1$ and hP2Y$_{12}$ receptors were studied separately. In the next series of experiments their localisation was studied after pairwise cotransfection of the HA-tagged receptor of one subtype with the FP-tagged receptor of the other. In **Figure 3.8a**, as a control, the HA-hP2Y$_1$ receptor (red) was coexpressed with eCFP. Whilst the HA-hP2Y$_1$ receptor expressed mainly at the plasma membrane, eCFP expression (cyan) was predominantly intracellular and superimposition with DAPI nuclear staining (blue) demonstrated little colocalisation with the HA-hP2Y$_1$ receptor, as indicated by the lack of white spot formation. In contrast, when the hP2Y$_{12}$-eCFP receptor (cyan) was coexpressed with HA-hP2Y$_1$ receptors (red), it is clear that both were expressed at the plasma membrane and that this is more noticeable in the merge image, where the overlap is represented as white spots (**Figure 3.8b**). Thus, colocalisation of HA-hP2Y$_1$ and hP2Y$_{12}$-eCFP receptors was not due to a non-specific interaction between the eCFP tag and HA-hP2Y$_1$ receptors.

Next, protein expression under these conditions was measured in cell lysates using western blotting. Similar to Figure 3.2b, three abundant protein bands were detected for the HA-hP2Y$_1$ receptor when expressed alone; one at 40 kDa, a ~52-72 kDa protein "smear" and a band between 80k-95 Da (**Figure 3.8c, lane 1**). Interestingly, the protein abundance of the 40 kDa and 80-95 kDa HA-hP2Y$_1$ receptor were reduced when coexpressed with eCFP (**lane 2**) and hP2Y$_{12}$-eCFP (**lane 3**). Confirmation of successful cotransfection of eCFP and hP2Y$_{12}$-eCFP receptor is shown in **Figure 3.8c middle panel**. The eCFP protein was detected at ~30 kDa (predicted molecular weight 26.9 kDa), with hP2Y$_{12}$-eCFP receptor expression detected between 72-95 kDa, as previously reported. Equal protein loading between samples was demonstrated by the α-Tubulin (55 kDa) immunoblot.

Western blot quantification analysis (**Figure 3.8d**) confirmed that the ~52-72 kDa for HA-hP2Y$_1$ receptor "smear" was not affected by coexpression of either eCFP or the hP2Y$_{12}$-eCFP receptor. However, coexpression of both did notably impact the abundance of the ~40 kDa and 80-95 kDa HA-hP2Y$_1$ bands, with a significant reduction ($p < 0.05$) in the expression of these bands when coexpressed with hP2Y$_{12}$-eCFP (**Figure 3.8d**).
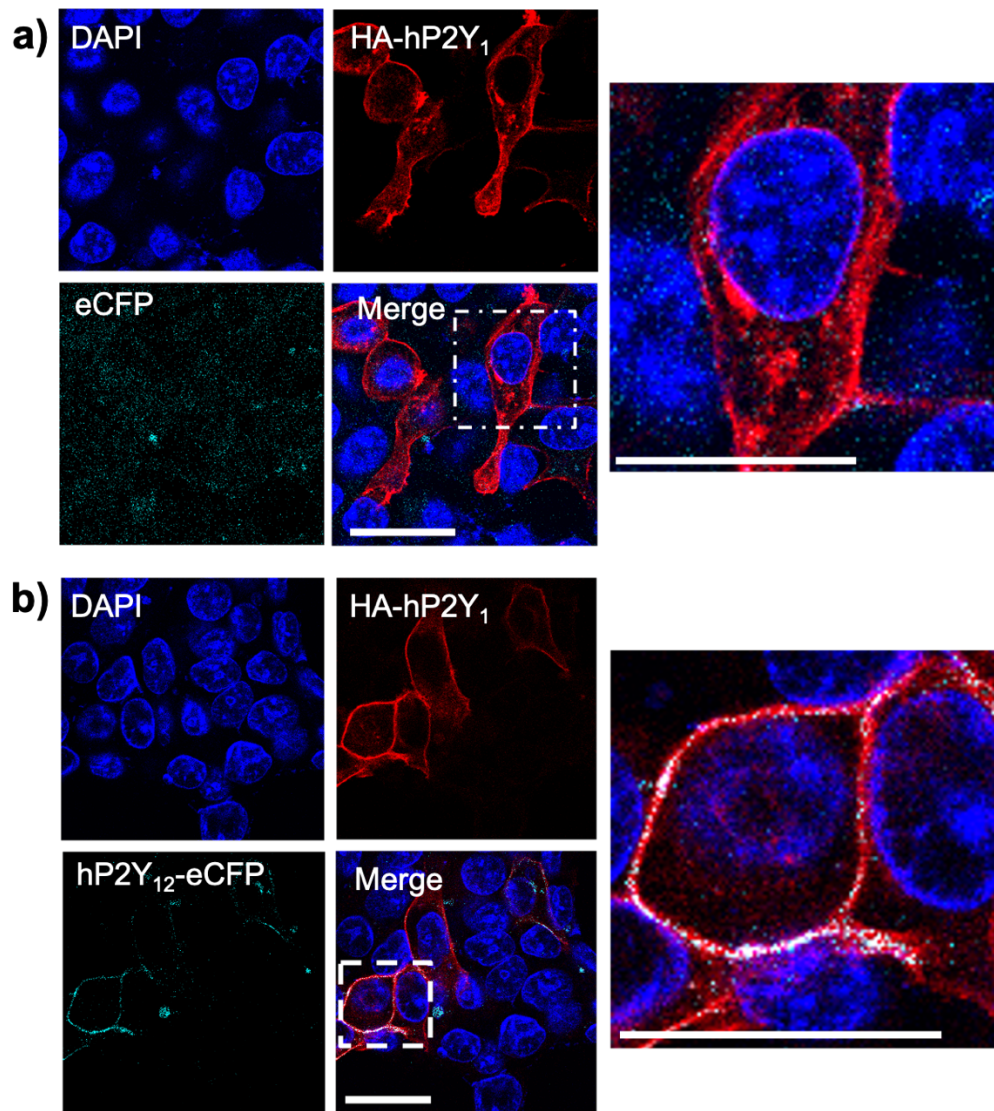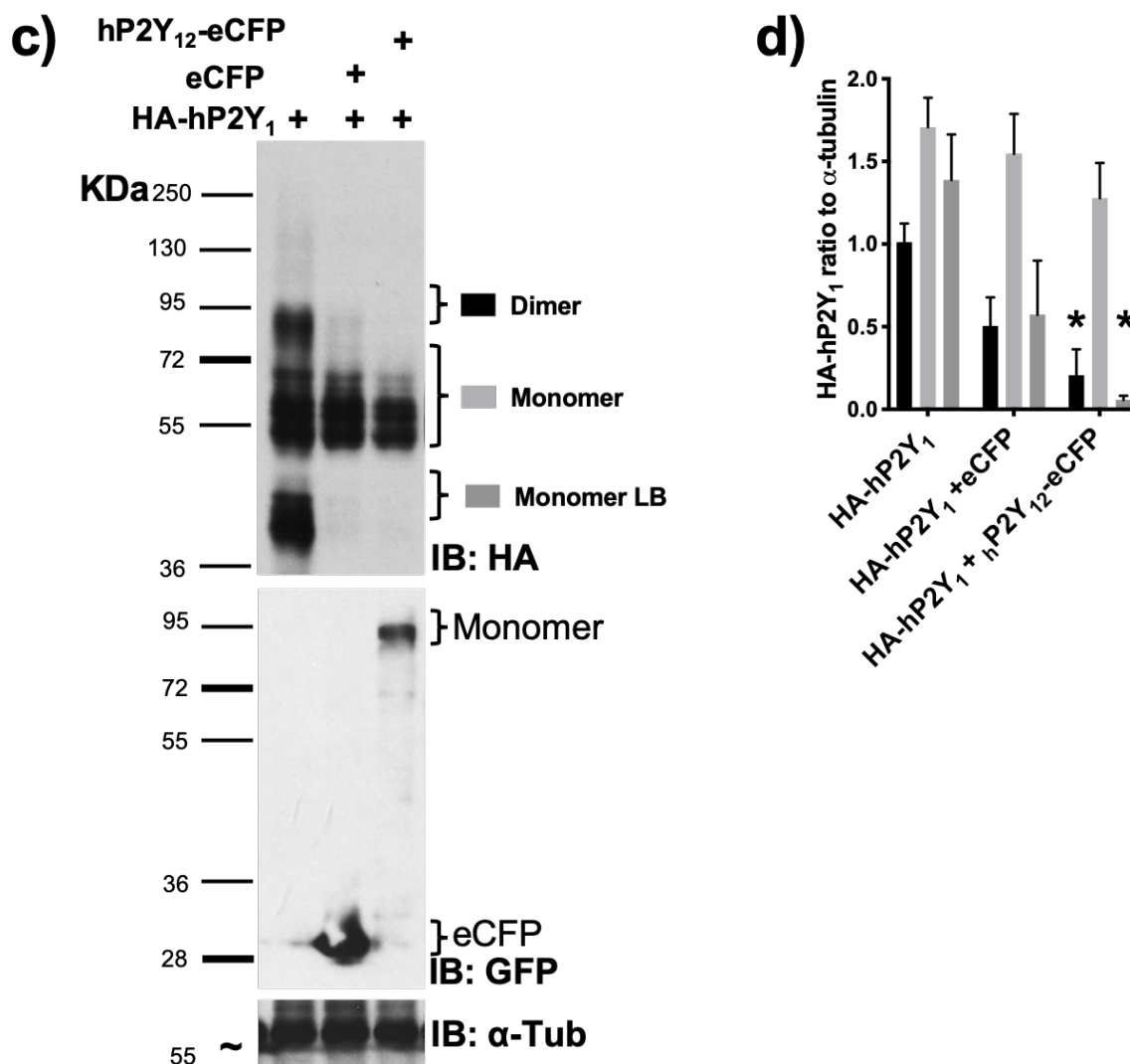
Figure 3.8: Colocalisation and protein expression patterns of HA-hP2Y$_1$ and hP2Y$_{12}$-eCFP receptors in tSA201 cells.

Representative images of fixed tSA201 cells 48 hours after cotransfection with **a)** HA-hP2Y$_1$ receptors and eCFP; **b)** HA-hP2Y$_1$ and hP2Y$_{12}$-eCFP receptors are shown. The top row of each shows nuclear staining by DAPI (left) and HA-hP2Y$_1$ receptors (right). The bottom rows show eCFP or hP2Y$_{12}$-eCFP receptor (left) and the overlay of all three images at the same (left), and greater (far right) magnification. The images were obtained using confocal microscopy and cells were visualised at 63x (oil) magnification (scale bars = 30 µm). **c)** A Western blot of whole cell lysates of tSA201 cells prepared 48 hours after transfection with HA-hP2Y$_1$ receptor (left-hand lane) and cotransfected with HA-hP2Y$_1$ receptors and eCFP (middle lane) and HA-hP2Y$_1$ and hP2Y$_{12}$-eCFP receptors (right-hand lane) is shown. Samples were probed with anti-HA then anti-GFP anti-bodies. Molecular weight markers are shown on the left. α-Tubulin (α-tub) was used to confirm equal loading of samples. **d)** The relative density of each band, as measured by densiometric analysis is shown. Data are expressed as mean ± s.e.m and are representative of three independent experiments. *P<0.05 compared to expression of the HA-hP2Y$_1$ receptor alone.

The opposite pairing of P2Y subtypes was studied next. In **Figure 3.9a**, as a control, the HA-hP2Y$_{12}$ receptor (red) was coexpressed with eYFP. Whilst the HA-hP2Y$_{12}$ receptor expressed mainly at the plasma membrane, eYFP expression (yellow) was predominantly intracellular and superimposition with DAPI nuclear staining (blue) demonstrated little colocalisation with the HA-hP2Y$_{12}$ receptor with no orange spot formation. In contrast, in **Figure 3.9b,** it is clear that the HA-hP2Y$_{12}$ receptor (red) expresses at the plasma membrane along with the hP2Y$_1$-eYFP receptor (yellow), and that this is more noticeable in the merge image, where the overlap forms orange spots. Thus, colocalisation of HA-hP2Y2$_1$ and hP2Y$_1$-eYFP receptors was not due to a non-specific interaction between the eYFP tag and HA-hP2Y$_{12}$ receptors.

Assessment of HA-hP2Y$_{12}$ receptor protein expression during cotransfection with eCFP or hP2Y$_1$-eYFP was carried out. Similar to the western blot data shown in Figure 3.4b, two clear HA-hP2Y$_{12}$ receptor protein bands were expressed when the receptor was expressed on its own (lane 1); one at ~40 kDa and a second migrating as a "smear" between ~45-72 kDa (**Figure 3.9c, upper panel**). Successful cotransfection with eYFP (lane 2) or hP2Y$_1$-eYFP receptor (lane 3) is shown in **Figure 3.9c middle panel**. The eYFP protein was expressed at ~30 kDa (predicted molecular weight 27.0 kDa), whilst three abundant bands were detected for hP2Y$_1$-eYFP (~55-72 kDa, ~72-95 kDa and the 130-250 kDa "smear"), as previously described. α-Tubulin (55 kDa) in **Figure 3.9c lower panel** demonstrates equal protein loading in each sample.

Whilst representative blots are shown in Figure 3.9c, quantitative analysis of all western blotting datasets (n=3) through densitometry of HA-hP2Y$_{12}$ receptor bands (**Figure 3.9d**) revealed that coexpression with the hP2Y$_1$-eYFP receptor, but not eYFP, resulted in a significant decrease (P<0.05) in the abundance of monomeric HA-hP2Y$_{12}$ receptors. This is presented as a reduction in the protein expression of the 45-72 kDa HA-hP2Y$_{12}$ receptor "smear". The representative blots presented in Figure 3.9c suggest increased abundance of the lower molecular weight HA-hP2Y$_{12}$ receptor band (monomeric LB band) during hP2Y$_1$-eYFP receptor coexpression, however this was not quantitatively different when all datasets were analysed.
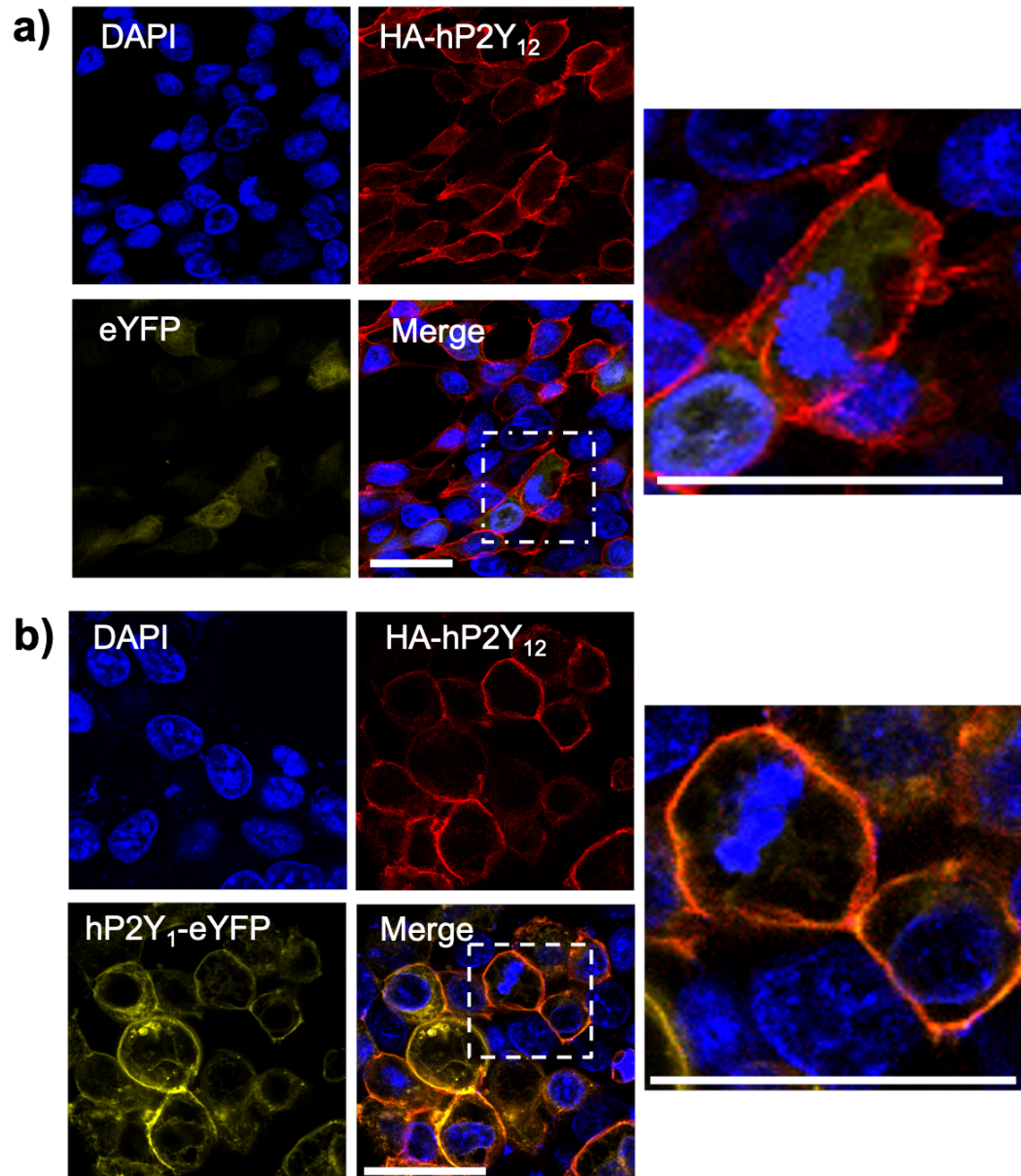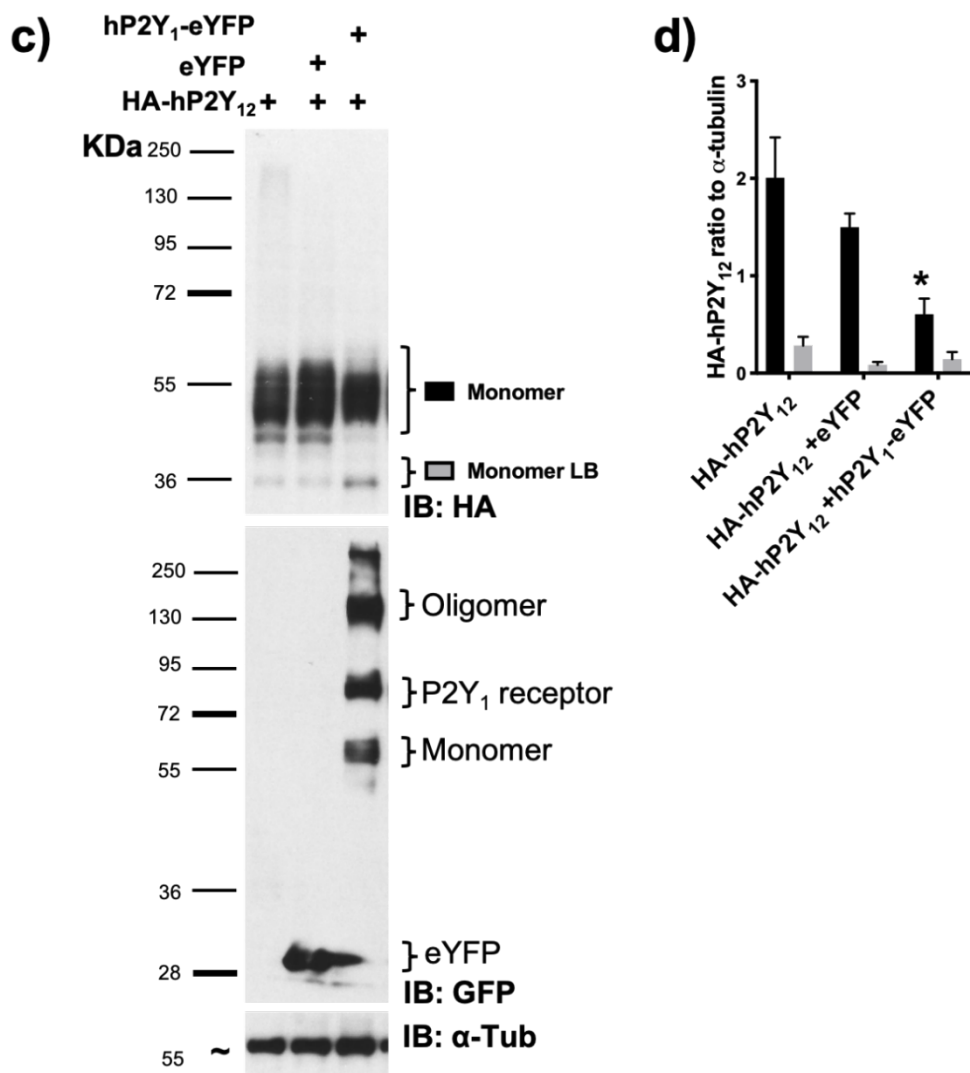
Figure 3.9: Colocalisation and protein expression patterns of HA-hP2Y$_{12}$ and hP2Y$_{1}$-eYFP receptors in tSA201 cells.

Representative images of fixed tSA201 cells 48 hours after cotransfection with **a)** HA-hP2Y$_{12}$ receptors and eYFP; **b)** HA-hP2Y$_{12}$ and hP2Y$_{1}$-eYFP receptors are shown. The top row of each shows nuclear staining by DAPI (left) and HA-hP2Y$_{12}$ receptors (right). The bottom rows show eYFP or hP2Y$_{1}$-eYFP receptors eYFP (left) and the overlay of all three images at the same (right) and greater (far right) magnification. The images were obtained using confocal microscopy and cells were visualised at 63x (oil) magnification (scale bars = 30 µm). **c)** A western blot of whole cell lysates of tSA201 cells prepared 48 hours after transfection with HA-hP2Y$_{12}$ receptor (left-hand lane) and cotransfected with HA-hP2Y$_{12}$ receptors and eYFP (middle lane) and HA-hP2Y$_{12}$ and hP2Y$_{1}$-eYFP receptors (right-hand lane). Samples were probed with anti-HA then anti-GFP antibodies. Molecular weight markers are shown on the left. α-Tubulin (α-tub) was used to confirm equal loading of samples. **d)** The relative density of each band, as measured by densiometric analysis is shown. Data are expressed as mean ± s.e.m are representative of three independent experiments. *$P<0.05$ compared to expression of the HA-hP2Y$_{12}$ receptor alone.

Finally, in this group of experiments, the effect of cotransfection on the efficiency of protein expression was determined by confocal microscopy by counting how many tSA201 cells exhibited fluorescence after cotransfection with both $P2Y_1$ and $P2Y_{12}$ receptors. **Figure 3.10** shows that when cells were cotransfected with HA-hP2Y$_1$ and hP2Y$_{12}$-eCFP receptors, 33.0% ±7.8 expressed HA-hP2Y$_1$ receptors and 27.4% ±7.3 expressed hP2Y$_{12}$-eCFP receptors, and for cells that were cotransfected with hP2Y$_1$-eYFP and HA-hP2Y$_{12}$ the values were 36.8% ±12.4 and 29.9% ±12.6 respectively. No significant difference between any of these values was observed. Also, there was no significant difference between these values and those obtained when each plasmid was expressed on its own, as shown in **Figure 3.5**.
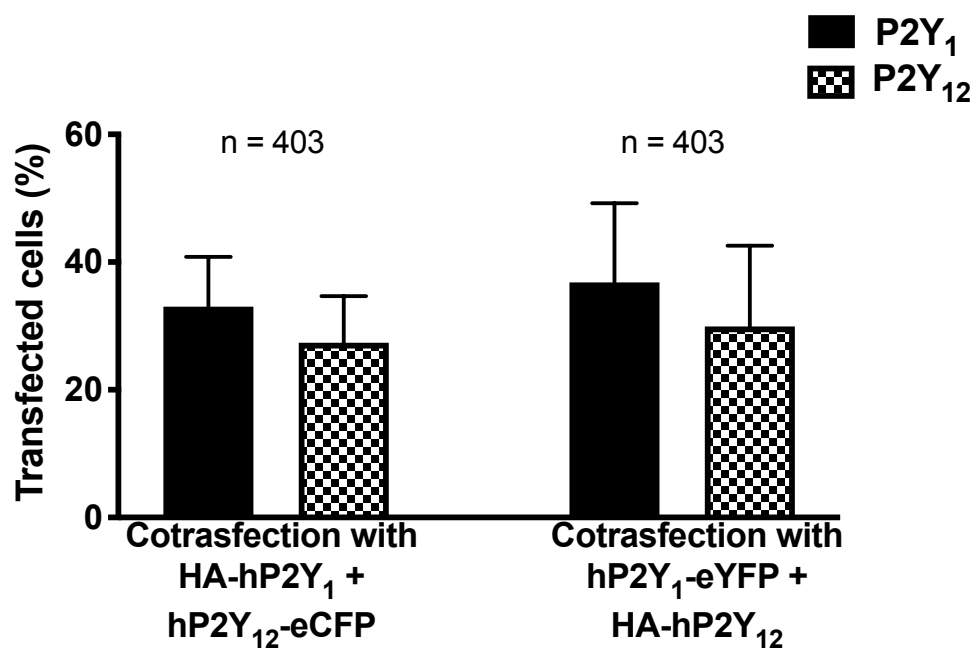
Figure 3.10: Transfection efficiency of tSA201 cells cotransfected with HA-hP2Y$_1$ and hP2Y$_{12}$-eCFP or hP2Y$_1$-eYFP and HA-hP2Y$_{12}$.

The percentage of tSA201 cells expressing HA-hP2Y$_1$ and hP2Y$_{12}$-eCFP receptors (left) and hP2Y$_1$-eYFP and HA-hP2Y$_{12}$ receptors (right) 48 hours after cotransfection, is shown. The values were derived by calculating the percentage of DAPI positive cells in a field that also showed P2Y receptor expression, as indicated by FP fluorescence or HA indirect immunofluorescence, as appropriate. Each bar is the mean (± s.e.m) obtained from three separate cotransfection experiments (n= number of cells).

2.4 Investigating the cellular colocalisation of P2Y$_1$ and P2Y$_{12}$ receptors in tSA201 cells

The cellular localisation of the coexpressed P2Y receptors was studied in more detail using confocal microscopy and line-scanning to assess receptor distribution profiles in transfected cells. First, a control experiment was performed in cells cotransfected with HA-hP2Y$_1$ receptors and eCFP (**Figure 3.11a**). The line scan of fluorescence (**Figure 3.11a, bottom, middle panel**)**,** shows that HA-hP2Y$_1$ receptors (red) express predominantly at the plasma membrane, while eCFP (cyan) expresses mainly intracellularly. The positive product of the differences from the mean (PDM) image (**Figure 3.11a, top, right-hand panel**) indicates very low overlap of pixels (white), with a Pearson correlation coefficient (PCC) value that is close to zero. The scatter plot of intensity distributions of both, plotted against one another (**Figure 3.11a, bottom, right-hand panel**) shows a low correlation of distribution of the two proteins. Thus, eCFP does not colocalise with HA-hP2Y$_1$ receptors in a non-specific manner.

Next, cells were cotransfected with HA-hP2Y$_1$ and hP2Y$_{12}$-eCFP receptors (**Figure 3.11b**). In contrast to above, the line scan of fluorescence (**Figure 3.11b, bottom, middle panel**) shows that both receptors express predominantly at the plasma membrane, similar to the data reported above in **Figure 3.8b**. Furthermore, the PDM image (**Figure 3.11b, top, right-hand panel**) indicates a high overlap of pixels (white), with a PCC value that is close to one. Finally, the scatter plot of intensity distributions of both, plotted against one another (**Figure 3.11b, bottom, right-hand panel**) shows a high correlation of distribution of the two proteins. Thus HA-hP2Y$_1$ and hP2Y$_{12}$-eCFP receptors appear to localise close to each other in the plasma membrane.
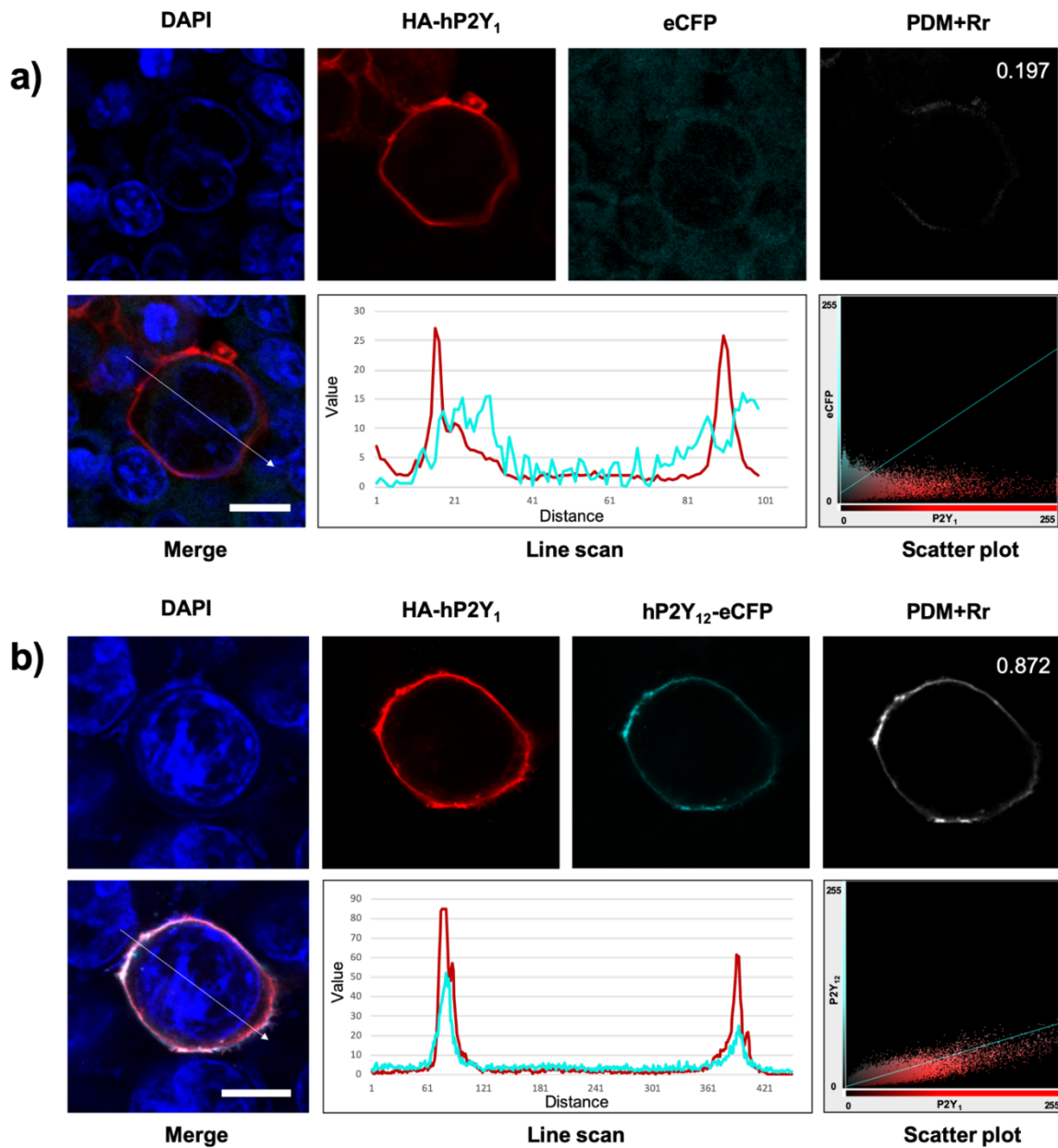
Figure 3.11: HA-hP2Y$_1$ and hP2Y$_{12}$-eCFP receptors colocalise in tSA201 cells.
Confocal microscopy of tSA201 cells showed colocalisation of HA-hP2Y$_1$ receptor and eCFP **(a);** HA-hP2Y$_1$ and hP2Y$_{12}$-eCFP **(b)** in tSA201 cell (scale bars = 10 μm). Line scans of fluorescence intensity indicate colocalisation of peak colour intensities and was applied to quantify colocalisation of both receptors with the HA and FP tag. Intensity scatter plots exhibit the distribution of cyan and red pixels for the represented images along with positive PDM value (product of the differences from the mean) and Rr=Pearson's correlation coefficient.

The opposite pairing of P2Y subtypes was studied next. Similar to eCFP, the eYFP (yellow) line scan of fluorescence (**Figure 3.12a, bottom, middle panel**), shows no overlap with HA-hP2Y$_{12}$ receptor (red) line scan, as eYFP is predominately intracellular and HA-hP2Y$_{12}$ receptors localise to the plasma membrane. The positive PDM image (**Figure 3.12a, top, right-hand panel**) shows that the overlap between the different pixels has a low PCC value that is close to zero. Furthermore, the scatter plot of intensity distributions of both, plotted against one another (**Figure 3.12a, bottom, right-hand panel**) shows a low correlation of distribution of the two proteins. Thus, eYFP does not colocalise with HA-hP2Y$_{12}$ receptors in a non-specific manner.

Next, cells were cotransfected with HA-hP2Y$_{12}$ and hP2Y$_1$-eYFP receptors (**Figure 3.12b**). In contrast to above, the line scan of fluorescence (**Figure 3.12b, bottom, middle panel**), shows that both receptors express predominantly at the plasma membrane, as previously reported in Figure 3.9b. Furthermore, the PDM image (**Figure 3.12b, top, right-hand panel**) indicates a high overlap of pixels (orange), with a PCC value that is close to one. Finally, the scatter plot of intensity distributions of both, plotted against one another (**Figure 3.12b, bottom, right-hand panel**) shows a high correlation of distribution of the two proteins. Thus HA-hP2Y$_{12}$ and hP2Y$_{12}$-eYFP receptors appear to localise close to each other in the plasma membrane.
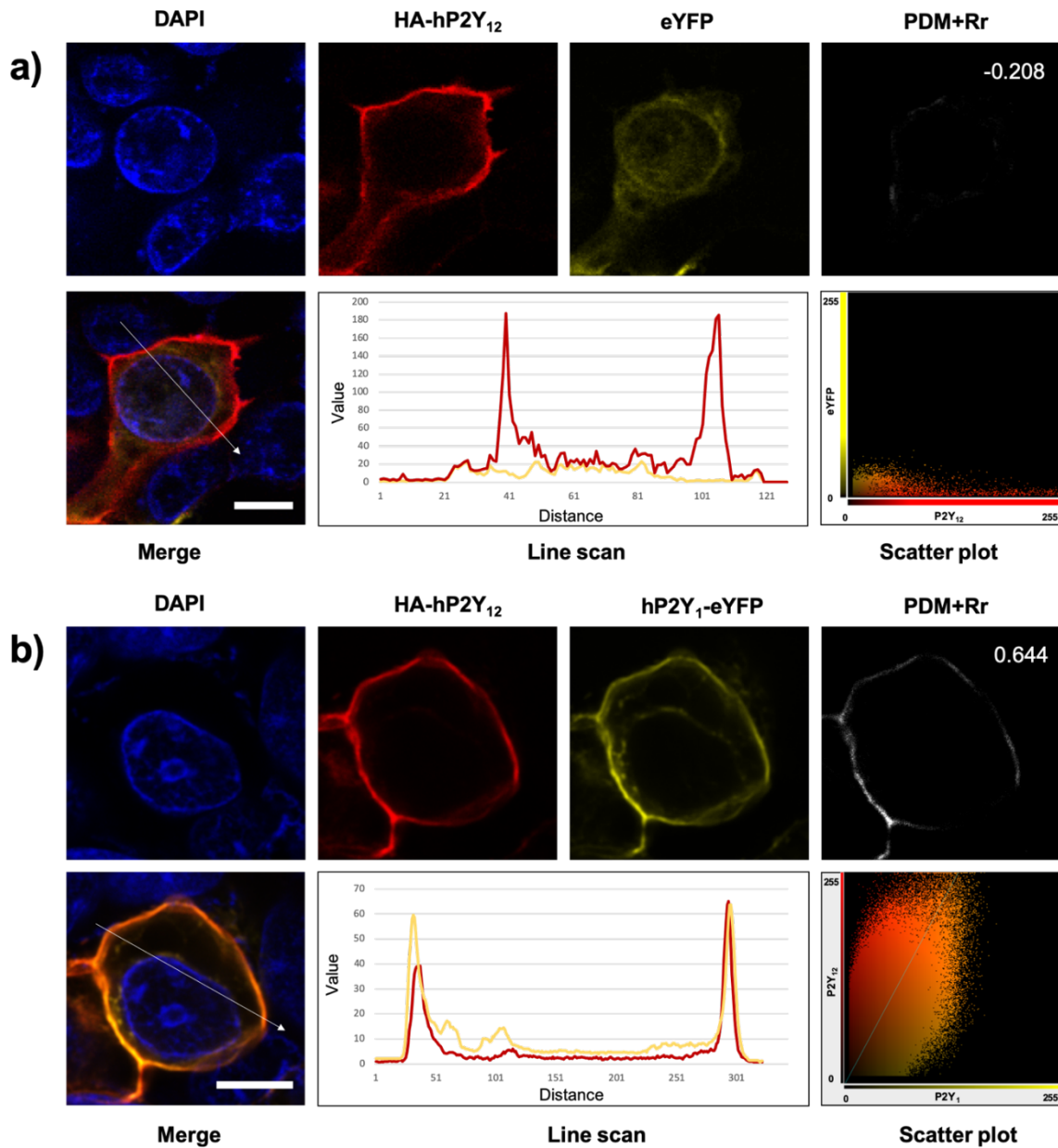
Figure 3.12: hP2Y$_1$ and hP2Y$_{12}$ receptors colocalise in tSA201 cells.
Confocal microscopy of tSA201 cells showed colocalisation of HA-hP2Y$_{12}$ receptor and eYFP **(a);** HA-hP2Y$_{12}$ and hP2Y$_1$-eYFP **(b)** in tSA201 cell (scale bars = 10 μm). Line scans of fluorescence intensity indicate colocalisation of peak colour intensities and was applied to quantify colocalisation of both receptors with the HA and FP tag. Intensity scatter plots exhibit the distribution of yellow and red pixels for the represented images along with positive PDM value (product of the differences from the mean) and Rr=Pearson's correlation coefficient.

Finally, the Pearson's coefficients for colocalisation of $P2Y_1$ and $P2Y_{12}$ receptors were analyzed statistically. As shown in **Figure 3.13**, the HA-$hP2Y_1$ receptor showed significantly more colocalisation with $hP2Y_{12}$-eCFP than with eCFP when coexpressed ($P<0.0001$). Likewise, the HA-$hP2Y_{12}$ receptor showed a significantly stronger localisation correlation when coexpressed with $hP2Y_1$-eYFP than when coexpressed with eCFP ($P<0.0001$).
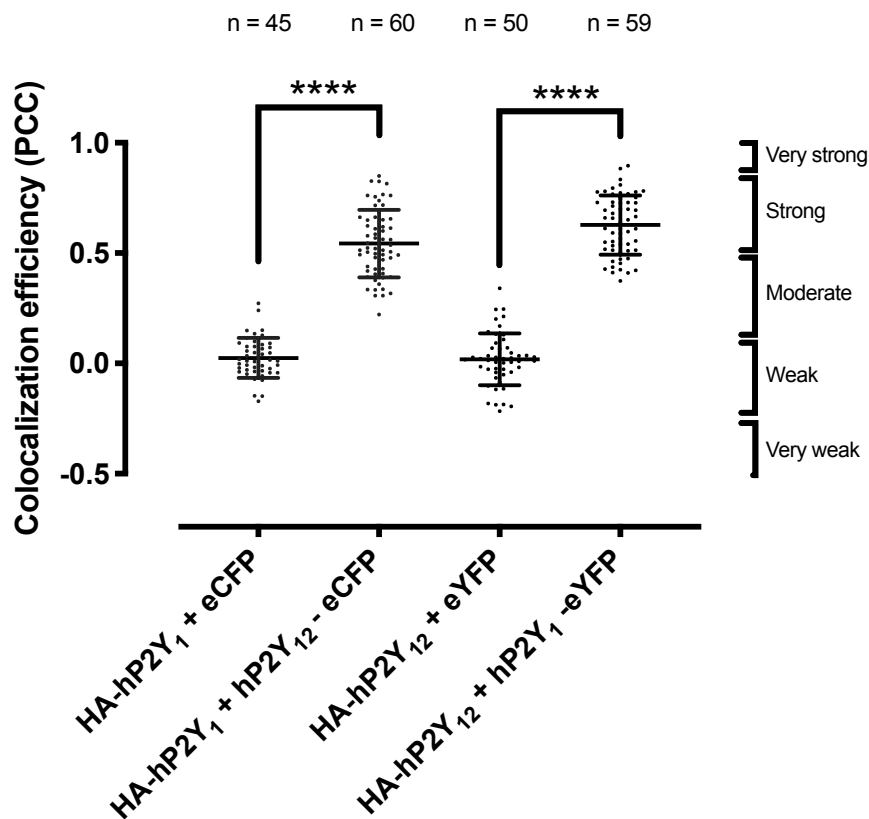
Figure 3.13: Pearson's correlation coefficients for $hP2Y_1$ and $hP2Y_{12}$ colocalisation.

The plot shows Pearson´s correlation coefficient values for the colocalisation measured in tSA201 cells cotransfected with (HA-$hP2Y_1$ and eCFP), (HA-$hP2Y_1$ and $hP2Y_{12}$-eCFP), (HA-$hP2Y_{12}$ and eYFP) and (HA-$hP2Y_{12}$ and $hP2Y_1$-eYFP). The data presented represents the average ± SD of n= 45-60 cells from three individual experiments. **** $P<0.0001$.

2.5   Investigation of cell surface expression of P2Y1 and P2Y12 receptors

The data described above indicate that recombinant $P2Y_1$ and $P2Y_{12}$ receptors localise mainly at the cell membrane when expressed in tSA201 cells, with evidence of colocalisation. The aim of the next set of experiments was to attempt to quantify the level of membrane expression by using an anti-HA antibody directed towards the extracellular HA tag. An overview of the approach used is presented in (**Figure 3.14**).
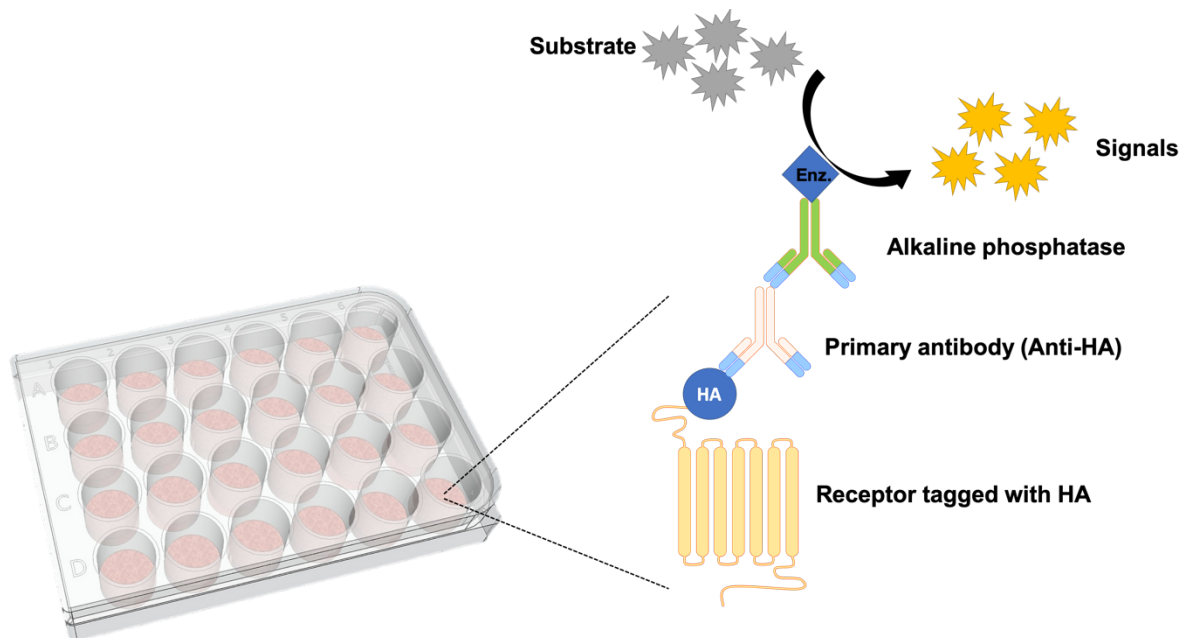
Figure 3.14: Overview of surface ELISA approach.
The schematic shows a brief overview of the cell surface ELISA method. It starts by adding anti-HA antibody to cells that express HA tagged receptors. Followed by adding anti-mouse IgG secondary antibody (conjugated with alkaline phosphatase), and alkaline phosphate substrate solution to develop signals, with absorbance measured at 405 nm using a microplate reader.

tSA201 cells transfected with $hP2Y_1$-eYFP or $hP2Y_{12}$-eCFP receptors showed no difference in absorbance compared with untransfected cells, consistent with the lack of extracellular HA tag (**Figure 3.15**). As expected, the HA tag surface expression was significantly higher in cells transfected with HA-$hP2Y_1$ or HA-$hP2Y_{12}$ receptors ($P<0.05$). There was, however, no significant difference between the two HA-tagged receptors.
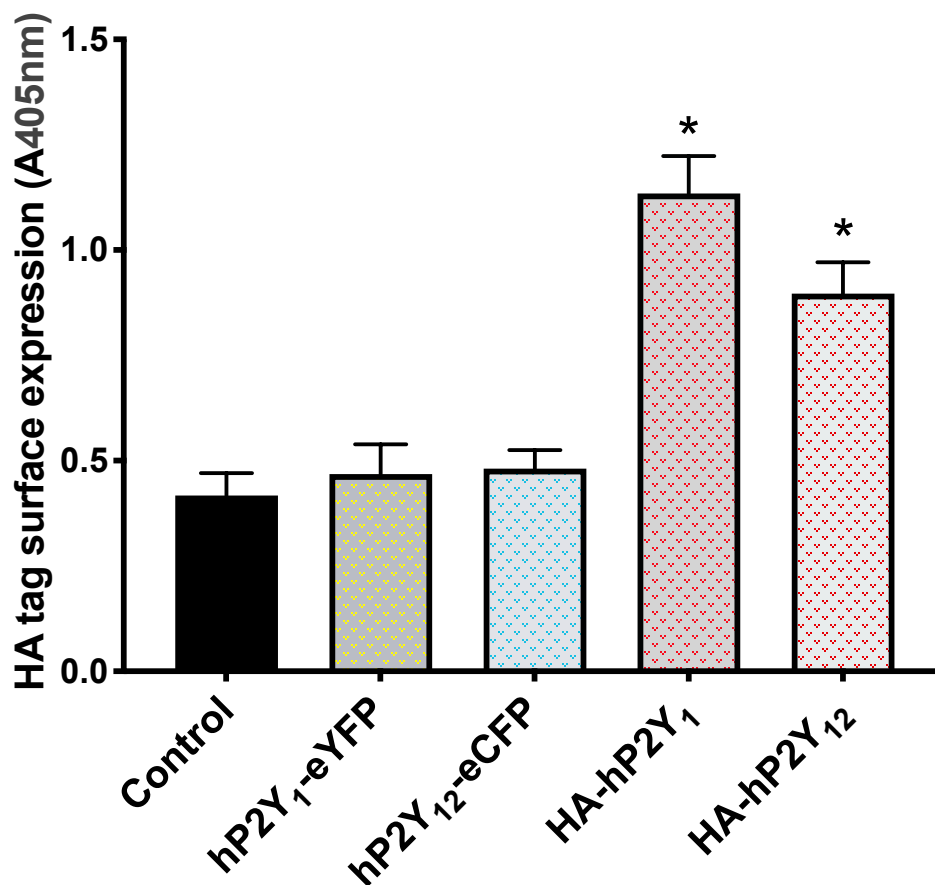
Figure 3.15: Cell surface expression of $hP2Y_1$-eYFP, $hP2Y_{12}$-eCFP, HA-$hP2Y_1$ and HA-$hP2Y_{12}$ detected using ELISA against HA.
The bars show the mean HA tag surface expression in tSA201 cells that were transfected with $hP2Y_1$-eYFP (yellow), $hP2Y_{12}$-eCFP (cyan), HA-$hP2Y_1$ (red) or HA-$hP2Y_{12}$ (red) alone, and in untransfected cells (control). Cell surface ELISA was performed and the assay plates were read at an absorbance wavelength of 405nM (A405 nm. These values are representative of three independent experiments performed in quadruplicate (*$P<0.05$ compared to the control).

So far, surface expression of HA-hP2Y$_1$ and HA-hP2Y$_{12}$ receptors have been investigated separately. In the next series of experiments their surface expression was studied after pairwise cotransfection of the HA-tagged variant of one subtype with the FP-tagged variant of the other. Thus, the HA-hP2Y$_1$ receptor was cotransfected with eCFP, hP2Y$_{12}$-eCFP or hP2Y$_1$-eYFP and the HA-hP2Y$_{12}$ receptor was cotransfected with eYFP, hP2Y$_{12}$-eCFP, hP2Y$_1$-eYFP or hPAR4-eYFP. The results in **Figure 3.16** shows that cell surface expression of the HA-hP2Y$_1$ receptor was unaffected by coexpression with any of the fluorescent proteins. Interestingly, HA-hP2Y$_{12}$ receptor surface expression was significantly reduced when coexpressed with hP2Y$_1$-eYFP or hPAR4-eYFP by ~30% and ~40% respectively (P<0.05), but were unaffected by eYFP or hP2Y$_{12}$-eCFP (**Figure 3.17**). This is the first time that hP2Y$_{12}$ receptor surface expression changes have been reported when coexpressed with PAR4 and P2Y$_1$ receptors.
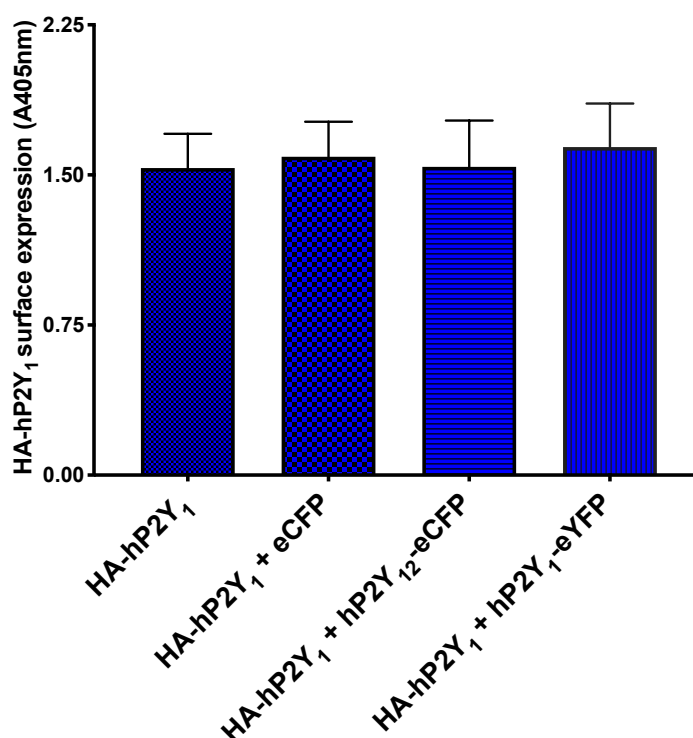
Figure 3.16: Cell surface HA ELISA to detect membrane expression of HA-hP2Y$_1$ receptor when coexpressed with other receptors
        The bars show the mean values of tSA201 cells that were cotransfected with HA tagged P2Y$_1$ receptor along with eCFP, hP2Y$_{12}$-eCFP or hP2Y$_1$-eYFP. Cell surface ELISA was performed and the assay plates were read at an absorbance wavelength of 405nm (A405nm). These values are representative of mean ± s.e.m of three independent experiments performed in quadruplicate.
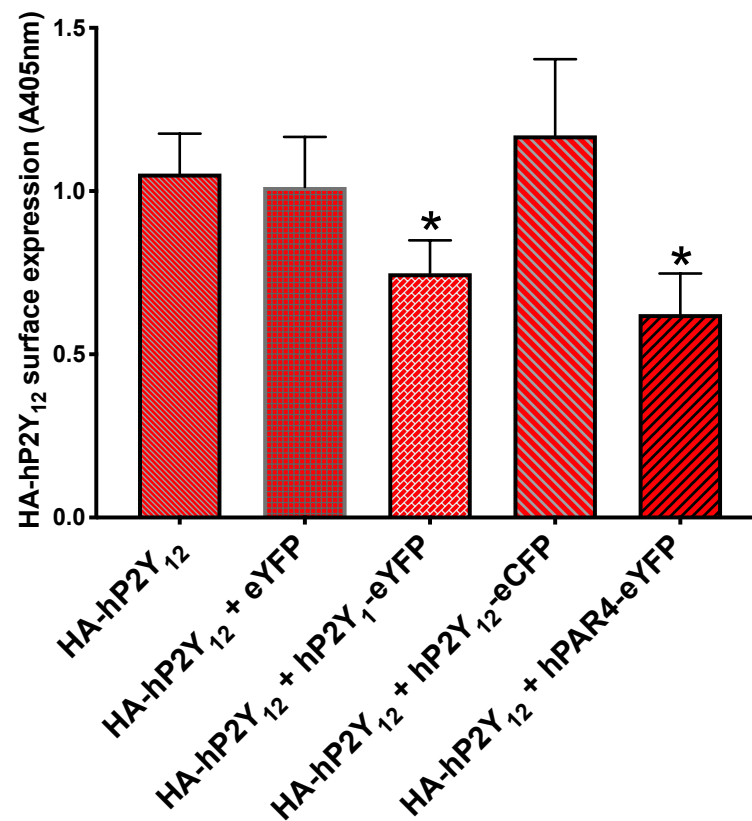
Figure 3.17: Cell surface HA ELISA to detect membrane expression of HA-hP2Y$_{12}$ receptor when coexpressed with other receptors

The bars show the mean values of tSA201 cells that were cotransfected with HA tagged P2Y$_{12}$ receptor along with eYFP, hP2Y$_1$-eYFP, hP2Y$_{12}$-eCFP or hPAR4-eYFP. Cell surface ELISA was performed and the assay plates were read at an absorbance wavelength of 405nm (A405nm). These values are representative of the mean ± s.e.m from three independent experiments performed in quadruplicate (*P<0.05, compared to HA-hP2Y$_{12}$).

2.6 Surface biotinylation of P2Y$_1$ and P2Y$_{12}$ receptors

The aim of the following experiments was to use an alternative strategy to measure changes in surface expression. An additional benefit of this approach is the ability to differentiate intracellular and surface receptor populations from the protein bands expressed. Biotinylation is a technique that that can be used to study GPCR localisation and trafficking (Hislop and Zastrow, 2011). It works by labeling the protein present at the plasma membrane with biotin, with subsequent isolation of biotin-bound protein from the total protein pool in the cell lysate by using a resin (**Figure 3.18**). For clarity, samples were named as follows: the biotinylated proteins (surface), the non-biotinylated proteins (intracellular) and the total protein extracts from WCL.
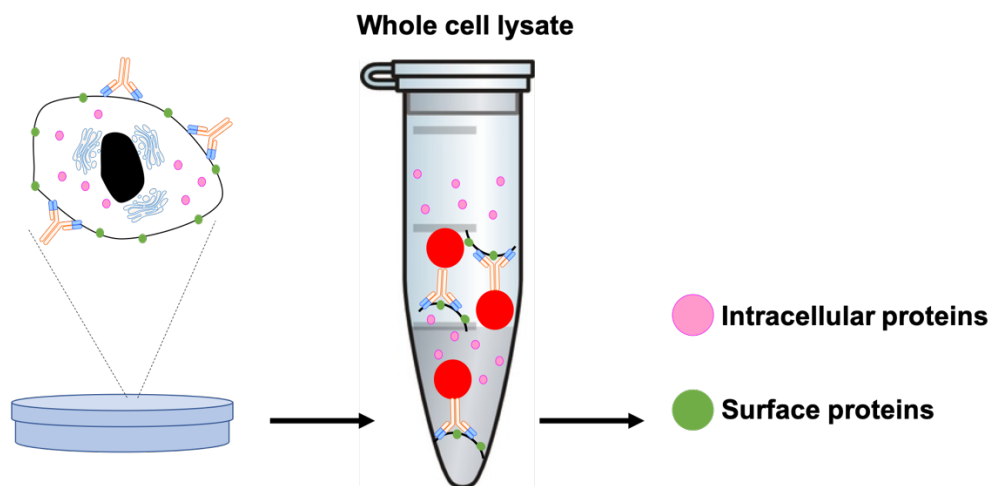
Figure 3.18: Schematic representation of cell surface biotinylation
The schematic shows a brief explanation of the cell surface biotinylation method. It starts with labeling cell surface proteins with biotin then lysing the cells and incubating with agarose beads (red) that attach to the biotin label. The beads will be attached to the surface protein (green), while the rest of the lysate will contain the intracellular proteins (pink).

Before identifying the expression of the receptors, it was essential to check the purity of the samples and avoid contamination between intracellular and surface proteins in the different samples. To do this, a mixture of different cell markers (Abcam cocktail), which contains intracellular markers (GRP78, ATP5a and GAPDH) and a surface marker (Na$^+$,K$^+$ ATPase) was used (**Figure 3.19a**). Samples are presented in triplicate and separated into surface (lane 1-3), intracellular (lane 4-6) and whole cell lysate (lane 7-9).

As shown in **Figure 3.19b** (top panel), all samples (lane 1-9) expressed a band at ~100 kDa which represents Na$^+$,K$^+$ ATPase, while the intracellular and WCL samples (lanes 4-9) expressed a ~75 kDa band and a low abundance ~60 kDa band, which represents GRP78 and ATP5a, respectively. In **Figure 3.19b** (bottom panel). GAPDH (37 kDa) expression was not detected in surface samples (lanes 1-3), but a band was expressed in all other lanes for intracellular and WCL samples (lanes 4-9).

The lack of GRP78, ATP5a and GAPDH expression in surface samples (lanes 1-3), which were positive for Na$^+$,K$^+$ ATPase, confirm that the surface fractions are pure. However, it is clear that Na$^+$,K$^+$ ATPase can be expressed both at the cell surface and intracellularly, as it was detected in all lanes.

a)

Name of the protein	Band size (kDa)	Target
Sodium Potassium ATPase	112/100	Plasma Membrane Marker
GRP78	78/75	Endoplasmic Reticulum Marker
ATP5a	60/60	Mitochondrial Membrane Marker
GAPDH	37/38	Cytosolic Marker

b)
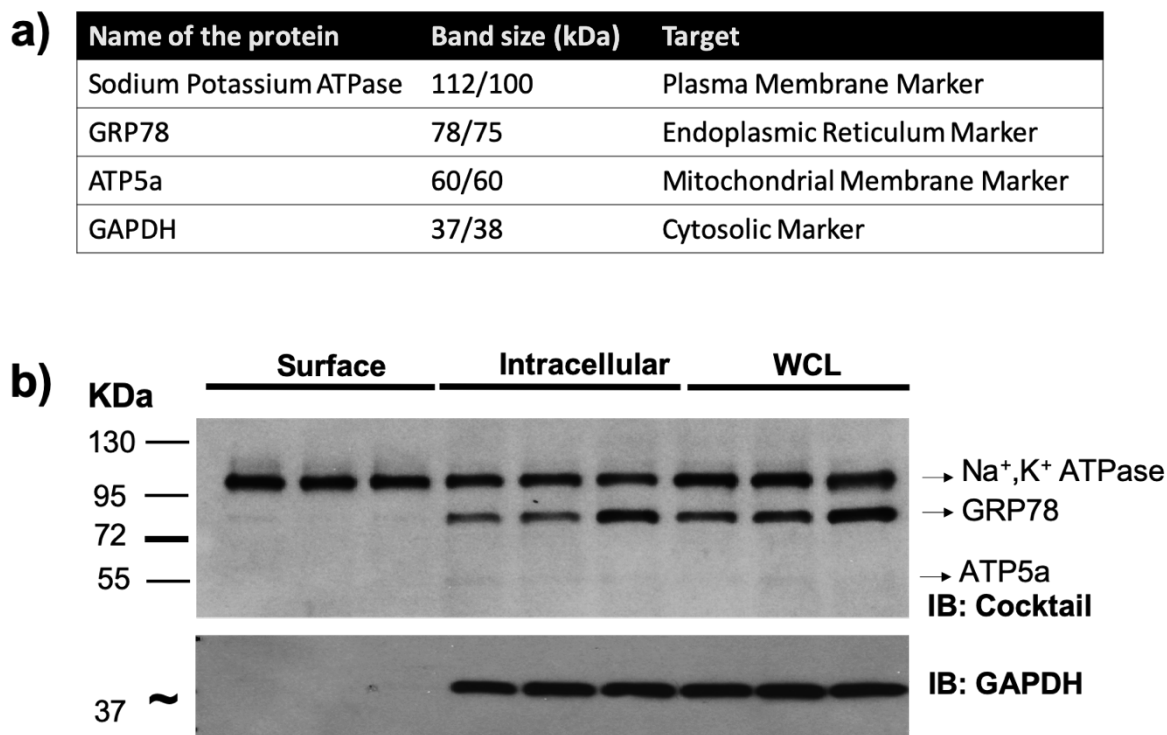
Figure 3.19: Surface biotinylation analysis of different cell lysate fractions processed by western blotting.

     a) The table indicates the protein name and target, with proposed band sizes (adapted from Abcam cocktail antibody protocol). **b)** A Western blot of surface, intracellular and whole cell lysates of tSA201 cells prepared 48 hours after transfection. Whole cells lysate (WCL) indicates the total receptors in the cells and (intracellular) indicates the fraction that was separated from the biotinylated, cell surface sample, while (surface) indicates biotinylated samples. **b, upper panel**) Abcam cocktail anti-body used to identify intracellular and surface markers, and **b, lower panel**) anti-GAPDH was used as an intracellular marker. Molecular weight markers are shown on the left. Data are representative of 3 individual experiments.

The first surface biotinylation experiment allowed for differentiation of protein bands to be detected between the surface and intracellular expression of receptors in cells cotransfected with HA-hP2Y$_1$ and CFP or HA-hP2Y$_1$ and hP2Y$_{12}$-eCFP receptors. Untransfected cells were included as a negative control for these experiments.

As shown in **Figure 3.20,** untransfected cells (UT, lanes 1, 4 and 7) did not present any non-specific bands when probed for anti-HA (top panel) or anti-GFP (middle panel), but expressed GAPDH (bottom panel) in both intracellular and WCL, but not surface, samples. When cells were cotransfected with HA-hP2Y$_1$ and eCFP (lanes 2, 5 and 8), or HA-hP2Y$_1$ and hP2Y$_{12}$-eCFP (lanes 3, 6 and 9), surface samples revealed three bands for HA-hP2Y$_1$; a faint ~36 kDa band, an abundant 50-72 kDa "smear", and a less abundant band migrating between 72-250 kDa (**top panel, lane 2 and 3**). Interestingly, the high molecular weight expression of HA-hP2Y$_1$ receptors migrating at 72-250 kDa was negligible in intracellular and WCL samples (**top panel lanes 5-9**).

No band for eCFP was detected in the surface sample (**middle panel, lane 2**), but it was expressed as a <28 kDa protein in intracellular and WCL samples (**middle panel, lanes 5 and 8**). This is consistent with the intracellular localisation of eCFP and lack of interaction with HA-hP2Y$_1$ receptors, as previously shown in Figure 3.8a.

Surface expression of hP2Y$_{12}$-eCFP revealed two clear bands; one abundantly expressed between 72-95 kDa and a higher molecular weight band resolving between 130-250 kDa (**middle panel, lane 3**). The 72-95 kDa band was less abundant in intracellular and WCL samples, (**lanes 3, 6 and 9**), however expression of the high molecular weight band was unique to surface samples (**lane 3**). Finally, **Figure 3.20** (bottom panel), shows that GAPDH was absent in the surface lanes, but present in the intracellular and WCL lanes, confirming the purity of the samples.
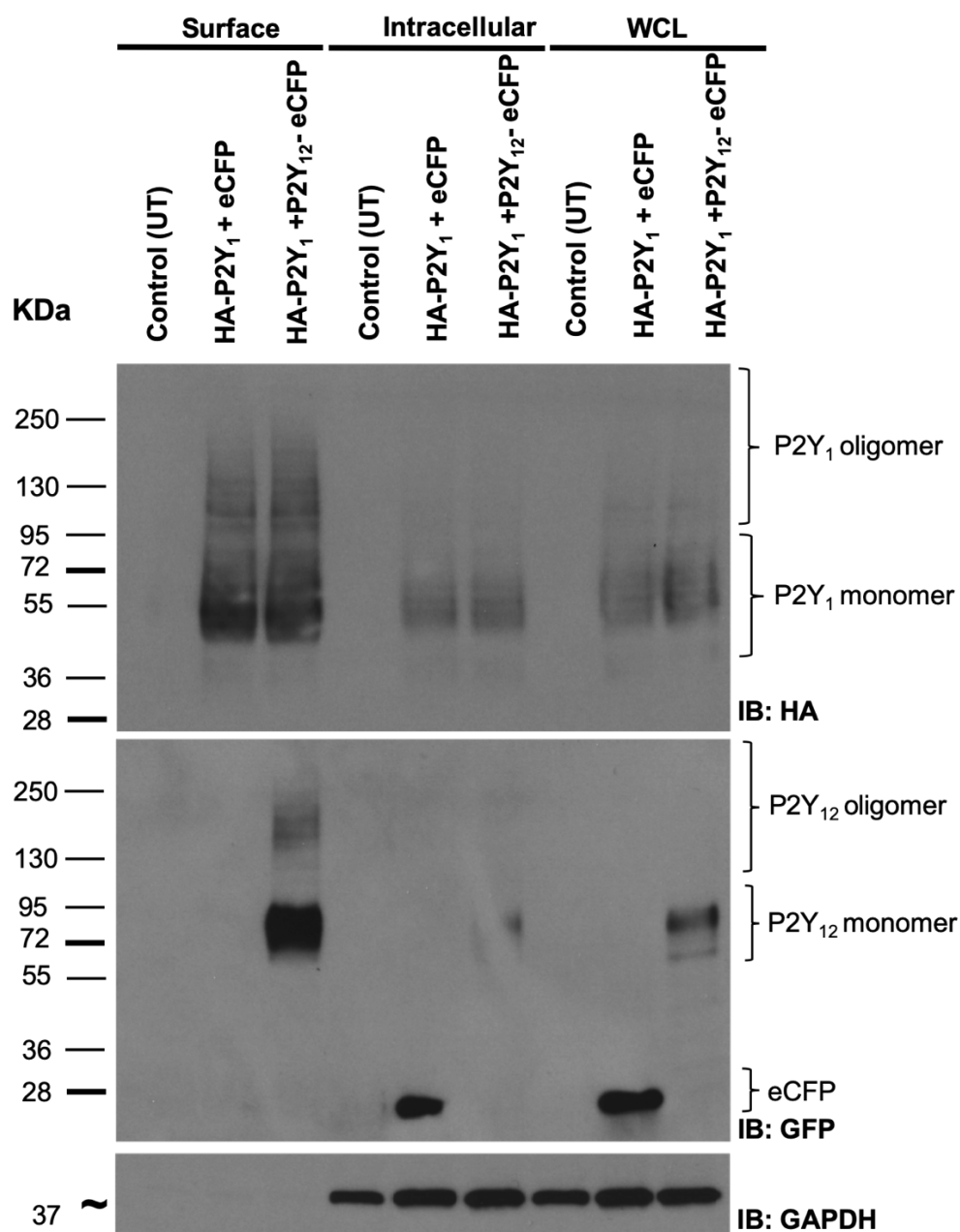
Figure 3.20: Representative surface biotinylation assay of coexpressed HA-hP2Y$_1$ and hP2Y$_{12}$-eCFP receptors in tSA201 cells.

A western blot of surface, intracellular and whole cell lysates (WCL) of tSA201 cells prepared 48 hours after cotransfection with HA-hP2Y$_1$ and eCFP (lanes 2, 5 and 8) or HA-hP2Y$_1$ and hP2Y$_{12}$-eCFP (lanes 3, 6, and 9). Untransfected cells were used as control (lanes 1, 4 and 7). (WCL) indicates the total receptors in the cells, (intracellular) indicates the samples that were not biotinylated, while (surface) indicates biotinylated samples. Samples were probed with anti-HA, anti-GFP then anti-GAPDH antibodies. Molecular weight markers are shown on the left. Data are representative of 3 individual experiments.

Surface biotinylation experiments were then repeated in cells cotransfected with HA-hP2Y$_{12}$ and eYFP or HA-hP2Y$_{12}$ and hP2Y$_1$-eYFP receptors. As shown in **Figure 3.21,** untransfected cells (UT, lanes 1, 4 and 7) did not present any non-specific bands when probed for anti-HA (top panel) or anti-GFP (middle panel), but expressed GAPDH (bottom panel) in both intracellular and WCL, but not surface, samples. When cells were cotransfected with HA-hP2Y$_{12}$ and eYFP (lanes 2, 5 and 8), or HA-hP2Y$_{12}$ and hP2Y$_1$-eYFP (lanes 3, 6 and 9), surface samples revealed three bands for HA-hP2Y$_{12}$; a faint ~36 kDa band, an abundant 50-70 kDa band, and a less abundant "smear" migrating between 72-130 kDa (**top panel, lane 2 and 3**). Interestingly, high molecular weight expression of HA-hP2Y$_{12}$ receptors migrating at 72-130 kDa was not expressed in intracellular and WCL samples (**top panel lanes 5-9**) and was not detected in previous results in Figure 3.4b. eYFP was not detected in the surface sample (**middle panel, lane 2**), but was expressed as a <28 kDa protein in intracellular and WCL samples (**middle panel, lanes 5 and 8**). This is consistent with the intracellular localisation of eYFP and lack of interaction with HA-hP2Y$_{12}$ receptors, as previously shown in Figure 3.9a.

Surface expression of hP2Y$_1$-eYFP revealed three bands; one at ~55 kDa, an abundant band between ~72-95 kDa and a higher molecular weight band resolving as a "smear" between 130-250 kDa (middle panel, lane 3). This band pattern was similar in WCL samples (middle panel, lane 9), however a different pattern emerged for intracellular samples (middle panel, lane 6). The only prominent hP2Y$_1$-eYFP band detected in intracellular samples migrated between the 95-130 kDa marker. Finally, **Figure 3.21** (bottom panel), shows that GAPDH was absent in the surface lanes, but present in the intracellular and WCL lanes, confirming the purity of the samples.

It was clear from both sets of biotinylation data that the higher molecular weight receptor protein bands for both receptors were largely expressed at the cell surface and not representative of intracellular receptor expression. We propose that these bands are receptor oligomers, as annotated in Figures 3.20 and 3.21. The lower molecular weight bands for both receptors, annotated as monomers, spanned surface and intracellular regions. These data suggest successful differentiation between the surface and intracellular localisation of P2Y$_1$ and P2Y$_{12}$ receptor expression.
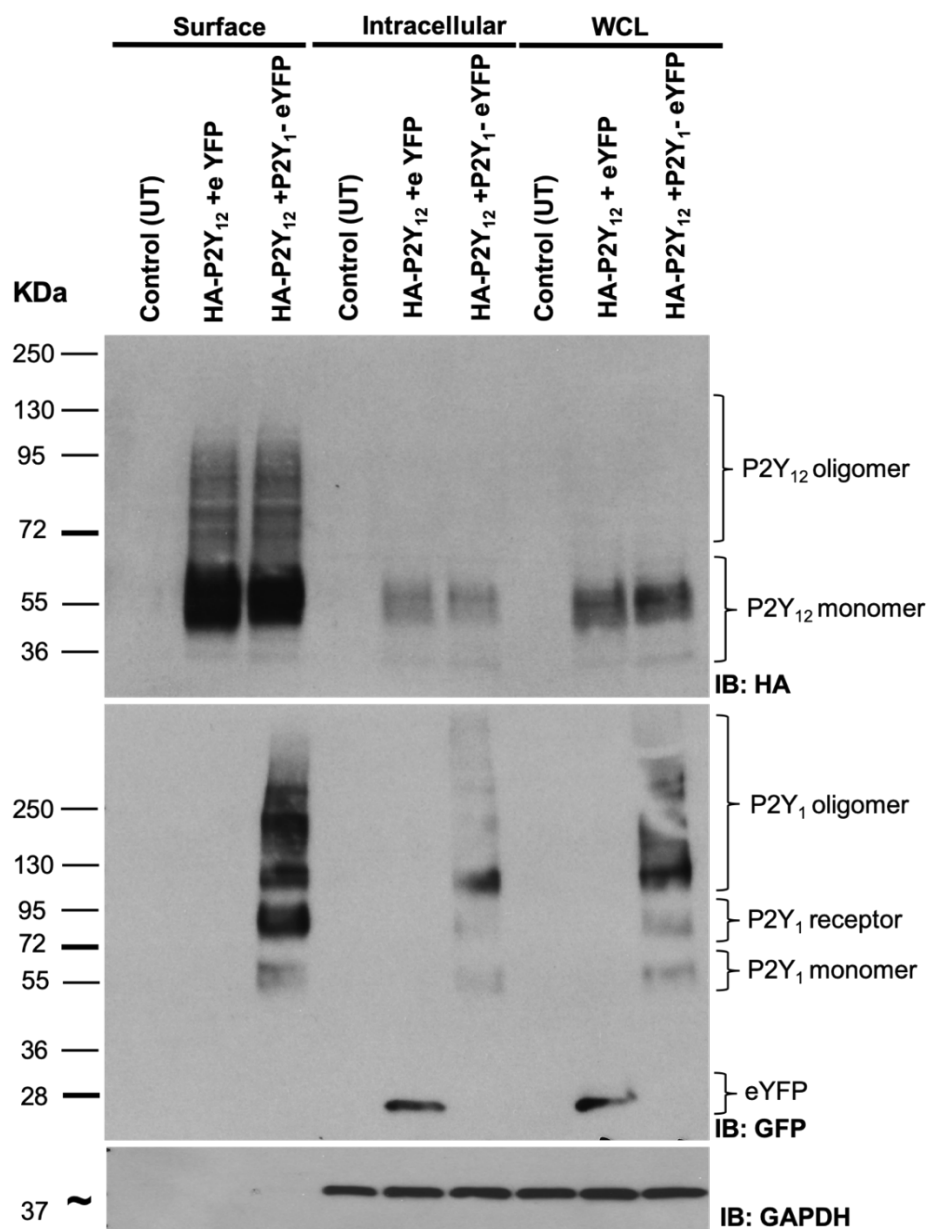
Figure 3.21: Representative surface biotinylation assay of coexpressed tagged hP2Y₁-eYFP and HA-hP2Y₁₂ receptors in tSA201 cells.
A western blot of surface, intracellular and whole cell lysates (WCL) of tSA201 cells prepared 48 hours after cotransfection with HA-hP2Y$_{12}$ and eYFP (lanes 2, 5 and 8); HA-hP2Y$_{12}$ and hP2Y$_1$-eYFP (lanes 3, 6 and 9). Untransfected cells were used as a control (lanes 1, 4 and 7). (WCL) indicates the total receptors in the cells and (intracellular) indicates the samples that were not biotinylated, while (surface) indicates biotinylated samples. Samples were probed with anti-HA, anti-GFP then anti-GAPDH antibodies. Molecular weight markers are shown on the left. Data are representative of 3 individual experiments.

2.7 The Influence of N-linked glycosylation on localisation and expression of P2Y$_1$ and P2Y$_{12}$ Receptors

It was clear from the previous receptor expression studies that transfection of the epitope-tagged receptors resulted in distinct expression of protein bands across a range of different molecular weights. Biotinylation experiments helped to categorize each protein band in relation to the surface and intracellular localised expression profiles. Whilst the bands expressed coincided closely with the predicted molecular weights of receptor monomers, dimers and oligomers, there were some bands that resolved at a molecular weight that did not all into either category. For example, Figure 3.4b revealed an abundant band that migrated as a "smear" between ~55-72 kDa for HA-hP2Y$_{12}$ receptors (predicted molecular weight 40.5 kDa). The molecular weight of this protein band is too high to represent monomers, but too small to represent HA-hP2Y$_{12}$ receptor homodimers. Likewise, the 95 kDa protein band seen in hP2Y$_1$-eYFP transfected cells. Biotinylation experiments suggested that this band was largely expressed at the plasma membrane, with a low level of intracellular expression (Figure 3.21). It was, therefore proposed that these bands are due to P2Y$_1$ and P2Y$_{12}$ receptors being post-translationally modified.

GPCR expression at the plasma membrane can be increased through the process of N-linked glycosylation, the addition of N-glycans during biosynthetic processing (Moradi et al., 2016). There are several chemical tools that can be used to inhibit N-linked glycosylation and so enable the glycosylation status of proteins to be determined (Esko et al., 2015). Here, this section focused on taking a pharmacological approach by using a specific inhibitor of N-linked glycosylation, tunicamycin, to deglycosylate receptors to assess the subsequent impact upon hP2Y$_1$ and hP2Y$_{12}$ receptor localisation and expression.

tSA201 cells were transfected with HA-hP2Y$_1$ or HA-hP2Y$_{12}$ receptor plasmid for 24 hours. They were then incubated for 16 hours in serum-free media containing 2 μg/ml tunicamycin, followed by incubation in modified DMEM for 8 hours.

Confocal microscopy confirmed that membrane localisation of HA-hP2Y$_1$ and HA-hP2Y$_{12}$ receptors was not impacted by tunicamycin (**Figure 3.22a**). Tunicamycin did, however, result in a reduction of the molecular weight of HA-hP2Y$_1$ bands, as determined by western blotting (**Figure 3.22b**). Untransfected controls (lanes 1 and 2) did not express any HA-positive proteins (top panel), but did express α-tubulin (bottom panel). In the absence of tunicamycin, two abundant bands were detected for HA-hP2Y$_1$ (lane 3); one at ~40 kDa and a second band that resolved as a continuous "smear" migrating from ~55-130 kDa. In the presence of tunicamycin (lane 4), the original ~40 kDa band was reduced and resolved below the <36 kDa molecular weight marker. Tunicamycin also reduced the continuous ~55-130 kDa "smear" to a lower molecular weight "smear" between ~45-72 kDa (**Figure 3.22b, top panel**). In cells transfected with HA-hP2Y$_{12}$ receptors, one band was detected at ~55 kDa (lane 5), which appeared to be unaffected by tunicamycin (lane 6). Interestingly, treatment with tunicamycin resulted in the appearance of a lower molecular weight band above the 36 kDa marker, which coincided with the predicted molecular weight for the P2Y$_{12}$ receptor. In **Figure 3.22b, (lower panel)** α-tubulin expression (55 kDa) was similar in each lane, confirming equal protein loading of across all samples.

These results confirmed that glycosylation does not play a role in regulating surface localisation of HA-hP2Y$_1$ or HA-hP2Y$_{12}$ receptors, but does influence the protein expression profile pattern and molecular weight of protein bands resolved by western blotting.
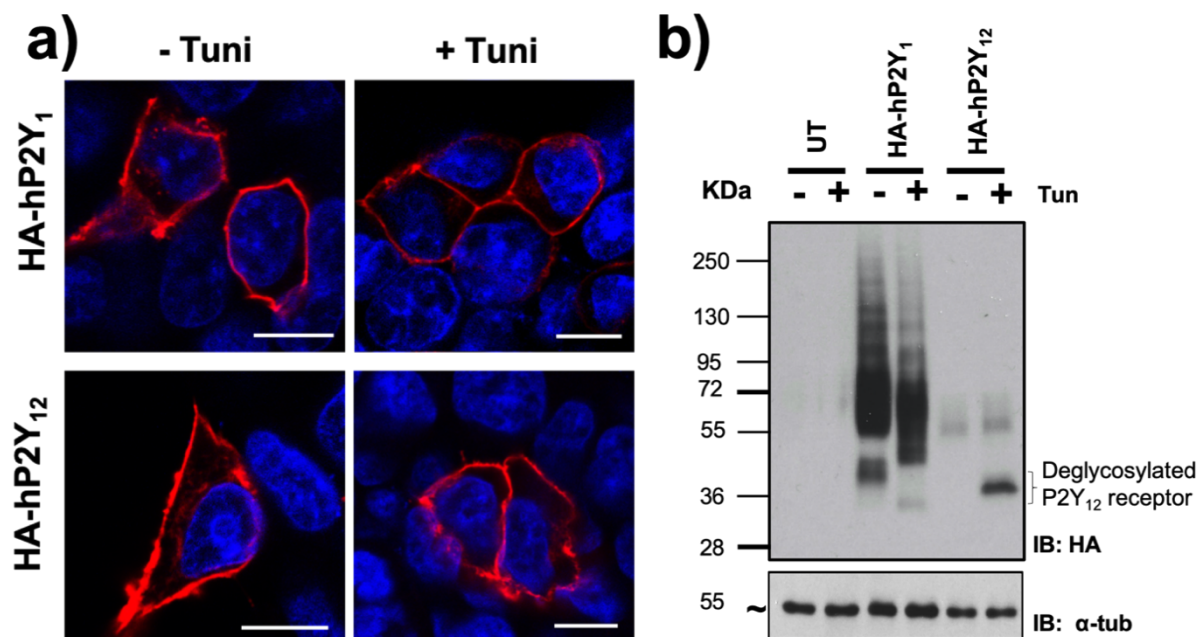
Figure 3.22: Effect of tunicamycin treatment on cell surface expression and glycosylation of HA-hP2Y$_1$ and HA-hP2Y$_{12}$ receptors.

  a) Representative images of tSA201 cells 48 hours after transfection with HA-P2Y$_1$ (top row) and HA-hP2Y$_{12}$ (bottom row) receptor without (left column) and after (right column) treatment with 2 µg/ml of tunicamycin for 16 hours, are shown. Cells were subjected to indirect immunostaining of the HA tag expression and visualised at 63x (oil) magnification (scale bar = 10 µm); (red) HA and (blue) DAPI for nuclear staining. **b)** A western blot of whole cell lysates of tSA201 cells prepared 48 hours after transfection with HA-hP2Y$_1$ receptor (lanes 3 and 4) and HA-hP2Y$_{12}$ receptor (lanes 5 and 6) without **(-)** and after **(+)** treatment with tunicamycin. Untransfected (UT) samples were used as control (lanes 1 and 2). Samples were probed with anti-HA antibody (top panel), then reprobed with anti-α-tubulin (α-tub) antibody to confirm equal loading of samples (lower panel). Data are representative of 3 individual experiments.

These experiments were repeated in cells transfected with the FP-tagged hP2Y$_1$ hP2Y$_{12}$ receptors. Confocal microscopy confirmed that the membrane localisation of hP2Y$_1$-eYFP and hP2Y$_{12}$-eCFP receptors were unaffected by tunicamycin (**Figure 3.23a**), however, an intracellular pool of both receptors became more prominent compared to untreated samples.

In agreement with results obtained for HA-tagged receptors, tunicamycin similarly impacted the molecular weight of protein bands expressed for FP-tagged receptors in western blots (**Figure 3.23b**). In the absence of tunicamycin, several bands were detected for hP2Y$_1$-eYFP receptor (lane 1); one band ~55 kDa, a second band between 72-95 kDa followed by a continuous protein "smear" from ~95 kDa to > 250 kDa (**Figure 3.23b, top panel**). In the presence of tunicamycin (lane 2), hP2Y$_1$-eYFP receptor, the original 55 kDa band decreased below the 55 kDa molecular marker, a new band appeared below the 72 kDa marker, which coincided with a decrease in the abundance of the 72-95 kDa. The molecular weight of this new band resolved at the same size as the predicted molecular weight for the hP2Y$_1$-eYFP receptor (68 kDa). The continuous smear from 95 kDa to >250 kDa was largely unaffected by tunicamycin.

In cells transfected with hP2Y$_{12}$-eCFP receptors (**Figure 3.23b, top panel, lane 3**), one abundant band of 72-95 kDa was expressed in the absence of tunicamycin. Following treatment with tunicamycin (lane 4), the abundance of this band decreased, which coincided with the appearance of a new lower molecular weight band resolving between the 55-72 kDa marker. The size of this new band corresponds with the predicted molecular weight for the hP2Y$_{12}$-eCFP receptor (66 kDa). Finally, for cells that were transfected with eCFP (lanes 5 and 6), a band was expressed above the 28 kDa marker expressed, which remained unchanged in the absence and presence of tunicamycin. In **Figure 3.23b, (lower panel)** α-tubulin expression was similar in each lane at 55 kDa.

Based on these results, P2Y1 and P2Y$_{12}$ receptors undergo N-linked glycosylation, which accounts for the different band sizes resolved by western blotting. However, pharmacological dysregulation of glycosylation by tunicamycin does not impact surface localisation of either receptor.
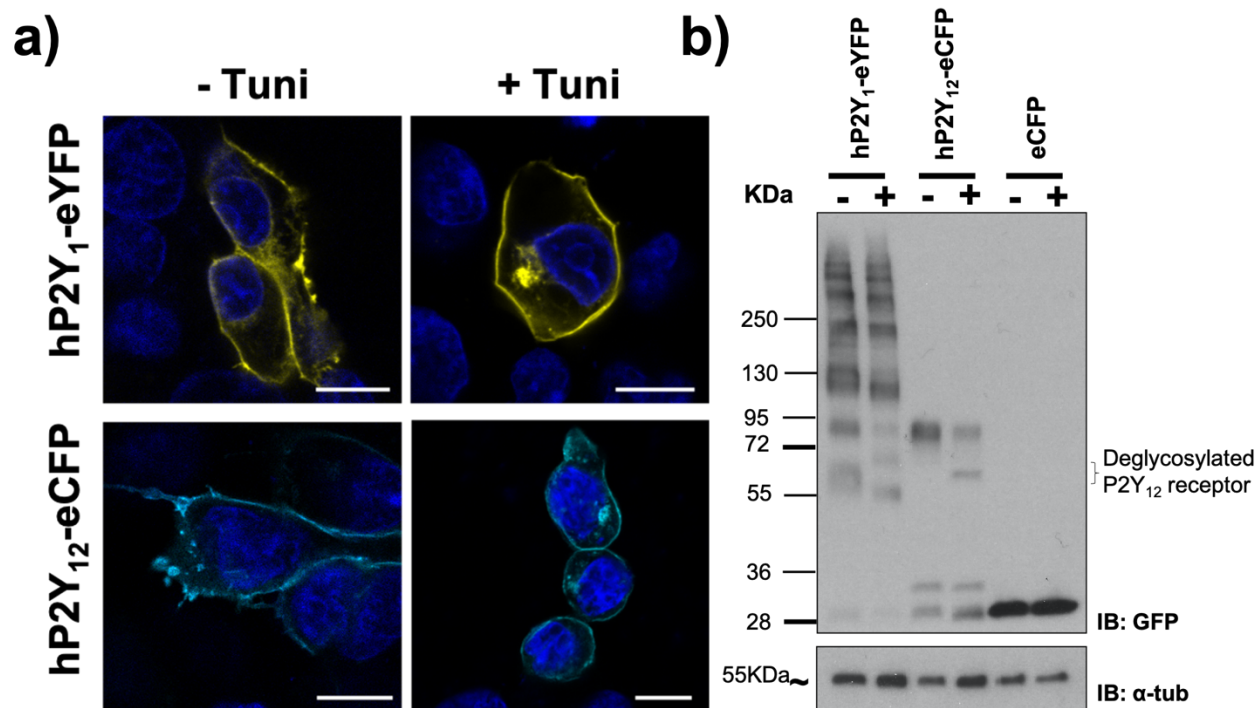
Figure 3.23: Effect of tunicamycin treatment on cell surface expression and glycosylation of hP2Y$_1$-eYFP and hP2Y$_{12}$-eCFP receptors.
a) Representative images of tSA201 cells 48 hours after transfection with hP2Y$_1$-eYFP (top row) and hP2Y$_{12}$-eCFP (bottom row) receptor without (left column) and after (right column) treatment with 2 μg/ml of tunicamycin for 16 hours are shown. Cells were visualised at 63x (oil) magnification (scale bar = 10 μm); (yellow) eYFP, (cyan) eCFP and (blue) DAPI for nuclear staining. **b)** A western blot of whole cell lysates of tSA201 cells prepared 48 hours after transfection with hP2Y$_1$-eYFP receptor (Lane 1 and 2), hP2Y$_{12}$-eCFP receptor (Lane 3 and 4) and eCFP (Lane 5 and 6) without **(-)** and after **(+)** treatment with tunicamycin. Samples were probed with an anti-GFP antibody (top panel) and reprobed with an α-Tubulin (α-tub) antibody to confirm equal loading of samples (lower panel). Data are representative of 3 individual experiments.

2.8 The influence of disulphide bonds on P2Y$_1$ and P2Y$_{12}$ receptor expression and coexpression

Disulphide bonds have an essential role in protein folding and stability (Darby and Creighton, 1995). The P2Y$_1$ receptor has two disulphide bonds, one that connects the N-terminus (Cys42) to extracellular end of transmembrane 7 (TM7) (Cys296), which is a critical region for receptor activation. The other disulphide bond connects TM3 (Cys124) to the second extracellular loop (Cys202), which is thought to be critical for proper receptor trafficking to the cell surface (Hoffmann et al., 1999; Moro et al., 1999; Zhang et al., 2015). In contrast, the P2Y$_{12}$ receptor only has one disulphide bond that links the N-terminus (Cys17) with TM7 (Cys270) (Zhang et al., 2014b), which are important sites for receptor expression (Mansour et al., 2020). Other residues, (Cys97) and (Cys175), are able to interact with the thiol moieties of drug metabolites, such as clopidogrel (Savi et al., 2006). The next experiments, therefore, focused on the involvement of disulphide bonds in protein expression of the epitope tagged P2Y$_1$ and P2Y$_{12}$ receptors. This was carried out by using different concentrations of dithiothreitol (DTT) to reduce disulphide bonds (Alliegro, 2000).

All blotting experiments conducted in the previous sections of this thesis were carried out using reducing conditions with a final concentration of 50 mM DTT in the sample buffer as standard. Here, experiments were carried out to identify if removal of or lower concentrations of DTT influenced HA-hP2Y$_1$, hP2Y$_1$-eYFP, HA-hP2Y$_{12}$ or hP2Y$_{12}$-eCFP receptor expression. Transfected cells were lysed in sample buffer with no DTT (control) or in sample buffer containing 3 different concentrations of DTT (0.5, 10 and 50 mM) as described previously by for P2Y$_{12}$ receptors (Savi et al,. 2006). Changes in receptor expression and multimerization was quantified using immunoblotting with densitometry analysis of the different protein bands.

As shown in **Figure 3.24a**, in the absence of DTT (lane 1) the HA-P2Y$_1$ receptors were expressed as two bands; one was a lower molecular weight "smear", which migrated at between 55-95 kDa and the second band was a highly abundant "smear" resolving from 130 kDa to >250 kDa. The latter band was annotated as being P2Y$_1$ oligomers. Increasing the concentration of DTT from 0.5 to 50 mM (lanes 2-4) resulted in a significant loss of this high molecular weight HA-P2Y$_1$ receptor complex, as shown in the representative blot (a) and densitometry data presented in **Figure**

3.24b. This coincided with the appearance of lower molecular weight bands at ~40 kDa, which has been described in previous sections for monomeric HA-P2Y$_1$ receptor expression. Treatment with 50 mM DTT resulted in expression that was approximately one third of the control value (P<0.05). The intensities of the dimer band (~80 kDa) and monomer "smear" at ~55-95 kDa were unchanged, but the 40 kDa lower band (LB) monomer form was nearly doubled, though this effect was not significant.

Experiments were repeated to assess the impact of DTT upon hP2Y$_1$-eYFP receptor expression (**Figure 3.24c**). In the absence of DTT (lane 1), three bands were detected in hP2Y$_1$-eYFP transfected cells; one band resolved above the 55 kDa marker, a second band migrated between 72-95 kDa and an abundant continuous "smear" was expressed from 130 kDa to >250 kDa. Unlike previous results demonstrating DTT sensitivity of HA-hP2Y$_1$ receptor expression, increasing concentrations of DTT (lanes 2-4) did not significantly change the expression levels of any of these hP2Y$_1$-eYFP bands. This was quantified by densitometry of the different bands, shown in **Figure 3.24d**. Total α-tubulin expression across the samples are shown for each representative blot (55 kDa). It should be noted that some experiments experienced changes in the migration of α-tubulin when DTT concentrations were changed (see **Figure 3.24a, bottom panel**).

These results highlight clear differences in the DTT sensitivity between the HA and FP epitope tagged hP2Y$_1$ receptors. Whilst HA-hP2Y$_1$ receptor expression appear sensitive to DTT concentration, hP2Y$_1$-eYFP receptors expression display resistance to disulphide bond reduction by DTT. This will be discussed later.
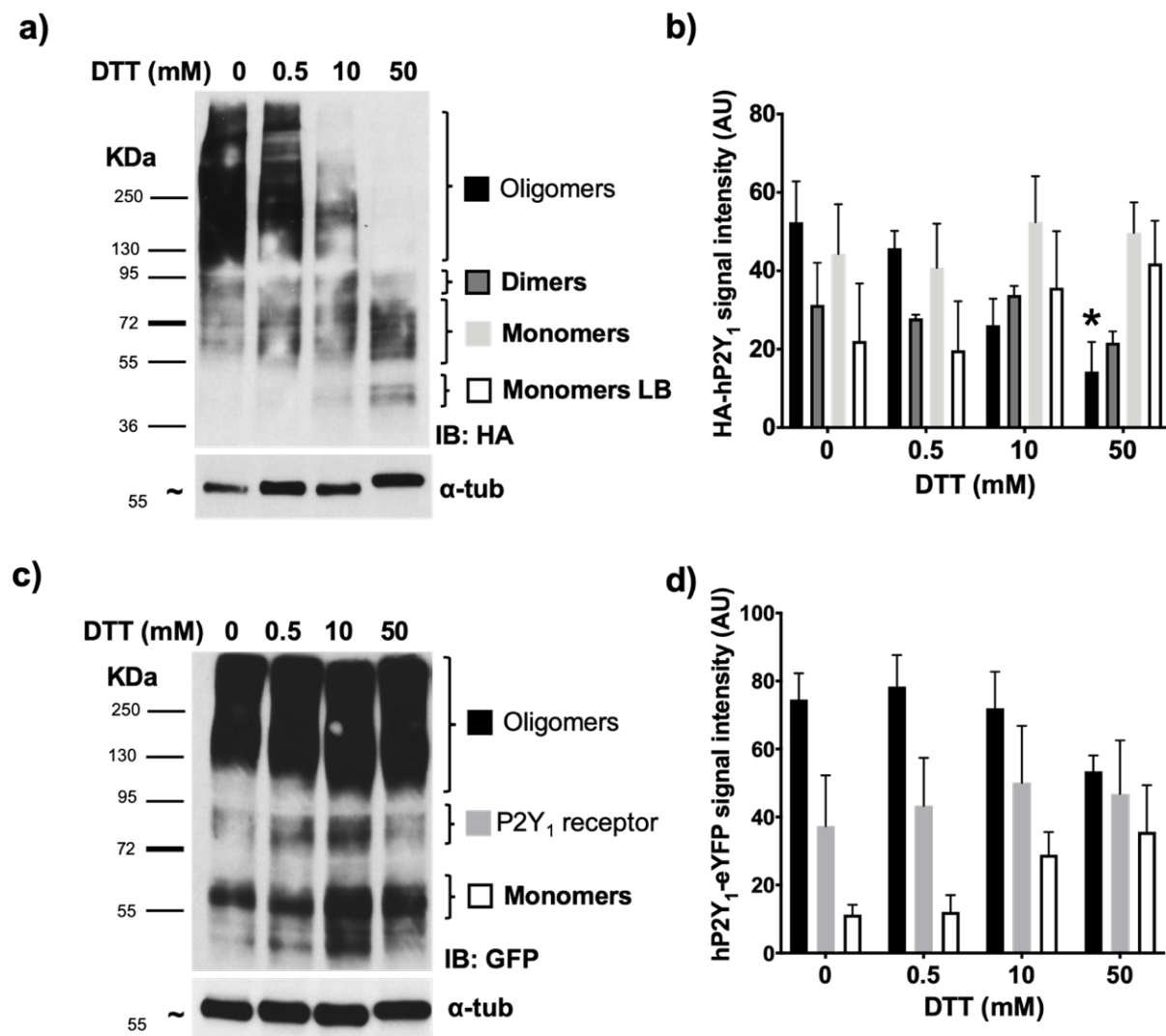
Figure 3.24: Disruption of the oligomeric form of P2Y$_1$ expressed in tSA201 cells by DTT.

Immunoblots of receptor expression in whole cell lysates of tSA201 cells transfected with HA-hP2Y$_1$ **(a)** and hP2Y$_1$-eYFP receptors **(c)** in the absence (0) and presence of DTT (0.5, 10 and 50 mM) are shown. The receptors were detected using specific antibodies against HA **(a)** and GFP **(c)** respectively. Molecular weight markers are shown on the left. Blots shown were reprobed with an α-Tubulin (α-tub) antibody to confirm equal loading of samples (a and c, lower panel). The data are expressed as mean ± s.e.m of the band signal intensity for HA-hP2Y$_1$ **(b)** and hP2Y$_1$-eYFP **(d)** receptor as measured by densitometry from three individual experiments. *$P < 0.05$ compared to the untreated cells.

Experiments were repeated to assess the sensitivity of the HA and FP-epitope tagged $P2Y_{12}$ receptors to DTT. In the absence of DTT (**Figure 3.25a, lane 1**), HA-$P2Y_{12}$ receptors were expressed as three abundant bands; one > the 36 kDa marker, a second "smear" between ~45-72 kDa and a high molecular weight continuous "smear", which migrated from 95 kDa to >250 kDa. Increasing the concentration of DTT from 0.5 to 50 mM (**lanes 2-4**) resulted in a significant loss of this high molecular weight HA-$P2Y_{12}$ receptor complex, as shown in the representative blot (a) and densitometry data presented in **Figure 3.25b**. The other HA-$P2Y_{12}$ receptors bands were not significantly affected by DTT treatment. These results mirror those obtained for HA-$hP2Y_1$ receptor expression.

Next, the effect of DTT upon $hP2Y_{12}$-eCFP receptor expression was assessed (**Figure 3.25c**). In the absence of DTT (lane 1), two bands were detected in $hP2Y_{12}$-eCFP transfected cells; one resolved between the 72-95 kDa molecular marker and the second migrated as an abundant continuous "smear" from 130 kDa to >250 kDa. Increasing the concentration of DTT to 10 mM (lane 3) and 50 mM (lane 4) resulted in a significant loss of the high molecular weight $hP2Y_{12}$-eCFP complex ($P<0.05$). The other $hP2Y_{12}$-eCFP receptors bands were not significantly affected by DTT treatment. Blotting results were quantified by densitometry of the different receptor bands, shown in **Figure 3.25d**. Total α-tubulin expression (55 kDa) across the samples is shown for each representative blot in **Figure 3.25a, c, bottom panel**.

These results highlight that both HA and FP epitope tagged $hP2Y_{12}$ receptors display sensitivity to disulphide reduction by DTT, with expression of the high molecular weight receptor complex more susceptible to disruption. Of the plasmids tested, only the $hP2Y_1$-eYFP receptor oligomeric complex displayed resistance to DTT-dependent disulphide bond disruption.
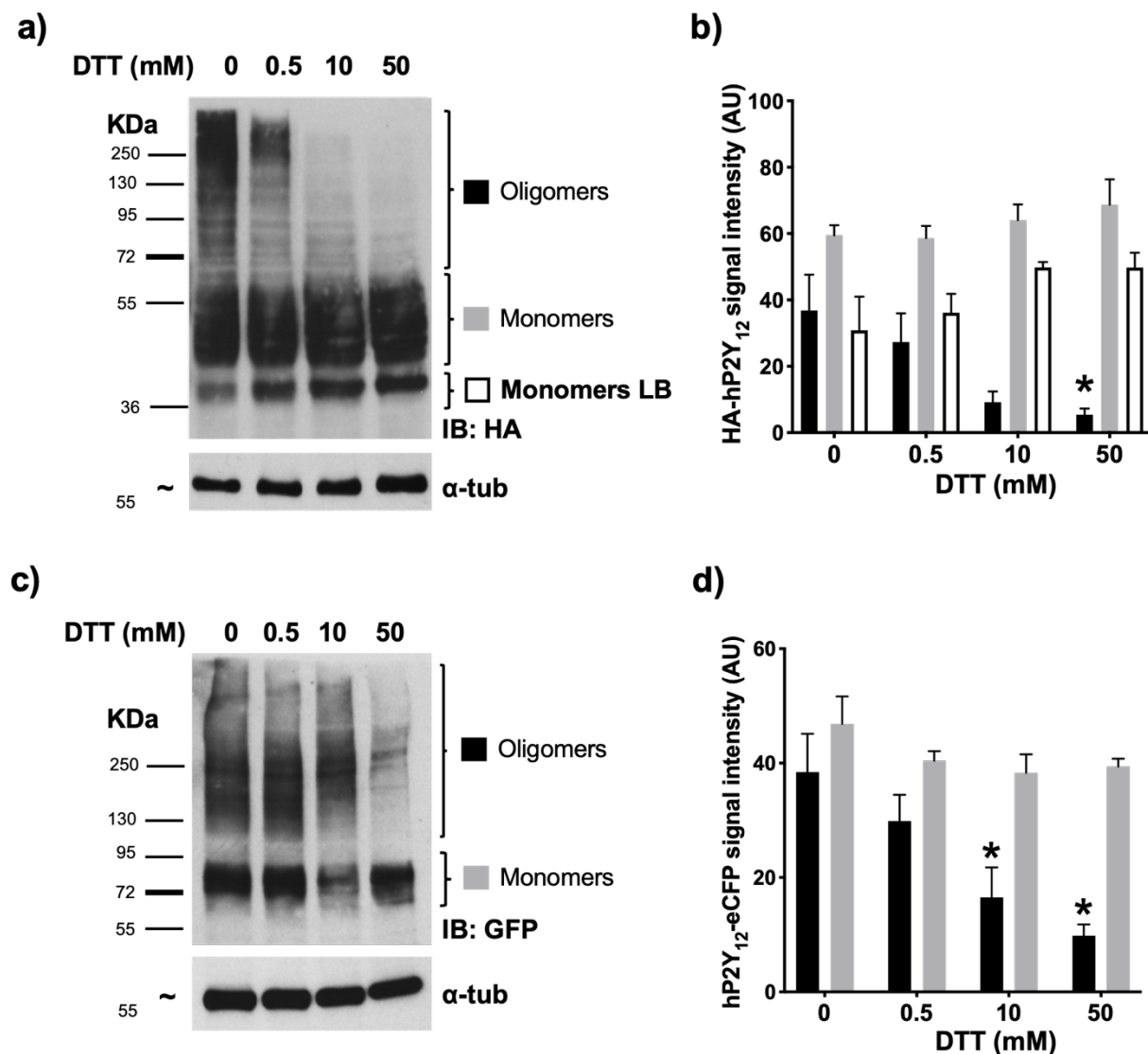
Figure 3.25: Disruption of the oligomeric form of P2Y$_{12}$ receptor expressed in tSA201 cells by DTT.

Immunoblots of receptor expression in whole cell lysates of tSA201 cells transfected with HA-hP2Y$_{12}$ **(a)** and hP2Y$_{12}$-eCFP receptors **(c)** in the absence (0) and presence of DTT (0.5, 10 and 50 mM) are shown. The receptors were detected using specific antibodies against HA **(a)** and GFP **(c)** respectively. Molecular weight markers are shown on the left. Blots shown were reprobed with an α-Tubulin (α-tub) antibody to confirm equal loading of samples (a and c, lower panel). The data are expressed as mean ± s.e.m of the band signal intensity for HA-hP2Y$_{12}$ **(b)** and hP2Y$_{12}$-eCFP **(d)** receptor as measured by densitometry from three individual experiments. *P<0.05 compared to the untreated cells.

2.9   ADP-dependent internalisation of hP2Y$_1$ & hP2Y$_{12}$ receptors

All the experiments carried out have placed focus on receptor expression in the absence of agonists, with the receptors presumed to be in their inactive state. An increasing amount of data suggests that quaternary complexes can be regulated by ligand binding (Milligan et al., 2019), and that Class A GPCR dimers (Calibiro et al., 2013) may be transient. Previous studies have even demonstrated that agonist-dependent co-internalisation of the hP2Y$_{12}$-PAR4 heteromeric complex are important to trigger specific cell signalling events (Smith et al., 2017). Here, the aim was to optimise epitope tagged ADP-induced internalisation and assess the impact of receptor coexpression on these events.

Visualisation of receptor internalisation in fixed cells using confocal microscopy (**Figure 3.26**). tSA201 cells expressing hP2Y$_1$-eYFP or hP2Y$_{12}$-eCFP were treated with ADP (10µM) for 5 and 30 minutes. As previously described, both receptors were evident at cell surface (**Figure 3.26**, left column). In the first 5 minutes post ADP (10µM) treatment, it was clear in both receptors are expressed on the cell membrane, which indicate the starting of internalisation (**Figure 3.26**, middle column). At 30 minutes post treatment with ADP, both hP2Y$_1$-eYFP and hP2Y$_{12}$-eCFP receptor remain expressing on cell membrane (**Figure 3.26**, right column). For that, more sensitive technique is needed to quantify the surface expression of the receptors.
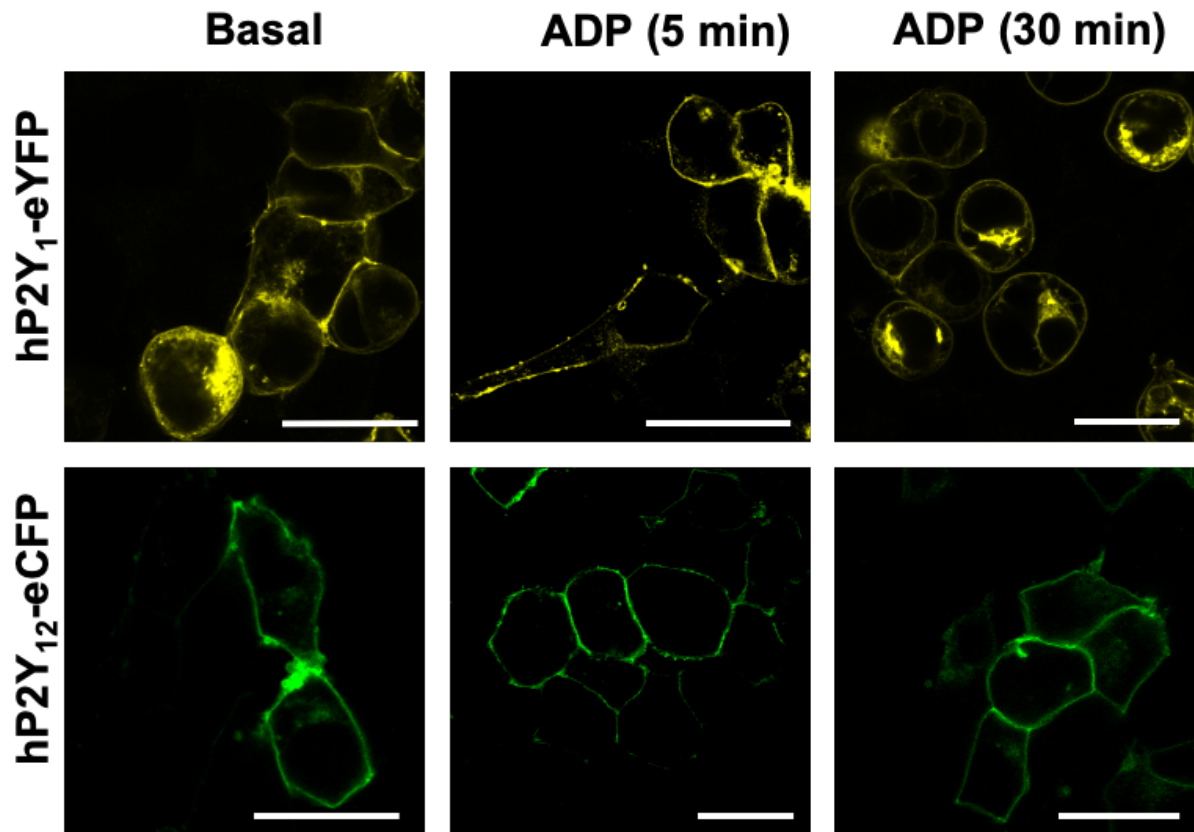
Figure 3.26: Visualisation of ADP-promoted internalisation of hP2Y$_1$ and hP2Y$_{12}$ receptors.

Representative images of fixed tSA201 cells 48 hours after cotransfection with hP2Y$_1$-eYFP receptors (top row) and hP2Y$_{12}$-eCFP receptors (bottom row) are shown. The nuclear staining by DAPI (blue), hP2Y$_1$-eYFP receptors (yellow) and hP2Y$_{12}$-eCFP (green). The untreated cells (left column) were compared to cells that treated with ADP for 5 minutes (middle column) and 30 minutes (right column). The images were obtained using confocal microscopy and cells were visualised at 63x (oil) magnification (scale bars = 20 µm).

Surface ELISA was used to quantify changes in receptor expression at the plasma membrane (**Figure 3.27**). tSA201 cells expressing HA-hP2Y$_1$ or HA-hP2Y$_{12}$ alone or coexpressing HA-hP2Y$_1$ and hP2Y$_{12}$-eCFP or HA-hP2Y$_{12}$ and hP2Y$_1$-eYFP is shown. Cells treated with ADP (10µM) showed a loss of surface HA receptor expression over a time course of 0, 5, 15, 30 or 60 minutes. When HA-hP2Y$_1$ and HA-hP2Y$_{12}$ receptors were expressed on their own, ADP (10µM) induced their internalisation, with a loss of surface HA signal detected after 5 minutes, which reached peak at 15-30 minutes (28.9 ± 3.9% and 20.8 ± 7.8%, respectively). Receptor recycling was evident, with surface receptor recovery observed after 60 minutes exposure to ADP. This was more notable for HA-hP2Y$_{12}$ than HA-hP2Y$_1$ receptors. Interestingly, when each HA-tagged receptor was coexpressed with the other subtype that was FP-tagged (i.e. HA-hP2Y$_1$ with hP2Y$_{12}$-eCFP and HA-hP2Y$_{12}$ with hP2Y$_1$-eYFP), ADP (10µM) no longer induced internalisation of the receptors. Thus, coexpression of hP2Y$_1$ and hP2Y$_{12}$ receptors block their internalisation induced by ADP. These events have not been reported before and warrants further investigation to address the question of whether HA-hP2Y$_1$ or HA-hP2Y$_{12}$ receptors form heterodimers.
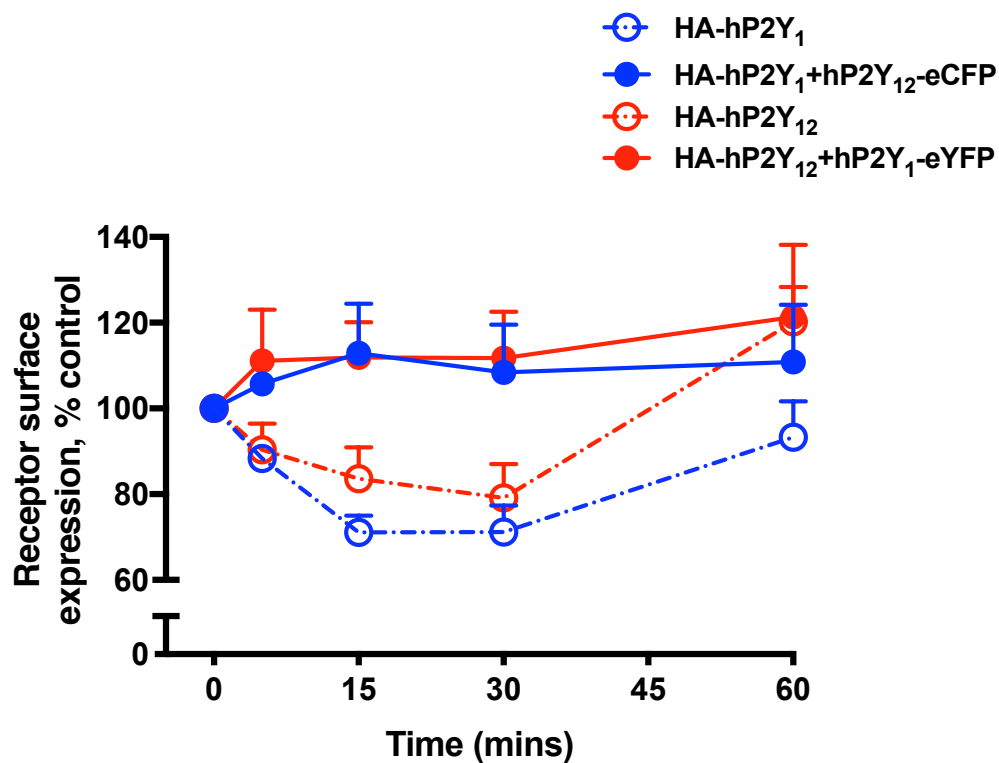
Figure 3.27: ADP-promoted internalisation of hP2Y$_1$ and hP2Y$_{12}$ receptors.
The graph shows the HA-hP2Y$_1$ and HA-hP2Y$_{12}$ receptor expression levels at the plasma membrane of tSA201 cells when transfected on their own or cotransfected with hP2Y$_{12}$-eCFP or hP2Y$_1$-eYFP respectively, before (0 min) or during administration of ADP (10 µM) for 60 min. Cell surface expression was measured using ELISA at an absorbance wavelength of 405 nm (A405 nm). The data are expressed as a percentage of the control HA-tagged receptor expression measured immediately before addition of ADP and represent the average ± standard error in duplicate from three individual experiments.

3   Discussion

The outcomes of the basic experiments performed in this chapter not only provided valuable insights into receptor transfection efficiency, but also confirmed preservation of typical GPCR transmembrane localisation, with the identification of distinct protein bands profiles that allowed for discrimination between surface and intracellular receptor populations. Furthermore, characterization of Ca^{2+} signalling mediated by the epitope-tagged P2Y receptors showed that the fusion of the tags to the receptors did not impact the ability of the receptors to function.

Plasma membrane expression

In the current study, tSA201 cells provided an ideal model in which to investigate the functional expression of $P2Y_1$ and $P2Y_{12}$ receptors, as this system has been reported to produce consistently high levels of recombinant protein expression, with minimal toxicity to the cell (Venkatachalan et al., 2007). In my experiments, all $P2Y_1$ and $P2Y_{12}$ tagged receptors retained plasma membrane surface expression, irrespective of the location or type of tag. This is consistent with previous studies in 1312N1, CHO and HEK293 cells that reported that HA-tagged $P2Y_1$ and $P2Y_{12}$ receptors express at the cell surface (Mundell et al., 2008; Smith et al., 2017, Zhong et al., 2004; Savi et al., 2006).

Whilst these data reveal no issues with the HA-tag on the extracellular region of each receptor, a concern was that the C-terminal tagging of the receptors with eCFP and eYFP may affect receptor expression or function. This was because of the presence of Postsynaptic Density 95/disc large/Zonula occludens-1 (*PDZ*)-binding *motifs* at the extreme C-tail of $P2Y_1$ and $P2Y_{12}$ receptors (Nisar et al., 2011, 2012; Cunningham et al., 2013b), which play a major role in the recruitment of important PDZ-binding proteins, such as the Na^+-H^+ Exchanger Regulatory factor-1 (NHERF-1), in receptor endocytosis. Other studies have also implicated the C-terminal region as an important feature for receptor-mediated G_q activation (Ding 2005). The present demonstration of effective internalisation of $hP2Y_1$-eYFP and $hP2Y_{12}$-eCFP receptors in response to ADP shows that C-terminal tagging was not an issue. This is consistent with previous studies using rat $P2Y_1$-GFP-expressing HEK293 cells (Tulapurkar et al., 2004) and tagged $P2Y_1$ plasmids in Jurkat cells (Baurand et

al., 2000), which did not find any issues related to receptor endocytosis in these recombinant systems. A C-terminal hexahistidine tag has also been reported to not compromise receptor function (Hoffmann et al., 1999). Thus, P2Y$_1$ and P2Y$_{12}$ receptors appear to be able to tolerate C-terminal tagging with eYFP and eCFP.

The influence of disulphide bonds

The data obtained in this study for expression of HA-hP2Y$_{12}$ and hP2Y$_{12}$-eCFP receptors showed good agreement and align with published findings (Savi et al., 2006). HA-hP2Y$_{12}$ and hP2Y$_{12}$-eCFP receptor expression were both found to be sensitive to the thiol reducing agent, DTT, which breaks the disulphide bonds formed in the receptors. That was consistent with previous data (Savi et al., 2006; Ding et al., 2009). This indicates that disulphide bonds play an important role in the formation of hP2Y$_{12}$ receptor oligomers. The hP2Y$_{12}$ receptor crystallized as a dimer, but without disulphide bonds between the two receptors (Zhang et al., 2014b). It may be that breaking S-S bonds in the extracellular region of the hP2Y$_{12}$ receptor changes its conformation, which in turn alters the ability of hP2Y$_{12}$ receptors to interact physically with each other.

The same agreement was not, however, always observed between expression of HA-hP2Y$_1$ and hP2Y$_1$-eYFP receptors, as there were clear differences in the sensitivity to DTT-mediated reduction. HA-hP2Y$_1$ receptors were readily reduced upon increasing concentrations of DTT, as seen by the loss of high molecular weight receptor expression, suggesting a role for disulphide bonds in the formation of multimeric HA-hP2Y$_1$ complexes. The presence of the C-terminal eYFP tag on the P2Y$_1$ receptor, however, appeared to confer resistance to DTT, indicating potential protein stabilization differences between HA-hP2Y$_1$ and hP2Y$_1$-eYFP receptor plasmids.

The importance of extracellular disulphide bonds is known for hP2Y$_1$ ligand recognition (Moro et al., 1998; Neumann et al., 2020) with mutational analysis of Cys^{124} and Cys^{202} demonstrating that disulphide bonding between these cysteines is critical for proper receptor trafficking of the human P2Y$_1$ receptor to the cell surface (Hoffmann et al., 1999). Blotting data from that study, probing for the C-terminal hexahistidine epitope tag, revealed a similar P2Y$_1$ receptor expression profile, with the typical high molecular weight 'smear'. Interestingly, mutational analysis of all critical

cysteine residues (with alanine substitution) did not affect the abundance of the high molecular weight receptor bands expressed, which coincides with the lack of DTT effect in hP2Y$_1$-eYFP expressed in tSA201 cells. Whilst these blots were processed by SDS-PAGE, the reducing conditions were not stated in the methods. Presumably, no reducing agent was added to samples due to the purpose of the study and the critical role of DTT in reducing disulphide bonds, which would have prevented the role of cysteine residues being addressed. In light of the differences observed between HA-hP2Y$_1$ and hP2Y$_1$-eYFP receptor expression under reducing conditions, going forward it would be prudent to use a combination of different techniques to assess receptor-receptor interactions that do not solely rely upon either receptor and expression analysis via blotting where reducing conditions may add complications to data interpretation. Therefore, in subsequent chapters, co-immunoprecipitation, which is a standard technique for detection of protein-protein interaction, will be used in combination with microscopy-based approaches, including proximity ligation assay (PLA) and fluorescence lifetime imaging microscopy Förster resonance energy transfer (FLIM-FRET).

Receptors trafficking

Surface biotinylation experiments confirmed high molecular weight P2Y complexes were typically expressed at the cell surface, however it was clear that whilst all epitope tagged receptors were N-glycosylated, this was not essential for hP2Y$_1$ or hP2Y$_{12}$ receptor delivery to the cell surface. This is consistent with a previous study which identified that the addition process of the oligosaccharide may increase the molecular weight of the receptor, but does not affect P2Y$_{12}$ receptor folding and cell surface delivery (Zhong et al., 2004). That study highlighted N-linked glycosylation as being essential for the surface expression for other purinergic receptors like P2X receptor, however, no role for glycosylation was found for either P2Y$_1$ or P2Y$_{12}$ receptors in facilitating cell surface delivery.

Functional expression of receptors

Functional receptor expression was assessed using Ca^{2+} flux in response to ADP as the bioassay. In the present study, overexpression of HA-hP2Y$_1$ or hP2Y$_1$-

YFP receptor cDNA caused a leftward shift in the ADP concentration-response curve, with a corresponding decrease in the EC_{50} in compare with endogenous $P2Y_1$ experiments. This is consistent with there being a raised number of binding sites present and receptor overexpression (Chen et al., 2000). Overexpression of either tagged receptor also caused a significant reduction in the Hill slope compared to endogenous $hP2Y_1$ responses. The EC_{50} value for ADP acting at the endogenous $hP2Y_1$ receptor in tSA201 cells is similar to previously published values obtained in other HEK-293 type cell lines (Mundell and Benovic, 2000; Werry et al., 2002; Jones et al., 2014). Receptor overexpression results in a higher receptor density, which increases proportional occupancy (Jarvis and Thompson, 2019).

In the current study, AR-C69931MX significantly suppressed the Ca^{2+} response evoked by ADP in tSA201 cells in which either of the $hP2Y_{12}$ receptor plasmids was expressed, with responsiveness to ADP restored after washout. This demonstrated that $hP2Y_{12}$ receptors were functionally expressed, as AR-C69931MX has no effect on the endogenous $hP2Y_1$ receptors inducing the Ca^{2+} signal (Suzuki et al., 2011) and in the absence of $hP2Y_{12}$ receptor transfection (Kennedy, unpublished data). The data are also consistent with the electrophysiological data of Shrestha et al., (2010), which suggested that recombinant $hP2Y_{12}$ receptors interact with endogenous $hP2Y_1$ receptors to produce AR-C69931MX-sensitive responses. The current data also indicated that the presence of tags did not interfere with $hP2Y_1$ and $hP2Y_{12}$ receptor activity and they could be functionally expressed in the tSA201 cell line for further investigations.

Receptors internalisation

In the current study, ADP induced internalisation of both receptors within 5 minutes and maximum internalisation was seen at 15 to 30 minutes. The internalisation was not maintained, however, and the cell surface expression of both subtypes recovered after 60 minutes exposure to ADP. The same concentration of ADP, 10µM, also activated and internalised both receptors in platelets (Jin et al., 1998; Cattaneo, 2015). The process underlying internalisation was not studied further here, but NHERF-1 and -2, which are PDZ motif-binding proteins, regulate $P2Y_1$ and $P2Y_{12}$ receptor internalisation via interacting with their C-terminal tail (Nisar et al., 2011,

2012; Cunningham et al., 2013b). The small GTP-binding protein, ADP ribosylation factor 6 (Arf6), also regulates dynamin-dependent $P2Y_1$ and $P2Y_{12}$ receptor internalisation in human platelets (Kanamarlapudi et al., 2012). The recycling mechanism for $P2Y_1$ and $P2Y_{12}$ receptors are not similar. $P2Y_1$ receptor internalisation depends on PKC activity (Mundell et al., 2006; Reiner et al., 2009), and they were then recycled slowly by Sorting Nexin 1 (Nisar et al., 2010). In contrast, $P2Y_{12}$ receptor internalisation depends on GRK2 and GRK6 activities (Hardy et al., 2005), and they are then recycled rapidly back to the plasma membrane via a Rab4/11-dependent trafficking pathway (Cunningham et al., 2013a). In platelets, the recycling for both $P2Y_1$ and $P2Y_{12}$ receptors play a vital role in keeping the receptor more responsive to endogenous ADP (Mundell et al., 2008).

Interestingly, when $P2Y_1$ and $P2Y_{12}$ receptors were coexpressed, ADP-induced internalisation was abolished. There are many ways that this data could be interpreted. While this could be a feature of potential dimerisation, it may also be an artifact of overexpression. As previously mentioned, the mechanisms of internalisation of both $P2Y_1$ and $P2Y_{12}$ receptors relies upon interaction with PDZ proteins NHERF1/2 (**Figure 3.28**). In the event where both receptors are over-expressed, there will be a higher demand for endogenous NHERF1/2 to accommodate efficient internalisation. In the absence of sufficient NHERF levels, receptor internalisation may be reduced. While this was not followed up here, to test this theory, experiments could be repeated with over-expression of NHERF in addition to both receptors to assess if internalisation reappears.

A previous study found that the coexpression of the $P2Y_1$ receptor with the $P2Y_{11}$ receptor had the opposite effect in that it promoted agonist-induced internalisation of the $P2Y_{11}$ receptor (Ecke et al., 2008). This was inhibited by the $P2Y_1$ selective antagonist, MRS2179, but not by the selective $P2Y_{11}$ antagonist, NF157. Whilst the $P2Y_1$ receptor is regulated by NHERF1/2, there is no studies prove that the $P2Y_{11}$ receptor is also regulated by NHERF1/2. Thus, the lack of internalisation of both $P2Y_1$ and $P2Y_{12}$ receptor in the current study, may be due to the high demand for NHERF1/2. Following on from these studies, the ability of $P2Y_1$ and $P2Y_{12}$ receptors to form heterodimers was tested.
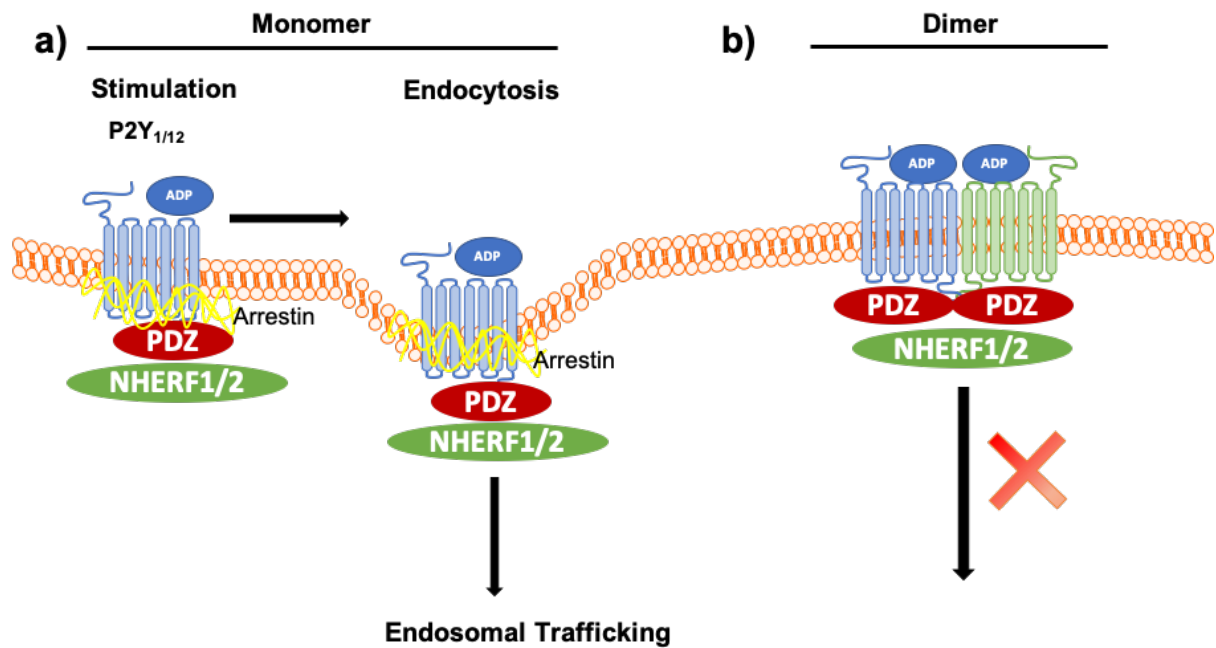
Figure 3.28: Possible internalisation mechanism for P2Y$_1$ and P2Y$_{12}$ receptors.
  a) Receptor activation causes Arrestin to bind to the receptor and promote phosphorylation. The interaction between Arrestin and NHERF1/2 directs the receptor to a distinct population of clathrin-coated pits for internalisation. **b)** The coexpression of both P2Y$_1$ and P2Y$_{12}$ receptor leads to both activated receptors to remain on the cell surface.

Chapter Four

Investigating heterodimer formation between P2Y$_1$ and P2Y$_{12}$ receptor

1   Introduction

The results in **Chapter thee** demonstrated that both recombinant $P2Y_1$ and $P2Y_{12}$ receptors were predominantly colocalised in the plasma membrane with a high PCC. When the $P2Y_1$ receptor was coexpressed with the $P2Y_{12}$ receptor, it decreased $P2Y_{12}$ receptor surface expression in the recombinant system. Deglycosylation did not inhibit $P2Y_1$ and $P2Y_{12}$ receptor expression at the membrane, indicating that N-linked glycosylation has no role in membrane localisation. $P2Y_{12}$ oligomers, with both tags, were dissociated by the reducing agent, DTT, to its monomeric form, whereas only $P2Y_1$ oligomers with an HA (N-terminus) tag and not $P2Y_1$ oligomers with a YFP (C-terminus) tag were reduced to its monomeric form. These results confirmed the presence of disulphide bonds in these receptors. However, differences in the tagging having an impact upon the sensitivity to DTT. From the experiments carried out in **Chapter three**, both $P2Y_1$ and $P2Y_{12}$ receptors were internalised by the agonist ADP. This was blocked entirely when these receptors were coexpressed with each other. By using ADP-evoked Ca^{2+} release as a bioassay, the presence of endogenous $P2Y_1$ receptor in tSA201 cells was confirmed. Furthermore, when $P2Y_{12}$ receptors were expressed, the inhibitory effects of AR-C69931MX on ADP-evoked Ca^{2+} release were consistent with the suggestion of a protein-protein interaction between the $P2Y_1$ and $P2Y_{12}$ receptors. Thus, in this chapter the focus was on investigating dimer formation between $P2Y_1$ and $P2Y_{12}$ receptors, with a multi-pronged approach adopted by employing several complimentary methods to assess potential receptor-receptor interactions.

The experiments carried out in this chapter aimed to identify if there is a physical association between $P2Y_1$ and $P2Y_{12}$ receptors. Co-IP experiments were used to identify if the interaction takes place between $P2Y_1$ and $P2Y_{12}$ receptor in lysed tSA201 cells. PLA experiments were applied to visualise the interaction between the receptors. Also, the effects of $P2Y_1$ and $P2Y_{12}$ receptor agaonists and antagonists on dimer formation were investigated. FLIM-FRET was used to further characterise the interaction between the receptors and to measure the possible distance between the protomers before and after treatment with ligands.

2   Results

2.1   Determination of physical interaction between $P2Y_1$ and $P2Y_{12}$ receptors via co-immunoprecipitation

Co-IP, used with western blotting, is a valuable technique for isolating proteins of interest from lysed cells (Hall, 2005). For the past several decades this method been key for the study of protein–protein interactions and is often the tool of choice when investigating GPCR dimerisation.

In the next experiments, co-IP was used to detect interaction between $P2Y_1$ and $P2Y_{12}$ receptors **(Figure 4.1)**. tSA201 cells were either untransfected (lane 1 and 4) or cotransfected with HA-$P2Y_1$ and CFP (lanes 2 and 5) or HA-$P2Y_1$ and $P2Y_{12}$-eCFP (lanes 3 and 6), and samples were treated with 50mM of DTT. In untransfected cells (lanes 1 and 4) no bands were detected when probed with either anti-GFP (top panel) or anti-HA (middle panel) antibodies. Immunoprecipitation (IP) of the HA tag was performed (lanes 1-3) and confirmed expression and immunoprecipitation of the HA-$P2Y_1$ receptor (lanes 2 and 3, middle panel). Whole cell lysates (WCL, lanes 4-6) were used to identify total receptor expression, the band pattern for the HA-$P2Y_1$ receptor was similar to that described in previous experiments in chapter 3. Three abundant protein bands were detected for the HA-h$P2Y_1$ receptor when expressed alone; one at 40 kDa, a ~52-95 kDa protein "smear" and a higher molecular weight protein smear between 130-250 kDa. No expression of HA-$P2Y_1$ receptor was detected following immunoblotting for the FP tag using an anti-GFP antibody (IB: GFP, top panel, lanes 2 and 5). Similarly, no CFP expression was detected in IP lane 2 but it was detected in WCL lane 5 (~30kDa). This confirmed successful CFP transfection, but no interaction between HA-$P2Y_1$ receptors and the CFP tag (lanes 2 and 5).

When $P2Y_{12}$-eCFP was coexpressed with the HA-$P2Y_1$ receptor and probed with the anti-GFP antibody (top panel), a high molecular weight complex ~130 to >250KDa was detected in IP lane 3 and WCL lane 6. A second low abundance band was also detected between 72-95 kDa in IP lane 3, which was more abundant in WCL lane 6. The presence of $P2Y_{12}$-eCFP in the HA-IP lane confirmed that HA- $P2Y_1$ could retrieve $P2Y_{12}$-eCFP receptors when coexpressed, which suggests that these receptors may interact physically. Interestingly, when coexpressed with $P2Y_{12}$-eCFP

receptors, the ~40 kDa HA-P2Y$_1$ receptor band was no longer detected (middle panel, lanes 4 and 6). α-Tubulin levels (IB: α-Tubulin, bottom panel) were measured and confirmed no contamination of non-specific proteins in the IP lanes (1-3) and demonstrated equal protein levels between lanes in WCL lanes (4-6).
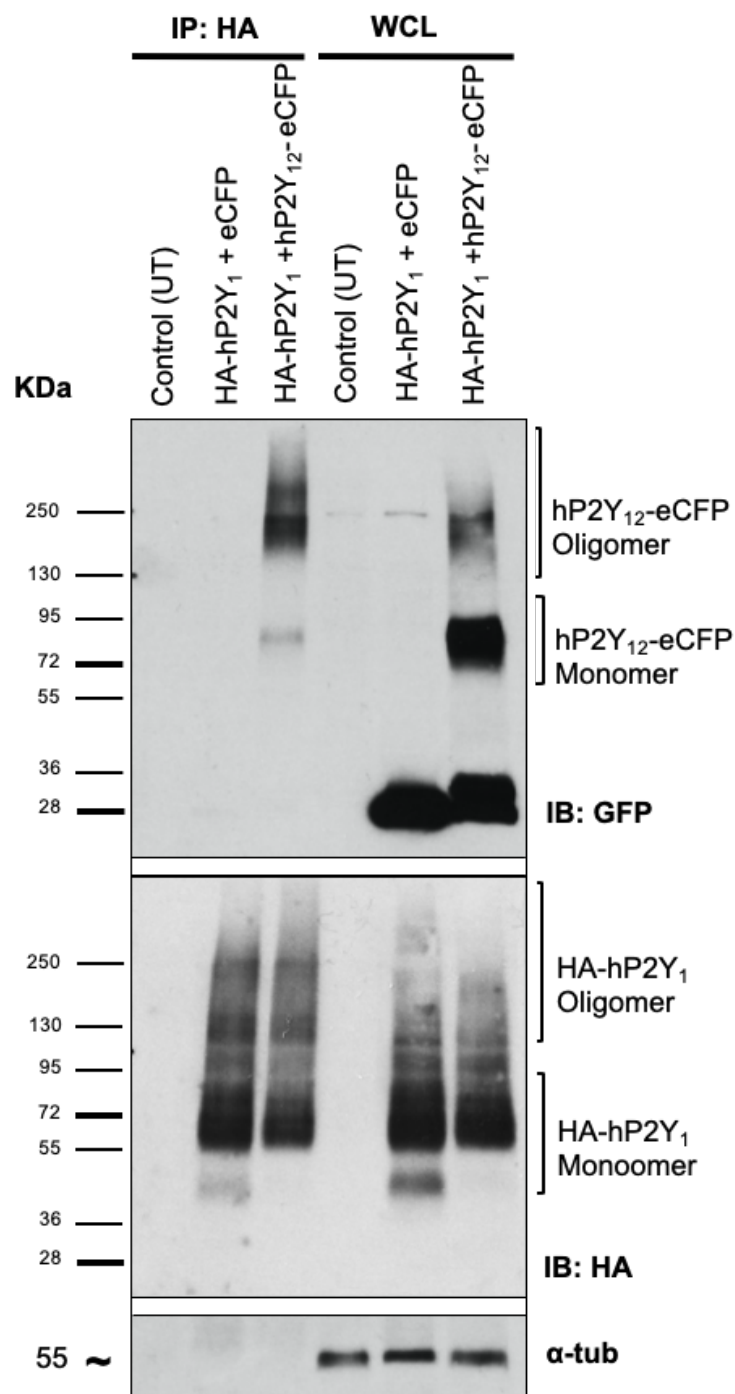
Figure 4.1: HA co-IP of coexpressed HA-hP2Y$_1$ and hP2Y$_{12}$-eCFP receptors in tSA201 cells.

tSA201 cells were cotransfected with hP2Y$_{12}$-eCFP, along with HA-hP2Y$_1$ receptors or eCFP; other samples had no cDNA added as a control or were untransfected cells (UT). Whole cells lysate (WCL) indicates the total receptors present in the cells, while IP: HA indicates the samples that were immunoprecipitated for the HA tag. HA-hP2Y$_1$ and hP2Y$_{12}$-eCFP coexpression was assessed by immunoblotting with an anti-GFP antibody in the top panel and an anti-HA antibody in the middle panel. α-Tubulin (α-tub) was used to confirm equal loading of samples. Data are representative of 3 individual experiments.

The reciprocity of the receptor association was investigated using alternatively tagged receptors. This time, HA-P2Y$_{12}$ receptors were immunoprecipitated and coexpressed with either YFP or hP2Y$_1$-eYFP (**Figure 4.2**). Similar to the previous experiments, whole cell lysates (WCL, lanes 4-6) were used to identify total receptor expression. In untransfected cells (lanes 1 and 4) no bands were detected when probed with either anti-GFP (top panel) or anti-HA (middle panel) antibodies. Immunoprecipitation (IP) of the HA tag was performed (lanes 1-3) and confirmed expression and immunoprecipitation of the HA-P2Y$_{12}$ receptor (lanes 2 and 3, middle panel). The band pattern for HA-P2Y$_{12}$ receptor was similar to that described in previous experiments in chapter 3. Three abundant protein bands were detected for the HA-hP2Y$_{12}$ receptor when expressed alone; one at >36kDa kDa, a ~40-72 kDa protein "smear" and higher molecular weight protein band between 130-250 kDa. Interestingly, the higher bands were not detected in WCL lane 5 and receptor expression appeared lower when coexpressed with P2Y$_1$-eYFP. No expression of the HA-P2Y$_{12}$ receptor was detected following immunoblotting for the FP tag using an anti-GFP antibody (IB: GFP, top panel, lanes 2 and 5). Similarly, no YFP expression was detected in IP lane 2, but was detected in WCL lane 5 (~30kDa). This confirmed successful YFP transfection, but no interaction between HA-P2Y$_{12}$ receptors and the YFP tag (lanes 2 and 5).

When P2Y$_1$-YFP was coexpressed with HA-P2Y$_{12}$ receptors and probed with the anti-GFP antibody (top panel), a series of P2Y$_1$-eYFP bands were detected in IP lane 3 at 55 kDa, ~72 kDa and an abundant high molecular weight protein 'smear' from ~130 to >250KDa. While these bands were also visible in WCL lane 6, the 72kDa band was more abundant and more bands were noted in the ~130 to >250KDa 'smear'. The presence of P2Y$_1$-eYFP in the HA-IP lane confirmed that HA-P2Y$_{12}$ could retrieve P2Y$_1$-eYFP receptors when coexpressed. These results confirm reciprocation of P2Y$_1$ and P2Y$_{12}$ receptor association, independently of the tagging strategy employed. Interestingly, when coexpressed with P2Y$_1$-eYFP receptors, expression of the HA-P2Y$_{12}$ receptor was notably lower, with the higher molecular weight bands no longer detected (middle panel, lanes 4 and 6). α-Tubulin levels (IB: α-Tubulin, bottom panel) were measured and confirmed no contamination of non-specific proteins in the IP lanes (1-3) and demonstrated equal protein levels between lanes in WCL lanes (4-6).
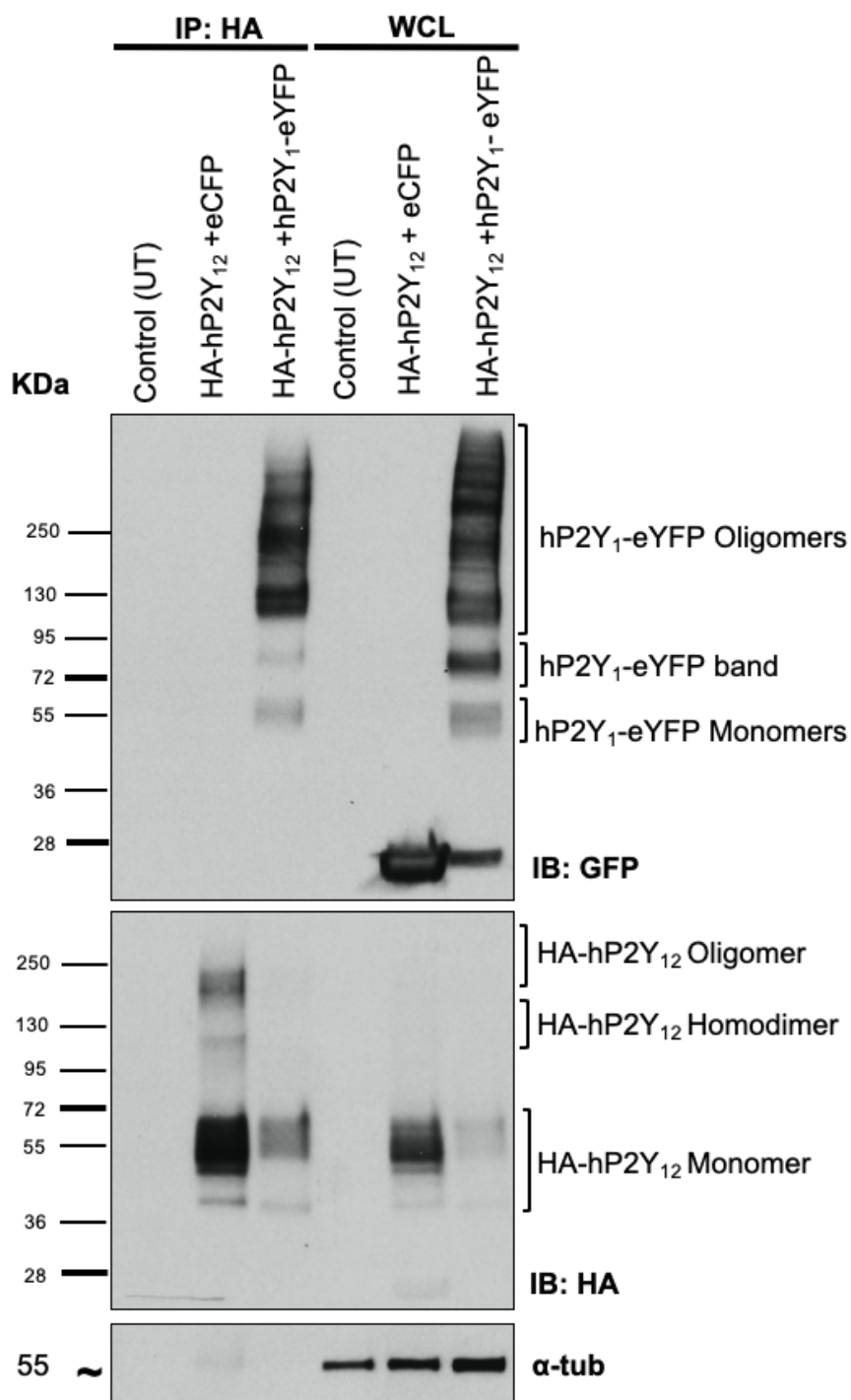
Figure 4.2: HA co-IP of coexpressed hP2Y$_1$-eYFP and HA-hP2Y$_{12}$ receptors in tSA201 cells.
tSA201 cells were cotransfected with HA-hP2Y$_{12}$ receptors along with hP2Y$_1$-eYFP receptors or eCFP; other samples had no cDNA added, as a control or were untransfected cells (UT). Whole cells lysate (WCL) indicates the total receptors in the cells while IP: HA indicates the samples that were immunoprecipitated for the HA tag. HA-hP2Y$_{12}$ and hP2Y$_1$-eYFP coexpression was assessed by immunoblotting with an anti-GFP antibody in the top panel and an anti-HA antibody in the middle panel. α-Tubulin (α-tub) was used to confirm equal loading of samples. Data are representative of 3 individual experiments.

2.2 Using the Proximity Ligation Assay to detect and localise the interactions of P2Y$_1$ and P2Y$_{12}$ receptors

While co-IP studies confirmed association between P2Y$_1$ and P2Y$_{12}$ receptors, further validation of heteromer formation and localisation was investigated. Proximity ligation assay (PLA) is a powerful tool to study protein-protein interactions that has been used previously to validate the existence of GPCR homo- and heteroreceptor complexes in their native environment (Borroto-Escuela et al., 2016; Gomes et al., 2016). For example, the A$_{2A}$-D$_2$ dimer has been detected using PLA in rodent brains (Trifilieff et al., 2011) and in the adult human ventral striatum (Zhu et al., 2019). The aim of the following experiments was, therefore, to further validate the interaction between P2Y$_1$ and P2Y$_{12}$ receptors using PLA in order to increase confidence in the positive association between these two receptors. tSA201 cells were cotransfected with the HA-tagged variant of one subtype and the FP-tagged variant of the other. Highly selective antibodies were used to detect HA and GFP tags prior to performing *in situ* PLA, as shown in the schematic in (**Figure 4.3**).
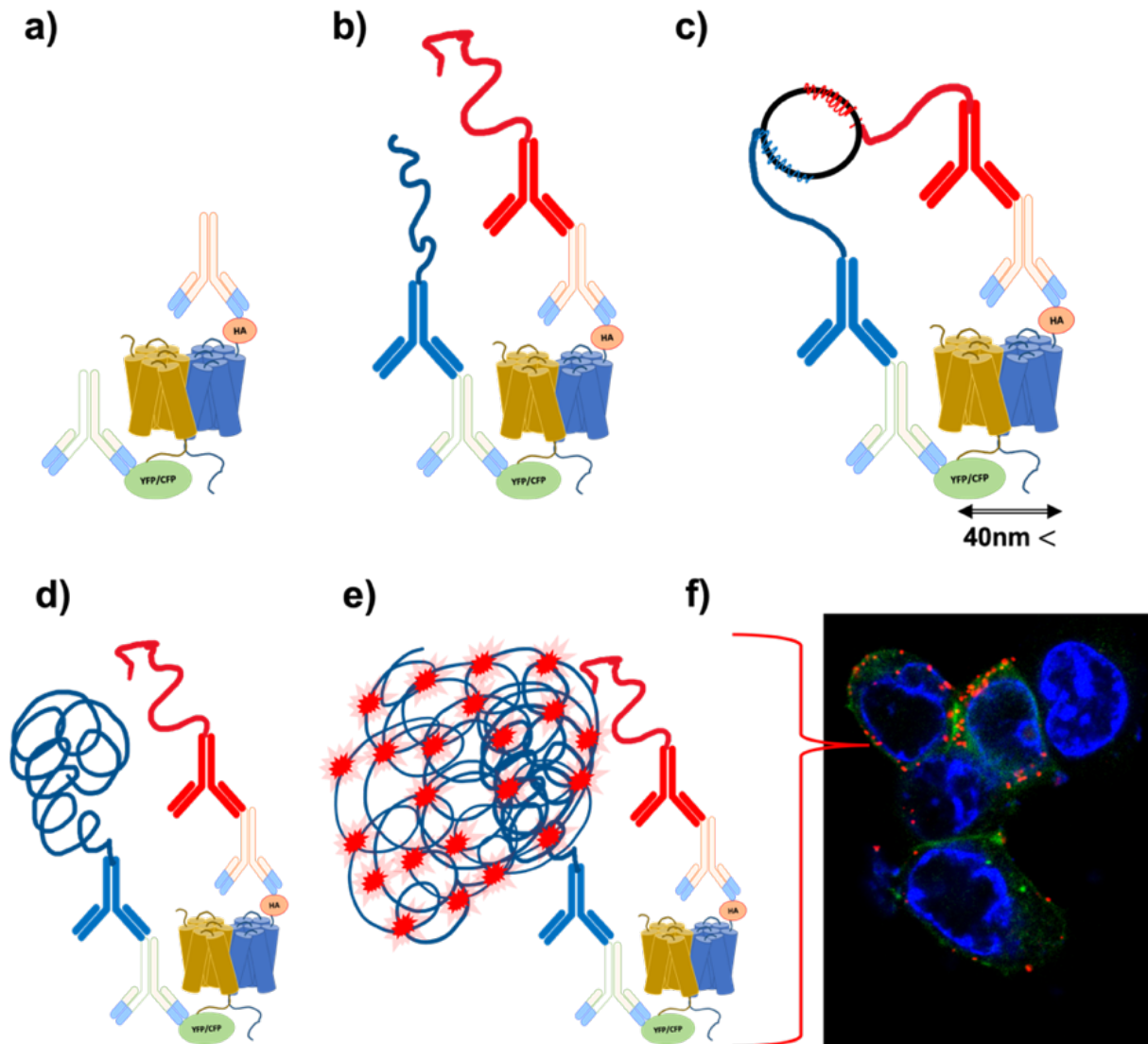
Figure 4.3: Schematic representation of indirect PLA to detect receptor heteromers

  The orange receptor represents the FP-tagged receptor and the blue receptor represents the HA-tagged receptor. Samples are first incubated with **a)** anti-HA and anti-GFP primary antibodies that recognize the HA and GFP tags. **b)** Secondary antibodies coupled with oligonucleotides (PLA probes) bind to the primary antibodies (i.e., the PLA probes PLUS and MINUS. **c)** When the PLA probes are in close proximity (< 40nm), connector oligos join the PLA probes and become ligated. **d)** The resulting closed, circular DNA template becomes amplified by DNA polymerase. **e)** Complementary detection oligos coupled to fluorochromes hybridize to repeating sequences in the amplicons. **f)** PLA signals are detected by fluorescent microscopy as discrete spots and indicate a protein-protein interaction.

As a control, an experiment was carried out by coexpressing HA-hP2Y$_{12}$ receptors with eYFP (**Figure 4.4** top row), or HA-hP2Y$_1$ receptors with eCFP (**Figure 4.4** second row). eCFP and eYFP expression was predominantly intracellular (green), with no positive PLA signal, which indicates that the two protomers are not in close proximity (<40nm). As a negative control to detect potential unspecific signal, the assay was also performed in cells that only expressed hP2Y$_{12}$-eCFP, and no PLA signal was detected here either (**Figure 4.4** third row).

In **Figure 4.4** (fourth row)**,** it is clear that hP2Y$_1$-eYFP (green) was expressed at the plasma membrane and a positive PLA signal was detected (red dots) which indicates close proximity between hP2Y$_1$-eYFP and HA-hP2Y$_{12}$ receptors. To confirm the result, the opposite pairing of P2Y subtypes was studied next. hP2Y$_{12}$-eCFP expressed at the plasma membrane (green) and an abundant PLA signal (red dots) was observed, indicating close proximity of the hP2Y$_{12}$-eCFP and HA-hP2Y$_1$ receptors (**Figure 4.4,** bottom row). Thus, coexpression of the two P2Y receptor subtypes generated a positive PLA signal, which indicate that the two protomers were less than 40 nm apart (Gomes et al, 2018). The number of positive spots per cell was quantified and is plotted in **Figure 4.5**. Positive PLA signals were negligible in cells coexpressing HA-tagged variant of one subtype and eCFP or eYFP, while coexpression of both receptors produced a high PLA signal.
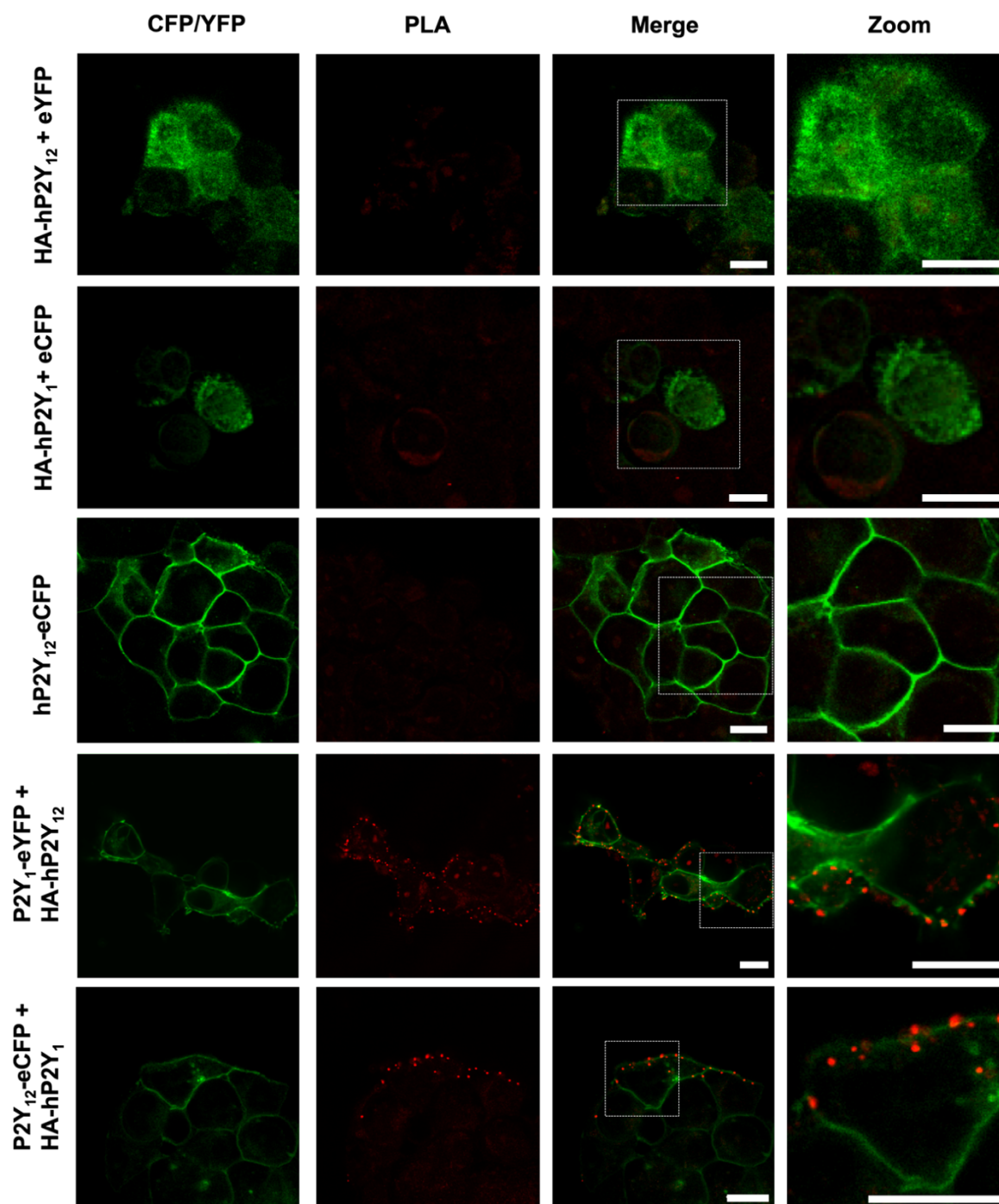
Figure 4.4: Representative confocal images of PLA between P2Y$_1$ and P2Y$_{12}$ receptors.

Images of tSA201 cells fixed 48 hours after cotransfection with HA-hP2Y$_{12}$ and eYFP (top row); HA-hP2Y$_1$ and eCFP (second row), transfected with hP2Y$_{12}$-eCFP alone (third row), cotransfected with hP2Y$_1$-eYFP and HA-hP2Y$_{12}$ (fourth row); or hP2Y$_{12}$-eCFP and HA-hP2Y$_1$ (bottom row). The representative images show hP2Y$_{12}$-eCFP, hP2Y$_1$-eYFP, eYFP and eCFP fluorescence (CFP/YFP column), the PLA signal (PLA column), overlay of both (merge column) and magnification of specific areas of the merged images (zoom column). Cells were visualised using confocal microscopy, at 63x (oil) magnification (scale bar = 10 µm), using a 605 nm excitation filter setting to detect the PLA signal and a 430 nm excitation filter setting to detect CFP or YFP fluorescence. Data are representative of 3 individual experiments.

146
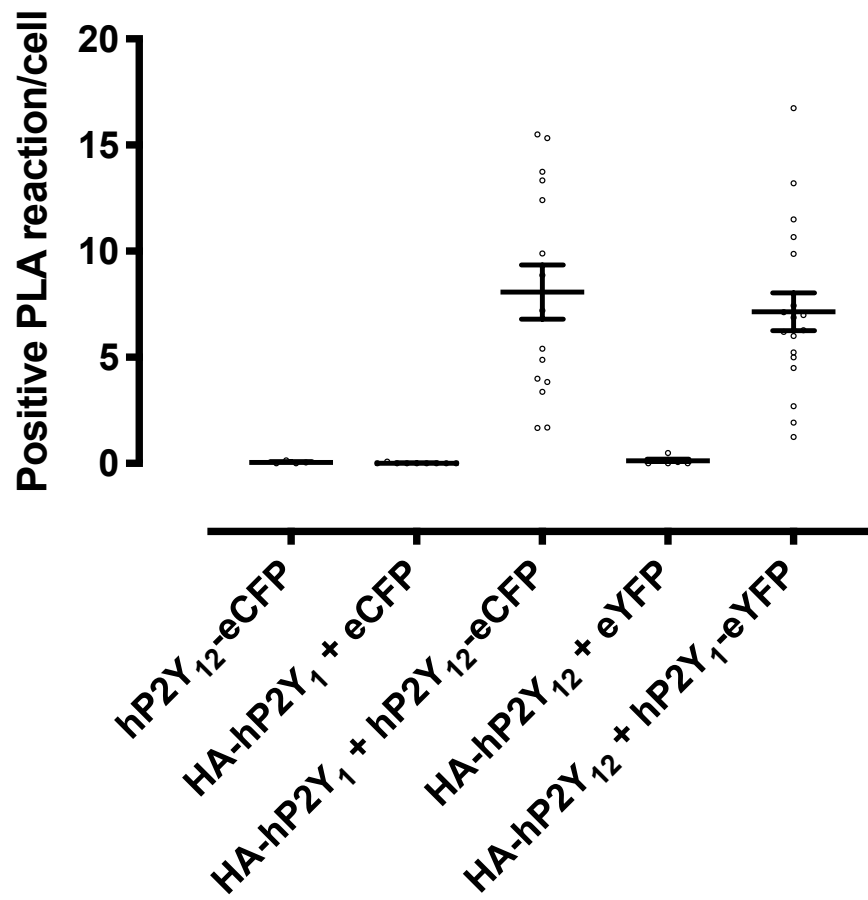
Figure 4.5: Quantification of positive PLA signals per cell.
The plot shows the number of PLA signals in tSA201 cells that were transfected with hP2Y$_{12}$-eCFP or cotransfected with HA-hP2Y$_{1}$ and eCFP; HA-hP2Y$_{1}$ and hP2Y$_{12}$-eCFP; HA-hP2Y$_{12}$ and eYFP; HA-hP2Y$_{12}$ and hP2Y$_{1}$-eYFP. The wide horizontal bars represent the mean values obtained from 20 cells for each column from two separate experiments. The narrow horizontal bars represent the sem.

Quantification of PLA signals per cell was carried out initially using a single a plane of a cell. This, may not, however, provide an accurate measurement of the PLA signal. As shown in the Z-stack image series in **Figure 4.6**, in tSA201 cells cotransfected with hP2Y$_{12}$-eCFP and HA-hP2Y$_1$ receptors, the number and location of the PLA signal differed from one focal plane to the next. In one plane (**Figure 4.6A**), the hP2Y$_{12}$-eCFP receptor was expressed clearly at the cell membrane (green), with abundant PLA signals (red dots) observed. However, as the focal plane moved through the cell (**Figure 4.6B-I**), the localisation and number of PLA signals changed. As shown in **Figure 4.6 (i,ii,iii)**, the distribution of positive PLA signal throughout the cell has been grossly underestimated in Figure 4.5, with positive signals merging. Thus, counting individual spots may not be the most accurate way to quantify this type of data and may lead to misinterpretation and observational bias of spot definition. On this basis, it was decided to not quantify PLA data in future experiments.
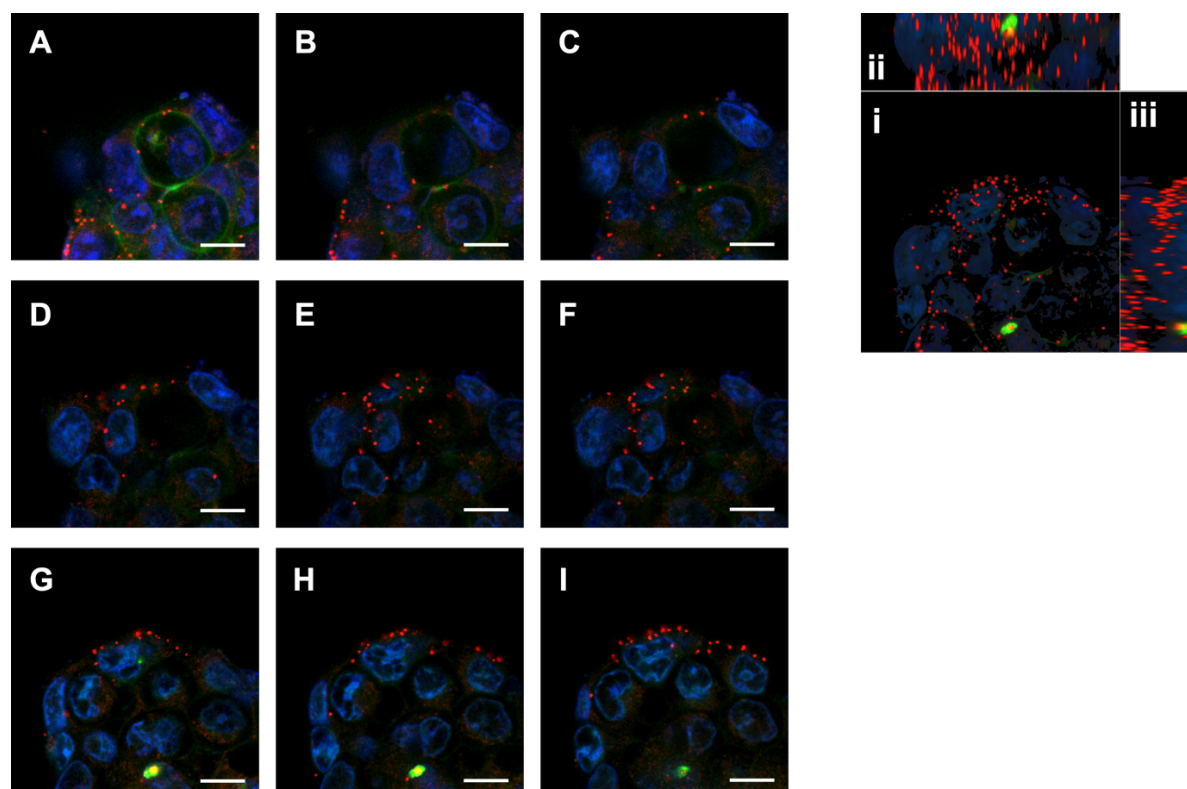
Figure 4.6: Z-stacks showing P2Y$_1$-P2Y$_{12}$ heterodimerisation using PLA.
Z-stacks of tSA201 cells transfected with HA-hP2Y$_1$ and hP2Y$_{12}$-eCFP, generated using confocal microscopy, are shown. Images were taken at 1 μm intervals, starting at the top of the cells (A) and progressively moving downwards (B-I). On the top right is **(i)** an example of a focal plane of the cells, **(ii)** the side view of the z-stack, viewed in the *x* and *z* plane of (i), while **(iii)** the view is of the *y* and *z* plane of (i). Cells were visualised using confocal microscopy at 63x (oil) magnification (scale bar = 10 μm) using a 430 nm excitation filter setting to detect CFP (green) and a 380 nm excitation filter to detect DAPI nuclear stain (blue). PLA signals are shown in (red) and were detected using a 605 nm excitation filter setting.

2.3 Effect of hP2Y$_1$ & hP2Y$_{12}$ receptor agonists and antagonists on PLA signal

After determining the interaction between P2Y$_1$ and P2Y$_{12}$ receptors using the PLA approach, further experiments were carried out to identify if the proposed dimer was influenced by the presence of their agonists or antagonists. tSA201 cells cotransfected with hP2Y$_{12}$-eCFP and HA-hP2Y$_1$ were treated for 5 or 30 minutes with ADP (10µM), the selective P2Y$_1$ agonist, MRS2365 (3µM), the P2Y$_1$ negative allosteric modulator, BPTU (1µM), the selective P2Y$_1$ antagonist, MRS2179 (10µM) or the selective P2Y$_{12}$ antagonist, AR-C69931MX (1µM) and changes in receptor interaction measured using PLA. Untreated cells were used as a control.

Similar to previous experiments, in the absence of receptor agonists or antagonists, cells expressed hP2Y$_{12}$-eCFP receptors at the cell membrane (green), and an abundant PLA signal (red dots) was observed, confirming the interaction between hP2Y$_{12}$-eCFP and HA-hP2Y$_1$ receptors (**Figure 4.7,** top panel). Furthermore, treating the cells with P2Y$_1$ and P2Y$_{12}$ agonists, ADP (second and third panel) or MRS2365 (fourth and bottom panel) did not appear to affect the PLA signal obtained.
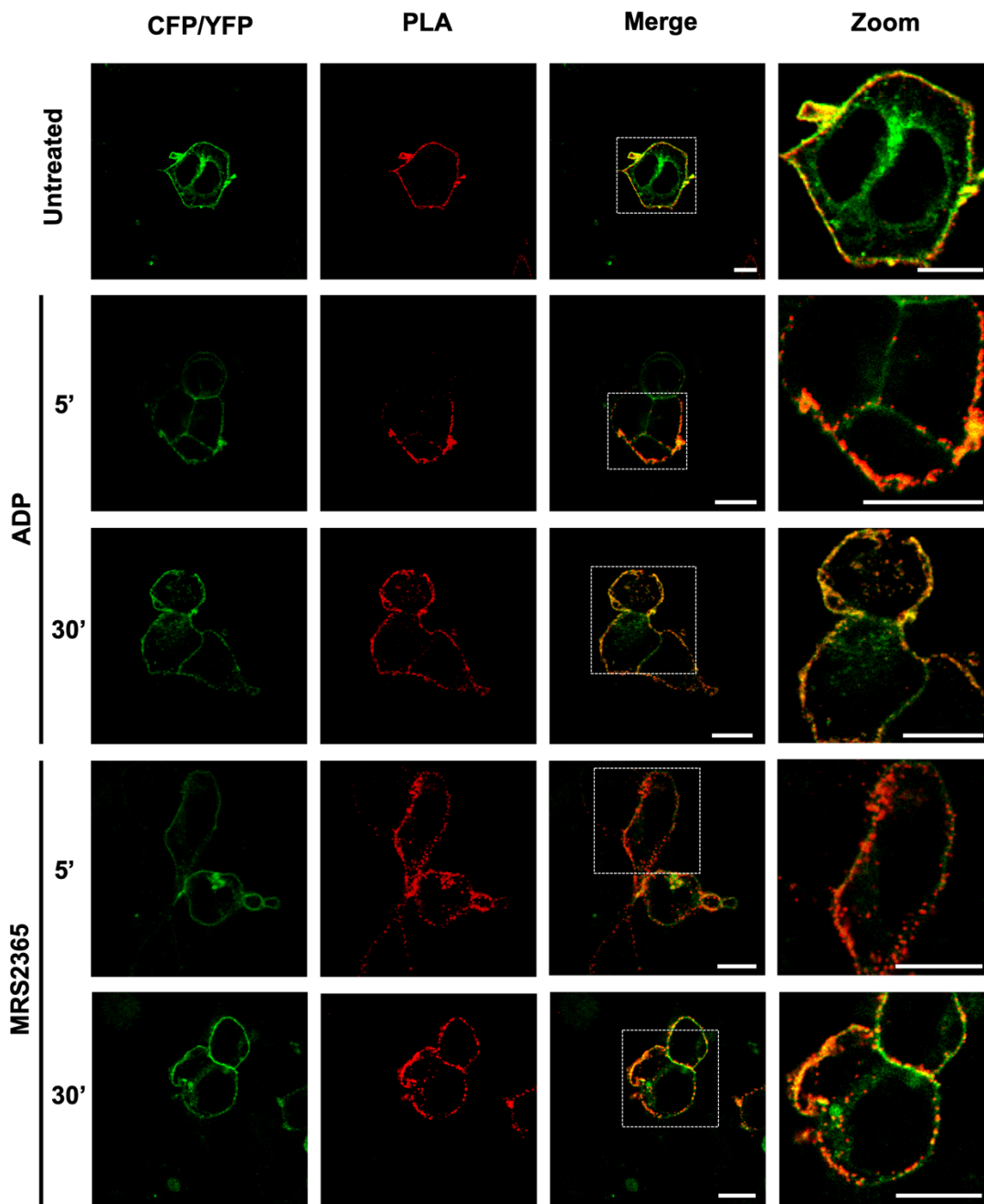
Figure 4.7: The effects of hP2Y$_1$ and hP2Y$_{12}$ receptor agonists on PLA signals.
Images of tSA201 cells fixed 48 hours after cotransfection with hP2Y$_{12}$-eCFP and HA-hP2Y$_1$ receptors are shown. The top row shows cells that were not exposed to an agonist, while the other rows show cells that had been exposed to ADP (10μM) or MRS2365 (3μM) for 5 or 30 minutes. The representative images show hP2Y$_{12}$-eCFP fluorescence (CFP/YFP column), the PLA signal (PLA column), overlay of both (merge column) and magnification of specific areas of the merged images (zoom column). Cells were visualised using confocal microscopy, cells were visualised at 63x (oil) magnification (scale bar = 10 μm) using a 605 nm excitation filter setting to detect the PLA signal and a 430 nm excitation filter setting to detect CFP fluorescence. Data are representative of 2 individual experiments.

When cells were treated with the $P2Y_1$ antagonists, BPTU (1µM) or MRS2179 (10µM), (**Figure 4.8**) a positive PLA signal was still detected at both 5 and 30 minute treatment points, which resembled untreated control PLA signals. Interestingly, following treatment with the $P2Y_{12}$ antagonist AR-C69931MX (1µM) (**Figure 4.9**) the PLA signals (red dots) were less intense at 5 minutes and more unevenly distributed at 30 minutes when compared to the PLA signals observed in untreated cells.
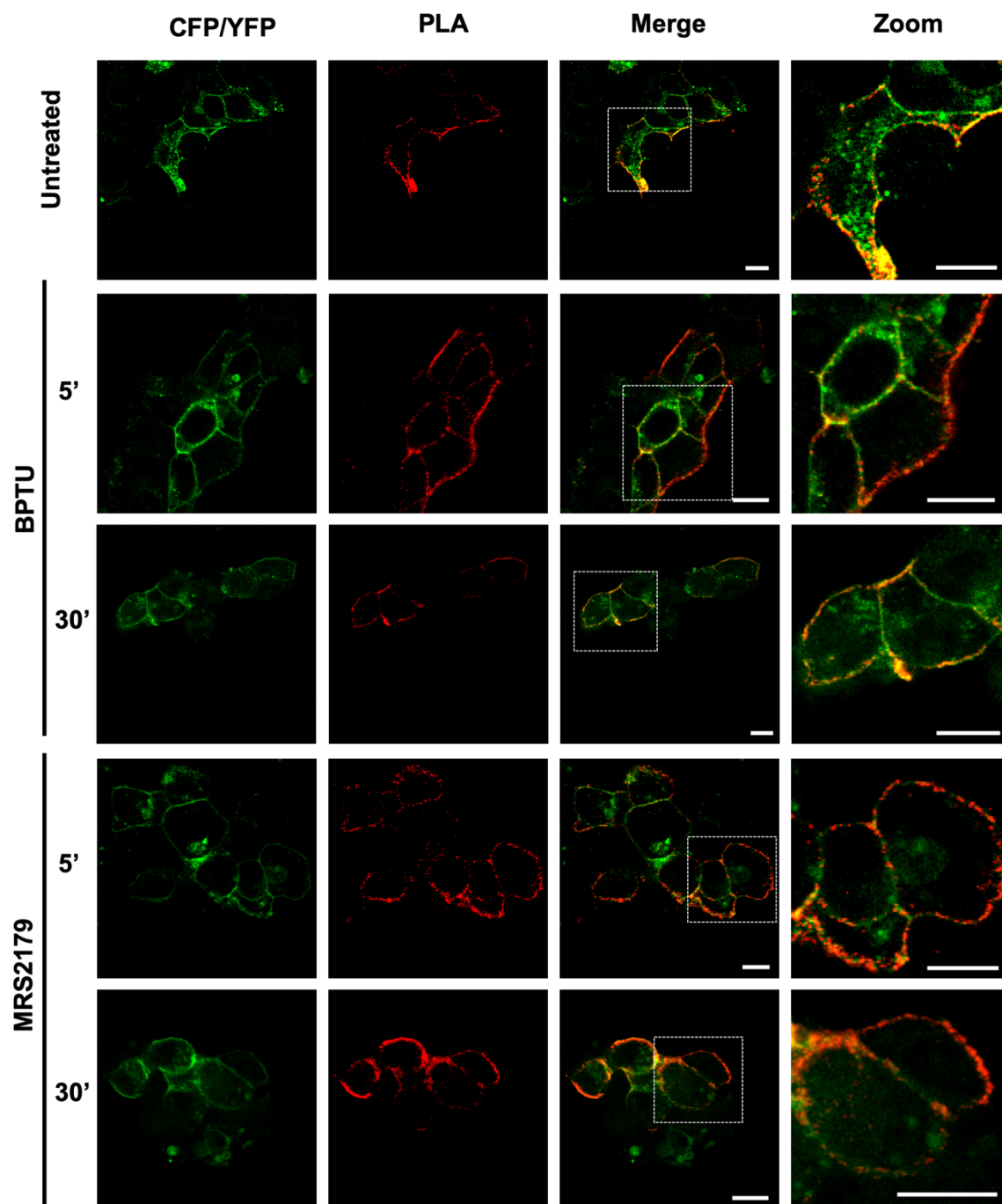
Figure 4.8: The effects of hP2Y$_1$ receptor antagonists on PLA signals.
Images of tSA201 cells fixed 48 hours after cotransfection with hP2Y$_{12}$-eCFP and HA-hP2Y$_1$ receptors are shown. The top row shows cells that were not exposed to an antagonist, while the other rows show cells that had been exposed to BPTU (1µM) or MRS2179 (10µM) for 5 or 30 minutes. The representative images show hP2Y$_{12}$-eCFP fluorescence (CFP/YFP column), the PLA signal (PLA column), overlay of both (merge column) and magnification of specific areas of the merged images (zoom column). Cells were visualised using confocal microscopy, cells were visualised at 63x (oil) magnification (scale bar = 10 µm) using a 605 nm excitation filter setting to detect the PLA signal and a 430 nm excitation filter setting to detect CFP fluorescence. Data are representative of 2 individual experiments.
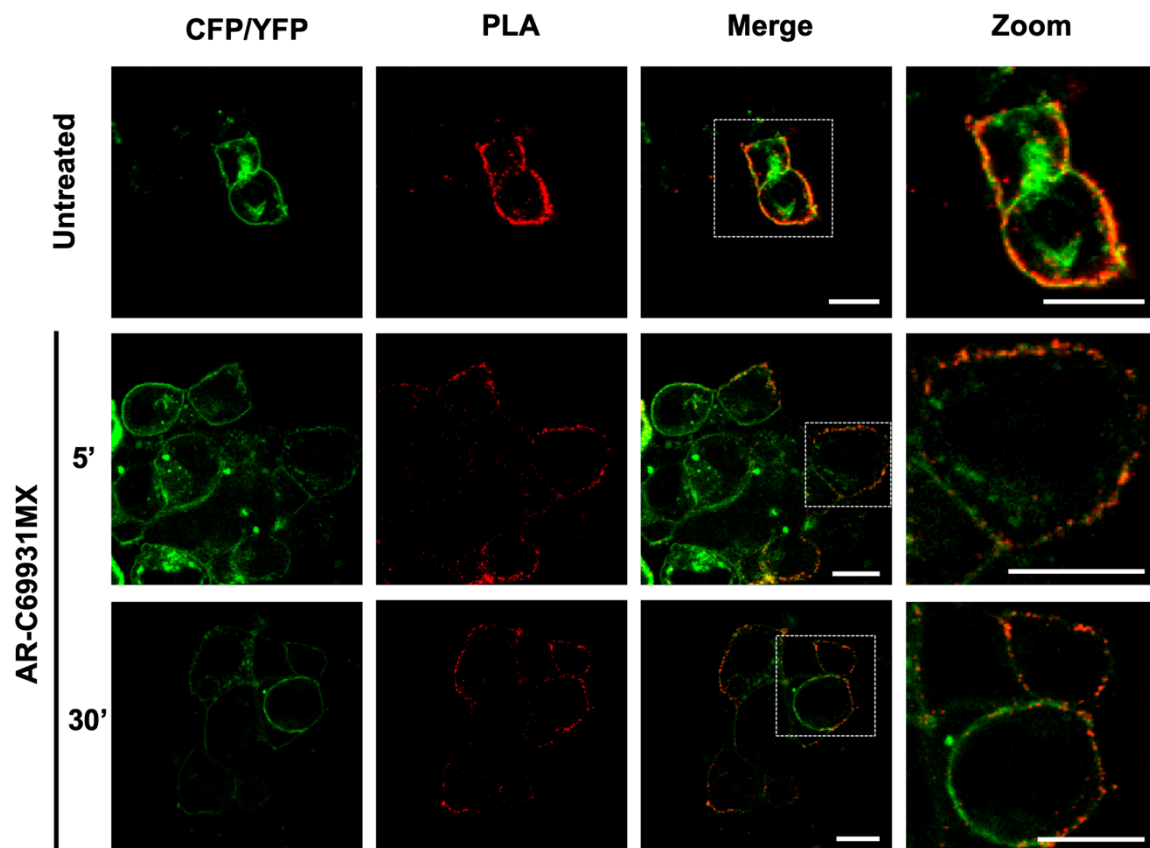
Figure 4.9: The effects of an hP2Y$_{12}$ receptor antagonist on PLA signals.
Images of tSA201 cells fixed 48 hours after cotransfection with hP2Y$_{12}$-eCFP and HA-hP2Y$_1$ receptors are shown. The top shows cells that were not exposed to AR-C69931MX, while the other rows show cells that had been exposed to AR-C69931MX (1µM) for 5 or 30 minutes. The representative images show hP2Y$_{12}$-eCFP fluorescence (CFP/YFP column), the PLA signal (PLA column), overlay of both (merge column) and magnification of specific areas of the merged images (zoom column). Cells were visualised using confocal microscopy, cells were visualised at 63x (oil) magnification (scale bar = 10 µm) using a 605 nm excitation filter setting to detect the PLA signal and a 430 nm excitation filter setting to detect CFP fluorescence. Data are representative of 2 individual experiments.

2.4 Investigating the physical interaction of P2Y$_1$ and P2Y$_{12}$ receptors via FLIM-FRET technique

Both co-IP and PLA experiments rely upon permeabilisation or lysis of cells and the ability of antibodies to subsequently detect the epitopes of the proteins of interest. Förster resonance energy transfer (FRET) is a key fluorescence microscopy technique used in the study of protein-protein interactions (Margineanu et al., 2016, and does not rely upon permeabilising cells to enable antibody access to the cell interior. This technique is based on energy transfer between two fluorophores. When the (donor) fluorophore is excited, energy will be transferred directly to the (acceptor), which then emits a photon. FRET only occurs if the donor and acceptor fluorophores are in close proximity (typically <10 nm), and the emission spectrum of the donor and the absorption spectrum of the acceptor overlap, as shown in **Figure 4.10**.
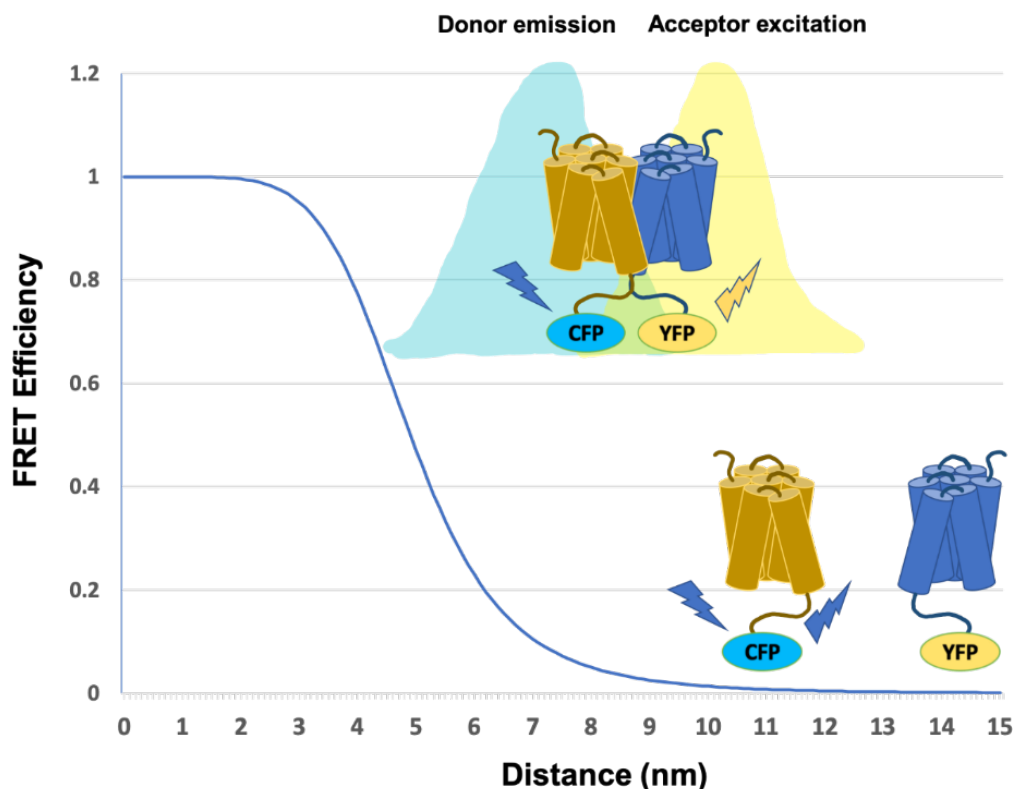
Figure 4.10: Schematic representation of FRET efficiency, which depends on the distance between the CFP-YFP pair.
The diagram shows two receptors tagged with CFP or YFP in a FRET situation and no FRET situation. In the FRET situation the receptors appear to interact with each other with a high FRET efficiency, while in the no FRET situation the receptors appear to be apart and with a low FRET efficiency. The FRET efficiency can be used to calculate the percentage of the energy transferred between CFP and YFP.

The most straightforward method for measuring FRET is Fluorescence Lifetime Imaging Microscopy (FLIM) (Margineanu et al., 2016). FLIM measures the lifetime of a fluorophore using a pulsed laser, and the lifetime reduces when FRET occurs, due to quenching the donor signal. The aim of using the FLIM-FRET technique for the following experiment was to quantify the energy transferred between the two receptors tagged with eCFP and eYFP and calculate the distance between them. To do so, tSA201 cells were transfected with $hP2Y_{12}$-eCFP (donor) or cotransfected with $hP2Y_{12}$-eCFP (donor) and eYFP (acceptor) as controls or with $hP2Y_{12}$-eCFP (donor) and $hP2Y_1$-eYFP (acceptor). Following excitation of the eCFP tagged receptor with a short laser pulse, the arrival time of single fluorescence photons is recorded to picosecond accuracy using time-correlated single-photon counting (TCSPC). The fluorescence lifetimes of the donor without acceptor (τ_D) and with acceptor (τ_{DA}) were measured then the FRET efficiency (E) was calculated using the following equation (Bajar et al., 2016):

$$E = 1 - (\tau DA/\tau D)$$

Also, the distance between donor and acceptor (r) was calculated using the following equation (Dacres et al., 2010):

$$r^6 = \frac{R_0^6}{E} - R_0^6$$

While R_0 is the critical distance (Förster distance) defined by quantum yield and extinction coefficient of donor and acceptor, which is 4.9 nm for eCFP/eYFP pair (Patterson et al., 2000).

The FRET efficiency was estimated in tSA201 cells transfected with hP2Y$_{12}$-eCFP as the fluorescence lifetime of the donor and hP2Y$_1$-eYFP as the energy acceptor. In **Figure 4.11a**, the green colour represents a long lifetime for hP2Y$_{12}$-eCFP, while yellow and red colours indicate a reduction of mean fluorescence lifetime because of energy transfer between the donor and acceptor. **Figure 4.11b** show the mean values of fluorescence lifetime of selected pixels of a cell's plasma membrane. It was noted that average donor fluorescence lifetime was significantly reduced when the acceptor was expressed in the cells when compared to the value attained from cells that expressed hP2Y$_{12}$-eCFP (donor) only **Figure 4.11b**. The donor mean fluorescence lifetime was 1.595 ns, and when coexpressed with eYFP as an acceptor there was no significant reduction in lifetime. However, when hP2Y$_{12}$-eCFP (donor) was coexpressed with hP2Y$_1$-eYFP (acceptor) the fluorescence lifetime was significantly reduction to 1.2 ns. The τ_D value decreased upon coexpression of both receptors. Additionally, the energy transfer efficiency was 24.8% when measurements were taken from cells cotransfected with hP2Y$_{12}$-eCFP and hP2Y$_1$-eYFP. Thus, these experiments provide more evidence for a close interaction between P2Y$_{12}$ and P2Y$_1$ receptors.
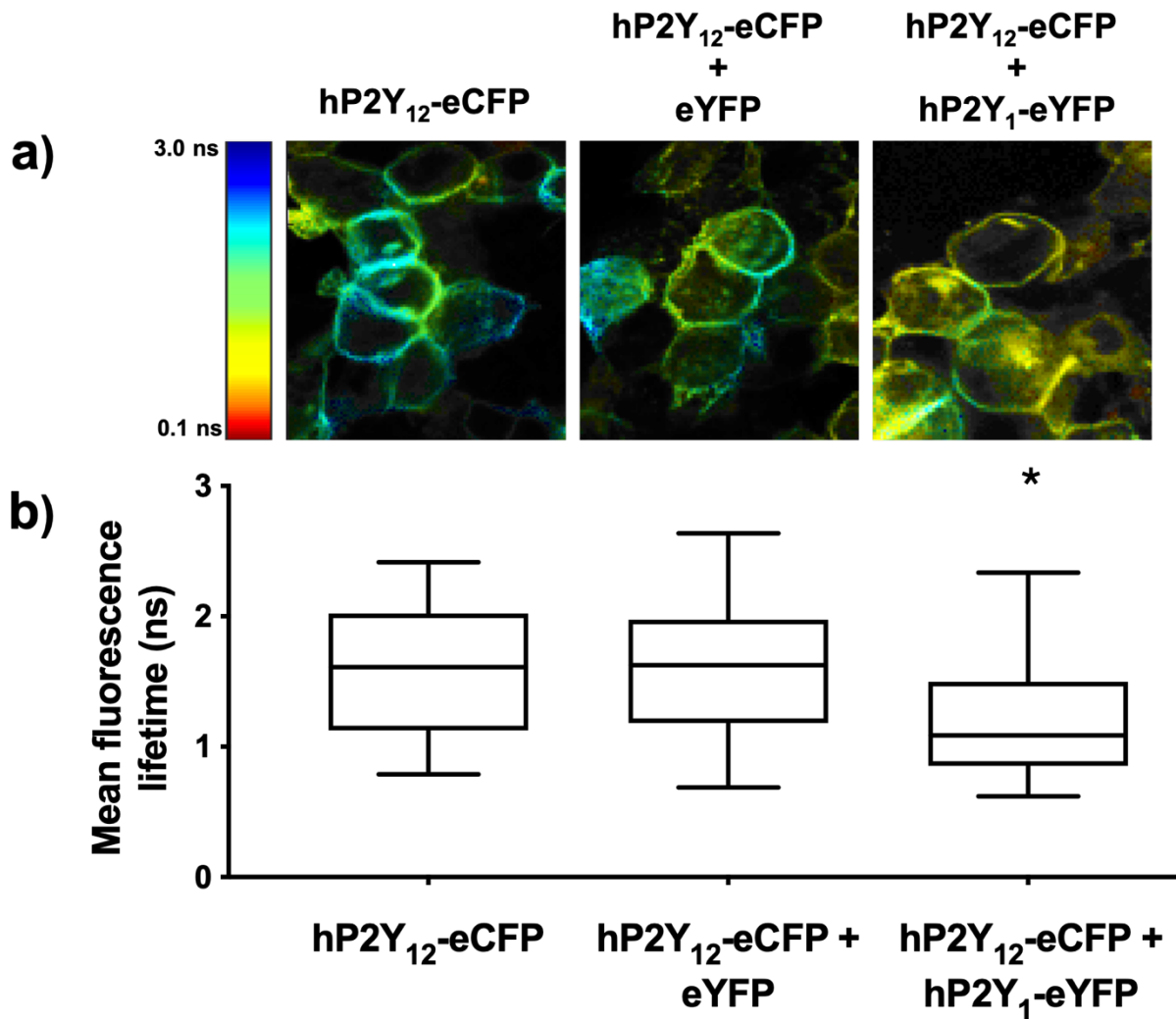
Figure 4.11: Interaction between P2Y₁ and P2Y₁₂ receptors assessed by FLIM-FRET.

a) Representative images are presented in a continuous pseudo-colour scale representing fluorescence lifetime values (0.1 - 3.0 ns) obtained by Laser Scanning Microscope (LSM) in tSA201 cells transfected with hP2Y₁-eCFP on its own (left-hand panel) or cotransfected with eYFP (middle panel) or hP2Y₁-eYFP (right-hand panel). **b)** The graph shows the mean ± SED values of fluorescence lifetimes obtained by analysis of regions of 60 pixels selected from the plasma membrane of 100 cells in 3 individual experiments. *P<0.05 compared to the hP2Y₁₂-eCFP receptor lifetime.

2.5   Impact of P2Y$_1$ and P2Y$_{12}$ ligands on FLIM-FRET responses

After confirming the interaction between P2Y$_1$ and P2Y$_{12}$ using the FLIM-FRET approach, the impact of P2Y$_1$ and P2Y$_{12}$ ligands on this interaction was studied in tSA201 cells cotransfected with hP2Y$_{12}$-eCFP and hP2Y$_1$-eYFP, followed by treatment with ADP (10µM), the selective P2Y$_1$ agonist, MRS2365 (3µM), BPTU (1µM), MRS2179 (10µM) or AR-C69931MX (1µM) for 5 or 30 minutes prior to FLIM-FRET imaging. **Figure 4.12** shows representative images for each experimental protocol and **Figure 4.13** the mean data obtained. Consistent with the previous experiment, the mean fluorescence lifetime for the donor was 1.25 ns, with energy transfer efficiency about 21.9% (**Figure 4.13, Table 4.1**). None of the drug treatments had any significant effect on the fluorescence lifetime of the donor, except for 30 minutes exposure to AR-C69931MX, where the lifetime was significantly shortened to 1.03ns. Under these conditions the distance between both protomers was calculated to be 5.4nm and the energy transfer efficiency was 35.2%. Thus AR-C69931MX appeared to bring the two protomers closer together and so increase the efficiency of energy transfer.
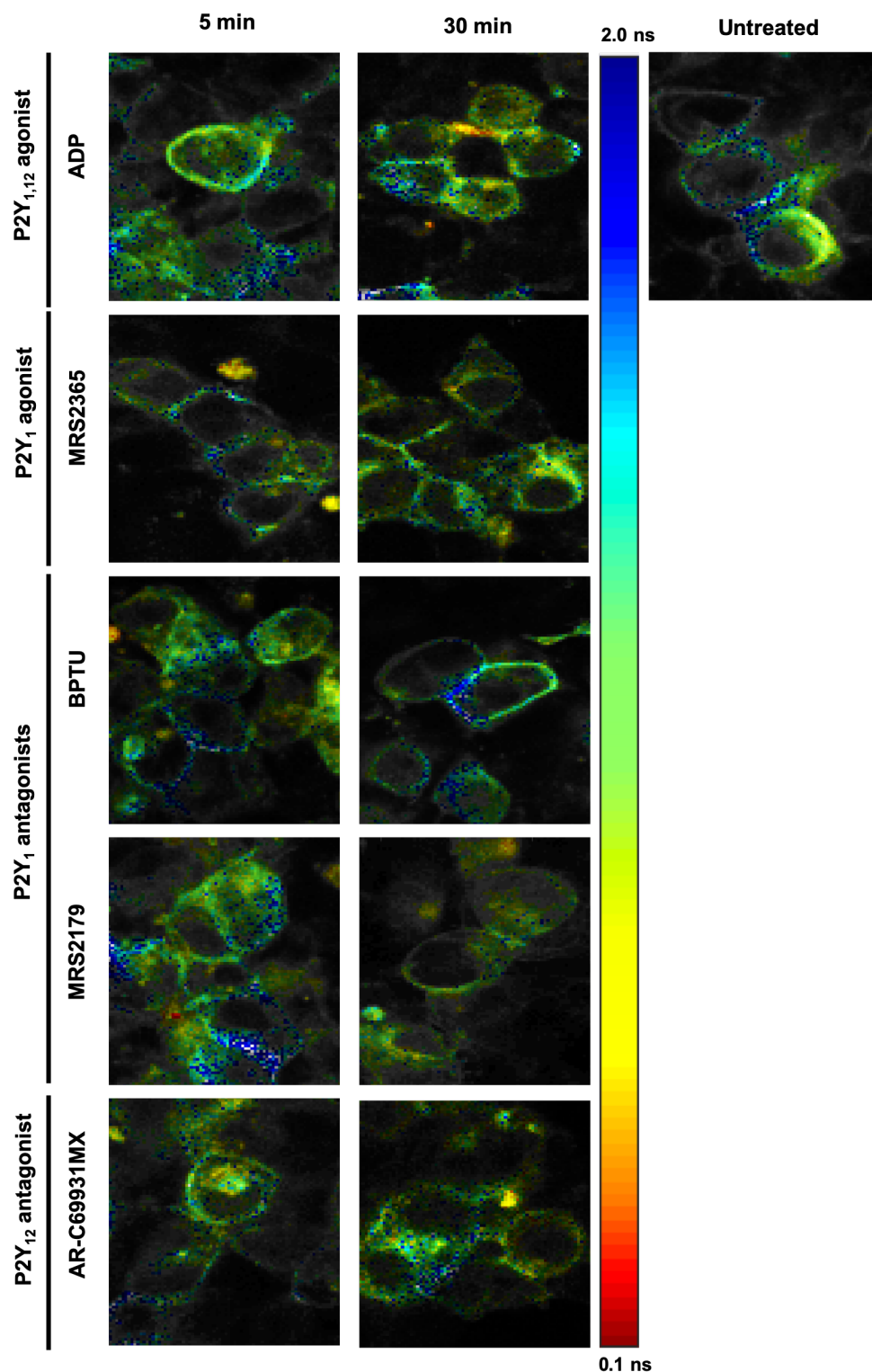
Figure 4.12: Interaction between P2Y$_1$ and P2Y$_{12}$ receptors assessed by FLIM-FRET post-treatment with ligands.

Fluorescence lifetimes were measured by Laser Scanning Microscope (LSM) in cotransfected tSA201 cells with hP2Y$_1$-eCFP and hP2Y$_1$-eYFP that were treated with ADP, MRS2365, BPTU, MRS2179 and AR-C69931MX for 5 min (left column) and 30 min (right column). Images are presented in a continuous pseudo-colour scale representing the time values ranging from 0.1 – 2.0 ns.
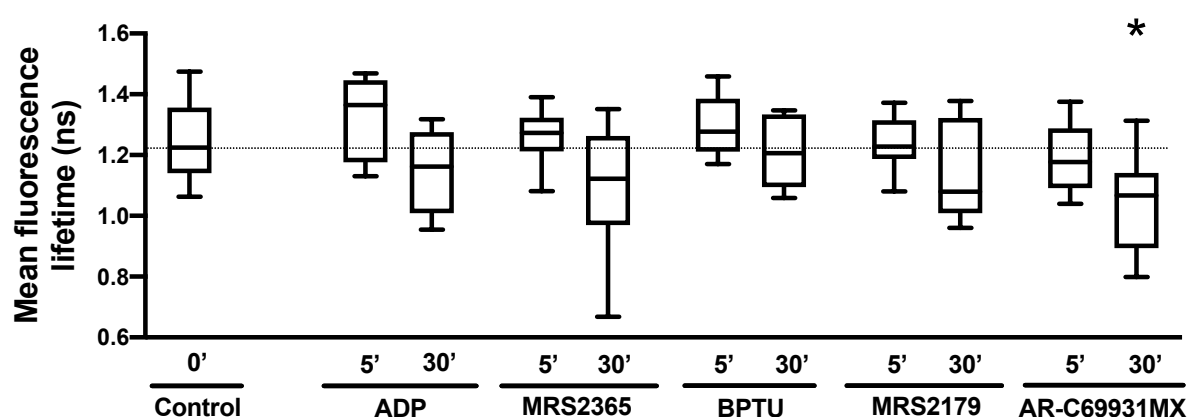
Figure 4.13: Plotted values of P2Y$_1$ and P2Y$_{12}$ receptors assessed by FLIM-FRET post-treatment with ligands.

Analysed data of fluorescence lifetimes obtained from cotransfected with donor hP2Y$_{12}$-eCFP and acceptor hP2Y$_1$-eYFP. Untreated cells used as control. The data represent the mean values ±SED of 3 images of 106 from 3 individual experiments. *P<0.05 compared to the untreated samples lifetime.

Table 4.1: Fluorescence lifetime and energy transferred

Ligands	Treatment time (min)	The fluorescence lifetimes (τ_D)	FRET efficiency (E) %	Distance (nm)
Untreated	0	1.25	21.9	6.0
ADP	5	1.32	17.2	6.4
	30	1.15	27.8	5.7
MRS2369	5	1.27	20.6	6.1
	30	1.10	31.3	5.6
BPTU	5	1.30	18.6	6.2
	30	1.22	23.5	5.9
MRS2179	5	1.24	22.3	6.0
	30	1.14	28.4	5.7
AR-C69931MX	5	1.19	25.3	5.8
	30	1.03	35.2	5.4

3   Discussion

This chapter focused on investigating the physical interaction between recombinant, epitope-tagged $P2Y_1$ and $P2Y_{12}$ receptors when coexpressed in tSA201 cells. This was relatively straightforward to carry out due to the availability of well-characterized, epitope tag-selective antibodies. The data obtained using three different techniques were all consistent with a close physical interaction between the two receptors. Indeed, the FLIM-FRET data indicated that they were approximately 6 nm apart. The interaction was unaffected by the $P2Y_1$ and $P2Y_{12}$ agonist, ADP, the selective $P2Y_1$ agonist MRS2365 and the selective $P2Y_1$ antagonists, BPTU and MRS2179. The selective $P2Y_{12}$ antagonist, AR-C69931MX, on the other hand appeared to bring the two receptors closer together. Thus, these data are consistent with the close physical interaction between $P2Y_1$ and $P2Y_{12}$ receptors proposed by Shrestha et al., (2010).

Confirmation of the $P2Y_1$/$P2Y_{12}$ receptor dimer by co-IP

Co-IP is one of the fundamental methods for investigating proteins interactions in the same cellular complex. However, it cannot indicate the number of other proteins involved between the two receptors in the complex. For the first time, the physical interaction between $P2Y_1$ and $P2Y_{12}$ receptors was demonstrated here by co-IP in tSA201 cells coexpressing both receptors. The formation of a detectable higher molecular weight protein of ~130 to >250 kDa expressing an FP tag was visible in samples expressing both receptors, which indicated the physical association between the two receptors. The multiple bands and the smear shown on the western blots might indicate various post-translationally modified forms of the receptors. This could be due to processes such as glycosylation (Yoshioka et al., 2001; Zhong et al., 2004) and formation of homodimers, which both $hP2Y_1$ (Choi et al., 2008) and $hP2Y_{12}$ (Savi et al., 2006) receptors have been acknowledged to form.

The main concerns when using co-IP to study protein-protein interactions is that the receptors' hydrophobic domains might nonspecifically aggregate together after solubilization, which might result in an artifactual co-IP result (Angers et al., 2002). However, the coexpression of the HA-$hP2Y_1$ receptor with eCFP and the HA-

hP2Y$_{12}$ receptor with eCFP did not produce any co-IP bands, implying that the interaction between the receptors was not simply due to protein aggregation. It was also noticeable that P2Y$_{12}$ receptor showed lower expression in the Western blot when it coexpressed with P2Y$_1$ receptors, similar to the results from the previous chapter, as P2Y$_1$ receptor might impact the dynamic formation of P2Y$_{12}$ receptor.

Confirmation of the dimer via biophysical methods

Another approach taken to investigate the interaction between P2Y$_1$ and P2Y$_{12}$ receptors was the very sensitive in situ PLA method, which generates a signal only when both targets are in close proximity (< 40nm). The PLA approach has been used previously for GPCR heterodimer detection, for example the A$_{2A}$-D$_2$ dimer in rodent brain (Trifilieff et al., 2011) and in the adult human ventral striatum (Zhu et al., 2019). However, this method is dependent upon on the quality of the antibodies used, but that is unlikely to be an issue here as the specificity of both anti-HA and anti-GFP antibodies was characterized previously in **Chapter three** using standard fluorescence immunohistochemistry and confocal microscopy. The results obtained in this chapter demonstrate that when both receptors were coexpressed in tSA201 cell they generated PLA signals that localised to the plasma membrane. That is consistent with the results of the co-IP experiments and indicate that the PLA approach is valid for the future detection of native receptors, which will be discussed in the next chapter.

Although previous techniques yielded valuable information, more evidence was needed to confirm the interaction. In this study we used FRET approach to test the interaction between both receptors, however, this was not the first time that this approach was used to detect the P2Y$_1$ and P2Y$_{12}$ receptors physical interaction. As the previous study was done by Schicker et al. (2009) confirmed the interaction between two rat P2Y$_1$ and P2Y$_{12}$ receptors in tSA201 cells using FRET method. However, in this study, we used human P2Y$_1$ and P2Y$_{12}$ receptors tagged with FRET-based methods use fluorescent proteins, such as the CFP and YFP (Bajar et al., 2016). Also, FLIM was used to measure FRET to determine the lifetime of the donor. Working closely with the physics department at the University of Strathclyde we managed to employ FLIM-FRET for GPCR dimerisation study (Li et al., 2020), which

made us one of the few researchers to apply that on GPCR and the first to apply that approach in the purinergic field. In this thesis experiments, the variant with $hP2Y_{12}$-eCFP as the donor and $hP2Y_1$-eYFP as acceptor was chosen for these studies. Indeed, the measured fluorescence lifetime in cells transfected only with the donor (1.59 ns) was significantly higher compared to cells transfected additionally with the acceptor (1.25 ns), providing strong evidence for the $P2Y_1$-$P2Y_{12}$ dimer formation. Moreover, the energy transfer efficiency was about 24.8% between the donor and the acceptor. The unchanged donor fluorescence lifetime (1.58 ns) obtained for a negative sample control, in where cells were cotransfected with the $hP2Y_{12}$-eCFP receptor (donor) and with unfused eYFP confirmed the reliability of the chosen model. FLIM-FRET approach was used to characterizing the interactions of another GPCR Class A member, which is GPR17 homodimer expressed in HEK293 cells (Yang et al., 2020). In Yang et al. (2020) study they used a different pair than our current study, which is GFP as the FRET donor and mCherry as the FRET acceptor. However, there is no significant difference in using different FRET pairs as long as the donor has the highest quantum yield and the acceptor has the highest absorbance with significant overlap in their spectra. Other paper used the same approach to detect the dissociation of the heterotrimeric G-proteins (Mystek et al., 2019), which helps a lot in understanding the receptor from signaling perspective. Unfortunately, we did not have fluorescent tagged G proteins at this moment in time.

The impact of ligands on the $P2Y_1$-$P2Y_{12}$ dimer

Because both pairs of P2Y receptor plasmids generated PLA signals successfully, only one pair was used (HA-$hP2Y_1$ and $hP2Y_{12}$-eCFP receptors) when studying the effects of ligands. Most highly selective $P2Y_1$ and $P2Y_{12}$ receptor ligands had no effect on the FLIM-FRET signal in cells that coexpressed $hP2Y_{12}$-eCFP as the donor and $hP2Y_1$-eYFP as acceptor shortened. Interestingly, however, 30 minutes exposure to the selective $P2Y_{12}$ antagonist, AR-C69931MX (1μM), shortened the τ_D significantly, increased FRET efficiency between $hP2Y_{12}$-eCFP and $hP2Y_1$-eYFP to 35.2% and reduced the distance between the donor and acceptor from 6 nm to 5.4 nm that argue for the interaction of between the $P2Y_1$ and $P2Y_{12}$ receptors. It has been

suggested that high FRET efficiency values could be an indication of the presence of multiple FRET acceptors (Vogel et al., 2006; Koushik et al., 2009), which in this case, 30 minutes after the addition of AR-C69931MX (1µM) caused more of $hP2Y_1$-eYFP receptors to be closer to $hP2Y_{12}$-eCFP receptors. However, estimating distances between the donor and the acceptor relies on certain assumptions, such as that the energy transfer occurs between a single donor and a single acceptor, with a discrete separation between them (Vogel et al., 2014). Also, that the distance represents a homogeneous population of dimers, all with the same separation, and that both donor and acceptor chromophores do not participate in the photo-physical process (blinking or bleaching) that might alter their ability to act as a FRET donor or acceptor (Vogel et al., 2014). Nevertheless, the presence of multiple oligomers is one of the assumptions, as both $P2Y_1$ and $P2Y_{12}$ receptors can form a dimer with another GPCRS (Ribeiro-Filho et al., 2016; Smith et al., 2017), or a homodimer (Choi et al., 2008).

Numerous studies have shown that the addition of ligands changes the rate of formation of GPCR homo- and heterodimers (Abadir et al., 2006; Łukasiewicz et al., 2010; Espinoza et al., 2011). For examples, colocalisation and interaction between AT_2 and B_2 receptors was detected using C-FRET microscopy (Abadir et al., 2006). It has been noticed that the combined treatment of an AT_2 agonist and a B_2 antagonist lead to an increase in AT_2–B_2 heterodimer formation, because both ligands caused an increase in both receptors' expression. Nevertheless, the B_2 antagonist significantly increased the AT_2 and B_2 receptors expression, but slightly increased the AT_2–B_2 heterodimer formation (Abadir et al., 2006). In another study was aimed to detect the dimer formation between HT_{2A} and D_2 receptors using FRET approach (Łukasiewicz et al., 2010). The level of FRET efficiency for the formed dimer was recused upon the addition of HT_{2A} and D_2 agonist and antagonists (Łukasiewicz et al., 2010). The presence of $P2Y_1$ and $P2Y_{12}$ homo-dimers, which are likely to have formed simultaneously with the $P2Y_1$-$P2Y_{12}$ heterodimer, may have influenced the effect of the AR-C69931MX. It is possible that the addition of AR-C69931MX weakened homo-dimerisation, which lead to an increase in energy transfer from the $P2Y_1$-$P2Y_{12}$ heterodimer. Unfortunately, we cannot distinguish homo-dimers as in this case both receptors will be tagged with the same fluorescent protein. Also, it is possible that the presence of AR-C69931MX might influence rearrangements of the protomer pair in a way that alters distance and receptors location, as both receptors are known to

internalise during the activation process (Jin et al., 1998; Cattaneo, 2015). The obtained results confirm the existence of $P2Y_1$-$P2Y_{12}$ dimers in the recombinant system, and the addition of AR-C69931MX changed the distance, influenced the rearrangements of the protomers or changed the promotion of hetero-dimerisation over homo-dimerisation.

ADP, MRS2365, BPTU, MRS2179 and AR-C69931MX did not appear to induce relocalisation of the PLA signals from the plasma membrane. Previous studies, such as Bohmer et al. (2013) and Lin et al. (2014) compared the control and treated samples by counting the PLA signals. However, PLA generated signals is hard to quantify and the quantification of it is not reliable, as the number of PLA signals differ from one plane to another across z-stacks, with individual spots merging throughout the volume of the cell. Consequently, we choose not to quantify PLA signals for the following experiments in order to avoid misinterpreting the data. Also, the amount of the primary antibodies present can impact the number of PLA signals, and/or can cause coalescence of positive PLA signals that cannot be accurately quantified (SigmaAldrich, 2020). Like any experiment, PLA has limitations, as we cannot confirm a direct interaction between the receptors, as they might interact through an adapter protein. Also, the distance between the receptors cannot be accurately determined, as it will depend on the size of the receptors, the tags, the primary proximity probes, the direct-conjugated proximity probes and the length of the attached oligonucleotides (Borroto-Escuela et al., 2016). Thus, it is important to use a FRET approach to compliment this finding, even though according to Weibrecht et al. (2010) there is no significant difference between the functional distance detected in PLA and FRET assays.

Previous studies on P2Y receptor heterodimerisation

A previous study provided evidence for the formation of a constitutive heterodimer between $hP2Y_1$ and $hP2Y_{12}$ receptors based on FRET studies in the tSA201 cell line where cotransfection of the two receptors lead to a significant FRET signal (Schicker et al., 2009). However, the difference between Schicker study and the current study is they used rat P2Y receptors, while in the current study human

receptors were used. Therefore, this is the first study to successfully demonstrate heterodimerisation between human $hP2Y_1$ and $hP2Y_{12}$ receptors using a combination of complimentary approaches. Schicker et al., (2009) used the $P2X_2$ receptor homodimer tagged with CFP and YFP as a positive control, while the interaction between ecto-nucleoside triphosphate diphosphohydrolases 1 (NTPD1)-YFP and $P2X_2$-CFP was used as a negative control. Unfortunately, the authors did not study the effect of ligands on the dimer, unlike in the current study. However, it shows that $P2Y_1$-$P2Y_{12}$ dimerisation occurs across different species.

Previous studies show that both $P2Y_1$ and $P2Y_{12}$ receptors can form heterodimers with other GPCRs. For instance, based on co-IP and FRET studies, $P2Y_1$ receptors showed a heteromeric association with $P2Y_2$ as well as $P2Y_4$ receptors, although there was no direct association between $P2Y_2$ and $P2Y_4$ receptors (Ribeiro-Filho et al., 2016). Using the same approaches in HEK293 cells, the $P2Y_1$ receptor was found to form a heterodimer with $P2Y_{11}$ receptors (Ecke et al., 2008). On the other hand, in a recent study by Khan et al. (2014) in HEK-293T cells using a BRET approach, it was found that PAR4 and $P2Y_{12}$ receptors dimerise, which was confirmed by Smith et al. (2017) in COS-7 cells using co-IP.

Also, other studies that used the same approach show that the coexpression of adenosine receptor subtypes were associated with an increase in FRET signal, for instance, adenosine A_1 or A_{2A} receptors when coexpressed with $hP2Y_1$ or $hP2Y_{12}$ receptors. A_1-$P2Y_1$ heterodimers were reported by Yoshioka et al., (2001; 2002), and the physical interaction for both $hP2Y_1$ and $hP2Y_{12}$ with A_{2A} receptors was confirmed by co-IP (Schicker et al., 2009). As it is known that HEK-293T cells (Suzuki et al., 2011) and the parent HEK-293 cell line (Inbe et al., 2004) endogenously express A_1 and A_{2A} receptors, it might be possible that a third or possibly more partners may be involved in what is referred to here as dimer formation. The same could be suggested for crosstalk between $hP2Y_1$ and $hP2Y_{12}$ receptors in tSA201 cells, for example, a possible multimeric $P2Y_1$-$P2Y_{12}$-A_{2A} receptor complex may exist (Nakata et al., 2010).

In summary, the data reported in this thesis so far are consistent with formation of a physical interaction between recombinant $P2Y_1$ and $P2Y_{12}$ receptors coexpressed in tSA201 cells. This then leads to two vital question, which are whether this is also true for native receptors endogenously expressed in cells in vivo and if so, what are the functions of the dimer?

Chapter Five

Expression, dimerisation and functional characterization of endogenous P2Y$_1$ and P2Y$_{12}$ receptors

1   Introduction

One of the major challenges in the GPCR dimerisation field is the detection of native dimers. In our studies, all experiments so far have relied upon over-expression of tagged $P2Y_1$ and $P2Y_{12}$ receptors, with dimerisation detected in a recombinant system. While confidence in the data has been provided through the different approaches used so far (co-IP, PLA and FLIM-FRET) that have each independently detected $P2Y_1$ and $P2Y_{12}$ heterodimersation in transfected cell systems, the same confidence cannot be provided that these receptors dimerise when expressed endogenously at native levels in physiologically relevant cell systems.

$P2Y_1$ and $P2Y_{12}$ receptors express natively in many cells, such as platelets, where they play an important role in aggregation (Hechler and Gachet, 2011). Both receptors also play a role in regulating pain signalling (Bailey and Connor, 2005; DuPen et al., 2007, Pan et al., 2008). Microglial cells are known to express a variety of P2X and P2Y receptors (Farber and Kettenmann, 2006). For example, $P2Y_1$, $P2Y_2$ and $P2Y_4$ receptors all mediated the activation of a K^+ current (Farber and Kettenmann, 2006). Also, $P2Y_{12}$ receptors and other $G_{(i/o)}$- coupled P2Y receptors are involved in microglial activation through a change in microglial morphology from resting to amoeboid form, which helps microglia migrate to an injury site (Honda et al., 2001). In this study, microglial cells were used as models to test endogenous $P2Y_1$ and $P2Y_{12}$ receptor expressions and interactions.

The experiments carried out in this chapter started with validating the microglial phenotype using specific markers. The expression of endogenous $P2Y_1$ and $P2Y_{12}$ receptors was visualised by immunofluorescence and physical association between them was studied using PLA.

2   Results

2.1   Validating microglial cells using a microglial marker

The BV-2 mouse microglial cells were gifted from Dr Hui-Rong Jiang (University of Strathclyde), while the HMC3 human microglial cells were obtained from ATCC. The suppliers state that both cell lines are microglial-like cells and the following experiments aimed to confirm this by using a microglial marker. The BV-2 cells generated by transduction of neonatal primary microglia with the v-raf/v-myc carrying J2 retrovirus, while the HMC3 cells were originate from the CHME-5 cell line (Timmerman et al., 2018). The marker that was used was the ionized calcium-binding adaptor 1 (Iba1), which is a protein that is expressed at high levels in microglial cells (Imai & Kohsaka, 2002). Iba1 also used to visualise morphological changes specific to microglial activity (Imai & Kohsaka, 2002). The following cells were dual stained with Iba1 and rhodamine phalloidin, a marker for F-actin, which is a component of the actin cytoskeleton that contributes to activation of microglia and determines the cell shape (Imai & Kohsaka, 2002).

In **Figure 5.1a**, it was clear that BV-2 mouse microglial cells expressed Iba1 (green). Furthermore, rhodamine phalloidin (red) positively stained F-actin and revealed intercellular structures for BV-2 cells. The merge image shows the expression of Iba1 inside the cells. Human microglial cells HMC3 also expressed Iba1 (green), mainly in the nucleus, which was different from BV-2 Iba1 localisation. Interestingly, rhodamine phalloidin (red) revealed different F-actin expression compared to the BV-2 cells (**Figure 5.1b)**.
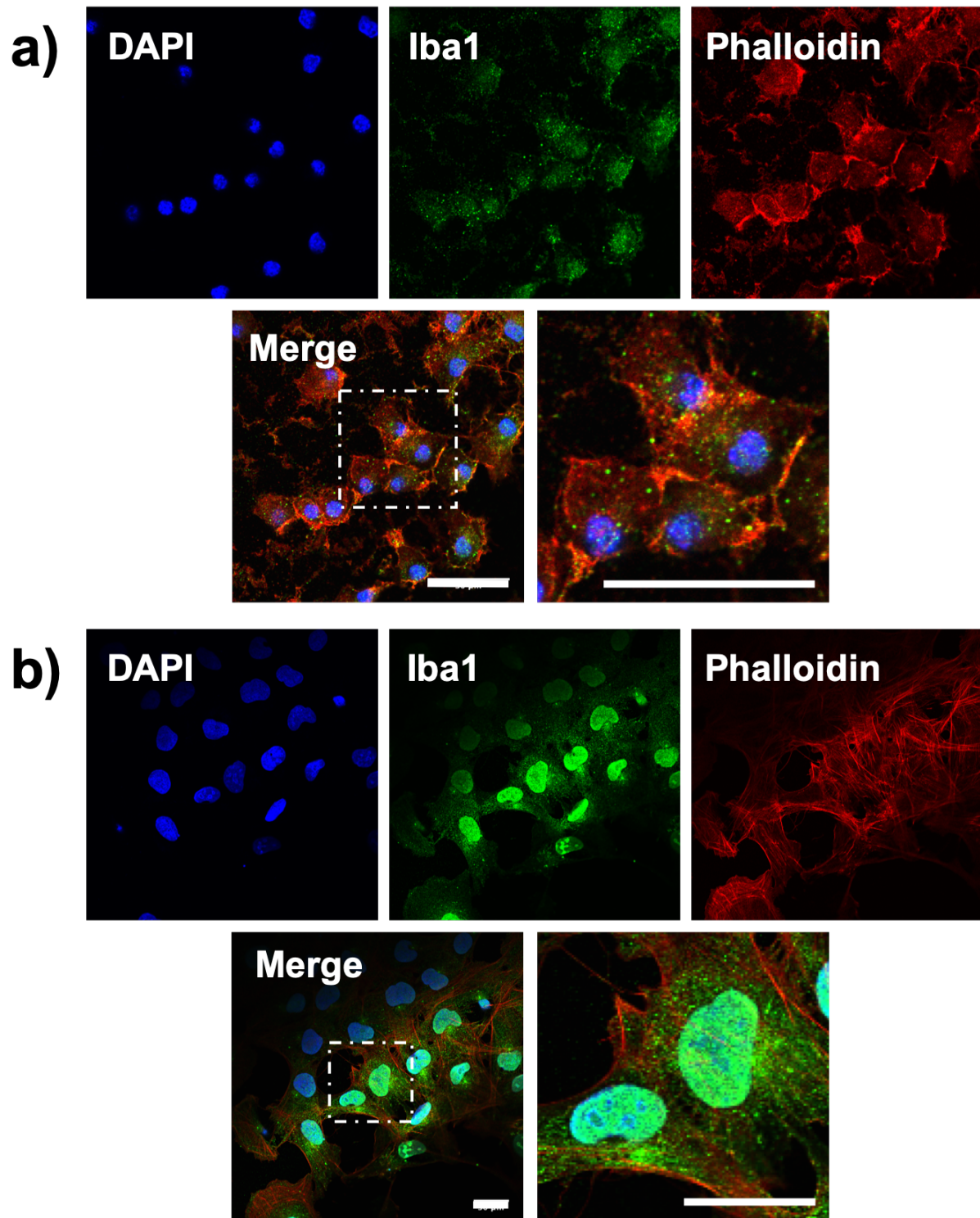
Figure 5.1: Indirect immunofluorescence of Iba1 expressed in microglial cells.
Representative images of fixed **a)** BV-2 and **b)** HMC3 cells are shown. The top row of each shows nuclear staining by DAPI (left), Iba1 (middle) and F-actin was observed by rhodamine phalloidin (right). The bottom rows show the overlay of all three images at the same (left) or greater (right) magnification. The images were obtained using confocal microscopy and cells were visualised at 63x (oil) magnification (scale bars = 30 μm), (n=2).

2.2   P2Y$_1$ and P2Y$_{12}$ receptors expression in BV-2 and HMC3 cells

To detect the presence of endogenous P2Y$_1$ and P2Y$_{12}$ receptors in microglial cells, selective endogenous antibodies were needed. An anti-P2Y$_1$ antibody, obtained from Santa-Cruz, was used that was raised against amino acid residues 146-265, which is near the C-terminus of hP2Y$_1$ (Santa Cruz Biotechnology, 2020). An anti-P2Y$_{12}$ antibody was obtained from Alomone, which was raised against amino acid residues 125-142 on the 2nd IL of hP2Y$_{12}$ (Alomone, 2020). As a control, P2Y$_1$ and P2Y$_{12}$ antibodies were used to stain tSA201 cells transfected with HA-hP2Y$_1$ and HA-hP2Y$_{12}$ receptors, respectively. In **Figure 5.2**, both P2Y$_1$ receptor and P2Y$_{12}$ receptors were detected by the primary antibodies, with signals detected both intracellularly and at the plasma membrane (green).
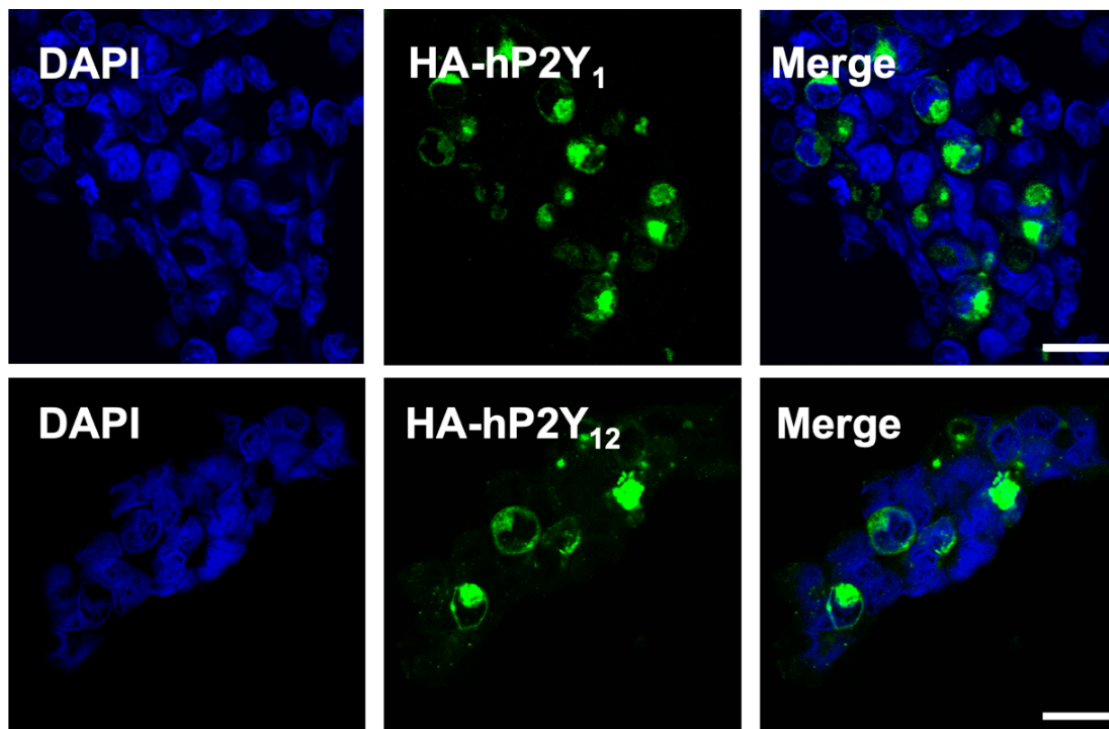
Figure 5.2: Indirect immunofluorescence of P2Y$_1$ and P2Y$_{12}$ receptors expressed in tSA201 cells.
Representative images of fixed tSA201 cells 48 hours after transfection with HA-hP2Y$_1$ (top row) and HA-hP2Y$_{12}$ (bottom row) receptors are shown. They show nuclear staining by DAPI (left-hand column), HA-hP2Y$_1$ and HA-hP2Y$_{12}$ staining (middle column) and overlay of both (right-hand column) and were visualised at 63x (oil) magnification using confocal microscopy (scale bar = 20 μm).

Next, experiments were designed to investigate the cellular localisation of $P2Y_1$ and $P2Y_{12}$ receptors in HMC3 and BV-2 cells by visualising the expression using confocal microscopy. Both cell lines were co-stained with $P2Y_1$ and $P2Y_{12}$ antibodies, alongside DAPI as a marker for the nucleus. In BV-2 cells, the $P2Y_1$ receptor was detected mainly intracellularly (red), while the $P2Y_{12}$ receptor was expressed intracellularly and cell surface (green). The merged image demonstrates the colocalisation of $P2Y_1$ and $P2Y_{12}$ receptors, as the overlap is represented as orange spots (**Figure 5.3a**). In HMC3 cells, $P2Y_1$ receptor was not readily detected (red), while $P2Y_{12}$ receptor expression was predominantly intracellular with overlapping expression with DAPI nuclear staining (blue). Thus, both receptors were colocalised in BV-2 cells, while HMC3 cells expressed the $P2Y_{12}$ receptor, but not the $P2Y_1$ receptor, albeit in an uncharacteristic nuclear localisation (**Figure 5.3b**).
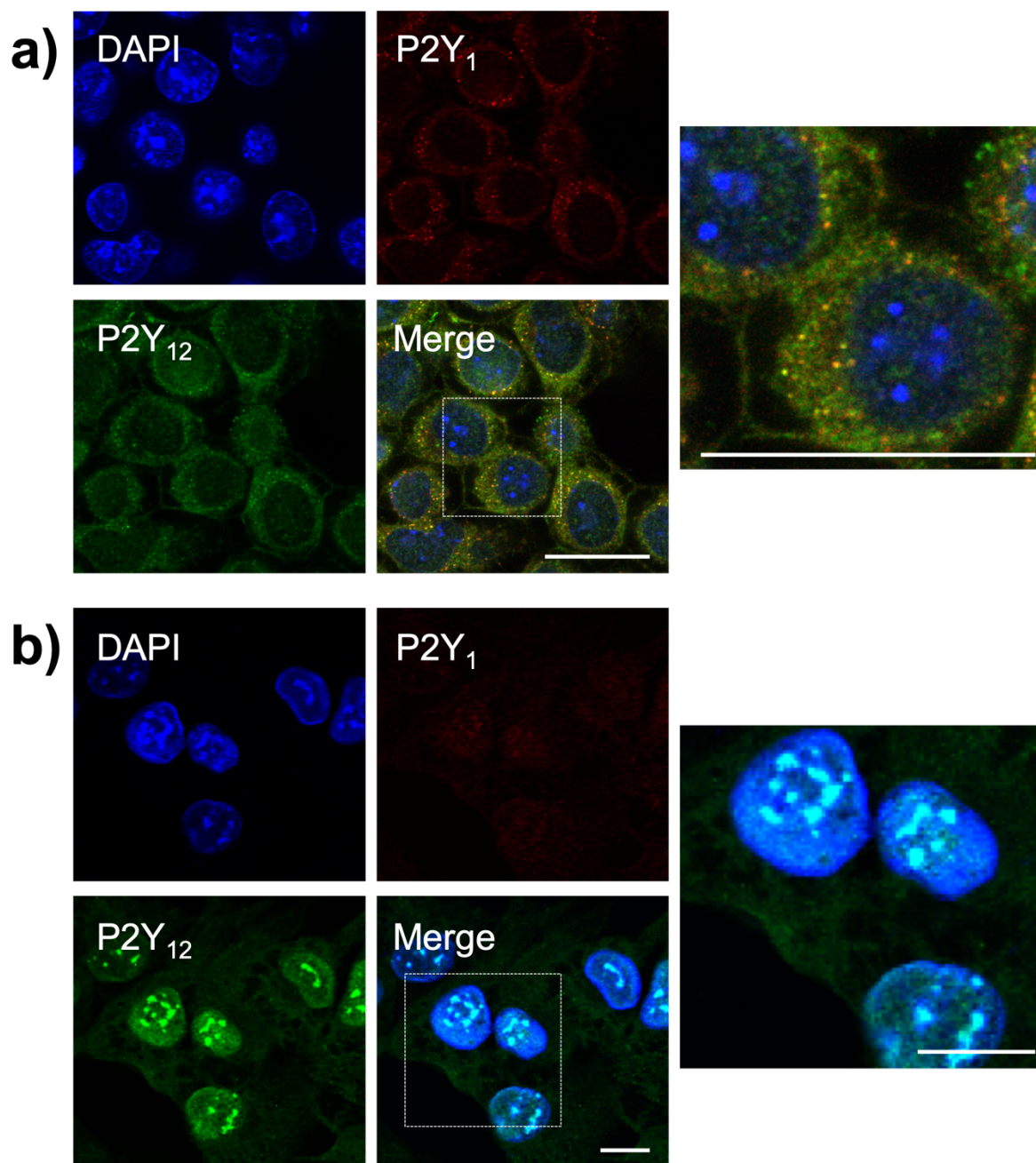
Figure 5.3: Testing endogenous P2Y$_1$ and P2Y$_{12}$ antibodies in BV-2 and HMC3 cells.

Representative images of fixed **a)** BV-2 and **b**) HMC3 cells are shown. The top row of each shows nuclear staining by DAPI (left) and P2Y$_1$ receptor staining (right). The bottom rows show hP2Y$_{12}$ receptor staining (left) and the overlay of all three images at the same (right) and greater (far right) magnification. The images were obtained using confocal microscopy and cells were visualised at 63x (oil) magnification (scale bars = 20 μm).

Next, P2Y$_1$ and P2Y$_{12}$ receptor expression was assessed using western blotting of tSA201, BV-2 and HMC3 cells and compared to the expression in tSA201 cells transfected with HA-hP2Y$_1$ or HA-hP2Y$_{12}$ receptor. **Figure 5.4** top panel, shows that when samples were probed with the anti-HA antibody, no staining was apparent in any of the cell lines, apart from those expressing HA-hP2Y$_1$ and HA-hP2Y$_{12}$ receptors. The patterns of staining were similar to those already described in chapter 3. **Figure 5.4** (middle-upper panel) shows that when samples were probed with the anti-P2Y$_1$ antibody, all lanes showed a band at ~50 kDa, which probably represents the P2Y$_1$ receptor monomer, as the predicted molecular weight is 42 kDa, as well as another band at ~63 kDa.

Figure 5.4 (middle-lower panel) shows that tSA201, BV-2 and HMC3 cell lines expressed a P2Y$_{12}$ monomer band at ~50 kDa, another band at ~72 kDa and a P2Y$_{12}$ dimer band at ~100 kDa. HMC3 cells expressed a dense band at ~36 kDa. However, when the HA-hP2Y$_1$ receptor was expressed in tSA201 cells, the intensity of all P2Y$_{12}$ receptor bands was reduced, except the band at ~72 kDa. On the other hand, when the HA-hP2Y$_{12}$ receptor was expressed in tSA201 cells, the P2Y$_{12}$ receptor expression appeared as a smear from 40 to >250, kDa with a prominent band at ~72 kDa. α-Tubulin staining demonstrates equal loading of the samples **Figure 5.4** bottom panel.
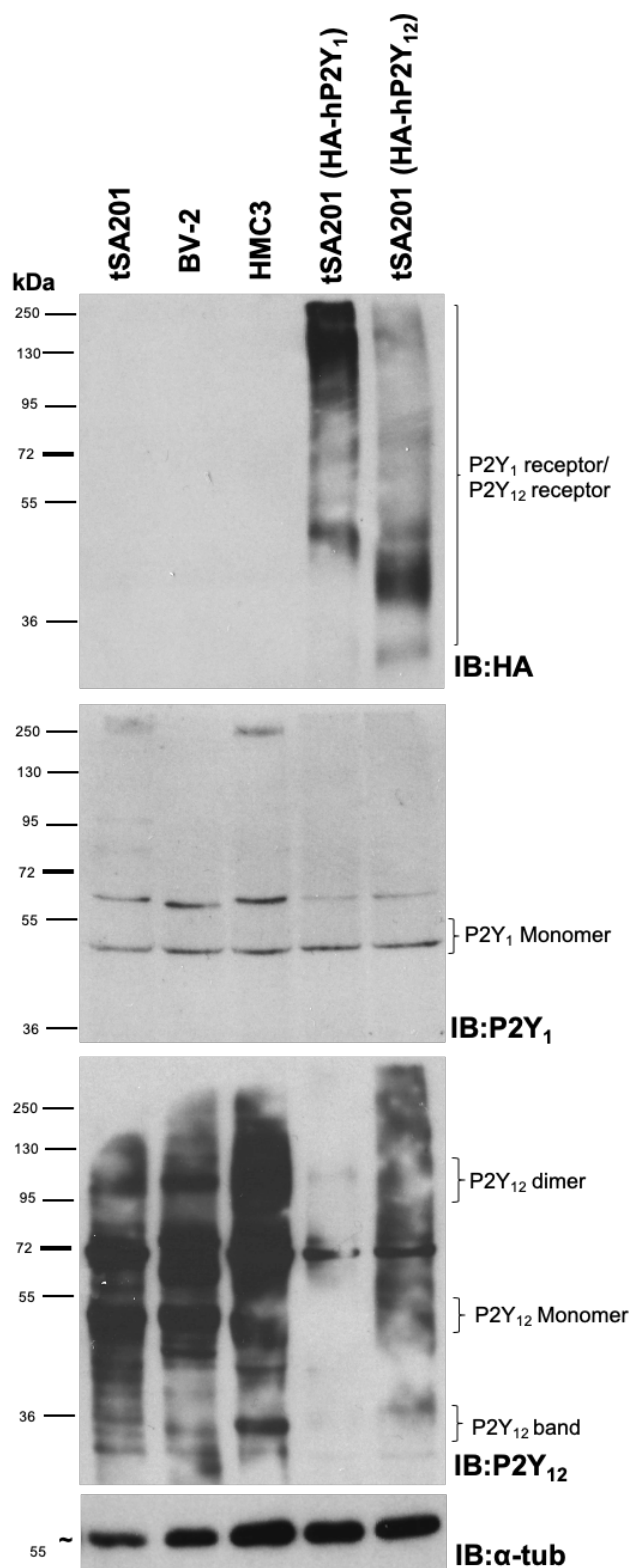
Figure 5.4: P2Y$_1$ and P2Y$_{12}$ expression in different cell lines.
Western blots of whole cell lysates of tSA201 (lane 1), BV-2 (lane 2) and HMC3 (lane 3) cells and tSA201 cells prepared 48 hours after transfection with HA-hP2Y$_1$ receptors (lane 4) or HA-hP2Y$_{12}$ receptors (lane 5) are shown. Samples were probed with anti-HA, (top panel) anti-P2Y$_1$ (middle upper panel), then anti-P2Y$_{12}$ (middle lower panel) antibodies. Molecular weight markers are shown on the left. α-Tubulin (α-tub) was used to confirm equal loading of samples (bottom panel).

The gene expression was verified with Real-Time (RT) PCR to detect $P2Y_1$ and $P2Y_{12}$ mRNA expression using species-specific sets of primers for each. Both $P2Y_1$ and $P2Y_{12}$ receptor mRNA was detected in BV-2 cells, whereas only $P2Y_{12}$ receptor expression was detected in HMC3 cells (**Figure 5.5**).
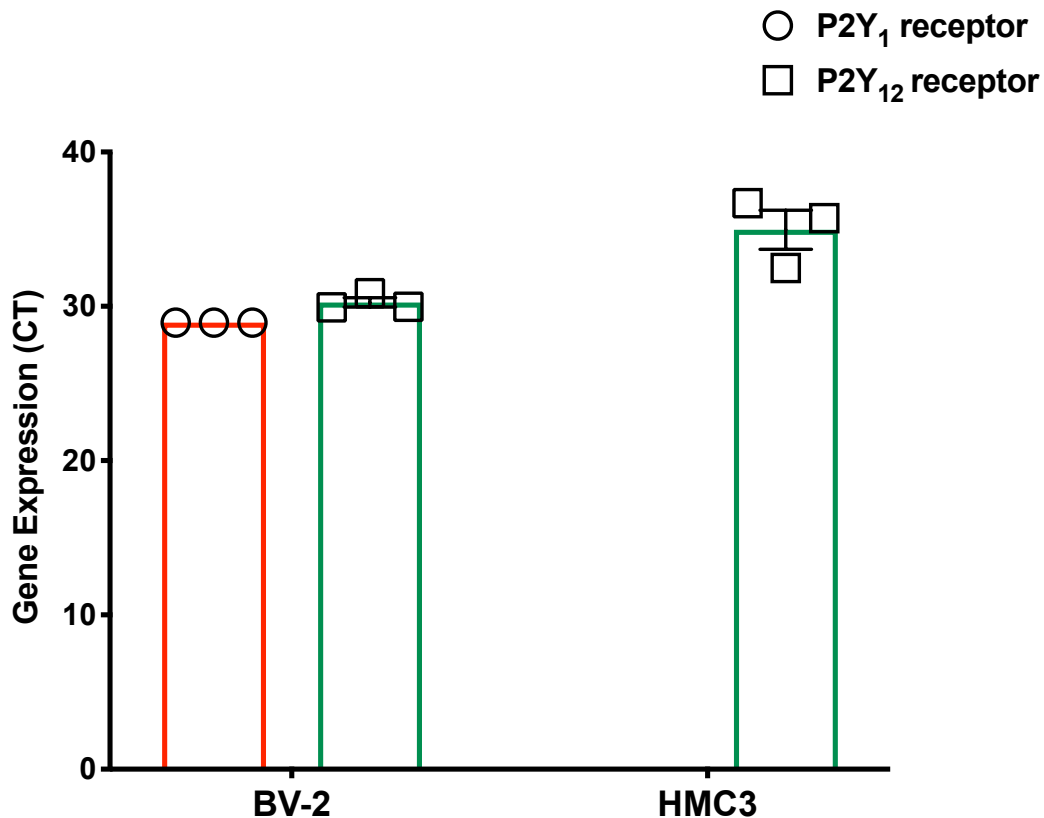
Figure 5.5: Relative expression of $P2Y_1$ and $P2Y_{12}$ receptors in BV-2 and HMC3 cells.
RT-PCR analysis of the mRNA expression levels of $P2Y_1$ (red) and $P2Y_{12}$ (green) receptors in BV-2 (n=3; n=3) and HMC3 (n=1; n=3) cells is shown. mRNA expression is expressed as cycle threshold (ct) of gene expression of the receptors. Data values shown are the mean ± SEM.

2.3 Ca^{2+} flux imaging of BV-2 and HMC3 cells with P2Y$_1$ and P2Y$_{12}$ agonists

These data reveal differences in the expression of P2Y$_1$ and P2Y$_{12}$ receptor mRNA and protein in BV-2 and HMC3 cells. The next experiments examined whether this leads to differences in functional expression of the P2Y$_1$ receptor using a Ca^{2+} flux assay. The concentration-dependent rise in fluorescence signal that indicated the release of Ca^{2+} was evoked by ADP, endogenous agonist, and MRS2365.

In BV-2 cells, ADP (10 nM-10 µM) evoked a concentration-dependent rise in cytoplasmic Ca^{2+} (**Figure 5.6**, purple), with an EC$_{50}$= 826.4 nM (95 % cl. 387.8 – 1761 nM) and an E$_{max}$ of 2.2 $\pm$ 0.09 signal/background (n=5). The selective P2Y$_1$ agonist, MRS2365 (0.3 nM-30 µM), also evoked a concentration-dependent rise in cytoplasmic Ca^{2+}, but the concentration-responses curves were shifted to the left compared with that of ADP (EC$_{50}$ = 12.3 nM (95 % cl. 4.1 – 37.2 nM)) and the E$_{max}$ was lower (1.7 $\pm$ 0.07 signal/background) (n=6) (**Figure 5.6**, blue).

In HMC3 cells, ADP (1 µM- 3 mM) also evoked a concentration-dependent rise in cytoplasmic Ca^{2+} (**Figure 5.6**, black), but with a much higher EC$_{50}$ (138 µM (95 % cl. 54.4 – 349.6µM)) and very low E$_{max}$ (1.6 $\pm$ 0.16 signal/background compared to BV-2 cells (n=5). Interestingly, MRS2365 (100 nM-100 µM), did not evoke a concentration-dependent rise in cytoplasmic Ca^{2+} (n=3) (**Figure 5.6**, grey). These results are consistent with the RT-PCR and IF data above and are consistent with low expression of P2Y$_1$ receptors in HMC3 cells.
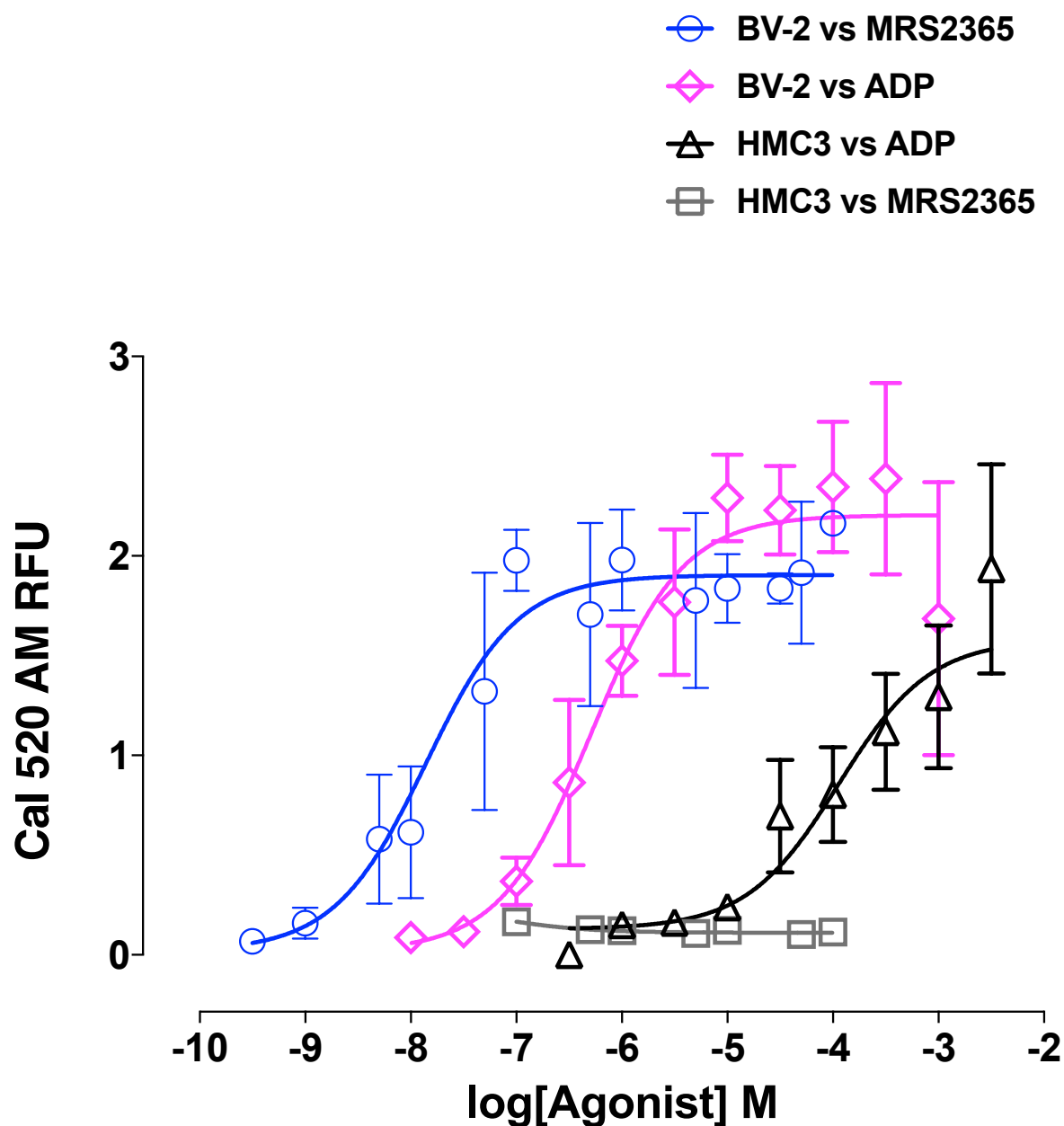
Figure 5.6: The effect of P2Y$_1$ receptor agonists on intracellular Ca^{2+} levels in BV-2 and HMC3 cells.

The mean peak amplitude of responses evoked by ADP and MRS2365 in BV-2 and HMC3 cells is shown. n=5 for ADP and n=6 for MRS2365 in BV-2 cells and n=5 for ADP and n=3 for MRS2365 in HMC3 cells. Responses are expressed as signal/background. Vertical lines show s.e.m..

2.4   Investigating the cellular colocalisation of endogenous P2Y$_1$ and P2Y$_{12}$ receptors in BV-2 cells

The data above indicate that only BV-2 cells express both P2Y$_1$ and P2Y$_{12}$ receptors at appreciable levels. So, for the next set of experiments, the cellular localisation of the native P2Y receptors was studied in BV-2 cells using confocal microscopy and line-scanning. BV-2 cells were double-stained with anti-P2Y$_1$ and anti-P2Y$_{12}$ receptor anti-bodies (**Figure 5.7**). The line scan of fluorescence (**Figure 5.7, bottom, middle panel),** shows that both express predominantly inside the cell, with some receptor localisation evident at the membrane. Furthermore, the PDM image (**Figure 5.7, top, right-hand panel)** indicates a high overlap of pixels (white), with a PCC value that is close to one. Finally, the scatter plot of intensity distributions of both, plotted against one another (**Figure 5.7, bottom, right-hand panel)** shows a high correlation of distribution of the two proteins. Thus, P2Y$_1$ and P2Y$_{12}$ receptors appear to localise close to each other, around the nucleus.

Finally, the PCC for colocalisation of P2Y$_1$ and P2Y$_{12}$ receptors were analyzed statistically. As shown in **Figure 5.8**, The P2Y$_1$ and P2Y$_{12}$ receptors showed strong colocalisation in BV-2 cells, which was similar to the colocalisation between the recombinant receptors expressed in tSA201 cells.
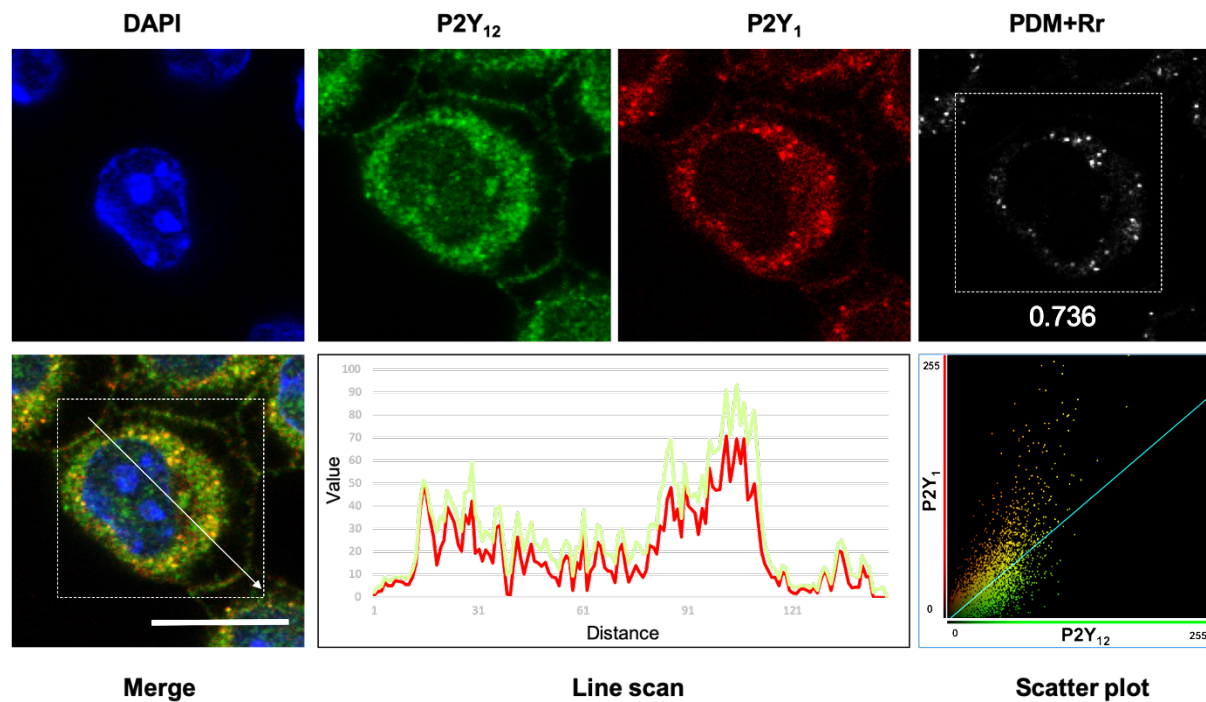
Figure 5.7: P2Y$_1$ and P2Y$_{12}$ colocalise in BV-2 cells.

Representative images of the same field of BV-2 cells show: top row- nuclear staining with DAPI (blue), anti-P2Y$_{12}$ receptor antibody staining (green), anti-P2Y$_1$ receptor antibody staining (red) and the positive PDM value of the overlaid P2Y$_1$ and P2Y$_{12}$ and Rr=Pearson's correlation coefficient. The bottom row shows overlay of the three staining images, with the location of the line scan indicated by the diagonal white line (left hand panel), the line scans of the P2Y$_1$ and P2Y$_{12}$ fluorescence intensity across the cells (middle panel) and a scatter plot P2Y$_1$ vs P2Y$_{12}$ fluorescence intensity. Images were obtained by confocal microscopy at 63x (oil) magnification (scale bars = 10 µm).
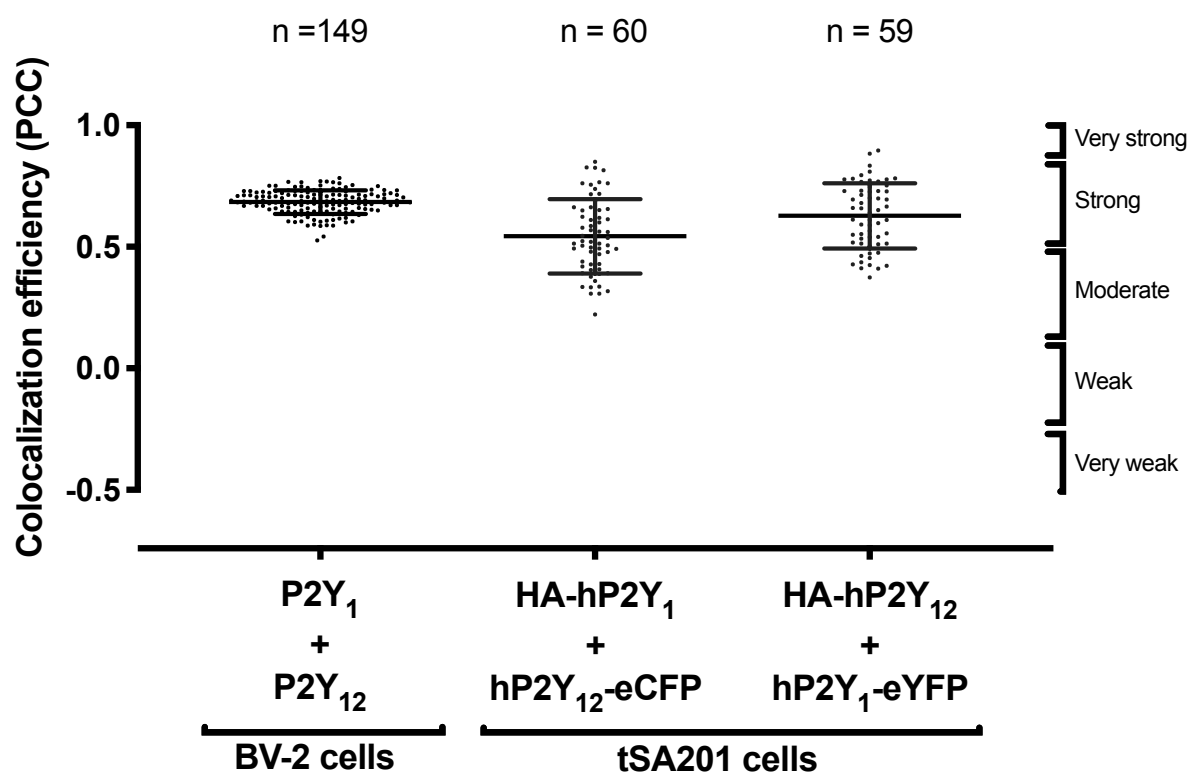
Figure 5.8: Pearson's Correlation Coefficients for colocalisation in BV-2 cells.

The plot shows Pearson's correlation coefficient values for the colocalisation measured in BV-2 cells (native $P2Y_1$ and $P2Y_{12}$) compared to tSA201 cells cotransfected with (HA-$hP2Y_1$ and eCFP), (HA-$hP2Y_1$ and $hP2Y_{12}$-eCFP), (HA-$hP2Y_{12}$ and eYFP) and (HA-$hP2Y_{12}$ and $hP2Y_1$-eYFP). The data presented represents the average ± SD of n= 59-149 cells from three individual experiments. The tSA201 cell data were previously shown in Figure 3.13 and are included here for comparison.

2.5 Optimisation of proximity ligation assay (PLA) using endogenous antibodies

After employing PLA in the recombinant system in **Chapter four** using selective antibodies against the tags, the next step was to confirm if this technique is also effective when using antibodies directed against $P2Y_1$ and $P2Y_{12}$ receptors themselves, before applying it to detect endogenous heterodimer. To do so, tSA201 cells were cotransfected with HA-$hP2Y_1$ and $hP2Y_{12}$-eCFP receptors then fixed, permeabilized, and incubated with primary antibodies under the following 4 conditions: (**Figure 5.9a**) anti-HA and anti-GFP, (**Figure 5.9b**) anti-HA and anti-$P2Y_{12}$, (**Figure 5.9c**) anti-GFP and anti-$P2Y_1$ or (**Figure 5.9d**) anti-$P2Y_{12}$ and anti-$P2Y_1$ primary antibodies. Following the incubation with the primary antibodies, PLA was carried out as previously described.
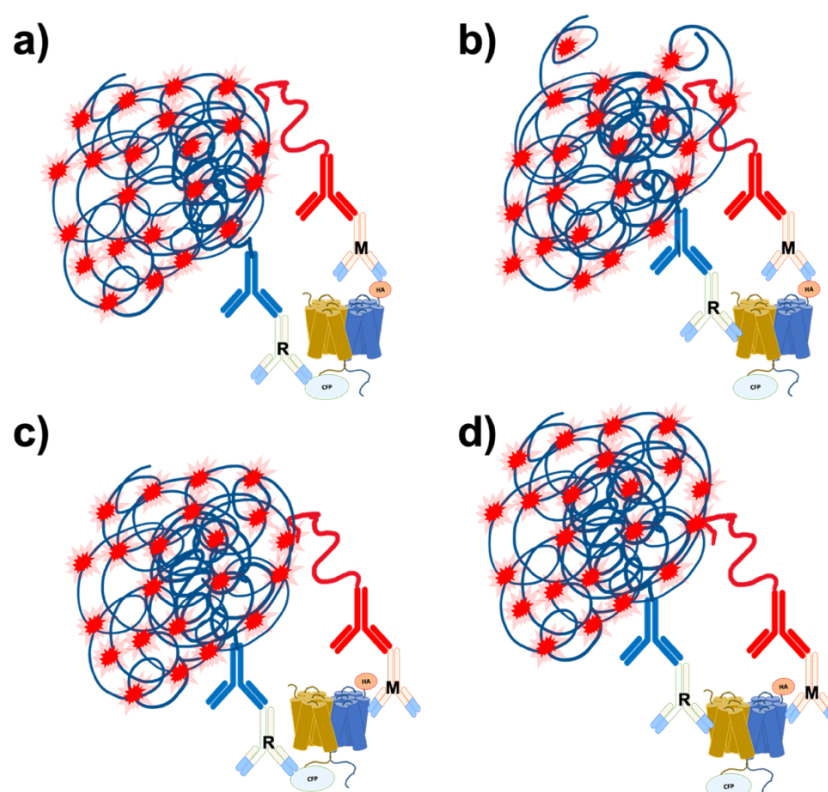
Figure 5.9: Schematic representation of indirect PLA to detect HA-$hP2Y_1$-$hP2Y_{12}$-eCFP heteromer.
The yellow receptor represents $P2Y_{12}$ receptor and the cyan tag represents the eCFP tag, while the blue receptor represents $P2Y_1$ receptors and the red tag represents the HA tag. Samples were incubated with **a)** anti-HA and anti-GFP, **b)** anti-HA and anti-$P2Y_{12}$, **c)** anti-GFP and anti-$P2Y_1$ or **d)** anti-$P2Y_{12}$ and anti-$P2Y_1$ primary antibodies (R=Rabbit source; M=Mouse source). Secondary antibodies coupled with oligonucleotides (PLA probes) bind to the primary antibodies and form the signals that detected by fluorescent microscopy.

To begin, tSA201 cells incubated with anti-HA and anti-GFP primary antibodies were used as a control, as in chapter four. **Figure 5.10a** shows $hP2Y_{12}$-eCFP expression at the plasma membrane (green) and an abundant PLA signal (red dots) between the coexpressed receptors. PLA was subsequently carried out in transfected cells using anti-HA and anti-$P2Y_{12}$ antibodies (**Figure 5.10b**) and anti-GFP and anti-$P2Y_1$ antibodies (**Figure 5.10c**). Both protocols revealed $hP2Y_{12}$-eCFP expression at the plasma membrane (green) and a clear PLA signal (red dots), though the PLA signal was less in cells that were incubated with anti-GFP and anti-$P2Y_1$ antibodies. Finally, PLA carried out using antibodies directed against endogenous sequences within the $P2Y_1$ and $P2Y_{12}$ receptors produced a clear PLA signal (red dots) (**Figure 5.10d**). Thus, antibodies against amino acid sequences within $P2Y_1$ and $P2Y_{12}$ receptors can be used to measure protein-protein interactions using PLA, though it must be noted that the receptors here were over-expressed.
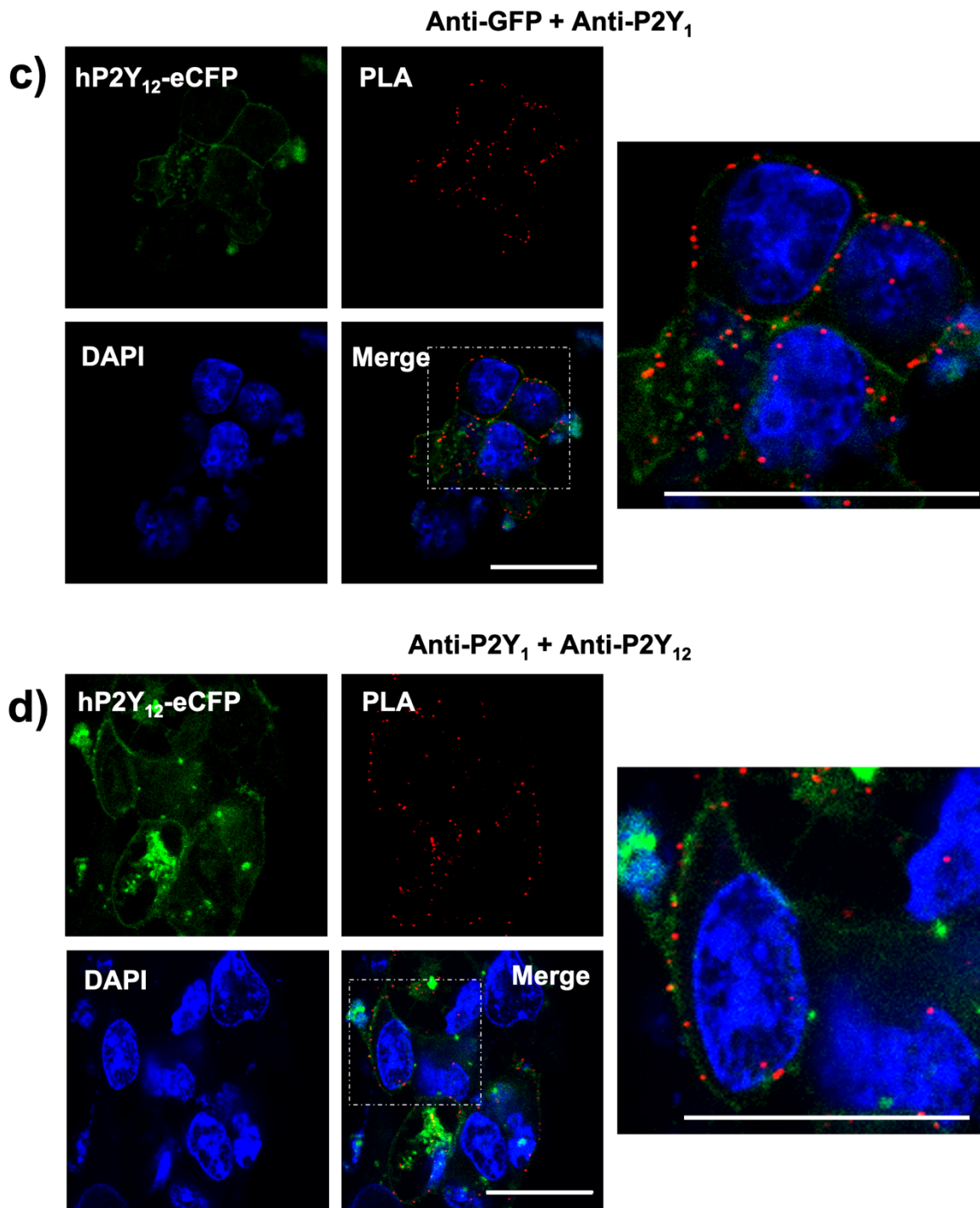
Figure 5.10: PLA between HA-hP2Y$_1$ and hP2Y$_{12}$-eCFP receptors with different primary antibodies incubations.

The images show fixed tSA201 cells 48 hours after cotransfection with HA-hP2Y$_1$ and hP2Y$_{12}$-eCFP. Cells were stained with **a)** anti-HA and anti-GFP; **b)** anti-P2Y$_{12}$ and anti-HA; **c)** anti-GFP and anti-P2Y$_1$; **d)** anti-P2Y$_1$ and P2Y$_{12}$ antibodies, then PLA was performed. The top row of each shows hP2Y$_{12}$-eCFP (left) and PLA (right) staining. The bottom rows show nuclear staining by DAPI (left) and the overlay of all three images at the same (right), and greater (far right) magnification. The images were obtained using confocal microscopy and cells were visualised at 63x (oil) magnification (scale bars = 20 µm). Data are representative of 2 individual experiments.

2.6 Investigating the physical interaction of endogenous P2Y$_1$ and P2Y$_{12}$ receptors via PLA

Having confirmed an interaction between recombinant P2Y$_1$ and P2Y$_{12}$ receptors using antibodies directed against endogenous epitopes, the aim of the next set of experiments was to investigate interaction between the native receptors in BV-2 and HMC3 cells.

In **Figure 5.11a,** PLA was performed in BV-2 cells and the images show PLA signals (red dots) around the cell nucleus, which indicate close proximity between endogenous P2Y$_1$ and P2Y$_{12}$ receptors. However, no PLA signal was seen in HMC3 cells (**Figure 5.11b**), which was not surprising given the lack of P2Y$_1$ receptor expression in this cell line. Thus, these data confirm that nativeP2Y$_1$ and P2Y$_{12}$ receptor can physically interact in BV-2 microglial cells.
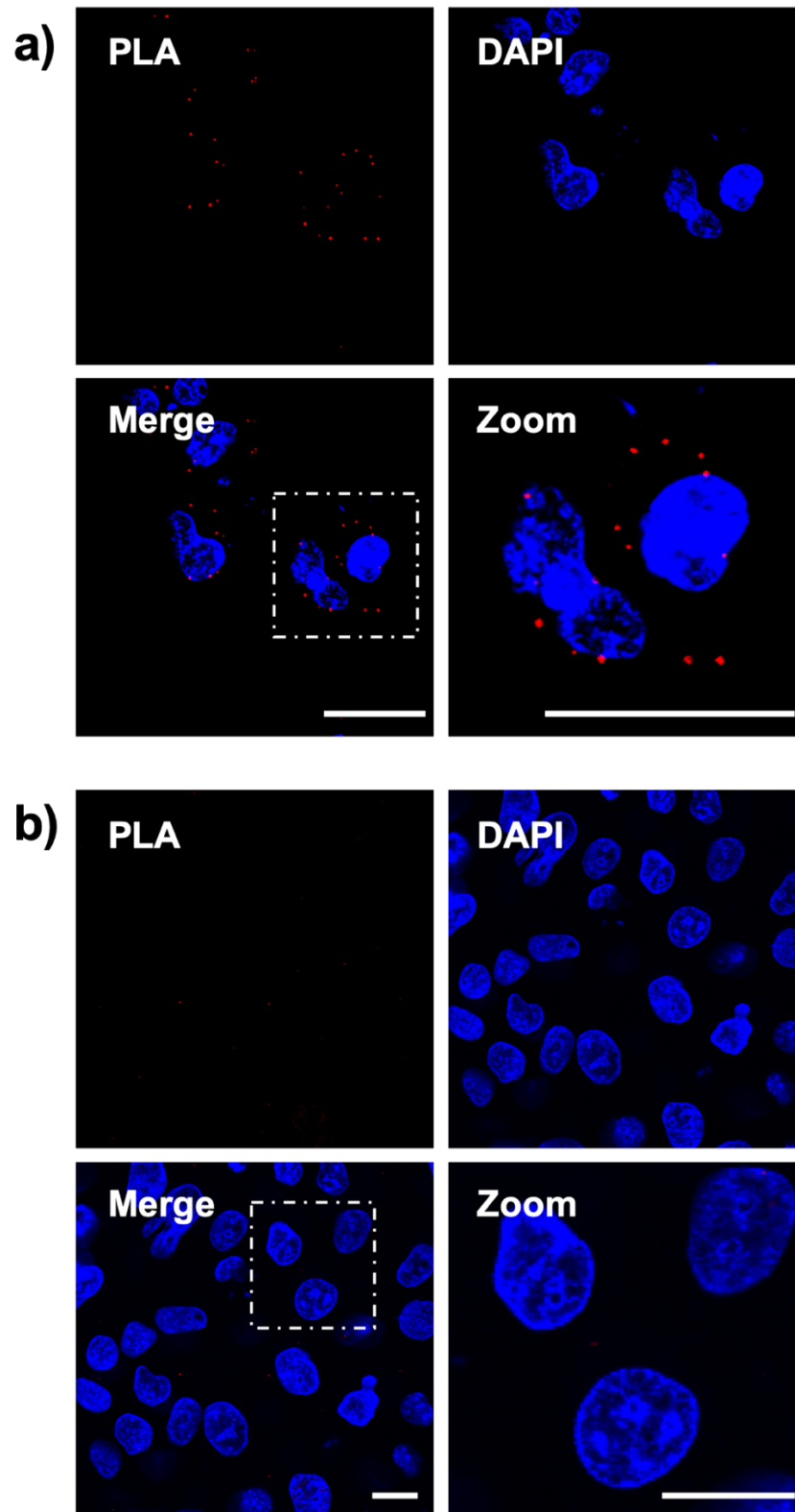
Figure 5.11: PLA between endogenous P2Y$_1$ and P2Y$_{12}$ receptors.
Images of fixed **(a)** BV-2 and **(b)** HMC3 cells are shown. The top row of each shows PLA (left) and nuclear staining by DAPI (right). The bottom rows show the overlay of the two images at the same (left) and greater magnification (right). The images were obtained using confocal microscopy and cells were visualised at 63x (oil) magnification (scale bars = 20 μm). Data are representative of 2 individual experiments.

2.7 Effect of different ligands on endogenous $P2Y_1$ & $P2Y_{12}$ receptor expression in BV-2 cells

The aim of the next series of experiments was to determine the effects of exposure to $P2Y_1$ and $P2Y_{12}$ receptor agonists and antagonists for 5 or 30 minutes on the expression of the native receptors in BV-2 cells. First, the effects of the $P2Y_1$ and $P2Y_{12}$ agonist, ADP (10μM) and the selective $P2Y_1$ agonist, MRS2365 (3μM) (Bourdon et al., 2006) were investigated (**Figure 5.12**). In untreated cells (**Figure 5.12,** 1st row) $P2Y_1$ receptors expressed mainly intracellularly (red), and $P2Y_{12}$ receptors were expressed intracellularly and at the cell surface (green), which is similar to the data shown in **Figure 5.3a**. Post treatment with ADP for 5 minutes (**Figure 5.12,** 2nd row), $P2Y_1$ receptor (red) expression appeared to be unchanged, while $P2Y_{12}$ receptors (green) expressed internally and localised at the periphery of the cell in vesicular structures. The overlay images of the two channels indicate that there is no close colocalisation of the $P2Y_1$ and $P2Y_{12}$ receptors. 30 minutes post treatment with ADP (**Figure 5.12,** 3rd row), $P2Y_1$ receptors again showed similar expression intracellularly (red), whilst $P2Y_{12}$ receptor expressed intracellularly and at cell surface (green) with slight change in receptor morphology. When BV-2 cells were treated with MRS2365 for 5 (**Figure 5.12,** 4th row) and 30 (**Figure 5.12,** 5th row) minutes, $P2Y_1$ and $P2Y_{12}$ receptor expression was similar to that in the untreated cells.
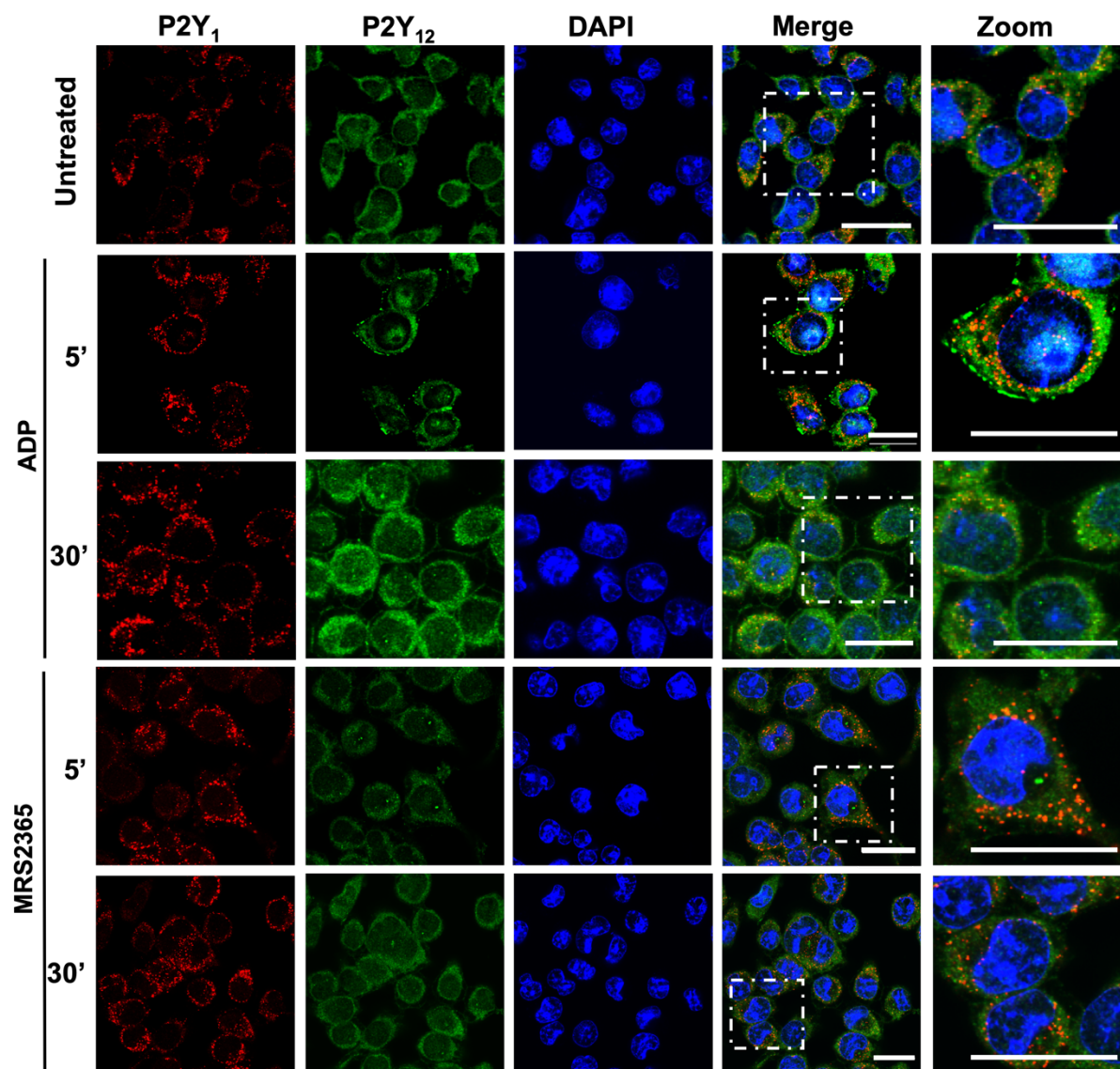
Figure 5.12: Endogenous P2Y$_1$ and P2Y$_{12}$ receptors expressed in BV-2 cells post-treatment with P2Y$_1$ and P2Y$_{12}$ agonists.

Representative images of fixed BV-2 are shown. On the top row is untreated cells, while the other rows are cells treated with ADP and MRS2365 for 5 min and 30 min, as indicated. The images show P2Y$_1$ receptor staining (P2Y$_1$ column), P2Y$_{12}$ receptor staining (P2Y$_{12}$ column), nuclear staining by DAPI (DAPI column), overlay of both (Merge column) and magnification (Zoom column). Cells were visualised using confocal microscopy at 63x (oil) magnification (scale bar = 20 µm) using (Ex: 555 nm) filter setting to detect P2Y$_1$, while (Ex: 488 nm) filter setting to detect P2Y$_{12}$. Data are representative of 2 individual experiments.

The second set of experiments determined the effects of the $P2Y_1$ negative allosteric modulator, BPTU (1µM) (Mane et al., 2016) and the selective orthosteric $P2Y_1$ antagonist, MRS2179 (10µM) (Mitchell et al., 2012). The untreated cells (**Figure 5.13,** 1st row) showed similar results as the untreated cells in the previous experiments. Post treatment with BPTU for 5 minutes (**Figure 5.13,** 2nd row), $P2Y_1$ receptor (red) expression was unchanged, while $P2Y_{12}$ receptor (green) localised at the periphery of the cell in structures with no overlap with $P2Y_1$ receptor. Also, the $P2Y_{12}$ receptor became almost undetectable intracellularly. 30 minutes post treatment with BPTU (**Figure 5.13,** 3rd row), $P2Y_1$ receptor showed similar expression intracellularly (red), and $P2Y_{12}$ receptor (green) localised intracellularly just like the untreated cells. After BV-2 cells were treated with MRS2179 for 5 (**Figure 5.13,** 4th row) and 30 (**Figure 5.13,** 5th row) minutes, $P2Y_1$ and $P2Y_{12}$ showed the same results as the untreated cells.
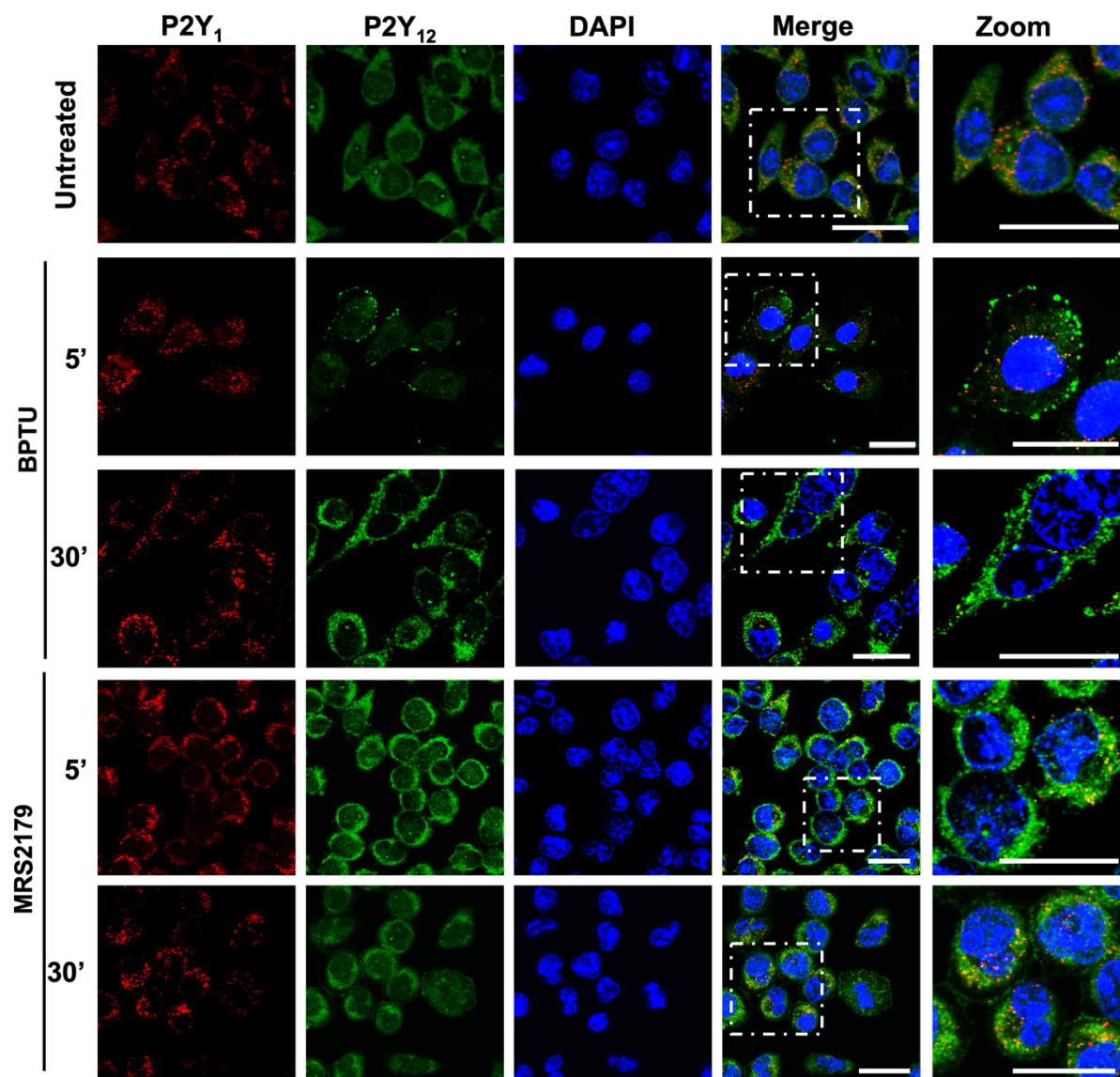
Figure 5.13: Endogenous P2Y$_1$ and P2Y$_{12}$ receptors expressed in BV-2 cells post-treatment with P2Y$_1$ antagonists.

Representative images of fixed BV-2 are shown. On the top row is untreated cells, while the other rows are cells were treated with BPTU and MRS2179 for 5 min and 30 min. The representative show P2Y$_1$ (P2Y$_1$ column), P2Y$_{12}$ (P2Y$_{12}$ column), nuclear staining by DAPI (DAPI column), overlay of both (Merge column) and magnification (Zoom column). Using confocal microscopy, cells were visualised at 63x (oil) magnification (scale bar = 20 μm) using (Ex: 555 nm) filter setting to detect P2Y$_1$, while (Ex: 488 nm) filter setting to detect P2Y$_{12}$. Data are representative of 2 individual experiments.

The third set of experiments visualised the expression of the receptors in BV-2 cells before and after treatment with the selective $P2Y_{12}$ antagonist, AR-C69931MX (1µM) (Mitchell et al., 2012) (**Figure 5.14**). The untreated cells (**Figure 5.14,** 1st row) showed similar results as the untreated cells in the previous experiments. Post treatment with AR-C69931MX for 5 minutes (**Figure 5.14,** 2nd row), $P2Y_1$ receptor (red) expression remained changed, but some of $P2Y_{12}$ receptors (green) localised at the periphery of the cell in vesicular structures and some localised intracellularly. Also, a change in cell morphology was observed. 30 minutes post treatment with AR-C69931MX (**Figure 5.14,** 3rd row), $P2Y_1$ and $P2Y_{12}$ showed the same results as the untreated cells.
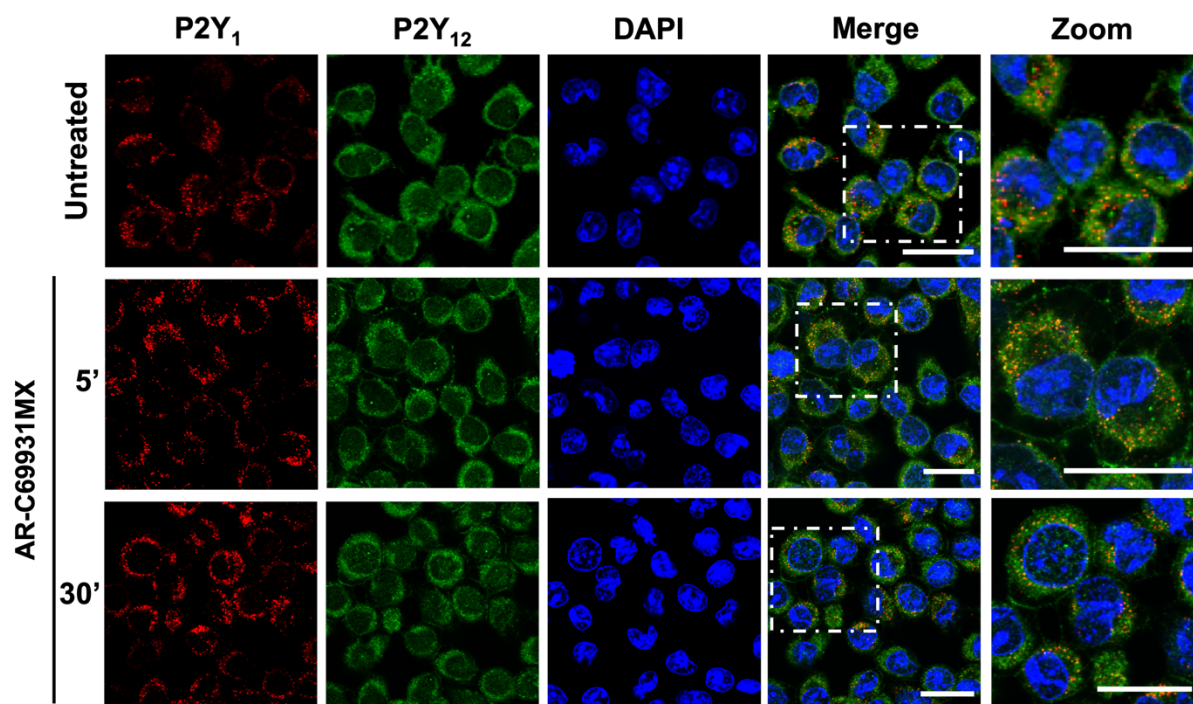
Figure 5.14: Endogenous P2Y$_1$ and P2Y$_{12}$ receptors expressed in BV-2 cells post-treatment with P2Y$_{12}$ antagonist.

Representative images of fixed BV-2 are shown. On the top row is untreated cells, while the other rows are cells were treated with AR-C69931MX for 5 min and 30 min. The representative show P2Y$_1$ (P2Y$_1$ column), P2Y$_{12}$ (P2Y$_{12}$ column), nuclear staining by DAPI (DAPI column), overlay of both (Merge column) and magnification (Zoom column). Using confocal microscopy, cells were visualised at 63x (oil) magnification (scale bar = 20 µm) using (Ex: 555 nm) filter setting to detect P2Y$_1$, while (Ex: 488 nm) filter setting to detect P2Y$_{12}$. Data are representative of 2 individual experiments.

The final set of these experiments determined the expression of receptors in BV-2 cells using western blotting. **Figure 5.15** (top panel) shows that when samples were probed with the anti-P2Y$_{12}$ antibody, P2Y$_{12}$ receptors resolved as 3 bands at ~30, ~50, ~70 kDa and a higher molecular band between 95 and 130 kDa. The ~50 kDa probably represents the P2Y$_{12}$ monomer form, while the bands between 95 and 130 kDa, might represent the dimer form of the receptor. α-Tubulin expression was similar in each lane at 55 kDa (**Figure 5.15,** bottom panel).

Due to the noticeable change in P2Y$_{12}$ dimer band intensity after treatment with P2Y$_1$ and P2Y$_{12}$ agonists and antagonist, the bands were quantified from the upper panel. The dimer form of the P2Y$_{12}$ receptor showed a significant increase upon the addition of MRS2365 for 5 and 30 minutes, as well as 5 minutes exposure to BPTU and MRS2179 ($P<0.05$) (**Figure 5.16**).
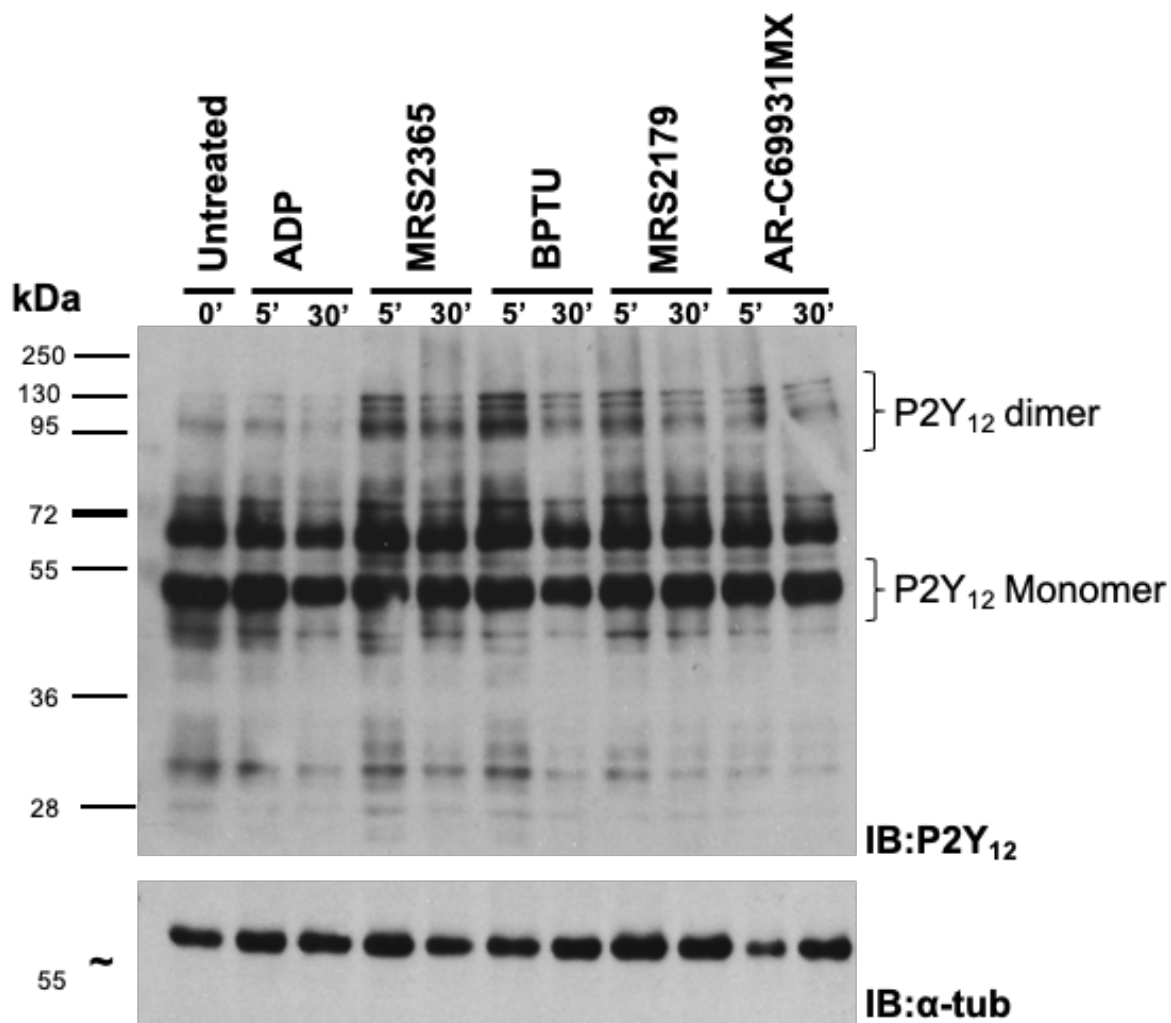
Figure 5.15: The effects of P2Y$_1$ and P2Y$_{12}$ receptor ligands on P2Y$_{12}$ receptors in BV-2 cells.

Immunoblots of P2Y$_{12}$ receptor expression in whole cell lysates of BV-2 cells before and after exposure of the cells to 10µM ADP, 3µM MRS2365, 1µM BPTU, 10µM MRS2179 and 1µM AR-C69931MX for 5 or 30 minutes are shown. The receptors were detected using specific antibodies against P2Y$_{12}$ receptor (top panel). Molecular weight markers are shown on the left. α-Tubulin (α-tub) was used to confirm equal loading of samples (bottom panel).
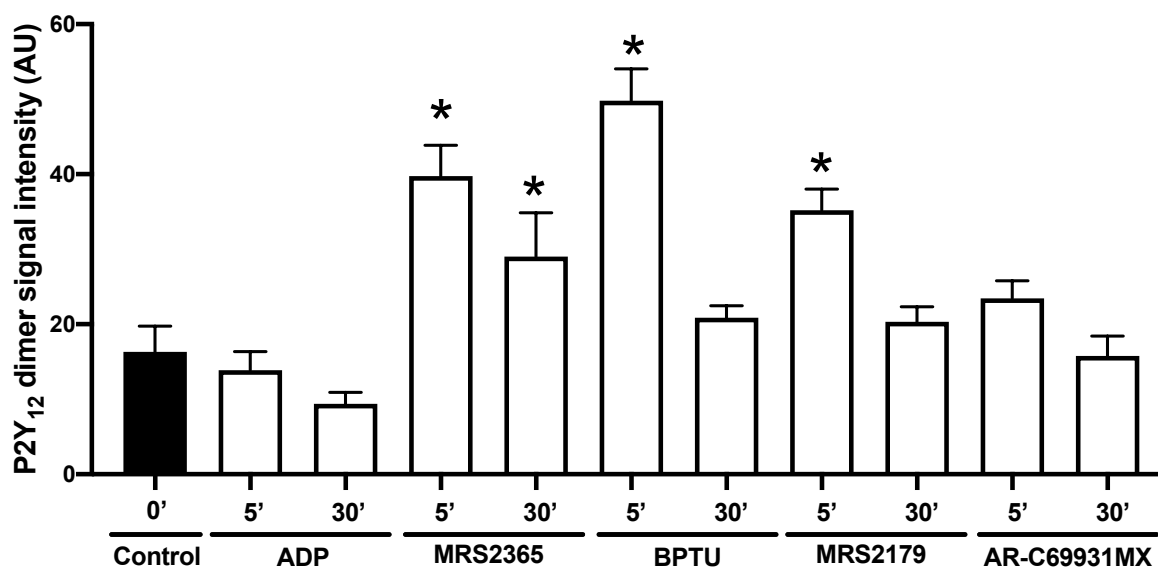
Figure 5.16: Quantification of P2Y$_{12}$ dimer bands' signal intensity post-treatment.
Densitometric quantification of endogenous P2Y$_{12}$ protein levels in BV-2 cell before and after exposure of the cells to 10µM ADP, 3µM MRS2365, 1µM BPTU, 10µM MRS2175, and 1µM AR-C69931MX for 5 or 30 minutes. The data are expressed as band intensity of receptor as measured by densitometry. The data presented represents the average ± standard error from three individual experiments. * $P<0.05$ compared to untreated cells.

2.8 Effect of AR-C69931MX on Ca^{2+} influx in BV-2 cells

Previous experiments in this thesis have shown that the highly selective P2Y$_{12}$ antagonist, AR-C69931MX, inhibits ADP-induced rises in intracellular Ca^{2+} in tSA201 cells expressing recombinant hP2Y$_{12}$ receptors (**Chapter three)**, but not in UT cells (Kennedy, unpublished observations). Therefore, the effect of AR-C69931MX on ADP-induced mobilization of intracellular Ca^{2+} in BV-2 cells was studied.

ADP (300 nM) induced an increase in intracellular Ca^{2+} levels in BV-2 cells, which was 1.7 ± 0.2 RFU, which was reduced to 0.5 ± 0.04 RFU, (n=4, P<0.05) in the presence of AR-C69931MX (1 µM) (**Figure 5.17a,c**). MRS2365 (10nM) also increased intracellular Ca^{2+}, though only to 0.8 ± 0.2 RFU and this was unaffected by AR-C69931MX (1 µM) (0.8 ± 0.1 RFU, n=3) (**Figure 5.17b,d**).
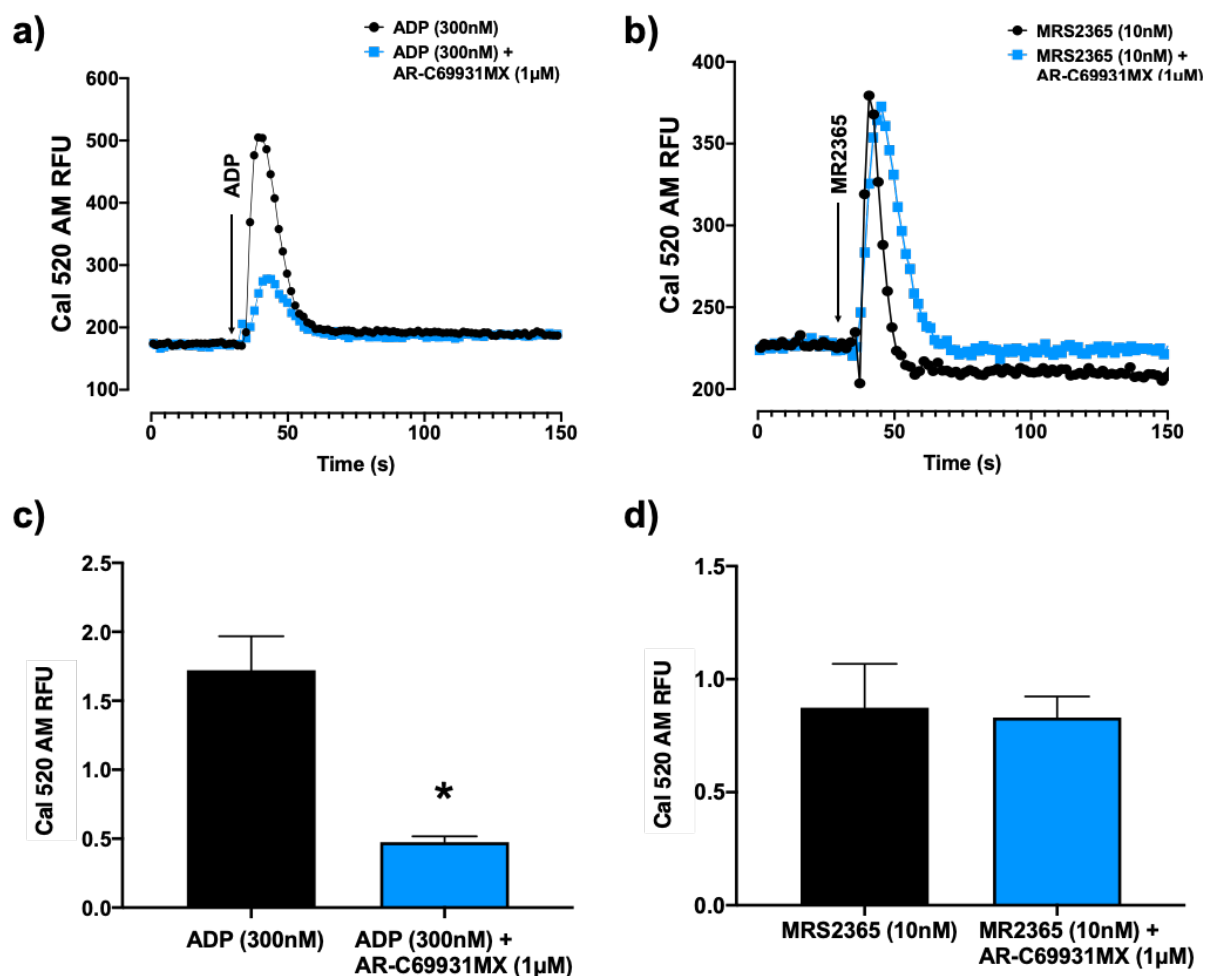
Figure 5.17: The effect of ADP and MRS2365 along with AR-C69931MX on intracellular Ca^{2+} levels in BV-2 cells.

The superimposed traces show changes in Cal-520 fluorescence evoked by superfusion of cells with **a)** ADP (300 nM) and **b)** MRS2365 (10 nM) in the absence and presence of AR-C69931MX (1 µM) in BV-2 cells. The mean peak amplitude of responses evoked by **c)** ADP (300 nM) and **d)** MRS2365 (10 nM) in the absence, presence and after washout of AR-C69931MX (1 µM) in BV-2 cells expressing are shown (mean ± s.e.m). *P<0.05 compared to in the absence of AR-C69931MX.

3   Discussion

In this chapter, the focus was to determine the interaction between native $P2Y_1$ and $P2Y_{12}$ receptors in an attempt to translate the findings from the recombinant expression system to a relevant cellular model. The data obtained in the immortalised human HMC3 and mouse BV-2 microglia cell lines showed that both expressed the microglial cell marker protein, Iba1 and $P2Y_{12}$ receptors, but $P2Y_1$ receptors could only be identified clearly in the BV-2 cells. Furthermore, PLA revealed a close association between the native $P2Y_1$ and $P2Y_{12}$ receptors in BV-2 cells. Finally, the selective $P2Y_{12}$ antagonist, AR-C69931MX inhibited the ADP-induced rise in cytoplasmic Ca^{2+} levels in BV-2 cells, but was ineffective against MRS3265. Thus, these PLA and Ca^{2+} signalling data support the proposal of Shrestha et al., (2010) that $P2Y_1$ and $P2Y_{12}$ receptors form a functional heteromer.

Cell lines confirmation

In this study the microglial BV-2 and HMC3 cell lines were used to study interactions between native $P2Y_1$ and $P2Y_{12}$ receptors because microglia are known to express several purinergic receptors, including $P2Y_1$ and $P2Y_{12}$ receptors (Farber and Kettenmann, 2006). Ideally, primary microglia would have been used, but microglia isolated from human brain and spinal cord are hard to obtain (Rodhe, 2013) and isolating microglia from animals is time-consuming, produces fewer cells and is more expensive than using cell lines. One of the advantages of using the immortal cell lines over primary cells is that they are a homogenous population of cells, derived from one clone, which improves the consistency of results and allows easier comparison with other studies using the same cell line (Rodhe, 2013). This is especially useful in an initial, investigatory study such as was carried out here. A potential disadvantage, however, is that the immortalization process might cause the loss of some important microglial characteristics or markers (Rodhe, 2013), such as CD11b and Iba1 proteins (Garcia-Mesa et al., 2017). Here, both BV-2 and HMC3 cells expressed Iba1 protein, consistent with them being microglial cells. Interestingly, the two cell lines differed in the structure of their actin network, as revealed by labelling of F-actin by rhodamine phalloidin. The BV-2 cells have three-dimensional networks that are present throughout the cytoplasm, while HMC3 cells have two-dimensional or planar networks

that are web-like and associated with the plasma membrane. These data confirmed previous reports of Reimer et al. (2018) and Dello Russo et al. (2018), respectively.

Selectivity of P2Y receptor antibodies

Studying the expression of endogenous GPCRs can be challenging due to the lack of highly selective antibodies (Massotte, 2015). Nonetheless, in this chapter, antibodies against endogenous epitopes within $P2Y_1$ and $P2Y_{12}$ receptor were used to study the receptors' expression in BV-2 and HMC3 cell. The antibodies were first tested using tSA201 cells in which HA-tagged $P2Y_1$ or $P2Y_{12}$ receptors had been expressed. This produced staining mainly at the cell membrane, which was similar to than seen when the cells were exposed to an anti-HA antibody. This gave us confidence that these antibodies could be used to detect endogenous $P2Y_1$ and $P2Y_{12}$ receptors in the microglial cells. The antibodies were also tested and optimised for PLA experiments by using tSA201 cells transfected with $P2Y_1$ and $P2Y_{12}$ receptors. As reported in **Chapter four**, $P2Y_1$ and $P2Y_{12}$ receptor can form a dimer that generates a PLA signal. The positive PLA signals gave us the confidence to use these antibodies in testing the physical interaction between the native receptors.

Differential expression of $P2Y_1$ and $P2Y_{12}$ receptor in BV-2 and HMC3 cells

In BV-2 cells endogenous $P2Y_{12}$ receptor localised mainly in intracellularly and on the cell surface, while in the HMC3 cells they expressed all over the cell, but localised mainly in the nucleus. When blotting the lysates of these cells, they expressed endogenous $P2Y_{12}$ monomers and dimers, which is a similar finding to Makkawi et al. (2015), who used the same antibody on platelet samples and observed bands at 50kDa, 100kDa and 220kDa. Interestingly, HMC3 cells have an extra band at ~35 kDa, which is probably an unmodified form of $P2Y_{12}$ receptor, as the predicted molecular weight is 39 kDa. On the other hand, endogenous $P2Y_1$ receptors in BV-2 cells localised mainly intracellularly, while in HMC3 cells, it was challenging to detect $P2Y_1$ receptor under the microscope. The lysed cells showed that both cell lines expressed endogenous $P2Y_1$ receptors, with a band at ~50 kDa. A similar band was seen by Wu et al., (2017) in samples prepared from the distal colon of rats, using the

same antibody. We have seen a band at this MW across these studies, even in tsA201 cells overexpressing the heavier HA-hP2Y$_1$ receptor. Thus, the P2Y$_1$ antibody (Santa-Cruz Biotechnology) is not specific to P2Y$_1$ receptors and so is unreliable for blotting experiments. Finally, when HA-hP2Y$_1$ receptors were overexpressed in tSA201 cells, expression of the endogenous P2Y$_{12}$ receptors was greatly reduced, which is consistent with the data reported in **Chapter three**. On the other hand, when HA-hP2Y$_{12}$ receptors were overexpressed in tSA201 cells, the endogenous P2Y$_{12}$ receptors immunoblotted as a smear, similar to that seen for HA-hP2Y$_{12}$ receptors.

In this study, RT-PCR confirmed the presence of mRNA of the P2Y$_{12}$ receptor in both cell lines, and confirmed the presence of mRNA of P2Y$_1$ receptor in BV-2 but not HMC3 cells. This is consistent with previous studies using RT-PCR that BV-2 cells express P2Y$_1$ and P2Y$_{12}$ receptors (Brautigam et al. 2005; Crain et al. 2009). In contrast, Jiang et al., (2017) reported that BV-2 cells express mRNA of P2Y$_{12}$ receptors, as well as P2Y$_{2,6,13,14}$ receptors, but not the P2Y$_1$ receptor. Dello Russo et al., (2018) reported that HMC3 cells, express the P2Y$_{12}$ receptor, but Rawat and Spector, (2017) claimed that they express significantly lower levels of the P2Y$_{12}$ receptor in compare to other microglial cells. To date, no other studies have investigated the expression of P2Y$_1$ receptors in HMC3 cells.

In this study, ADP and MRS2365, the selective P2Y$_1$ receptor agonist, increased cytoplasmic Ca^{2+} levels in BV-2 cells, but only ADP was effective in HMC3 cells. This could indicate that HMC3 cells lack functional P2Y$_1$ receptors and that ADP increased Ca^{2+} levels by another mechanism, such as the activation of P2Y$_{12}$ receptors. These do not couple to the Gq G protein (Bodor et al., 2003), but they can mediate activation of phosphatidylinositol-4,5-bisphosphate 3-kinase (PI3-K) through Gβγ, which can play a role in Ca^{2+} signalling (Koupenova and Ravid, 2018). This is consistent with unpublished data from the Kennedy lab show that MRS2365 is a partial agonist at recombinant P2Y$_1$ receptors expressed in 1321N1 cells. Partial agonists can lose all agonist activity at low levels of receptor expression and the level of P2Y$_1$ receptor expression in HMC3 cells is, at best, low. Thus, this may explain the lack of agonist activity of MRS2365. The simplest way to test this hypothesis would be to determine if the selective P2Y$_1$ antagonist, MRS2179, inhibits the responses to ADP in HMC3 cells. In addition, as partial agonists occupy the receptors and block the responses of full agonists at low levels of receptor expression, the effect of adding

MRS2365 along with ADP could be investigated. Unfortunately, time limitations prevented me from carrying out these experiments.

Native P2Y$_1$ and P2Y$_{12}$ receptors physical interaction

In view of the very low level of P2Y$_1$ receptor expression in BV2 cells, the colocalisation of P2Y$_1$ and P2Y$_{12}$ receptors was only studied in BV-2 cells. The immunofluorescence data showed that endogenous P2Y$_1$ and P2Y$_{12}$ receptors colocalised mainly intracellularly, as that is where the line scan intensity for both receptors overlapped. Also, there was strong overlap in pixels between both channels of P2Y$_1$ and P2Y$_{12}$ receptors, with a high PCC number close to 1. This correlation is similar to the data from recombinant receptors reported in **Chapter three**. Consistent with this, *in situ* PLA produced a positive signal in BV-2 cells, though unsurprisingly, not in HCM3 cells. This, to the best of our knowledge is the first demonstration of dimerisation of native P2Y$_1$ and P2Y$_{12}$ receptors.

Native P2Y$_1$ and P2Y$_{12}$ receptors activation, trafficking and signalling in microglia

In this study, P2Y$_1$ receptors localised mainly intracellularly and did not relocate upon addition of receptor ligands. On the other hand, P2Y$_{12}$ receptor localised intracellularly and at the cell membrane, and the addition of ADP for 30 minutes showed a sign of P2Y$_{12}$ receptor activation in the cell surface and changed the cell morphology by forming a 'honeycomb' structure, which suggest that there are cell morphology changes. This is a similar finding to data produced in rat primary cultured microglia by Honda et al., (2001), who reported that stimulation with ADP and ATP showed a sing of the plasma membrane ruffling, increased chemokinesis and produced chemotaxis via G$_{i/o}$-coupled P2Y receptors. On the other hand, the selective P2Y$_1$ agonist, MRS2365, did not cause any visible change in cell morphology, which might indicate that P2Y$_1$ receptor does not play a role in changing microglia's cell morphology. Unfortunately, no P2Y$_{12}$ selective agonist is commercially available to complement our study.

Interestingly, 5 minutes after adding the P2Y$_1$ negative allosteric modulator, BPTU, resulted in a sign of activating P2Y$_{12}$ receptor and a dramatic degradation of

the receptor intracellularly. But in 30 minutes post-treatment with BPTU, the majority of the $P2Y_{12}$ receptor was transported from membrane to the cytoplasm as a part of endosomes. The selective $P2Y_1$ antagonist, MRS2179, did not activate the $P2Y_{12}$ receptor but caused a change in the cell morphology. The addition of the $P2Y_{12}$ selective antagonist, AR-C69931MX, initially showed a sign of activation of the $P2Y_{12}$ receptor with a change in cell morphology. These effects reversed after 30 minutes of AR-C69931MX addition. Interestingly, the $P2Y_1$ ligands, MRS2365, BPTU and MRS2179, all increased $P2Y_{12}$ homodimer formation in BV-2 cells, which needs further investigation. Thus, this characterisation was outwith the period of this study however work is now under way to confirm using more developed methods such as automated morphological analysis tool which developed by Heindl et al. (2018) to study microglia morphology.

Finally, AR-C69931MX inhibited, but did not abolish, the ADP-induced rise in cytoplasmic Ca^{2+} levels in BV-2 cells. This is the same as the data shown in **Figure 3.7** in tSA201 cells transfected with HA-$hP2Y_{12}$ or $hP2Y_{12}$-eCFP receptors. In contrast, AR-C69931MX did not suppress the Ca^{2+} response induced by MRS2365 in BV-2 cells, which is consistent with AR-C69931MX acting directly and competitively on $P2Y_{12}$ receptors and with no effect of the $P2Y_1$ receptors (Suzuki et al., 2011). Indeed, molecular docking simulations based on the crystal structure of the $P2Y_{12}$ receptor indicated that AR-C69931MX occupies the same orthosteric binding pocket as ADP (Zhang et al., 2014a). In other potential view that AR-C69931MX blocks $P2Y_{12}$ receptor to reduce ADP-signal through this receptor as there was no effect on signal induced by MRS2365. However, our working hypothesis is that $P2Y_1$ and $P2Y_{12}$ receptors form a functional heteromer, which is activated when both orthosteric binding sites are occupied by ADP. AR-C69931MX acts by binding to the $P2Y_{12}$ receptor and so prevents activation of the dimer by ADP. Alternatively, ADP may only need to bind to the $P2Y_1$ receptor half of the dimer to activate it and by binding to the $P2Y_{12}$ receptor, AR-C69931MX prevents the physical rearrangement that underlies activation of the dimer. The lack of effect against the activation by MRS2365 may be because MRS2365 (and ADP) also acts via $P2Y_1$ homomers to induce Ca^{2+} release. That a component of the Ca^{2+} rise induced by ADP was resistant to AR-C69931MX is consistent with a second mode of action of ADP that is independent of $P2Y_{12}$

receptors. Regardless, these data suggest that $P2Y_1$ and $P2Y_{12}$ receptors form a functional heteromer as proposed by Shrestha et al., (2010).

Chapter Six

General Discussion

Understanding a receptor's dynamic response to pharmacological treatment is essential, as many factors, such as receptor localisation, trafficking and dimerisation, regulate receptor activity. The data presented in this thesis demonstrated heterodimerisation between recombinant $P2Y_1$ and $P2Y_{12}$ receptors, and, for the first time, between native $P2Y_1$ and $P2Y_{12}$ receptors. Coexpression of these receptors resulted in inhibition of receptor internalisation and altered $P2Y_1$ receptor Ca^{2+} mobilization by ADP. Coexpression also altered receptor pharmacology, with inhibition of $P2Y_{12}$ receptors using a selective antagonist impacting on $P2Y_1$ receptor signalling, in both recombinant and native cell models. To fully appreciate the implications of these findings, it is important to recognize where comparisons can be made with other GPCR dimer models.

$P2Y_1$ and $P2Y_{12}$ heterodimer formation – lessons from other GPCR families

The studies carried out in this thesis were conducted *in vitro* and presented evidence that reaffirm the existence of constitutive heterodimers between $P2Y_1$ and $P2Y_{12}$ when expressed in the same cell system. Interaction between $P2Y_1$ and $P2Y_{12}$ receptor was first proposed to be of functional importance back in 2010 when it was demonstrated that $P2Y_1$ and $P2Y_{12}$ receptors modulate the activity of two-pore potassium (K_{2P}) ion channels in neurons (Shrestha et al., 2010). These authors also suggested that $P2Y_{12}$ receptor could facilitate in $P2Y_1$ receptor co-activation and that this could be the consequence of formation of a functional dimer between these two receptors. Prior to these findings, Schicker et al., (2009) used $P2Y_1$ and $P2Y_{12}$ receptors as part of a study exploring physical interactions between receptors channels responsive to adenine nucleotides and nucleosides. They demonstrated a plethora of combinatorial dimer possibilities across the purine family of GPCRs. Additionally, heterodimerisation of rat $P2Y_1$ and $P2Y_{12}$ receptors was confirmed through FRET experiments in the tSA201 cell line, as well as $P2Y_1$ dimerisation with $P2Y_1$, $P2Y_2$ or $P2Y_{13}$ receptors and $P2Y_{12}$ dimerisation with $P2Y_{12}$, $P2Y_2$ or $P2Y_{13}$ receptors. The functional significance of any of these interactions were not, however, explored. While these studies focused upon the rat P2Y subtypes, the work in this thesis sought to investigate human P2Y heterodimer formation with the aim of bridging the gap between dimerisation and functional relevance of P2Y receptor interaction in native cell systems.

Several studies have examined constitutive GPCR heterodimerisation and identified far-reaching consequences upon receptor function both in vitro and in vivo. Examples of these dimers are β_2-adrenoreceptor with β_2-, β_1-, BK2, or AT1 receptors (Haack and McCarty, 2011). In the current study it was noticeable that the disulphide bonds in the receptors play a role in oligomer formation for P2Y$_{12}$ receptors, which is consistent with previous reports (Savi et al., 2006; Ding et al., 2009). HA-tagged P2Y$_1$ receptors showed similar results as P2Y$_{12}$ receptors, however, the presence of the eYFP tag on the C-terminal of P2Y$_1$ receptor, makes the disulphide bond resistant to DTT. That raised the question, *what receptor domains are responsible for the interaction between receptors?*

Exploring the possible dimer interface between GPCR dimers

Understanding the interface and structural features of heterodimers may provide a superior understanding of the functional consequence of dimers and their implications in ligand binding pockets and receptor function. According to Filizola and Weinstein (2005), the transmembrane helices of GPCRs, most commonly TM4, TM5 and TM6, provide the interfaces for dimerisation of many GPCRs. An example for that is the heterodimer between the A$_{2A}$ and D$_2$ receptors, where it has been proposed by Canals et al. (2003) that TM5,6,7 of the D$_2$ receptor and TM3,4 of the A$_{2A}$ receptor is the main interface for interaction. On the other hand, Borroto-Escuela et al. (2010) proposed that TM4,5 of the D$_2$ receptor interacted with either TM4,5 or TM1,7 of the A$_{2A}$ receptor. Subsequently, Borroto-Escuela et al., (2018) used BRET and PLA approaches to study the regions involved in the heterodimer formed between A$_{2A}$ and D$_2$ receptors. They found that TM4 and TM5, and possibly TM6, acted as a primary interface for both D$_2$ and A$_{2A}$ receptors. They also found a reduction of heteromerization in BRET assays by peptides corresponding to TM5 of the D$_2$ receptor. TM5 or TM1 of class A GPCR have also been implicated in dimerisation (Greife et al., 2016; Dijkman et al., 2018). For example, TM5 of the GPR17 receptor plays a crucial role in its homodimerisation, in particular, a pair of phenylalanines (residues F229 and F233) that interact with each other (Yang et al., 2020). The effect of mutation of these residues to alanines was investigated *in silico* in order to assess

their role in dimerisation. The mutation did not affect the structure of the receptor; however, it disrupted GPR17 dimerisation.

While these studies provided key insights into the GPCR interfaces involved in dimerisation, agonist binding to receptors causes rearrangements of the transmembrane helices to allow efficient heterotrimeric G protein coupling and activation (Vizurraga et al., 2020). For example, TM6 has been shown to move outwards upon agonist binding (Zhou et al., 2019). In the $P2Y_{12}$ receptor, EL2 and TM5 play an essential role in ligand binding, while EL3 and TM6 are associated with abnormal receptor function and signal transduction (Mundell et al., 2018). On the other hand, in the $P2Y_1$ receptor, EL2 and TM6 and TM7 are associated with ligand binding (Li et al., 2017), while TM3, TM6, and TM7 directly contact the Gα protein (Yuan et al., 2016). Interestingly, while agonists for either receptor, as well as $P2Y_1$ antagonists, did not impact receptor interaction significantly in the present study, the $P2Y_{12}$ antagonist, AR-C69931MX, caused a shortening of the distance between the two receptors, as measured by FLIM-FRET. Thus, TM5 and 6 of $P2Y_{12}$ receptors and TM3, 6 and 7 of $P2Y_1$ receptor might contribute to the interface of interaction, but further research is needed to investigate this possibility.

Inhibition of $P2Y_1$ and $P2Y_{12}$ internalisation – artefact of over-expression or consequence of dimerisation?

The fluorescence microscopy experiments conducted to monitor receptor expression identified $P2Y_1$ and $P2Y_{12}$ localisation in the recombinant cell systems. $P2Y_1$ and $P2Y_{12}$ receptors were colocalised mainly on the cell membrane, consistent with previous studies demonstrating surface expression of HA-tagged $P2Y_1$ and $P2Y_{12}$ receptors in 1312N1, CHO and HEK293 cells (Mundell et al., 2008; Smith et al., 2017; Zhong et al., 2004; Savi et al., 2006). ADP induced internalisation was confirmed for both receptors, which aligns with previous studies (Mundell et al., 2006; Nisar et al., 2011), however, the coexpression of both $P2Y_1$ and $P2Y_{12}$ receptor prevented receptor internalisation in response to ADP, which has not been reported before. The major questions that these data raised was *is deficiency of receptor internalisation an artefact of over-expression or a phenotype of heterodimerisation?*

Recycling mechanisms for both receptors play an essential role in responsiveness to their endogenous agonist, ADP (Mundell et al., 2008). Interestingly, they have different recycling mechanisms, as $P2Y_1$ receptors internalisation depends upon PKC activity (Mundell et al., 2006; Reiner et al., 2009), whilst $P2Y_{12}$ receptor internalised via GRK2 and GRK6 activities (Hardy et al., 2005). Both receptors then recycle back to the plasma membrane; $P2Y_1$ receptor recycled slowly by Sorting Nexin 1 (Nisar at al., 2010), while $P2Y_{12}$ receptor recycled faster by a Rab4/11-dependent trafficking pathway (Cunningham et al., 2013a). *Is it possible that receptor heterodimerisation impacts the ability of these scaffolding proteins to engage the receptor for effective regulation of receptor trafficking?*

One of the unifying mechanisms of internalisation that applies to both receptors is the regulation of internalisation by NHERF-1 and -2 (Nisar et al., 2011, 2012; Cunningham et al., 2013b). Two possible explanations for the defective internalisation could be that heterodimerisation prevents effective PDZ-dependent engagement with these PDZ binding proteins, as PZD domains are able to homodimerise, such as in the glutamate receptor-interacting protein (GRIP) (Fanning et al., 2007). Also, the presence of the fluoresces protein at the C-terminus for one of the receptors prevented the engagement of the PDZ binding proteins. Alternatively, over-expression of $P2Y_1$ and $P2Y_{12}$ receptors may mean that there is insufficient endogenous NHERF levels to support recombinant receptor trafficking events. Confirmation of this would require additional experimentation to increase the cellular levels of NHERF1 to identify if internalisation of the heteromer is restored. This is something for future consideration in taking this work forward.

Zamel et al. (2020) reported internalisation deficits in PAR1 and AT1 receptor heterodimers whereby the internalisation of the AT1 receptor was inhibited upon simultaneous co-activation of AT1 and PAR1 receptors with angiotensin II and thrombin, respectively, in HEK293 cells. Using BRET assays, that study identified that dimer formation could help both receptors remain at the cell membrane, leading to stronger coupling to G proteins and signalling. Conversely, previous studies have also reported the dimer formation can influence the endocytic recruitment of GPCRs and enable receptor internalisation (Opalinski et al., 2017; Zhao et al., 2019). An example for that phenomenon is the $P2Y_1$-$P2Y_{11}$ dimer. The $P2Y_{11}$ receptor does not undergo agonist-induced endocytosis, when expressed on its own, but does when the $P2Y_1$ receptor is coexpressed (Ecke et al., 2008; Dreising and Kornum, 2016).

In the current study, PLA experiments indicated that the $P2Y_1$ and $P2Y_{12}$ dimer remains at the cell membrane, with no sign of internalisation, after addition of ligands. Thus, it is feasible that the heterodimer population of receptors represents an internalisation-deficient pool. Previous studies have indicated that the over-expression of GPCR may artificially cause GPCR dimerisation (Ferre et al., 2014; Franco et al., 2016; Milligan et al., 2019). However, in this study the dimer was confirmed using several approaches in the recombinant system, as well as, in the native system, in this case, BV-2 cells. These results allow us to report for the first time the existence of $P2Y_1$-$P2Y_{12}$ dimers natively. The physiological or pathophysiological implications of these findings require some focused consideration, however the impact upon cell signalling at the local level was then investigated.

Inhibition of $P2Y_1$ Ca^{2+} signalling upon $P2Y_{12}$ antagonist treatment.

In this study, the $P2Y_{12}$ antagonist, AR-C69931MX, inhibited the rise of Ca^{2+} evoked by ADP in tSA201 cells expressing recombinant $hP2Y_{12}$ receptors, confirming the results of previous unpublished experiments in the Kennedy lab. Moreover, AR-C69931MX also suppressed the rise of Ca^{2+} evoked by ADP, acting at native P2Y receptors in BV-2 cells. $P2Y_1$ receptors couple to G_q, which is responsible for inducing Ca^{+2} release, while $P2Y_{12}$ receptors couple to $G_{i/o}$ and so are unable to induce Ca^{2+} release directly. The lack of effect of AR-C69931MX on Ca^{2+} release evoked by MRS2365, a selective $P2Y_1$ agonist, in BV-2 cells indicates that AR-C69931MX's inhibitory action against ADP is not due to it interacting directly with $P2Y_1$ receptors to block them. So, the obvious question that arises from these data is, *how does a highly selective $P2Y_{12}$ antagonist inhibit Ca^{2+} mobilization when $P2Y_{12}$ receptor activation does not normally induce Ca^{2+} release*? As discussed in **Chapter five**, our working hypothesis is that $P2Y_1$ and $P2Y_{12}$ receptors form a functional heteromer, which is activated when both orthosteric binding sites are occupied by ADP. AR-C69931MX acts by binding to the $P2Y_{12}$ receptor and so prevents activation of the dimer by ADP.

An alternative explanation that must be considered is that physically-separated $P2Y_1$ and $P2Y_{12}$ receptors modulate each other's activity by cross-talk. Such a mechanism has been proposed in in platelets (Hardy et al., 2004) and C6 glioma cells (Barańska et al., 2004; Suplat et al. 2007; Wypych and Barańska, 2013), as AR-

C69931MX partially inhibited ADP-induced Ca^{2+} release in both. In platelets, $P2Y_{12}$ receptor activation potentiated Ca^{2+} signalling via inhibition of cAMP and activation of phosphatidylinositol-4,5-bisphosphate 3-kinase (PI3-K) through $G\beta\gamma$ and the $P2Y_1$ receptor negatively regulated PI3-K by coupling with Src kinase (Hardy et al., 2004; Koupenova and Ravid, 2018). One caveat is that other $P2Y_{12}$ antagonists, A3P5PS, A3P5P, and A2P5P, did not inhibit Ca^{2+} signalling in platelets (Jin et al., 1998). The reason for this difference is unclear. It would be interesting to investigate if $P2Y_{12}$ receptor activation might trans-activate $P2Y_1$ receptors, but a selective $P2Y_{12}$ agonist is not available. Another possibility is that $P2Y_{12}$ receptors could trans-inhibit $P2Y_1$ receptors. As in (Shrestha et al., 2010) it has been found that ADP induced inhibition for $K_{2P,}$ which was antagonised by AR-C69913MX and MRS2179, but not PTX, $G\alpha_i$ inhibitor. Thus, $P2Y_{12}$ receptor might play a role in trans-inhibiting $P2Y_1$ receptor.

Do $P2Y_1$ and $P2Y_{12}$ heterodimers present a potential new target for treating pain?

$P2Y_1$ and $P2Y_{12}$ receptors are both upregulated in nerve injuries and $P2Y_{12}$ receptors play an important role in developing pain behaviour induced by peripheral nerve injury (Liu et al., 2017, 2020). *In vitro* studies showed that the activation of the $P2Y_{12}$ receptor leads to the release of IL-1β, IL-6 and TNF-α from cultured dorsal spinal cord microglia cells (Liu et al., 2017). On the other hand, a $P2Y_1$ antagonist reduced IL-1β-induced thermal hypersensitivity in carrageenan-injected rats (Kwon et al., 2017). In another study, $P2Y_1$ antagonists inhibited $TRPV_1$ expression in dorsal root ganglion and prevented thermal hyperalgesia in a rat model of neuralgia (Kwon et al., 2014). Malin and Molliver (2010) saw a reduction of $P2Y_1$ mRNA and a rise in $P2Y_{12}$ mRNA during CFA-induced inflammation. The low expression of $P2Y_1$ mRNA during inflammation could be in order to reduce further nociceptive signaling, whilst the rise of $P2Y_{12}$ mRNA may provide anti-nociceptive drive. For that, the neurons can decrease pro-nociceptive signaling by balancing the expression of the $P2Y_{12}$ receptor. Thus, both $P2Y_1$ and $P2Y_{12}$ receptors may serve as key regulators of peripheral sensitization.

In this study, we investigated the interaction of $P2Y_1$ and $P2Y_{12}$ receptors in human and mouse microglial cells. Microglial cells are known to express a variety of purinergic receptors (Farber and Kettenmann, 2006), and they play a crucial role in the development and maintenance of chronic pain (Chen et al., 2018). Both human

(HMC3) and mouse (BV-2) microglial cells expressed Iba1, which is a protein that microglial cells express in a higher level (Imai & Kohsaka, 2002). In this study, BV-2 cells expressed both $P2Y_1$ and $P2Y_{12}$ receptors, which is consistent with previous study that used RT-PCR to investigate the expression (Brautigam et al. 2005; Crain et al. 2009). On the other hand, HMC3 cells expressed $P2Y_{12}$ receptor, which is consistent with Dello Russo et al. (2018) study, however, HMC3 did not express $P2Y_1$ receptor, and unfortunately there was no previous study published reporting expression of $P2Y_1$ in HMC3 cells. For these reasons, the decision was made to investigate native dimer detection in BV-2 cells. In this native system, $P2Y_1$ and $P2Y_{12}$ receptors were localised mainly intracellularly with some receptors expressed on the cell membrane, unlike the recombinant system expression which was on the plasma membrane of the cells. It may be that both P2Y receptors are normally expressed at only low levels at the plasma membrane of microglial cells and that a painful stimulus causes them to translocate from the cytoplasm into the plasma membrane, where they then contribute to development and maintenance of chronic pain.

Very few laboratories have successfully detected native dimers, largely due to the issues that plague GPCR research in identifying reliable and selective antibodies. Despite such reservations, we attempted to detect dimerisation between native $P2Y_1$ and $P2Y_{12}$ receptors in the BV-2 cells using antibodies direct against endogenous epitopes of the P2Y receptors and which had been used previously by Makkawi et al. (2015) to study $P2Y_{12}$ receptors in platelets and Wu et al. (2017) to study $P2Y_1$ receptors in distal colon of rats. The results showed that both receptors colocalised in the native in BV-2 cell system and dimer formation was confirmed using the PLA. This PLA approach has previously been used to detect native A_{2A}-D_2 dimer heterodimers in rodent brains (Trifilieff et al., 2011) and adult human ventral striatum (Zhu et al., 2019).

Could an allosteric modulator or bitopic ligand approaches be adopted for selective targeting of $P2Y_1$ and $P2Y_{12}$ heterodimers?

While identifying dimers presents a challenge, the future challenge is to understand how best to target GPCR dimers for the development of new regulators of GPCR function. The use of bifunctional compounds is one of the most current methods in targeting dimers in biological systems (Carli et al., 2018). These compounds are the

bivalent ligands that are composed of two chemical groups (pharmacophores), linked to each other by a spacer sequence of a specific length, which can simultaneously bind to both receptors in the dimer (Morphy and Rankovic, 2005). If the spacer between the two pharmacophores is shorter is it likely to be a dual-acting ligand, designed to deliver both ligands simultaneously, but without the expectation of simultaneous binding (Jorg et al., 2015).

However, this approach might lead to an increase in the local concentration of the second tethered pharmacophore following the binding of the first pharmacophore to its receptor, which will lead into a higher affinity for the second pharmacophore (Kuhhorn et al., 2011). A study that used a short homobivalent ligand for the hMC4R receptor reported that binding of one pharmacophore to one receptor drives the binding equilibrium of the second receptor towards higher receptor binding (Vagner et al., 2008). This approach could be applied to the $P2Y_1$-$P2Y_{12}$ dimer to inhance the binding affinity, as ADP acts as an agonist at both receptors.

This approach has several limitations, as targeting dimers is complicated because they are transiently formed with varying monomer/dimer ratio (Carli et al., 2018). Also, designing the bivalent ligands for $P2Y_1$-$P2Y_{12}$ dimer is not going to be easy due to the lack of the crystal structure of the dimer pair, as well as crosslinking studies for $P2Y_1$ and $P2Y_{12}$ homo- or heterodimers. The crystal structures of the $P2Y_1$ and $P2Y_{12}$ homodimers could, however, act as a starting point.

Challenges in the field of GPCR dimerisation

The physical interactions between both receptors in the recombinant system was assessed by biochemical and biophysical methods. The critical biochemical method is co-IP, which showed that $P2Y_1$ and $P2Y_{12}$ receptors could form a dimer. However, the main concern with using this approach is the aggregation between the two receptors caused by lysis buffer, which may lead to an artificial co-IP positive result (Angers et al., 2002). This can be avoided by using biophysical methods, which do not require the use of lysis buffer. In this study PLA and FLIM-FRET approaches were used to provide additional validation of dimer formation between $P2Y_1$ and $P2Y_{12}$ receptors. The PLA approach has been applied to detect other several GPCR dimers (Borroto-Escuela et al., 2016; Gomes et al., 2016) and Borroto-Escuela et al. (2018) detected A_{2A}–D_2 heterodimers in HEK293T cells that were transiently cotransfected

with both receptors. The PLA experiments indicate that $P2Y_1$ and $P2Y_{12}$ receptor are within 40 nm of each other, while the FLIM-FRET experiments confirmed the physical interaction and reduce the estimated distance to less than 10nm. FLIM-FRET has been used previously to detect the GPR17 homodimer expressed in HEK293 cells (Yang et al., 2020).

Future studies

Future work might benefit from testing receptor internalization in the recombinant system using double-tagged receptors such as (HA-$hP2Y_1$-eYFP and HA-$hP2Y_{12}$-eCFP); the FP might interrupt the internalization mechanism for both receptors due to its size and the binding location at the PDZ domain. This will give a better understanding as one of the receptors was tagged with an FP, which might help the receptor to remain on the cell surface and forced the other receptor to be on the cell membrane.

Also, future studies could benefit from using techniques that utilize purified proteins, such as fusion protein pull-downs followed by co-IP to identify if the interaction between the receptors was direct or indirect. As when performing co-IP on tSA201 cell lysates, it is possible that $P2Y_1$ and $P2Y_{12}$ receptor are linked via additional scaffolding proteins. Also, it could be beneficial to use FLIM-FRET in live cells, as it is a useful tool for imaging of live cells in thicker specimens (Storez et al., 2005), including, for example Caspase-3 activity in live cells (Savitsky et al., 2012). Unfortunately, our instrument was not capable of performing these experiments. This technique is also suitable for *in vivo* studies due to the low excitation intensity required, which causes no photobleaching, and can detect low levels of fluorescent proteins.

One of the approaches to investigate protein-protein interactions in live cells is bimolecular fluorescence complementation (BiFC) (Kerppola 2006). In the recent years, an extended approach, multicolour BiFC, has gained a lot of attention (Hu & Kerppola 2003). Multicolor BiFC was applied to study hetero- and homodimer formation for several GPCR receptors, for example, the A_{2A}–D_2 heterodimer and A_{2A} homodimer in CAD neuronal cell line expressing Venus (D_2-VN/A_{2A}-CC) and Cerulean (A_{2A}-CN/A_{2A}-CC) plasmids, respectively (Vidi et al., 2008). Similarly, the oligomerisation of CB_1 and D_2 receptor was studied in CAD cells that expressed CB_1-VN and D_2 receptor fused to the split fragments of Cerulean (D_2-CN, D_2-CC) (Przybyla

and Watts, 2010). They found that heterodimer formation between CB_1-VN and D_2-CC that produced Venus signal, while homodimer formation of D_2 receptor produced a Cerulean signal. This approach might be a useful to study the formation of $P2Y_1$ and $P2Y_{12}$ receptor post-treatment with different ligands to distinguish the formation of hetero- and homodimers between the receptors. As mentioned before from several studies that used methods like FRET and BRET, ligands addition might influence the changes in the rate of formation of homo- and heterodimers of GPCRs (Abadir et al., 2006; Łukasiewicz et al., 2010; Espinoza et al., 2011).

Moreover, from the signalling level, we can measure the cAMP to test $P2Y_{12}$ receptor signalling by raising the intracellular cAMP using forskolin, then comparing the effect of AR-C69931MX to the $P2Y_1$ antagonists, BPTU and MRS2179, to make the mechanism clearer between the receptors. Also, it would be worthwhile comparing the effect of AR-C69931MX on the $P2Y_1$-$P2Y_{12}$ dimer and Ca^{2+} signalling with other $P2Y_{12}$ antagonists, as this phenomenon could be unique to AR-C69931MX. Also, using a PI3-K inhibitor, such as wortmannin, could provide more understanding of PI3-K's contribution to the Ca^{2+} signalling. An example of such a behaviour was tested in previous literature as wortmannin managed to reduce platelet aggregation which is a similar result when the platelets were treated with internal calcium inhibitor TG (Sun et al., 2005). As mentioned before in this study, HMC3 cells do not express the $P2Y_1$ receptor. However, there was a slight rise of calcium signalling upon ADP addition, so by blocking PI3-K, we are eliminating the contribution of the $P2Y_{12}$ receptor into the calcium signalling.

The downstream signalling for $P2Y_1$-$P2Y_{12}$ dimer needs further investigation. *What G protein(s) does the dimer couple to and which G protein is responsible for inhibiting the K_{2P} ion channels?* Furthermore, *what is the functional purpose?* To address these questions future studies may benefit from using a newly developed method called "TRUPATH", which can determine which G proteins are activated, by measuring the heterotrimeric G protein dissociation via bioluminescence resonance energy transfer 2 (BRET2) (Olsen et al., 2020). Also, it would be interesting to investigate if the release of Gβγ subunits from G protein trimers plays a role in activating PI3-K. In this study, as measured by FLIM-FRET, the addition of AR-C69931MX enhanced the heterodimerisation between $P2Y_1$ and $P2Y_{12}$ receptors. It would be interesting to apply the FLIM-FRET approach on disease models as some

diseases are associated with mutations to receptors and disruption of dimers (Ploier et al., 2016).

Conclusion

In summary, these studies provide new additional evidence that $P2Y_1$ and $P2Y_{12}$ receptors can form a dimer in both recombinant and native systems. The findings principally suggest that the dimer expressed on the cell membrane in the recombinant system, while it expressed intracellularly in the native system. This study further shows that ADP induced internalisation of both $P2Y_1$ and $P2Y_{12}$ receptors; however, this internalisation was inhibited entirely when the receptors were coexpressed at the same time. Further investigation must be carried out to identify the reason. In the current study, a $P2Y_{12}$ receptor antagonist enhanced and stabilized the dimer, as well as inhibiting Ca^{2+} signalling mediated through the $P2Y_1$ receptor. Future studies could potentially be directed toward exploring the dimer interface and understanding the downstream signalling pathways. This understanding will provide the foundation for future studies evaluating the functional pharmacology of the $P2Y_1$-$P2Y_{12}$ heterodimer.

References

References

Abadir PM, Periasamy A, Carey RM, & Siragy HM (2006). Angiotensin II type 2 receptor-bradykinin B2 receptor functional heterodimerization. Hypertension 48**:** 316-322.

Abbracchio MP, Burnstock G, Boeynaems JM, Barnard EA, Boyer JL, Kennedy C*, et al.* (2006). International Union of Pharmacology LVIII: update on the P2Y G protein-coupled nucleotide receptors: from molecular mechanisms and pathophysiology to therapy. Pharmacol Rev 58**:** 281-341.

Adler J, & Parmryd I (2010). Quantifying colocalization by correlation: the Pearson correlation coefficient is superior to the Mander's overlap coefficient. Cytometry A 77**:** 733-742.

Adler J, & Parmryd I (2013). Colocalization analysis in fluorescence microscopy. Methods Mol Biol 931**:** 97-109.

Agnati LF, Ferre S, Lluis C, Franco R, & Fuxe K (2003). Molecular mechanisms and therapeutical implications of intramembrane receptor/receptor interactions among heptahelical receptors with examples from the striatopallidal GABA neurons. Pharmacol Rev 55**:** 509-550.

Agnati LF, Fuxe K, Zini I, Lenzi P, & Hokfelt T (1980). Aspects on receptor regulation and isoreceptor identification. Med Biol 58**:** 182-187.

Agnati LF, Fuxe K, Zoli M, Rondanini C, & Ogren SO (1982). New vistas on synaptic plasticity: the receptor mosaic hypothesis of the engram. Med Biol 60**:** 183-190.

Alam MS (2018). Proximity Ligation Assay (PLA). Curr Protoc Immunol 123**:** e58.

Albizu L, Cottet M, Kralikova M, Stoev S, Seyer R, Brabet I*, et al.* (2010). Time-resolved FRET between GPCR ligands reveals oligomers in native tissues. Nat Chem Biol 6**:** 587-594.

Algaier I, Jakubowski JA, Asai F, & von Kugelgen I (2008). Interaction of the active metabolite of prasugrel, R-138727, with cysteine 97 and cysteine 175 of the human P2Y12 receptor. J Thromb Haemost 6**:** 1908-1914.

Alhadeff R, Vorobyov I, Yoon HW, & Warshel A (2018). Exploring the free-energy landscape of GPCR activation. Proc Natl Acad Sci U S A 115**:** 10327-10332.

Alliegro MC (2000). Effects of dithiothreitol on protein activity unrelated to thiol-disulfide exchange: for consideration in the analysis of protein function with Cleland's reagent. Anal Biochem 282**:** 102-106.

Anti-P2Y12 Receptor Antibody. [Online] Available from https://www.alomone.com/p/anti-p2y12-receptor/APR-012
. [Accessed: 22 May 2020].

References

Alvarez-Curto E, Prihandoko R, Tautermann CS, Zwier JM, Pediani JD, Lohse MJ, *et al.* (2011). Developing chemical genetic approaches to explore G protein-coupled receptor function: validation of the use of a receptor activated solely by synthetic ligand (RASSL). Mol Pharmacol 80**:** 1033-1046.

Ando RD, Mehesz B, Gyires K, Illes P, & Sperlagh B (2010). A comparative analysis of the activity of ligands acting at P2X and P2Y receptor subtypes in models of neuropathic, acute and inflammatory pain. Br J Pharmacol 159**:** 1106-1117.

Angers S, Salahpour A, & Bouvier M (2002). Dimerization: an emerging concept for G protein-coupled receptor ontogeny and function. Annu Rev Pharmacol Toxicol 42**:** 409-435.

Apweiler R, Hermjakob H, & Sharon N (1999). On the frequency of protein glycosylation, as deduced from analysis of the SWISS-PROT database. Biochim Biophys Acta 1473**:** 4-8.

Aratake Y, Okuno T, Matsunobu T, Saeki K, Takayanagi R, Furuya S, *et al.* (2012). Helix 8 of leukotriene B4 receptor 1 inhibits ligand-induced internalization. FASEB J 26**:** 4068-4078.

Ardito F, Giuliani M, Perrone D, Troiano G, & Lo Muzio L (2017). The crucial role of protein phosphorylation in cell signaling and its use as targeted therapy (Review). Int J Mol Med 40**:** 271-280.

Audet M, & Bouvier M (2012). Restructuring G-protein- coupled receptor activation. Cell 151**:** 14-23.

Avissar S, Amitai G, & Sokolovsky M (1983). Oligomeric structure of muscarinic receptors is shown by photoaffinity labeling: subunit assembly may explain high- and low-affinity agonist states. Proc Natl Acad Sci U S A 80**:** 156-159.

Baba K, Benleulmi-Chaachoua A, Journe AS, Kamal M, Guillaume JL, Dussaud S, *et al.* (2013). Heteromeric MT1/MT2 melatonin receptors modulate photoreceptor function. Sci Signal 6**:** ra89.

Bailey CP, & Connor M (2005). Opioids: cellular mechanisms of tolerance and physical dependence. Curr Opin Pharmacol 5**:** 60-68.

Bajar BT, Wang ES, Zhang S, Lin MZ, & Chu J (2016). A Guide to Fluorescent Protein FRET Pairs. Sensors (Basel) 16.

Baneres JL, & Parello J (2003). Structure-based analysis of GPCR function: evidence for a novel pentameric assembly between the dimeric leukotriene B4 receptor BLT1 and the G-protein. J Mol Biol 329**:** 815-829.

Barragan-Iglesias P, Mendoza-Garces L, Pineda-Farias JB, Solano-Olivares V, Rodriguez-Silverio J, Flores-Murrieta FJ, *et al.* (2015). Participation of peripheral P2Y1, P2Y6 and P2Y11 receptors in formalin-induced inflammatory pain in rats. Pharmacol Biochem Behav 128**:** 23-32.

References

Barrot M (2012). Tests and models of nociception and pain in rodents. Neuroscience 211**:** 39-50.

Basbaum AI, Bautista DM, Scherrer G, & Julius D (2009). Cellular and molecular mechanisms of pain. Cell 139**:** 267-284.

Baurand A, Eckly A, Bari N, Leon C, Hechler B, Cazenave JP*, et al.* (2000). Desensitization of the platelet aggregation response to ADP: differential down-regulation of the P2Y1 and P2cyc receptors. Thromb Haemost 84**:** 484-491.

Baurand A, Raboisson P, Freund M, Leon C, Cazenave JP, Bourguignon JJ*, et al.* (2001). Inhibition of platelet function by administration of MRS2179, a P2Y1 receptor antagonist. Eur J Pharmacol 412**:** 213-221.

Beaulieu JM, & Gainetdinov RR (2011). The physiology, signaling, and pharmacology of dopamine receptors. Pharmacol Rev 63**:** 182-217.

Bellot M, Galandrin S, Boularan C, Matthies HJ, Despas F, Denis C*, et al.* (2015). Dual agonist occupancy of AT1-R-alpha2C-AR heterodimers results in atypical Gs-PKA signaling. Nat Chem Biol 11**:** 271-279.

Bennett GJ, & Xie YK (1988). A peripheral mononeuropathy in rat that produces disorders of pain sensation like those seen in man. Pain 33**:** 87-107.

Bernard ML, Peterson YK, Chung P, Jourdan J, & Lanier SM (2001). Selective interaction of AGS3 with G-proteins and the influence of AGS3 on the activation state of G-proteins. J Biol Chem 276**:** 1585-1593.

Billiau A, & Matthys P (2001). Modes of action of Freund's adjuvants in experimental models of autoimmune diseases. J Leukoc Biol 70**:** 849-860.

Birch RE, Schwiebert EM, Peppiatt-Wildman CM, & Wildman SS (2013). Emerging key roles for P2X receptors in the kidney. Front Physiol 4**:** 262.

Birdsall NJM (1982). Can different receptors interact directly with each other? Trends in Neurosciences 5**:** 137-138.

Bodor ET, Waldo GL, Hooks SB, Corbitt J, Boyer JL, & Harden TK (2003). Purification and functional reconstitution of the human P2Y12 receptor. Mol Pharmacol 64**:** 1210-1216.

Boeynaems J-M, Communi D, & Robaye B (2012). Overview of the pharmacology and physiological roles of P2Y receptors. Wiley Interdisciplinary Reviews: Membrane Transport and Signaling 1**:** 581-588.

Bohme I, & Beck-Sickinger AG (2009). Illuminating the life of GPCRs. Cell Commun Signal 7**:** 16.

References

Bohmer SA, Weibrecht I, Soderberg O, & Bohmer FD (2013). Association of the protein-tyrosine phosphatase DEP-1 with its substrate FLT3 visualized by in situ proximity ligation assay. PLoS One 8**:** e62871.

Bolte S, & Cordelieres FP (2006). A guided tour into subcellular colocalization analysis in light microscopy. J Microsc 224**:** 213-232.

Bondar A, & Lazar J (2014). Dissociated GalphaGTP and Gbetagamma protein subunits are the major activated form of heterotrimeric Gi/o proteins. J Biol Chem 289**:** 1271-1281.

Borroto-Escuela DO, Hagman B, Woolfenden M, Pinton L, Jiménez-Beristain A, Oflijan J*, et al.* (2016). In Situ Proximity Ligation Assay to Study
and Understand the Distribution and Balance of GPCR Homo- and Heteroreceptor Complexes in the Brain. In Receptor and Ion Channel Detection in the Brain: Methods and Protocols, Neuromethods. eds Luján R., & Ciruela F.: New York.

Borroto-Escuela DO, Rodriguez D, Romero-Fernandez W, Kapla J, Jaiteh M, Ranganathan A*, et al.* (2018). Mapping the Interface of a GPCR Dimer: A Structural Model of the A2A Adenosine and D2 Dopamine Receptor Heteromer. Front Pharmacol 9**:** 829.

Borroto-Escuela DO, Romero-Fernandez W, Tarakanov AO, Gomez-Soler M, Corrales F, Marcellino D*, et al.* (2010). Characterization of the A2AR-D2R interface: focus on the role of the C-terminal tail and the transmembrane helices. Biochem Biophys Res Commun 402**:** 801-807.

Bourdon DM, Mahanty SK, Jacobson KA, Boyer JL, & Harden TK (2006). (N)-methanocarba-2MeSADP (MRS2365) is a subtype-specific agonist that induces rapid desensitization of the P2Y1 receptor of human platelets. J Thromb Haemost 4**:** 861-868.

Brautigam VM, Frasier C, Nikodemova M, & Watters JJ (2005). Purinergic receptor modulation of BV-2 microglial cell activity: potential involvement of p38 MAP kinase and CREB. J Neuroimmunol 166**:** 113-125.

Brown DA, & Sihra TS (2008). Presynaptic signaling by heterotrimeric G-proteins. Handb Exp Pharmacol**:** 207-260.

Burnstock G (2004). Introduction: P2 receptors. Curr Top Med Chem 4**:** 793-803.

Burnstock G (2006). Purinergic signalling--an overview. Novartis Found Symp 276**:** 26-48; discussion 48-57, 275-281.

Burnstock G (2007). Physiology and pathophysiology of purinergic neurotransmission. Physiol Rev 87**:** 659-797.

Burnstock G (2009). Purinergic signalling: past, present and future. Braz J Med Biol Res 42**:** 3-8.

References

Burnstock G (2013). Purinergic mechanisms and pain--an update. Eur J Pharmacol 716**:** 24-40.

Burnstock G (2014). Purines and Purinoceptors: Molecular Biology Overview.

Burnstock G (2018). Purine and purinergic receptors. Brain Neurosci Adv 2**:** 2398212818817494.

Burnstock G, & Kennedy C (1985). Is there a basis for distinguishing two types of P2-purinoceptor? Gen Pharmacol 16**:** 433-440.

Cahill TJ, 3rd, Thomsen AR, Tarrasch JT, Plouffe B, Nguyen AH, Yang F*, et al.* (2017). Distinct conformations of GPCR-beta-arrestin complexes mediate desensitization, signaling, and endocytosis. Proc Natl Acad Sci U S A 114**:** 2562-2567.

Calebiro D, Nikolaev VO, Persani L, & Lohse MJ (2010). Signaling by internalized G-protein-coupled receptors. Trends Pharmacol Sci 31**:** 221-228.

Calebiro D, Rieken F, Wagner J, Sungkaworn T, Zabel U, Borzi A*, et al.* (2013). Single-molecule analysis of fluorescently labeled G-protein-coupled receptors reveals complexes with distinct dynamics and organization. Proc Natl Acad Sci U S A 110**:** 743-748.

Callen L, Moreno E, Barroso-Chinea P, Moreno-Delgado D, Cortes A, Mallol J*, et al.* (2012). Cannabinoid receptors CB1 and CB2 form functional heteromers in brain. J Biol Chem 287**:** 20851-20865.

Canals M, Marcellino D, Fanelli F, Ciruela F, de Benedetti P, Goldberg SR*, et al.* (2003). Adenosine A2A-dopamine D2 receptor-receptor heteromerization: qualitative and quantitative assessment by fluorescence and bioluminescence energy transfer. J Biol Chem 278**:** 46741-46749.

Canals M, Poole DP, Veldhuis NA, Schmidt BL, & Bunnett NW (2019). G-Protein-Coupled Receptors Are Dynamic Regulators of Digestion and Targets for Digestive Diseases. Gastroenterology 156**:** 1600-1616.

Cardullo RA (2007). Theoretical principles and practical considerations for fluorescence resonance energy transfer microscopy. Methods Cell Biol 81**:** 479-494.

Carli M, Kolachalam S, Aringhieri S, Rossi M, Giovannini L, Maggio R*, et al.* (2018). Dopamine D2 Receptors Dimers: How can we Pharmacologically Target Them? Curr Neuropharmacol 16**:** 222-230.

Carrington SJ, Hernandez CC, Swale DR, Aluko OA, Denton JS, & Cone RD (2018). G protein-coupled receptors differentially regulate glycosylation and activity of the inwardly rectifying potassium channel Kir7.1. J Biol Chem 293**:** 17739-17753.

Cattaneo M (2015). P2Y12 receptors: structure and function. J Thromb Haemost 13 Suppl 1**:** S10-16.

References

Cattaneo M, Lecchi A, Ohno M, Joshi BV, Besada P, Tchilibon S, *et al.* (2004). Antiaggregatory activity in human platelets of potent antagonists of the P2Y 1 receptor. Biochem Pharmacol 68**:** 1995-2002.

Chakrabarti S, Liu NJ, & Gintzler AR (2010). Formation of mu-/kappa-opioid receptor heterodimer is sex-dependent and mediates female-specific opioid analgesia. Proc Natl Acad Sci U S A 107**:** 20115-20119.

Chen G, Way J, Armour S, Watson C, Queen K, Jayawickreme CK, *et al.* (2000). Use of constitutive G protein-coupled receptor activity for drug discovery. Mol Pharmacol 57**:** 125-134.

Chen G, Zhang YQ, Qadri YJ, Serhan CN, & Ji RR (2018). Microglia in Pain: Detrimental and Protective Roles in Pathogenesis and Resolution of Pain. Neuron 100**:** 1292-1311.

Cherezov V, Rosenbaum DM, Hanson MA, Rasmussen SG, Thian FS, Kobilka TS, *et al.* (2007). High-resolution crystal structure of an engineered human beta2-adrenergic G protein-coupled receptor. Science 318**:** 1258-1265.

Chien EY, Liu W, Zhao Q, Katritch V, Han GW, Hanson MA, *et al.* (2010). Structure of the human dopamine D3 receptor in complex with a D2/D3 selective antagonist. Science 330**:** 1091-1095.

Chini B, & Parenti M (2009). G-protein-coupled receptors, cholesterol and palmitoylation: facts about fats. J Mol Endocrinol 42**:** 371-379.

Choi RC, Simon J, Tsim KW, & Barnard EA (2008). Constitutive and agonist-induced dimerizations of the P2Y1 receptor: relationship to internalization and scaffolding. J Biol Chem 283**:** 11050-11063.

Chou R, Fanciullo GJ, Fine PG, Adler JA, Ballantyne JC, Davies P, *et al.* (2009). Clinical guidelines for the use of chronic opioid therapy in chronic noncancer pain. J Pain 10**:** 113-130.

Chun L, Zhang WH, & Liu JF (2012). Structure and ligand recognition of class C GPCRs. Acta Pharmacol Sin 33**:** 312-323.

Civelli O, Reinscheid RK, Zhang Y, Wang Z, Fredriksson R, & Schioth HB (2013). G protein-coupled receptor deorphanizations. Annu Rev Pharmacol Toxicol 53**:** 127-146.

Conigrave AD, Lee JY, van der Weyden L, Jiang L, Ward P, Tasevski V, *et al.* (1998). Pharmacological profile of a novel cyclic AMP-linked P2 receptor on undifferentiated HL-60 leukemia cells. Br J Pharmacol 124**:** 1580-1585.

Coppi E, Pedata F, & Gibb AJ (2012). P2Y1 receptor modulation of Ca2+-activated K+ currents in medium-sized neurons from neonatal rat striatal slices. J Neurophysiol 107**:** 1009-1021.

References

Costa S, Almeida A, Castro A, & Domingues L (2014). Fusion tags for protein solubility, purification and immunogenicity in Escherichia coli: the novel Fh8 system. Front Microbiol 5**:** 63.

Cottet M, Albizu L, Comps-Agrar L, Trinquet E, Pin JP, Mouillac B, *et al.* (2011). Time resolved FRET strategy with fluorescent ligands to analyze receptor interactions in native tissues: application to GPCR oligomerization. Methods Mol Biol 746**:** 373-387.

Couve A, Filippov AK, Connolly CN, Bettler B, Brown DA, & Moss SJ (1998). Intracellular retention of recombinant GABAB receptors. J Biol Chem 273**:** 26361-26367.

Crain JM, Nikodemova M, & Watters JJ (2009). Expression of P2 nucleotide receptors varies with age and sex in murine brain microglia. J Neuroinflammation 6**:** 24.

Cunningham MR, Nisar SP, Cooke AE, Emery ED, & Mundell SJ (2013a). Differential endosomal sorting of a novel P2Y12 purinoreceptor mutant. Traffic 14**:** 585-598.

Cunningham MR, Nisar SP, & Mundell SJ (2013b). Molecular mechanisms of platelet P2Y(12) receptor regulation. Biochem Soc Trans 41**:** 225-230.

Cvejic S, & Devi LA (1997). Dimerization of the delta opioid receptor: implication for a role in receptor internalization. J Biol Chem 272**:** 26959-26964.

D'Ambrosi N, Iafrate M, Saba E, Rosa P, & Volonte C (2007). Comparative analysis of P2Y4 and P2Y6 receptor architecture in native and transfected neuronal systems. Biochim Biophys Acta 1768**:** 1592-1599.

D'Ambrosi N, Iafrate M, Vacca F, Amadio S, Tozzi A, Mercuri NB, *et al.* (2006). The P2Y(4) receptor forms homo-oligomeric complexes in several CNS and PNS neuronal cells. Purinergic Signal 2**:** 575-582.

Dacres H, Wang J, Dumancic MM, & Trowell SC (2010). Experimental determination of the Forster distance for two commonly used bioluminescent resonance energy transfer pairs. Anal Chem 82**:** 432-435.

Darby N, & Creighton TE (1995). Disulfide bonds in protein folding and stability. Methods Mol Biol 40**:** 219-252.

Davis D, Liu X, & Segaloff DL (1995). Identification of the sites of N-linked glycosylation on the follicle-stimulating hormone (FSH) receptor and assessment of their role in FSH receptor function. Mol Endocrinol 9**:** 159-170.

Day RN, & Davidson MW (2009). The fluorescent protein palette: tools for cellular imaging. Chem Soc Rev 38**:** 2887-2921.

Debnath B, Al-Mawsawi LQ, & Neamati N (2010). Are we living in the end of the blockbuster drug era? Drug News Perspect 23**:** 670-684.

References

Decaillot FM, Rozenfeld R, Gupta A, & Devi LA (2008). Cell surface targeting of mu-delta opioid receptor heterodimers by RTP4. Proc Natl Acad Sci U S A 105**:** 16045-16050.

DeCaprio J, & Kohl TO (2019). Tandem Immunoaffinity Purification Using Anti-FLAG and Anti-HA Antibodies. Cold Spring Harb Protoc 2019.

Decosterd I, & Woolf CJ (2000). Spared nerve injury: an animal model of persistent peripheral neuropathic pain. Pain 87**:** 149-158.

DeFea KA, Zalevsky J, Thoma MS, Dery O, Mullins RD, & Bunnett NW (2000). beta-arrestin-dependent endocytosis of proteinase-activated receptor 2 is required for intracellular targeting of activated ERK1/2. J Cell Biol 148**:** 1267-1281.

Dello Russo C, Cappoli N, Coletta I, Mezzogori D, Paciello F, Pozzoli G*, et al.* (2018). The human microglial HMC3 cell line: where do we stand? A systematic literature review. J Neuroinflammation 15**:** 259.

Delos Santos NM, Gardner LA, White SW, & Bahouth SW (2006). Characterization of the residues in helix 8 of the human beta1-adrenergic receptor that are involved in coupling the receptor to G proteins. J Biol Chem 281**:** 12896-12907.

Deval E, Gasull X, Noel J, Salinas M, Baron A, Diochot S*, et al.* (2010). Acid-sensing ion channels (ASICs): pharmacology and implication in pain. Pharmacol Ther 128**:** 549-558.

DeWire SM, Ahn S, Lefkowitz RJ, & Shenoy SK (2007). Beta-arrestins and cell signaling. Annu Rev Physiol 69**:** 483-510.

Dijkman PM, Castell OK, Goddard AD, Munoz-Garcia JC, de Graaf C, Wallace MI*, et al.* (2018). Dynamic tuneable G protein-coupled receptor monomer-dimer populations. Nat Commun 9**:** 1710.

Ding Z, Bynagari YS, Mada SR, Jakubowski JA, & Kunapuli SP (2009). Studies on the role of the extracellular cysteines and oligomeric structures of the P2Y12 receptor when interacting with antagonists. J Thromb Haemost 7**:** 232-234.

Ding Z, Tuluc F, Bandivadekar KR, Zhang L, Jin J, & Kunapuli SP (2005). Arg333 and Arg334 in the COOH terminus of the human P2Y1 receptor are crucial for Gq coupling. Am J Physiol Cell Physiol 288**:** C559-567.

Dong C, Filipeanu CM, Duvernay MT, & Wu G (2007). Regulation of G protein-coupled receptor export trafficking. Biochim Biophys Acta 1768**:** 853-870.

Dreisig K, & Kornum BR (2016). A critical look at the function of the P2Y11 receptor. Purinergic Signal 12**:** 427-437.

References

Dror RO, Mildorf TJ, Hilger D, Manglik A, Borhani DW, Arlow DH, *et al.* (2015). SIGNAL TRANSDUCTION. Structural basis for nucleotide exchange in heterotrimeric G proteins. Science 348**:** 1361-1365.

DuPen A, Shen D, & Ersek M (2007). Mechanisms of opioid-induced tolerance and hyperalgesia. Pain Manag Nurs 8**:** 113-121.

Dupre DJ, Rola-Pleszczynski M, & Stankova J (2012). Rescue of internalization-defective platelet-activating factor receptor function by EBP50/NHERF1. J Cell Commun Signal 6**:** 205-216.

Ebisuya M, Kondoh K, & Nishida E (2005). The duration, magnitude and compartmentalization of ERK MAP kinase activity: mechanisms for providing signaling specificity. J Cell Sci 118**:** 2997-3002.

Ecke D, Hanck T, Tulapurkar ME, Schafer R, Kassack M, Stricker R, *et al.* (2008). Hetero-oligomerization of the P2Y11 receptor with the P2Y1 receptor controls the internalization and ligand selectivity of the P2Y11 receptor. Biochem J 409**:** 107-116.

Egea SC, & Dickerson IM (2012). Direct interactions between calcitonin-like receptor (CLR) and CGRP-receptor component protein (RCP) regulate CGRP receptor signaling. Endocrinology 153**:** 1850-1860.

El Moustaine D, Granier S, Doumazane E, Scholler P, Rahmeh R, Bron P, *et al.* (2012). Distinct roles of metabotropic glutamate receptor dimerization in agonist activation and G-protein coupling. Proc Natl Acad Sci U S A 109**:** 16342-16347.

Emami-Nemini A, Roux T, Leblay M, Bourrier E, Lamarque L, Trinquet E, *et al.* (2013). Time-resolved fluorescence ligand binding for G protein-coupled receptors. Nat Protoc 8**:** 1307-1320.

Erb L, Garrad R, Wang Y, Quinn T, Turner JT, & Weisman GA (1995). Site-directed mutagenesis of P2U purinoceptors. Positively charged amino acids in transmembrane helices 6 and 7 affect agonist potency and specificity. J Biol Chem 270**:** 4185-4188.

Esko JD, Bertozzi C, & Schnaar RL (2015). Chemical Tools for Inhibiting Glycosylation. In Essentials of Glycobiology. eds rd, Varki A., Cummings R.D., Esko J.D., Stanley P., Hart G.W., Aebi M., Darvill A.G., Kinoshita T., Packer N.H., Prestegard J.H., Schnaar R.L., & Seeberger P.H.: Cold Spring Harbor (NY), pp 701-712.

Espinoza S, Salahpour A, Masri B, Sotnikova TD, Messa M, Barak LS, *et al.* (2011). Functional interaction between trace amine-associated receptor 1 and dopamine D2 receptor. Mol Pharmacol 80**:** 416-425.

Evron T, Daigle TL, & Caron MG (2012). GRK2: multiple roles beyond G protein-coupled receptor desensitization. Trends Pharmacol Sci 33**:** 154-164.

References

Fanning AS, Lye MF, Anderson JM, & Lavie A (2007). Domain swapping within PDZ2 is responsible for dimerization of ZO proteins. J Biol Chem 282**:** 37710-37716.

Farber K, & Kettenmann H (2006). Purinergic signaling and microglia. Pflugers Arch 452**:** 615-621.

Felce JH, Latty SL, Knox RG, Mattick SR, Lui Y, Lee SF, *et al.* (2017). Receptor Quaternary Organization Explains G Protein-Coupled Receptor Family Structure. Cell Rep 20**:** 2654-2665.

Fernandez-Duenas V, Llorente J, Gandia J, Borroto-Escuela DO, Agnati LF, Tasca CI, *et al.* (2012). Fluorescence resonance energy transfer-based technologies in the study of protein-protein interactions at the cell surface. Methods 57**:** 467-472.

Ferre S, Baler R, Bouvier M, Caron MG, Devi LA, Durroux T, *et al.* (2009). Building a new conceptual framework for receptor heteromers. Nat Chem Biol 5**:** 131-134.

Ferre S, Casado V, Devi LA, Filizola M, Jockers R, Lohse MJ, *et al.* (2014). G protein-coupled receptor oligomerization revisited: functional and pharmacological perspectives. Pharmacol Rev 66**:** 413-434.

Fiala GJ, Schamel WW, & Blumenthal B (2011). Blue native polyacrylamide gel electrophoresis (BN-PAGE) for analysis of multiprotein complexes from cellular lysates. J Vis Exp.

Filipek S, Teller DC, Palczewski K, & Stenkamp R (2003). The crystallographic model of rhodopsin and its use in studies of other G protein-coupled receptors. Annu Rev Biophys Biomol Struct 32**:** 375-397.

Filippov AK, Brown DA, & Barnard EA (2000). The P2Y(1) receptor closes the N-type Ca(2+) channel in neurones, with both adenosine triphosphates and diphosphates as potent agonists. Br J Pharmacol 129**:** 1063-1066.

Filippov AK, Choi RC, Simon J, Barnard EA, & Brown DA (2006). Activation of P2Y1 nucleotide receptors induces inhibition of the M-type K+ current in rat hippocampal pyramidal neurons. J Neurosci 26**:** 9340-9348.

Filizola M, & Weinstein H (2005). The study of G-protein coupled receptor oligomerization with computational modeling and bioinformatics. FEBS J 272**:** 2926-2938.

Förster T (1948). Zwischenmolekulare Energiewanderung und Fluoreszenz. Annalen der Physik 437**:** 55-75.

Fotiadis D, Liang Y, Filipek S, Saperstein DA, Engel A, & Palczewski K (2004). The G protein-coupled receptor rhodopsin in the native membrane. FEBS Lett 564**:** 281-288.

Franceschini A, & Adinolfi E (2014). P2X receptors: New players in cancer pain. World J Biol Chem 5**:** 429-436.

References

Franco R, Martinez-Pinilla E, Lanciego JL, & Navarro G (2016). Basic Pharmacological and Structural Evidence for Class A G-Protein-Coupled Receptor Heteromerization. Front Pharmacol 7**:** 76.

Fredriksson R, Lagerstrom MC, Lundin LG, & Schioth HB (2003). The G-protein-coupled receptors in the human genome form five main families. Phylogenetic analysis, paralogon groups, and fingerprints. Mol Pharmacol 63**:** 1256-1272.

Fredriksson S, Gullberg M, Jarvius J, Olsson C, Pietras K, Gustafsdottir SM*, et al.* (2002). Protein detection using proximity-dependent DNA ligation assays. Nat Biotechnol 20**:** 473-477.

Frydman J, Nimmesgern E, Erdjument-Bromage H, Wall JS, Tempst P, & Hartl FU (1992). EMBO J 11**:** 4767.

Gacasan SB, Baker DL, & Parrill AL (2017). G protein-coupled receptors: the evolution of structural insight. AIMS Biophys 4**:** 491-527.

Gafar H, Dominguez Rodriguez M, Chandaka GK, Salzer I, Boehm S, & Schicker K (2016). Membrane coordination of receptors and channels mediating the inhibition of neuronal ion currents by ADP. Purinergic Signal 12**:** 497-507.

Gahbauer S, & Bockmann RA (2016). Membrane-Mediated Oligomerization of G Protein Coupled Receptors and Its Implications for GPCR Function. Front Physiol 7**:** 494.

Galva C, Artigas P, & Gatto C (2012). Nuclear Na+/K+-ATPase plays an active role in nucleoplasmic Ca2+ homeostasis. J Cell Sci 125**:** 6137-6147.

Garcia-Mesa Y, Jay TR, Checkley MA, Luttge B, Dobrowolski C, Valadkhan S*, et al.* (2017). Immortalization of primary microglia: a new platform to study HIV regulation in the central nervous system. J Neurovirol 23**:** 47-66.

Garnier M, Zaratin PF, Ficalora G, Valente M, Fontanella L, Rhee MH*, et al.* (2003). Up-regulation of regulator of G protein signaling 4 expression in a model of neuropathic pain and insensitivity to morphine. J Pharmacol Exp Ther 304**:** 1299-1306.

Gasecka A, Rogula S, Eyileten C, Postula M, Jaguszewski MJ, Kochman J*, et al.* (2020). Role of P2Y Receptors in Platelet Extracellular Vesicle Release. Int J Mol Sci 21.

Gauldie SD, McQueen DS, Clarke CJ, & Chessell IP (2004). A robust model of adjuvant-induced chronic unilateral arthritis in two mouse strains. J Neurosci Methods 139**:** 281-291.

George SR, Fan T, Xie Z, Tse R, Tam V, Varghese G*, et al.* (2000). Oligomerization of mu- and delta-opioid receptors. Generation of novel functional properties. J Biol Chem 275**:** 26128-26135.

References

Gomes I, Fujita W, Chandrakala MV, & Devi LA (2013). Disease-specific heteromerization of G-protein-coupled receptors that target drugs of abuse. Prog Mol Biol Transl Sci 117**:** 207-265.

Gomes I, Gupta A, Filipovska J, Szeto HH, Pintar JE, & Devi LA (2004). A role for heterodimerization of mu and delta opiate receptors in enhancing morphine analgesia. Proc Natl Acad Sci U S A 101**:** 5135-5139.

Gomes I, Ijzerman AP, Ye K, Maillet EL, & Devi LA (2011). G protein-coupled receptor heteromerization: a role in allosteric modulation of ligand binding. Mol Pharmacol 79**:** 1044-1052.

Gomes I, Jordan BA, Gupta A, Trapaidze N, Nagy V, & Devi LA (2000). Heterodimerization of mu and delta opioid receptors: A role in opiate synergy. J Neurosci 20**:** RC110.

Gomes I, Sierra S, & Devi LA (2016). Detection of Receptor Heteromerization Using In Situ Proximity Ligation Assay. Curr Protoc Pharmacol 75**:** 2 16 11-12 16 31.

Goodman OB, Jr., Krupnick JG, Santini F, Gurevich VV, Penn RB, Gagnon AW, *et al.* (1996). Beta-arrestin acts as a clathrin adaptor in endocytosis of the beta2-adrenergic receptor. Nature 383**:** 447-450.

Granier S, Manglik A, Kruse AC, Kobilka TS, Thian FS, Weis WI, *et al.* (2012). Structure of the delta-opioid receptor bound to naltrindole. Nature 485**:** 400-404.

Granier S, Terrillon S, Pascal R, Demene H, Bouvier M, Guillon G, *et al.* (2004). A cyclic peptide mimicking the third intracellular loop of the V2 vasopressin receptor inhibits signaling through its interaction with receptor dimer and G protein. J Biol Chem 279**:** 50904-50914.

Greenwood C, Ruff D, Kirvell S, Johnson G, Dhillon HS, & Bustin SA (2015). Proximity assays for sensitive quantification of proteins. Biomol Detect Quantif 4**:** 10-16.

Greife A, Felekyan S, Ma Q, Gertzen CG, Spomer L, Dimura M, *et al.* (2016). Structural assemblies of the di- and oligomeric G-protein coupled receptor TGR5 in live cells: an MFIS-FRET and integrative modelling study. Sci Rep 6**:** 36792.

Griner EM, & Kazanietz MG (2007). Protein kinase C and other diacylglycerol effectors in cancer. Nat Rev Cancer 7**:** 281-294.

Guo H, An S, Ward R, Yang Y, Liu Y, Guo XX, *et al.* (2017). Methods used to study the oligomeric structure of G-protein-coupled receptors. Biosci Rep 37.

Gupta A, Decaillot FM, Gomes I, Tkalych O, Heimann AS, Ferro ES, *et al.* (2007). Conformation state-sensitive antibodies to G-protein-coupled receptors. J Biol Chem 282**:** 5116-5124.

References

Gurevich VV, & Benovic JL (1993). Visual arrestin interaction with rhodopsin. Sequential multisite binding ensures strict selectivity toward light-activated phosphorylated rhodopsin. J Biol Chem 268**:** 11628-11638.

Gustafsson MG (2000). Surpassing the lateral resolution limit by a factor of two using structured illumination microscopy. J Microsc 198**:** 82-87.

Haack KKV, & McCarty NA (2011). Functional Consequences of GPCR Heterodimerization: GPCRs as Allosteric Modulators. Pharmaceuticals (Basel) 4**:** 509-523.

Haga K, Kruse AC, Asada H, Yurugi-Kobayashi T, Shiroishi M, Zhang C*, et al.* (2012). Structure of the human M2 muscarinic acetylcholine receptor bound to an antagonist. Nature 482**:** 547-551.

Hall RA (2005). Co-Immunoprecipitation as a Strategy to Evaluate Receptor–Receptor or Receptor–Protein Interactions in G-Protein-Coupled Receptor–Protein Interactions. In G Protein-Coupled Receptor–Protein Interactions. ed Dowd S.R.G.a.B.F.

Ham J, & Evans BA (2012). An emerging role for adenosine and its receptors in bone homeostasis. Front Endocrinol (Lausanne) 3**:** 113.

Hanlon CD, & Andrew DJ (2015). Outside-in signaling--a brief review of GPCR signaling with a focus on the Drosophila GPCR family. J Cell Sci 128**:** 3533-3542.

Hardy AR, Conley PB, Luo J, Benovic JL, Poole AW, & Mundell SJ (2005). P2Y1 and P2Y12 receptors for ADP desensitize by distinct kinase-dependent mechanisms. Blood 105**:** 3552-3560.

Hardy AR, Jones ML, Mundell SJ, & Poole AW (2004). Reciprocal cross-talk between P2Y1 and P2Y12 receptors at the level of calcium signaling in human platelets. Blood 104**:** 1745-1752.

Harrison C, & van der Graaf PH (2006). Current methods used to investigate G protein coupled receptor oligomerisation. J Pharmacol Toxicol Methods 54**:** 26-35.

Hauser AS, Attwood MM, Rask-Andersen M, Schioth HB, & Gloriam DE (2017). Trends in GPCR drug discovery: new agents, targets and indications. Nat Rev Drug Discov 16**:** 829-842.

Hauser AS, Chavali S, Masuho I, Jahn LJ, Martemyanov KA, Gloriam DE*, et al.* (2018). Pharmacogenomics of GPCR Drug Targets. Cell 172**:** 41-54 e19.

Haynes SE, Hollopeter G, Yang G, Kurpius D, Dailey ME, Gan WB*, et al.* (2006). The P2Y12 receptor regulates microglial activation by extracellular nucleotides. Nat Neurosci 9**:** 1512-1519.

References

Hebert TE, Moffett S, Morello JP, Loisel TP, Bichet DG, Barret C, *et al.* (1996). A peptide derived from a beta2-adrenergic receptor transmembrane domain inhibits both receptor dimerization and activation. J Biol Chem 271**:** 16384-16392.

Hechler B, & Gachet C (2011). P2 receptors and platelet function. Purinergic Signal 7**:** 293-303.

Heindl S, Gesierich B, Benakis C, Llovera G, Duering M, & Liesz A (2018). Automated Morphological Analysis of Microglia After Stroke. Front Cell Neurosci 12**:** 106.

Hell SW, & Wichmann J (1994). Breaking the diffraction resolution limit by stimulated emission: stimulated-emission-depletion fluorescence microscopy. Opt Lett 19**:** 780-782.

Henning J, Strauss U, Wree A, Gimsa J, Rolfs A, Benecke R, *et al.* (2008). Differential astroglial activation in 6-hydroxydopamine models of Parkinson's disease. Neurosci Res 62**:** 246-253.

Herrick-Davis K, Weaver BA, Grinde E, & Mazurkiewicz JE (2006). Serotonin 5-HT2C receptor homodimer biogenesis in the endoplasmic reticulum: real-time visualization with confocal fluorescence resonance energy transfer. J Biol Chem 281**:** 27109-27116.

Hiller C, Kuhhorn J, & Gmeiner P (2013). Class A G-protein-coupled receptor (GPCR) dimers and bivalent ligands. J Med Chem 56**:** 6542-6559.

Hislop JN, & von Zastrow M (2011). Analysis of GPCR localization and trafficking. Methods Mol Biol 746**:** 425-440.

Hoffmann C, Moro S, Nicholas RA, Harden TK, & Jacobson KA (1999). The role of amino acids in extracellular loops of the human P2Y1 receptor in surface expression and activation processes. J Biol Chem 274**:** 14639-14647.

Hoffmann C, Ziegler N, Reiner S, Krasel C, & Lohse MJ (2008). Agonist-selective, receptor-specific interaction of human P2Y receptors with beta-arrestin-1 and -2. J Biol Chem 283**:** 30933-30941.

Hollopeter G, Jantzen HM, Vincent D, Li G, England L, Ramakrishnan V, *et al.* (2001). Identification of the platelet ADP receptor targeted by antithrombotic drugs. Nature 409**:** 202-207.

Honda S, Sasaki Y, Ohsawa K, Imai Y, Nakamura Y, Inoue K, *et al.* (2001). Extracellular ATP or ADP induce chemotaxis of cultured microglia through Gi/o-coupled P2Y receptors. J Neurosci 21**:** 1975-1982.

Horvath G, Goloncser F, Csolle C, Kiraly K, Ando RD, Baranyi M, *et al.* (2014). Central P2Y12 receptor blockade alleviates inflammatory and neuropathic pain and cytokine production in rodents. Neurobiol Dis 70**:** 162-178.

References

Hu CD, & Kerppola TK (2003). Simultaneous visualization of multiple protein interactions in living cells using multicolor fluorescence complementation analysis. Nat Biotechnol 21**:** 539-545.

Hu GM, Mai TL, & Chen CM (2017). Visualizing the GPCR Network: Classification and Evolution. Sci Rep 7**:** 15495.

Huang J, Chen S, Zhang JJ, & Huang XY (2013). Crystal structure of oligomeric beta1-adrenergic G protein-coupled receptors in ligand-free basal state. Nat Struct Mol Biol 20**:** 419-425.

Huang W, Manglik A, Venkatakrishnan AJ, Laeremans T, Feinberg EN, Sanborn AL*, et al.* (2015). Structural insights into micro-opioid receptor activation. Nature 524**:** 315-321.

Hucho T, & Levine JD (2007). Signaling pathways in sensitization: toward a nociceptor cell biology. Neuron 55**:** 365-376.

Hussl S, & Boehm S (2006). Functions of neuronal P2Y receptors. Pflugers Arch 452**:** 538-551.

Imai Y, & Kohsaka S (2002). Intracellular signaling in M-CSF-induced microglia activation: role of Iba1. Glia 40**:** 164-174.

Inbe H, Watanabe S, Miyawaki M, Tanabe E, & Encinas JA (2004). Identification and characterization of a cell-surface receptor, P2Y15, for AMP and adenosine. J Biol Chem 279**:** 19790-19799.

Ishikawa-Ankerhold HC, Ankerhold R, & Drummen GP (2012). Advanced fluorescence microscopy techniques--FRAP, FLIP, FLAP, FRET and FLIM. Molecules 17**:** 4047-4132.

Jaakola VP, Griffith MT, Hanson MA, Cherezov V, Chien EY, Lane JR*, et al.* (2008). The 2.6 angstrom crystal structure of a human A2A adenosine receptor bound to an antagonist. Science 322**:** 1211-1217.

Jacobson KA, Delicado EG, Gachet C, Kennedy C, von Kugelgen I, Li B*, et al.* (2020). Update of P2Y receptor pharmacology: IUPHAR Review 27. Br J Pharmacol 177**:** 2413-2433.

Jacobson KA, Ivanov AA, de Castro S, Harden TK, & Ko H (2009). Development of selective agonists and antagonists of P2Y receptors. Purinergic Signal 5**:** 75-89.

Jacobson KA, Jarvis MF, & Williams M (2002). Purine and pyrimidine (P2) receptors as drug targets. J Med Chem 45**:** 4057-4093.

Jagroop IA, Burnstock G, & Mikhailidis DP (2003). Both the ADP receptors P2Y1 and P2Y12, play a role in controlling shape change in human platelets. Platelets 14**:** 15-20.

References

Jarvis GE, & Thompson AJ (2019). Evidence for an effect of receptor density on ligand occupancy and agonist EC50. Sci Rep 9**:** 19111.

Jarvis MF (2010). The neural-glial purinergic receptor ensemble in chronic pain states. Trends Neurosci 33**:** 48-57.

Jayadev S, Smith RD, Jagadeesh G, Baukal AJ, Hunyady L, & Catt KJ (1999). N-linked glycosylation is required for optimal AT1a angiotensin receptor expression in COS-7 cells. Endocrinology 140**:** 2010-2017.

Ji RR, Xu ZZ, & Gao YJ (2014). Emerging targets in neuroinflammation-driven chronic pain. Nat Rev Drug Discov 13**:** 533-548.

Jiang P, Xing F, Guo B, Yang J, Li Z, Wei W, *et al.* (2017). Nucleotide transmitters ATP and ADP mediate intercellular calcium wave communication via P2Y12/13 receptors among BV-2 microglia. PLoS One 12**:** e0183114.

Jiang Q, Guo D, Lee BX, Van Rhee AM, Kim YC, Nicholas RA, *et al.* (1997). A mutational analysis of residues essential for ligand recognition at the human P2Y1 receptor. Mol Pharmacol 52**:** 499-507.

Jimenez-Vargas NN, Pattison LA, Zhao P, Lieu T, Latorre R, Jensen DD, *et al.* (2018). Protease-activated receptor-2 in endosomes signals persistent pain of irritable bowel syndrome. Proc Natl Acad Sci U S A 115**:** E7438-E7447.

Jin J, Daniel JL, & Kunapuli SP (1998). Molecular basis for ADP-induced platelet activation. II. The P2Y1 receptor mediates ADP-induced intracellular calcium mobilization and shape change in platelets. J Biol Chem 273**:** 2030-2034.

Jin LQ, Goswami S, Cai G, Zhen X, & Friedman E (2003). SKF83959 selectively regulates phosphatidylinositol-linked D1 dopamine receptors in rat brain. J Neurochem 85**:** 378-386.

Jones KA, Borowsky B, Tamm JA, Craig DA, Durkin MM, Dai M, *et al.* (1998). GABA(B) receptors function as a heteromeric assembly of the subunits GABA(B)R1 and GABA(B)R2. Nature 396**:** 674-679.

Jones S, Evans RJ, & Mahaut-Smith MP (2014). Ca2+ influx through P2X1 receptors amplifies P2Y1 receptor-evoked Ca2+ signaling and ADP-evoked platelet aggregation. Mol Pharmacol 86**:** 243-251.

Jorg M, May LT, Mak FS, Lee KC, Miller ND, Scammells PJ, *et al.* (2015). Synthesis and pharmacological evaluation of dual acting ligands targeting the adenosine A2A and dopamine D2 receptors for the potential treatment of Parkinson's disease. J Med Chem 58**:** 718-738.

Kaebisch C, Schipper D, Babczyk P, & Tobiasch E (2015). The role of purinergic receptors in stem cell differentiation. Comput Struct Biotechnol J 13**:** 75-84.

References

Kamal M, & Jockers R (2011). Biological Significance of GPCR Heteromerization in the Neuro-Endocrine System. Front Endocrinol (Lausanne) 2**:** 2.

Kanamarlapudi V, Owens SE, Saha K, Pope RJ, & Mundell SJ (2012). ARF6-dependent regulation of P2Y receptor traffic and function in human platelets. PLoS One 7**:** e43532.

Kaupmann K, Huggel K, Heid J, Flor PJ, Bischoff S, Mickel SJ*, et al.* (1997). Expression cloning of GABA(B) receptors uncovers similarity to metabotropic glutamate receptors. Nature 386**:** 239-246.

Kennedy C, Chootip K, Mitchell C, Syed NI, & Tengah A (2013). P2X and P2Y nucleotide receptors as targets in cardiovascular disease. Future Med Chem 5**:** 431-449.

Kerppola TK (2006). Design and implementation of bimolecular fluorescence complementation (BiFC) assays for the visualization of protein interactions in living cells. Nat Protoc 1**:** 1278-1286.

Khan A, Li D, Ibrahim S, Smyth E, & Woulfe D (2011). Direct Association of PAR4 with P2Y12 Is Required for PAR4-Induced Recruitment of Arrestin-2: Structural and Functional Analysis of a GPCR Heterodimer. Blood 118**:** 3253-3253.

Khan A, Li D, Ibrahim S, Smyth E, & Woulfe DS (2014). The physical association of the P2Y12 receptor with PAR4 regulates arrestin-mediated Akt activation. Mol Pharmacol 86**:** 1-11.

Khan S, Ullah MW, Siddique R, Nabi G, Manan S, Yousaf M*, et al.* (2016). Role of Recombinant DNA Technology to Improve Life. Int J Genomics 2016**:** 2405954.

Kim SH, & Chung JM (1992). An experimental model for peripheral neuropathy produced by segmental spinal nerve ligation in the rat. Pain 50**:** 355-363.

Kirkby NS, Lundberg MH, Chan MV, Vojnovic I, Solomon AB, Emerson M*, et al.* (2013). Blockade of the purinergic P2Y12 receptor greatly increases the platelet inhibitory actions of nitric oxide. Proc Natl Acad Sci U S A 110**:** 15782-15787.

Koessler J, Weber K, Koessler A, Yilmaz P, Boeck M, & Kobsar A (2016). Expression and function of purinergic receptors in platelets from apheresis-derived platelet concentrates. Blood Transfus 14**:** 545-551.

Koupenova M, & Ravid K (2018). Biology of Platelet Purinergic Receptors and Implications for Platelet Heterogeneity. Front Pharmacol 9**:** 37.

Koushik SV, Blank PS, & Vogel SS (2009). Anomalous surplus energy transfer observed with multiple FRET acceptors. PLoS One 4**:** e8031.

Kruse AC, Hu J, Pan AC, Arlow DH, Rosenbaum DM, Rosemond E*, et al.* (2012). Structure and dynamics of the M3 muscarinic acetylcholine receptor. Nature 482**:** 552-556.

References

Kruse AC, Ring AM, Manglik A, Hu J, Hu K, Eitel K, *et al.* (2013). Activation and allosteric modulation of a muscarinic acetylcholine receptor. Nature 504**:** 101-106.

Kuhhorn J, Gotz A, Hubner H, Thompson D, Whistler J, & Gmeiner P (2011). Development of a bivalent dopamine D(2) receptor agonist. J Med Chem 54**:** 7911-7919.

Kuhn H, Bennett N, Michel-Villaz M, & Chabre M (1981). Interactions between photoexcited rhodopsin and GTP-binding protein: kinetic and stoichiometric analyses from light-scattering changes. Proc Natl Acad Sci U S A 78**:** 6873-6877.

Kwon SG, Roh DH, Yoon SY, Choi SR, Choi HS, Moon JY, *et al.* (2017). Involvement of peripheral P2Y1 receptors and potential interaction with IL-1 receptors in IL-1beta-induced thermal hypersensitivity in rats. Brain Res Bull 130**:** 165-172.

Kwon SG, Roh DH, Yoon SY, Moon JY, Choi SR, Choi HS, *et al.* (2014). Blockade of peripheral P2Y1 receptors prevents the induction of thermal hyperalgesia via modulation of TRPV1 expression in carrageenan-induced inflammatory pain rats: involvement of p38 MAPK phosphorylation in DRGs. Neuropharmacology 79**:** 368-379.

Lagerstrom MC, & Schioth HB (2008). Structural diversity of G protein-coupled receptors and significance for drug discovery. Nat Rev Drug Discov 7**:** 339-357.

Lambright DG, Sondek J, Bohm A, Skiba NP, Hamm HE, & Sigler PB (1996). The 2.0 A crystal structure of a heterotrimeric G protein. Nature 379**:** 311-319.

Latorraca NR, Venkatakrishnan AJ, & Dror RO (2017). GPCR Dynamics: Structures in Motion. Chem Rev 117**:** 139-155.

Latremoliere A, & Woolf CJ (2009). Central sensitization: a generator of pain hypersensitivity by central neural plasticity. J Pain 10**:** 895-926.

Lechner SG, & Boehm S (2004). Regulation of neuronal ion channels via P2Y receptors. Purinergic Signal 1**:** 31-41.

Lee SP, So CH, Rashid AJ, Varghese G, Cheng R, Lanca AJ, *et al.* (2004). Dopamine D1 and D2 receptor Co-activation generates a novel phospholipase C-mediated calcium signal. J Biol Chem 279**:** 35671-35678.

Lefkowitz RJ, & Shenoy SK (2005). Transduction of receptor signals by beta-arrestins. Science 308**:** 512-517.

Lenertz LY, Baughman CJ, Waldschmidt NV, Thaler R, & van Wijnen AJ (2015). Control of bone development by P2X and P2Y receptors expressed in mesenchymal and hematopoietic cells. Gene 570**:** 1-7.

Leuchowius KJ, Weibrecht I, Landegren U, Gedda L, & Soderberg O (2009). Flow cytometric in situ proximity ligation analyses of protein interactions and post-translational modification of the epidermal growth factor receptor family. Cytometry A 75**:** 833-839.

References

Li K, Tan YH, Light AR, & Fu KY (2013). Different peripheral tissue injury induces differential phenotypic changes of spinal activated microglia. Clin Dev Immunol 2013**:** 901420.

Li R, Dang S, Yao M, Zhao C, Zhang W, Cui J*, et al.* (2020). Osthole alleviates neuropathic pain in mice by inhibiting the P2Y1-receptor-dependent JNK signaling pathway. Aging (Albany NY) 12**:** 7945-7962.

Li X, Zhou M, Huang W, & Yang H (2017). N-glycosylation of the beta2 adrenergic receptor regulates receptor function by modulating dimerization. FEBS J 284**:** 2004-2018.

Li Y, Natakorn S, Chen Y, Safar M, Cunningham MR, Tian J*, et al.* (2020). Investigations on average fluorescence lifetimes for visualizing multi-exponential decays. Frontiers in Physics, section Optics and Photonics Manuscript ID: 576862 (under revision).

Li Y, Yin C, Liu P, Li D, & Lin J (2017). Identification of a Different Agonist-Binding Site and Activation Mechanism of the Human P2Y1 Receptor. Sci Rep 7**:** 13764.

Liang YL, Khoshouei M, Radjainia M, Zhang Y, Glukhova A, Tarrasch J*, et al.* (2017). Phase-plate cryo-EM structure of a class B GPCR-G-protein complex. Nature 546**:** 118-123.

Limbird LE, Meyts PD, & Lefkowitz RJ (1975). Beta-adrenergic receptors: evidence for negative cooperativity. Biochem Biophys Res Commun 64**:** 1160-1168.

Lin HH (2013). G-protein-coupled receptors and their (Bio) chemical significance win 2012 Nobel Prize in Chemistry. Biomed J 36**:** 118-124.

Lin MZ, Marzec KA, Martin JL, & Baxter RC (2014). The role of insulin-like growth factor binding protein-3 in the breast cancer cell response to DNA-damaging agents. Oncogene 33**:** 85-96.

Lin T, Li K, Zhang FY, Zhang ZK, Light AR, & Fu KY (2007). Dissociation of spinal microglia morphological activation and peripheral inflammation in inflammatory pain models. J Neuroimmunol 192**:** 40-48.

Lin Y, & Smrcka AV (2011). Understanding molecular recognition by G protein betagamma subunits on the path to pharmacological targeting. Mol Pharmacol 80**:** 551-557.

Lipp P, & Reither G (2011). Protein kinase C: the "masters" of calcium and lipid. Cold Spring Harb Perspect Biol 3.

Liu PW, Yue MX, Zhou R, Niu J, Huang DJ, Xu T*, et al.* (2017). P2Y12 and P2Y13 receptors involved in ADPbetas induced the release of IL-1beta, IL-6 and TNF-alpha from cultured dorsal horn microglia. J Pain Res 10**:** 1755-1767.

References

Liverani E, Kilpatrick LE, Tsygankov AY, & Kunapuli SP (2014). The role of P2Y(1)(2) receptor and activated platelets during inflammation. Curr Drug Targets 15**:** 720-728.

Lohse MJ, Benovic JL, Codina J, Caron MG, & Lefkowitz RJ (1990). beta-Arrestin: a protein that regulates beta-adrenergic receptor function. Science 248**:** 1547-1550.

Lopez-Gimenez JF, Canals M, Pediani JD, & Milligan G (2007). The alpha1b-adrenoceptor exists as a higher-order oligomer: effective oligomerization is required for receptor maturation, surface delivery, and function. Mol Pharmacol 71**:** 1015-1029.

Łukasiewicz S, Polit A, Kędracka-Krok S, Wędzony K, Maćkowiak M, & Dziedzicka-Wasylewska M (2010). Hetero-dimerization of serotonin 5-HT2A and dopamine D2 receptors. Biochimica et Biophysica Acta (BBA) - Molecular Cell Research 1803**:** 1347-1358.

Luscher C, & Slesinger PA (2010). Emerging roles for G protein-gated inwardly rectifying potassium (GIRK) channels in health and disease. Nat Rev Neurosci 11**:** 301-315.

Luthardt J, Borvendeg SJ, Sperlagh B, Poelchen W, Wirkner K, & Illes P (2003). P2Y(1) receptor activation inhibits NMDA receptor-channels in layer V pyramidal neurons of the rat prefrontal and parietal cortex. Neurochem Int 42**:** 161-172.

Lutz S, Freichel-Blomquist A, Yang Y, Rumenapp U, Jakobs KH, Schmidt M*, et al.* (2005). The guanine nucleotide exchange factor p63RhoGEF, a specific link between Gq/11-coupled receptor signaling and RhoA. J Biol Chem 280**:** 11134-11139.

MacDonald L, Baldini G, & Storrie B (2015). Does super-resolution fluorescence microscopy obsolete previous microscopic approaches to protein co-localization? Methods Mol Biol 1270**:** 255-275.

Maggio R, Innamorati G, & Parenti M (2007). G protein-coupled receptor oligomerization provides the framework for signal discrimination. J Neurochem 103**:** 1741-1752.

Magni G, & Ceruti S (2019). The role of adenosine and P2Y receptors expressed by multiple cell types in pain transmission. Brain Res Bull 151**:** 132-143.

Maier-Peuschel M, Frolich N, Dees C, Hommers LG, Hoffmann C, Nikolaev VO*, et al.* (2010). A fluorescence resonance energy transfer-based M2 muscarinic receptor sensor reveals rapid kinetics of allosteric modulation. J Biol Chem 285**:** 8793-8800.

Makkawi M, Moheimani F, Alserihi R, Howells D, Wright M, Ashman L*, et al.* (2015). A complementary role for tetraspanin superfamily member CD151 and ADP purinergic P2Y12 receptor in platelets. Thromb Haemost 114**:** 1004-1019.

Malin SA, & Molliver DC (2010). Gi- and Gq-coupled ADP (P2Y) receptors act in opposition to modulate nociceptive signaling and inflammatory pain behavior. Mol Pain 6**:** 21.

References

Manders EM, Stap J, Brakenhoff GJ, van Driel R, & Aten JA (1992). Dynamics of three-dimensional replication patterns during the S-phase, analysed by double labelling of DNA and confocal microscopy. J Cell Sci 103 (Pt 3)**:** 857-862.

Mane N, Jimenez-Sabado V, & Jimenez M (2016). BPTU, an allosteric antagonist of P2Y1 receptor, blocks nerve mediated inhibitory neuromuscular responses in the gastrointestinal tract of rodents. Neuropharmacology 110**:** 376-385.

Manglik A, Kruse AC, Kobilka TS, Thian FS, Mathiesen JM, Sunahara RK, *et al.* (2012). Crystal structure of the micro-opioid receptor bound to a morphinan antagonist. Nature 485**:** 321-326.

Mangmool S, & Kurose H (2011). G(i/o) protein-dependent and -independent actions of Pertussis Toxin (PTX). Toxins (Basel) 3**:** 884-899.

Mansour A, Bachelot-Loza C, Nesseler N, Gaussem P, & Gouin-Thibault I (2020). P2Y12 Inhibition beyond Thrombosis: Effects on Inflammation. Int J Mol Sci 21.

Margeta-Mitrovic M, Jan YN, & Jan LY (2000). A trafficking checkpoint controls GABA(B) receptor heterodimerization. Neuron 27**:** 97-106.

Margineanu A, Chan JJ, Kelly DJ, Warren SC, Flatters D, Kumar S, *et al.* (2016). Screening for protein-protein interactions using Forster resonance energy transfer (FRET) and fluorescence lifetime imaging microscopy (FLIM). Sci Rep 6**:** 28186.

Marteau F, Le Poul E, Communi D, Communi D, Labouret C, Savi P, *et al.* (2003). Pharmacological characterization of the human P2Y13 receptor. Mol Pharmacol 64**:** 104-112.

Massotte D (2015). Editorial: Monitoring endogenous GPCRs: lessons for drug design. Front Pharmacol 6**:** 146.

Masuho I, Ostrovskaya O, Kramer GM, Jones CD, Xie K, & Martemyanov KA (2015). Distinct profiles of functional discrimination among G proteins determine the actions of G protein-coupled receptors. Sci Signal 8**:** ra123.

Meng XY, Mezei M, & Cui M (2014). Computational approaches for modeling GPCR dimerization. Curr Pharm Biotechnol 15**:** 996-1006.

Michel MC, Wieland T, & Tsujimoto G (2009). How reliable are G-protein-coupled receptor antibodies? Naunyn-Schmiedeberg's Archives of Pharmacology 379**:** 385-388.

Milligan G (2004). G protein-coupled receptor dimerization: function and ligand pharmacology. Mol Pharmacol 66**:** 1-7.

Milligan G (2009). G protein-coupled receptor hetero-dimerization: contribution to pharmacology and function. Br J Pharmacol 158**:** 5-14.

References

Milligan G, & Bouvier M (2005). Methods to monitor the quaternary structure of G protein-coupled receptors. FEBS J 272**:** 2914-2925.

Milligan G, & McGrath JC (2009). GPCR theme editorial. Br J Pharmacol 158**:** 1-4.

Milligan G, Ward RJ, & Marsango S (2019). GPCR homo-oligomerization. Curr Opin Cell Biol 57**:** 40-47.

Mitchell C, Syed NI, Tengah A, Gurney AM, & Kennedy C (2012). Identification of contractile P2Y1, P2Y6, and P2Y12 receptors in rat intrapulmonary artery using selective ligands. J Pharmacol Exp Ther 343**:** 755-762.

Moller TC, Hottin J, Clerte C, Zwier JM, Durroux T, Rondard P*, et al.* (2018). Oligomerization of a G protein-coupled receptor in neurons controlled by its structural dynamics. Sci Rep 8**:** 10414.

Moradi SV, Hussein WM, Varamini P, Simerska P, & Toth I (2016). Glycosylation, an effective synthetic strategy to improve the bioavailability of therapeutic peptides. Chem Sci 7**:** 2492-2500.

Moreno JL, Holloway T, & Gonzalez-Maeso J (2013). G protein-coupled receptor heterocomplexes in neuropsychiatric disorders. Prog Mol Biol Transl Sci 117**:** 187-205.

Moriyama T, Iida T, Kobayashi K, Higashi T, Fukuoka T, Tsumura H*, et al.* (2003). Possible involvement of P2Y2 metabotropic receptors in ATP-induced transient receptor potential vanilloid receptor 1-mediated thermal hypersensitivity. J Neurosci 23**:** 6058-6062.

Moro S, Guo D, Camaioni E, Boyer JL, Harden TK, & Jacobson KA (1998). Human P2Y1 receptor: molecular modeling and site-directed mutagenesis as tools to identify agonist and antagonist recognition sites. J Med Chem 41**:** 1456-1466.

Moro S, Hoffmann C, & Jacobson KA (1999). Role of the extracellular loops of G protein-coupled receptors in ligand recognition: a molecular modeling study of the human P2Y1 receptor. Biochemistry 38**:** 3498-3507.

Morphy R, & Rankovic Z (2005). Designed multiple ligands. An emerging drug discovery paradigm. J Med Chem 48**:** 6523-6543.

Mundell SJ, Barton JF, Mayo-Martin MB, Hardy AR, & Poole AW (2008). Rapid resensitization of purinergic receptor function in human platelets. J Thromb Haemost 6**:** 1393-1404.

Mundell SJ, & Benovic JL (2000). Selective regulation of endogenous G protein-coupled receptors by arrestins in HEK293 cells. J Biol Chem 275**:** 12900-12908.

Mundell SJ, Jones ML, Hardy AR, Barton JF, Beaucourt SM, Conley PB*, et al.* (2006). Distinct roles for protein kinase C isoforms in regulating platelet purinergic receptor function. Mol Pharmacol 70**:** 1132-1142.

References

Mundell SJ, Matharu AL, Nisar S, Palmer TM, Benovic JL, & Kelly E (2010). Deletion of the distal COOH-terminus of the A2B adenosine receptor switches internalization to an arrestin- and clathrin-independent pathway and inhibits recycling. Br J Pharmacol 159**:** 518-533.

Mundell SJ, Rabbolini D, Gabrielli S, Chen Q, Aungraheeta R, Hutchinson JL*, et al.* (2018). Receptor homodimerization plays a critical role in a novel dominant negative P2RY12 variant identified in a family with severe bleeding. J Thromb Haemost 16**:** 44-53.

Mystek P, Rysiewicz B, Gregrowicz J, Dziedzicka-Wasylewska M, & Polit A (2019). Ggamma and Galpha Identity Dictate a G-Protein Heterotrimer Plasma Membrane Targeting. Cells 8.

Naranjo AN, Chevalier A, Cousins GD, Ayettey E, McCusker EC, Wenk C*, et al.* (2015). Conserved disulfide bond is not essential for the adenosine A2A receptor: Extracellular cysteines influence receptor distribution within the cell and ligand-binding recognition. Biochim Biophys Acta 1848**:** 603-614.

Neumann A, Müller CE, & Namasivayam V (2020). P2Y1-like nucleotide receptors— Structures, molecular modeling, mutagenesis, and oligomerization. WIREs Computational Molecular Science 10**:** e1464.

Neves SR, Ram PT, & Iyengar R (2002). G protein pathways. Science 296**:** 1636-1639.

Nisar S, Daly ME, Federici AB, Artoni A, Mumford AD, Watson SP*, et al.* (2011). An intact PDZ motif is essential for correct P2Y12 purinoceptor traffic in human platelets. Blood 118**:** 5641-5651.

Nisar S, Kelly E, Cullen PJ, & Mundell SJ (2010). Regulation of P2Y1 receptor traffic by sorting Nexin 1 is retromer independent. Traffic 11**:** 508-519.

Nisar SP, Cunningham M, Saxena K, Pope RJ, Kelly E, & Mundell SJ (2012). Arrestin scaffolds NHERF1 to the P2Y12 receptor to regulate receptor internalization. J Biol Chem 287**:** 24505-24515.

Norambuena A, Poblete MI, Donoso MV, Espinoza CS, Gonzalez A, & Huidobro-Toro JP (2008). P2Y1 receptor activation elicits its partition out of membrane rafts and its rapid internalization from human blood vessels: implications for receptor signaling. Mol Pharmacol 74**:** 1666-1677.

O'Connor S, Montalescot G, & Collet JP (2011). The P2Y(12) receptor as a target of antithrombotic drugs. Purinergic Signal 7**:** 325-332.

Ohtsubo K, & Marth JD (2006). Glycosylation in cellular mechanisms of health and disease. Cell 126**:** 855-867.

References

Okada M, Nakagawa T, Minami M, & Satoh M (2002). Analgesic effects of intrathecal administration of P2Y nucleotide receptor agonists UTP and UDP in normal and neuropathic pain model rats. J Pharmacol Exp Ther 303**:** 66-73.

Olsen RHJ, DiBerto JF, English JG, Glaudin AM, Krumm BE, Slocum ST, *et al.* (2020). TRUPATH, an open-source biosensor platform for interrogating the GPCR transducerome. Nat Chem Biol 16**:** 841-849.

Opalinski L, Sokolowska-Wedzina A, Szczepara M, Zakrzewska M, & Otlewski J (2017). Antibody-induced dimerization of FGFR1 promotes receptor endocytosis independently of its kinase activity. Sci Rep 7**:** 7121.

Pacheco MA, & Jope RS (1997). Comparison of [3H]phosphatidylinositol and [3H]phosphatidylinositol 4,5-bisphosphate hydrolysis in postmortem human brain membranes and characterization of stimulation by dopamine D1 receptors. J Neurochem 69**:** 639-644.

Painter JT, & Crofford LJ (2013). Chronic opioid use in fibromyalgia syndrome: a clinical review. J Clin Rheumatol 19**:** 72-77.

Pan HL, Wu ZZ, Zhou HY, Chen SR, Zhang HM, & Li DP (2008). Modulation of pain transmission by G-protein-coupled receptors. Pharmacol Ther 117**:** 141-161.

Paoletta S, Sabbadin D, von Kugelgen I, Hinz S, Katritch V, Hoffmann K, *et al.* (2015). Modeling ligand recognition at the P2Y12 receptor in light of X-ray structural information. J Comput Aided Mol Des 29**:** 737-756.

Park M, Reddy GR, Wallukat G, Xiang YK, & Steinberg SF (2017). beta1-adrenergic receptor O-glycosylation regulates N-terminal cleavage and signaling responses in cardiomyocytes. Sci Rep 7**:** 7890.

Patterson GH, Piston DW, & Barisas BG (2000). Forster distances between green fluorescent protein pairs. Anal Biochem 284**:** 438-440.

Perez DM, & Karnik SS (2005). Multiple signaling states of G-protein-coupled receptors. Pharmacol Rev 57**:** 147-161.

Pin JP, Kniazeff J, Liu J, Binet V, Goudet C, Rondard P, *et al.* (2005). Allosteric functioning of dimeric class C G-protein-coupled receptors. FEBS J 272**:** 2947-2955.

Pin JP, Neubig R, Bouvier M, Devi L, Filizola M, Javitch JA, *et al.* (2007). International Union of Basic and Clinical Pharmacology. LXVII. Recommendations for the recognition and nomenclature of G protein-coupled receptor heteromultimers. Pharmacol Rev 59**:** 5-13.

Pioszak AA, Harikumar KG, Parker NR, Miller LJ, & Xu HE (2010). Dimeric arrangement of the parathyroid hormone receptor and a structural mechanism for ligand-induced dissociation. J Biol Chem 285**:** 12435-12444.

References

Piston DW, & Kremers GJ (2007). Fluorescent protein FRET: the good, the bad and the ugly. Trends Biochem Sci 32**:** 407-414.

Ploier B, Caro LN, Morizumi T, Pandey K, Pearring JN, Goren MA*, et al.* (2016). Dimerization deficiency of enigmatic retinitis pigmentosa-linked rhodopsin mutants. Nat Commun 7**:** 12832.

Poole DP, Amadesi S, Veldhuis NA, Abogadie FC, Lieu T, Darby W*, et al.* (2013). Protease-activated receptor 2 (PAR2) protein and transient receptor potential vanilloid 4 (TRPV4) protein coupling is required for sustained inflammatory signaling. J Biol Chem 288**:** 5790-5802.

Porzionato A, Stocco E, Guidolin D, Agnati L, Macchi V, & De Caro R (2018). Receptor-Receptor Interactions of G Protein-Coupled Receptors in the Carotid Body: A Working Hypothesis. Front Physiol 9**:** 697.

Przybyla JA, & Watts VJ (2010). Ligand-induced regulation and localization of cannabinoid CB1 and dopamine D2L receptor heterodimers. J Pharmacol Exp Ther 332**:** 710-719.

Rabani V, Montange D, Meneveau N, & Davani S (2018). Impact of ticagrelor on P2Y1 and P2Y12 localization and on cholesterol levels in platelet plasma membrane. Platelets 29**:** 709-715.

Raju NC, Eikelboom JW, & Hirsh J (2008). Platelet ADP-receptor antagonists for cardiovascular disease: past, present and future. Nat Clin Pract Cardiovasc Med 5**:** 766-780.

Ralevic V, & Burnstock G (1998). Receptors for purines and pyrimidines. Pharmacol Rev 50**:** 413-492.

Ramsay D, Kellett E, McVey M, Rees S, & Milligan G (2002). Homo- and hetero-oligomeric interactions between G-protein-coupled receptors in living cells monitored by two variants of bioluminescence resonance energy transfer (BRET): hetero-oligomers between receptor subtypes form more efficiently than between less closely related sequences. Biochem J 365**:** 429-440.

Rands E, Candelore MR, Cheung AH, Hill WS, Strader CD, & Dixon RA (1990). Mutational analysis of beta-adrenergic receptor glycosylation. J Biol Chem 265**:** 10759-10764.

Rashid AJ, So CH, Kong MM, Furtak T, El-Ghundi M, Cheng R*, et al.* (2007). D1-D2 dopamine receptor heterooligomers with unique pharmacology are coupled to rapid activation of Gq/11 in the striatum. Proc Natl Acad Sci U S A 104**:** 654-659.

Rasmussen SG, Choi HJ, Rosenbaum DM, Kobilka TS, Thian FS, Edwards PC*, et al.* (2007). Crystal structure of the human beta2 adrenergic G-protein-coupled receptor. Nature 450**:** 383-387.

References

Rasmussen SG, DeVree BT, Zou Y, Kruse AC, Chung KY, Kobilka TS, *et al.* (2011). Crystal structure of the beta2 adrenergic receptor-Gs protein complex. Nature 477**:** 549-555.

Rawat P, & Spector SA (2017). Development and characterization of a human microglia cell model of HIV-1 infection. J Neurovirol 23**:** 33-46.

Raykova D, Koos B, Asplund A, Gelleri M, Ivarsson Y, Danielson UH, *et al.* (2016). Let There Be Light! Proteomes 4.

Reimer M, Petrova Zustiak S, Sheth S, & Martin Schober J (2018). Intrinsic Response Towards Physiologic Stiffness is Cell-Type Dependent. Cell Biochem Biophys 76**:** 197-208.

Reiner S, Ziegler N, Leon C, Lorenz K, von Hayn K, Gachet C, *et al.* (2009). beta-Arrestin-2 interaction and internalization of the human P2Y1 receptor are dependent on C-terminal phosphorylation sites. Mol Pharmacol 76**:** 1162-1171.

Ren K, & Dubner R (1999). Inflammatory Models of Pain and Hyperalgesia. ILAR J 40**:** 111-118.

Retamal JS, Ramirez-Garcia PD, Shenoy PA, Poole DP, & Veldhuis NA (2019). Internalized GPCRs as Potential Therapeutic Targets for the Management of Pain. Front Mol Neurosci 12**:** 273.

Ribeiro-Filho AC, Buri MV, Barros CC, Dreyfuss JL, Nader HB, Justo GZ, *et al.* (2016). Functional and molecular evidence for heteromeric association of P2Y1 receptor with P2Y2 and P2Y4 receptors in mouse granulocytes. BMC Pharmacol Toxicol 17**:** 29.

Ricks TK, & Trejo J (2009). Phosphorylation of protease-activated receptor-2 differentially regulates desensitization and internalization. J Biol Chem 284**:** 34444-34457.

Rizzo MJ, Evans JP, Burt M, Saunders CJ, & Johnson EC (2018). Unexpected role of a conserved domain in the first extracellular loop in G protein-coupled receptor trafficking. Biochem Biophys Res Commun 503**:** 1919-1926.

Robson SC, Sevigny J, & Zimmermann H (2006). The E-NTPDase family of ectonucleotidases: Structure function relationships and pathophysiological significance. Purinergic Signal 2**:** 409-430.

Rodhe J (2013). Cell culturing of human and murine microglia cell lines. Methods Mol Biol 1041**:** 11-16.

Rovati GE, Capra V, & Neubig RR (2007). The highly conserved DRY motif of class A G protein-coupled receptors: beyond the ground state. Mol Pharmacol 71**:** 959-964.

Sadja R, Alagem N, & Reuveny E (2003). Gating of GIRK channels: details of an intricate, membrane-delimited signaling complex. Neuron 39**:** 9-12.

References

P2Y1 Antibody (E-1): sc-377324. [Online] Available from https://www.scbt.com/p/p2y1-antibody-e-1. [Accessed: 5 June 2020].

Sauvageau E, Rochdi MD, Oueslati M, Hamdan FF, Percherancier Y, Simpson JC*, et al.* (2014). CNIH4 interacts with newly synthesized GPCR and controls their export from the endoplasmic reticulum. Traffic 15**:** 383-400.

Savi P, Zachayus JL, Delesque-Touchard N, Labouret C, Herve C, Uzabiaga MF*, et al.* (2006). The active metabolite of Clopidogrel disrupts P2Y12 receptor oligomers and partitions them out of lipid rafts. Proc Natl Acad Sci U S A 103**:** 11069-11074.

Savitsky AP, Rusanov AL, Zherdeva VV, Gorodnicheva TV, Khrenova MG, & Nemukhin AV (2012). FLIM-FRET Imaging of Caspase-3 Activity in Live Cells Using Pair of Red Fluorescent Proteins. Theranostics 2**:** 215-226.

Sawutz DG, Lanier SM, Warren CD, & Graham RM (1987). Glycosylation of the mammalian alpha 1-adrenergic receptor by complex type N-linked oligosaccharides. Mol Pharmacol 32**:** 565-571.

Schaible HG, von Banchet GS, Boettger MK, Brauer R, Gajda M, Richter F*, et al.* (2010). The role of proinflammatory cytokines in the generation and maintenance of joint pain. Ann N Y Acad Sci 1193**:** 60-69.

Schicker K, Hussl S, Chandaka GK, Kosenburger K, Yang JW, Waldhoer M*, et al.* (2009). A membrane network of receptors and enzymes for adenine nucleotides and nucleosides. Biochim Biophys Acta 1793**:** 325-334.

Schicker KW, Chandaka GK, Geier P, Kubista H, & Boehm S (2010). P2Y1 receptors mediate an activation of neuronal calcium-dependent K+ channels. J Physiol 588**:** 3713-3725.

Scholz J, & Woolf CJ (2002). Can we conquer pain? Nat Neurosci 5 Suppl**:** 1062-1067.

Schoneberg T, Schultz G, & Gudermann T (1999). Structural basis of G protein-coupled receptor function. Mol Cell Endocrinol 151**:** 181-193.

Schulte G (2010). International Union of Basic and Clinical Pharmacology. LXXX. The class Frizzled receptors. Pharmacol Rev 62**:** 632-667.

Sekar RB, & Periasamy A (2003). Fluorescence resonance energy transfer (FRET) microscopy imaging of live cell protein localizations. J Cell Biol 160**:** 629-633.

Seltzer Z, Dubner R, & Shir Y (1990). A novel behavioral model of neuropathic pain disorders produced in rats by partial sciatic nerve injury. Pain 43**:** 205-218.

Shrestha SS, Parmar M, Kennedy C, & Bushell TJ (2010). Two-pore potassium ion channels are inhibited by both G(q/11)- and G(i)-coupled P2Y receptors. Mol Cell Neurosci 43**:** 363-369.

References

How Proximity Ligation Assay (PLA) Works. [Online] Available from https://www.sigmaaldrich.com/technical-documents/protocols/biology/how-pla-works.html. [Accessed: 24 April].

Skieterska K, Duchou J, Lintermans B, & Van Craenenbroeck K (2013). Detection of G protein-coupled receptor (GPCR) dimerization by coimmunoprecipitation. Methods Cell Biol 117**:** 323-340.

Smith TH, Li JG, Dores MR, & Trejo J (2017). Protease-activated receptor-4 and purinergic receptor P2Y12 dimerize, co-internalize, and activate Akt signaling via endosomal recruitment of beta-arrestin. J Biol Chem 292**:** 13867-13878.

So CH, Varghese G, Curley KJ, Kong MM, Alijaniaram M, Ji X, *et al.* (2005). D1 and D2 dopamine receptors form heterooligomers and cointernalize after selective activation of either receptor. Mol Pharmacol 68**:** 568-578.

Soderberg O, Leuchowius KJ, Gullberg M, Jarvius M, Weibrecht I, Larsson LG, *et al.* (2008). Characterizing proteins and their interactions in cells and tissues using the in situ proximity ligation assay. Methods 45**:** 227-232.

Spiering D, & Hodgson L (2011). Dynamics of the Rho-family small GTPases in actin regulation and motility. Cell Adh Migr 5**:** 170-180.

Sriram K, & Insel PA (2018). G Protein-Coupled Receptors as Targets for Approved Drugs: How Many Targets and How Many Drugs? Mol Pharmacol 93**:** 251-258.

St John Smith E (2018). Advances in understanding nociception and neuropathic pain. J Neurol 265**:** 231-238.

Storez H, Scott MG, Issafras H, Burtey A, Benmerah A, Muntaner O, *et al.* (2005). Homo- and hetero-oligomerization of beta-arrestins in living cells. J Biol Chem 280**:** 40210-40215.

Sun DS, Lo SJ, Tsai WJ, Lin CH, Yu MS, Chen YF, *et al.* (2005). PI3-kinase is essential for ADP-stimulated integrin alpha(IIb)beta3-mediated platelet calcium oscillation, implications for P2Y receptor pathways in integrin alpha(IIb)beta3-initiated signaling cross-talks. J Biomed Sci 12**:** 937-948.

Sun XD, Wang A, Ma P, Gong S, Tao J, Yu XM, *et al.* (2020). Regulation of the firing activity by PKA-PKC-Src family kinases in cultured neurons of hypothalamic arcuate nucleus. J Neurosci Res 98**:** 384-403.

Sunahara RK, & Taussig R (2002). Isoforms of mammalian adenylyl cyclase: multiplicities of signaling. Mol Interv 2**:** 168-184.

Suplat D, Krzeminski P, Pomorski P, & Baranska J (2007). P2Y(1) and P2Y(12) receptor cross-talk in calcium signalling: Evidence from nonstarved and long-term serum-deprived glioma C6 cells. Purinergic Signal 3**:** 221-230.

References

Suzuki T, Namba K, Tsuga H, & Nakata H (2006). Regulation of pharmacology by hetero-oligomerization between A1 adenosine receptor and P2Y2 receptor. Biochem Biophys Res Commun 351**:** 559-565.

Suzuki T, Obara Y, Moriya T, Nakata H, & Nakahata N (2011). Functional interaction between purinergic receptors: effect of ligands for A2A and P2Y12 receptors on P2Y1 receptor function. FEBS Lett 585**:** 3978-3984.

Syrovatkina V, Alegre KO, Dey R, & Huang XY (2016). Regulation, Signaling, and Physiological Functions of G-Proteins. J Mol Biol 428**:** 3850-3868.

Syu GD, Wang SC, Ma G, Liu S, Pearce D, Prakash A*, et al.* (2019). Development and application of a high-content virion display human GPCR array. Nat Commun 10**:** 1997.

Szymanska K, Kalafut J, Przybyszewska A, Paziewska B, Adamczuk G, Kielbus M*, et al.* (2018). FSHR Trans-Activation and Oligomerization. Front Endocrinol (Lausanne) 9**:** 760.

Tang TS, & Bezprozvanny I (2004). Dopamine receptor-mediated Ca(2+) signaling in striatal medium spiny neurons. J Biol Chem 279**:** 42082-42094.

Tao YX, & Conn PM (2014). Chaperoning G protein-coupled receptors: from cell biology to therapeutics. Endocr Rev 35**:** 602-647.

Terrillon S, & Bouvier M (2004). Roles of G-protein-coupled receptor dimerization. EMBO Rep 5**:** 30-34.

Tetsuka M, Saito Y, Imai K, Doi H, & Maruyama K (2004). The basic residues in the membrane-proximal C-terminal tail of the rat melanin-concentrating hormone receptor 1 are required for receptor function. Endocrinology 145**:** 3712-3723.

Thomas P, & Smart TG (2005). HEK293 cell line: a vehicle for the expression of recombinant proteins. J Pharmacol Toxicol Methods 51**:** 187-200.

Thompson AA, Liu W, Chun E, Katritch V, Wu H, Vardy E*, et al.* (2012). Structure of the nociceptin/orphanin FQ receptor in complex with a peptide mimetic. Nature 485**:** 395-399.

Timmerman R, Burm SM, & Bajramovic JJ (2018). An Overview of in vitro Methods to Study Microglia. Front Cell Neurosci 12**:** 242.

Tobin AB, Butcher AJ, & Kong KC (2008). Location, location, location...site-specific GPCR phosphorylation offers a mechanism for cell-type-specific signalling. Trends Pharmacol Sci 29**:** 413-420.

Townsend-Nicholson A, Altwaijry N, Potterton A, Morao I, & Heifetz A (2019). Computational prediction of GPCR oligomerization. Curr Opin Struct Biol 55**:** 178-184.

References

Tozaki-Saitoh H, Tsuda M, Miyata H, Ueda K, Kohsaka S, & Inoue K (2008). P2Y12 receptors in spinal microglia are required for neuropathic pain after peripheral nerve injury. J Neurosci 28**:** 4949-4956.

Traynor JR, & Neubig RR (2005). Regulators of G protein signaling & drugs of abuse. Mol Interv 5**:** 30-41.

Treede RD, Rief W, Barke A, Aziz Q, Bennett MI, Benoliel R*, et al.* (2015). A classification of chronic pain for ICD-11. Pain 156**:** 1003-1007.

Trifilieff P, Rives ML, Urizar E, Piskorowski RA, Vishwasrao HD, Castrillon J*, et al.* (2011). Detection of antigen interactions ex vivo by proximity ligation assay: endogenous dopamine D2-adenosine A2A receptor complexes in the striatum. Biotechniques 51**:** 111-118.

Tulapurkar ME, Laubinger W, Nahum V, Fischer B, & Reiser G (2004). Subtype specific internalization of P2Y1 and P2Y2 receptors induced by novel adenosine 5'-O-(1-boranotriphosphate) derivatives. Br J Pharmacol 142**:** 869-878.

Undie AS, Weinstock J, Sarau HM, & Friedman E (1994). Evidence for a distinct D1-like dopamine receptor that couples to activation of phosphoinositide metabolism in brain. J Neurochem 62**:** 2045-2048.

Urizar E, Claeysen S, Deupi X, Govaerts C, Costagliola S, Vassart G*, et al.* (2005). An activation switch in the rhodopsin family of G protein-coupled receptors: the thyrotropin receptor. J Biol Chem 280**:** 17135-17141.

Vagner J, Xu L, Handl HL, Josan JS, Morse DL, Mash EA*, et al.* (2008). Heterobivalent ligands crosslink multiple cell-surface receptors: the human melanocortin-4 and delta-opioid receptors. Angew Chem Int Ed Engl 47**:** 1685-1688.

Van Dyke RW (2004). Heterotrimeric G protein subunits are located on rat liver endosomes. BMC Physiol 4**:** 1.

Vartian N, & Boehm S (2001). P2Y receptor-mediated inhibition of voltage-activated Ca(2+) currents in PC12 cells. Eur J Neurosci 13**:** 899-908.

Velazquez B, Garrad RC, Weisman GA, & Gonzalez FA (2000). Differential agonist-induced desensitization of P2Y2 nucleotide receptors by ATP and UTP. Mol Cell Biochem 206**:** 75-89.

Venkatachalan SP, Bushman JD, Mercado JL, Sancar F, Christopherson KR, & Boileau AJ (2007). Optimized expression vector for ion channel studies in Xenopus oocytes and mammalian cells using alfalfa mosaic virus. Pflugers Arch 454**:** 155-163.

Verkhratsky A, Pankratov Y, Lalo U, & Nedergaard M (2012). P2X receptors in neuroglia. Wiley Interdiscip Rev Membr Transp Signal 1.

References

Vernier P, Cardinaud B, Valdenaire O, Philippe H, & Vincent JD (1995). An evolutionary view of drug-receptor interaction: the bioamine receptor family. Trends Pharmacol Sci 16**:** 375-381.

Vidi PA, Chemel BR, Hu CD, & Watts VJ (2008). Ligand-dependent oligomerization of dopamine D(2) and adenosine A(2A) receptors in living neuronal cells. Mol Pharmacol 74**:** 544-551.

Vischer HF, Castro M, & Pin JP (2015). G Protein-Coupled Receptor Multimers: A Question Still Open Despite the Use of Novel Approaches. Mol Pharmacol 88**:** 561-571.

Vischer HF, Watts AO, Nijmeijer S, & Leurs R (2011). G protein-coupled receptors: walking hand-in-hand, talking hand-in-hand? Br J Pharmacol 163**:** 246-260.

Vizurraga A, Adhikari R, Yeung J, Yu M, & Tall GG (2020). Mechanisms of adhesion G protein-coupled receptor activation. J Biol Chem 295**:** 14065-14083.

Vogel SS, Thaler C, & Koushik SV (2006). Fanciful FRET. Sci STKE 2006**:** re2.

Vogel SS, van der Meer BW, & Blank PS (2014). Estimating the distance separating fluorescent protein FRET pairs. Methods 66**:** 131-138.

von Kugelgen I, & Hoffmann K (2016). Pharmacology and structure of P2Y receptors. Neuropharmacology 104**:** 50-61.

Voscopoulos C, & Lema M (2010). When does acute pain become chronic? Br J Anaesth 105 Suppl 1**:** i69-85.

Waldhoer M, Fong J, Jones RM, Lunzer MM, Sharma SK, Kostenis E, *et al.* (2005). A heterodimer-selective agonist shows in vivo relevance of G protein-coupled receptor dimers. Proc Natl Acad Sci U S A 102**:** 9050-9055.

Waldo GL, Corbitt J, Boyer JL, Ravi G, Kim HS, Ji XD, *et al.* (2002). Quantitation of the P2Y(1) receptor with a high affinity radiolabeled antagonist. Mol Pharmacol 62**:** 1249-1257.

Wang D, Sun X, Bohn LM, & Sadee W (2005). Opioid receptor homo- and heterodimerization in living cells by quantitative bioluminescence resonance energy transfer. Mol Pharmacol 67**:** 2173-2184.

Wang J, Chen H, Seth A, & McCulloch CA (2003). Mechanical force regulation of myofibroblast differentiation in cardiac fibroblasts. Am J Physiol Heart Circ Physiol 285**:** H1871-1881.

Wang T, Nakagawa S, Miyake T, Setsu G, Kunisue S, Goto K, *et al.* (2020). Identification and functional characterisation of N-linked glycosylation of the orphan G protein-coupled receptor Gpr176. Sci Rep 10**:** 4429.

References

Wehbi VL, & Tasken K (2016). Molecular Mechanisms for cAMP-Mediated Immunoregulation in T cells - Role of Anchored Protein Kinase A Signaling Units. Front Immunol 7**:** 222.

Weibrecht I, Leuchowius KJ, Clausson CM, Conze T, Jarvius M, Howell WM, *et al.* (2010). Proximity ligation assays: a recent addition to the proteomics toolbox. Expert Rev Proteomics 7**:** 401-409.

Weick M, Wiedemann P, Reichenbach A, & Bringmann A (2005). Resensitization of P2Y receptors by growth factor-mediated activation of the phosphatidylinositol-3 kinase in retinal glial cells. Invest Ophthalmol Vis Sci 46**:** 1525-1532.

Weis WI, & Kobilka BK (2018). The Molecular Basis of G Protein-Coupled Receptor Activation. Annu Rev Biochem 87**:** 897-919.

Weisman GA, Woods LT, Erb L, & Seye CI (2012). P2Y receptors in the mammalian nervous system: pharmacology, ligands and therapeutic potential. CNS Neurol Disord Drug Targets 11**:** 722-738.

Werry TD, Christie MI, Dainty IA, Wilkinson GF, & Willars GB (2002). Ca(2+) signalling by recombinant human CXCR2 chemokine receptors is potentiated by P2Y nucleotide receptors in HEK cells. Br J Pharmacol 135**:** 1199-1208.

Wheatley M, Wootten D, Conner MT, Simms J, Kendrick R, Logan RT, *et al.* (2012). Lifting the lid on GPCRs: the role of extracellular loops. Br J Pharmacol 165**:** 1688-1703.

White JH, Wise A, Main MJ, Green A, Fraser NJ, Disney GH, *et al.* (1998). Heterodimerization is required for the formation of a functional GABA(B) receptor. Nature 396**:** 679-682.

Wilson BH, & Nelson J (2015). Sickle cell disease pain management in adolescents: a literature review. Pain Manag Nurs 16**:** 146-151.

Wu B, Chien EY, Mol CD, Fenalti G, Liu W, Katritch V, *et al.* (2010). Structures of the CXCR4 chemokine GPCR with small-molecule and cyclic peptide antagonists. Science 330**:** 1066-1071.

Wu H, Wacker D, Mileni M, Katritch V, Han GW, Vardy E, *et al.* (2012). Structure of the human kappa-opioid receptor in complex with JDTic. Nature 485**:** 327-332.

Wu J, Cheng Y, Zhang R, Liu D, Luo YM, Chen KL, *et al.* (2017). P2Y1R is involved in visceral hypersensitivity in rats with experimental irritable bowel syndrome. World J Gastroenterol 23**:** 6339-6349.

Wypych D, & Baranska J (2013). Cross-talk in nucleotide signaling in glioma C6 cells. Adv Exp Med Biol 986**:** 31-59.

References

Xu J, He J, Castleberry AM, Balasubramanian S, Lau AG, & Hall RA (2003). Heterodimerization of alpha 2A- and beta 1-adrenergic receptors. J Biol Chem 278: 10770-10777.

Xu L, Zhang Y, & Huang Y (2016). Advances in the Treatment of Neuropathic Pain. Adv Exp Med Biol 904: 117-129.

Yang J, Gong Z, Lu YB, Xu CJ, Wei TF, Yang MS, *et al.* (2020). FLIM-FRET-Based Structural Characterization of a Class-A GPCR Dimer in the Cell Membrane. J Mol Biol 432: 4596-4611.

Yawn BP, Buchanan GR, Afenyi-Annan AN, Ballas SK, Hassell KL, James AH, *et al.* (2014). Management of sickle cell disease: summary of the 2014 evidence-based report by expert panel members. JAMA 312: 1033-1048.

Yekkirala AS, Roberson DP, Bean BP, & Woolf CJ (2017). Breaking barriers to novel analgesic drug development. Nat Rev Drug Discov 16: 545-564.

Yoshioka K, Saitoh O, & Nakata H (2001). Heteromeric association creates a P2Y-like adenosine receptor. Proc Natl Acad Sci U S A 98: 7617-7622.

Yoshioka K, Saitoh O, & Nakata H (2002). Agonist-promoted heteromeric oligomerization between adenosine A(1) and P2Y(1) receptors in living cells. FEBS Lett 523: 147-151.

Yuan S, Chan HC, Vogel H, Filipek S, Stevens RC, & Palczewski K (2016). The Molecular Mechanism of P2Y1 Receptor Activation. Angew Chem Int Ed Engl 55: 10331-10335.

Zafar S, Nasir A, & Bokhari H (2011). Computational analysis reveals abundance of potential glycoproteins in Archaea, Bacteria and Eukarya. Bioinformation 6: 352-355.

Zamel IA, Palakkott A, Ashraf A, Iratni R, & Ayoub MA (2020). Interplay Between Angiotensin II Type 1 Receptor and Thrombin Receptor Revealed by Bioluminescence Resonance Energy Transfer Assay. Frontiers in Pharmacology 11.

Education in Microscopy and Digital Imaging. [Online] [Accessed: 17 April 2020].

Zhang D, Gao ZG, Zhang K, Kiselev E, Crane S, Wang J, *et al.* (2015). Two disparate ligand-binding sites in the human P2Y1 receptor. Nature 520: 317-321.

Zhang J, Zhang K, Gao ZG, Paoletta S, Zhang D, Han GW, *et al.* (2014a). Agonist-bound structure of the human P2Y12 receptor. Nature 509: 119-122.

Zhang K, Zhang J, Gao ZG, Zhang D, Zhu L, Han GW, *et al.* (2014b). Structure of the human P2Y12 receptor in complex with an antithrombotic drug. Nature 509: 115-118.

GPCR-EXP for Experimentlly-Solved and Predicted GPCR Structures. [Online] Available from https://zhanglab.ccmb.med.umich.edu/GPCR-EXP/. [Accessed: 4th July 2020].

References

Zhao C, DeGroot ACM, Hayden CC, Houser JR, Ali HA, LaMonica MF*, et al.* (2019). Receptor Heterodimerization Modulates Endocytosis through Collaborative and Competitive Mechanisms. Biophys J 117**:** 646-658.

Zhao X, Li G, & Liang S (2013). Several affinity tags commonly used in chromatographic purification. J Anal Methods Chem 2013**:** 581093.

Zhong X, Kriz R, Seehra J, & Kumar R (2004). N-linked glycosylation of platelet P2Y12 ADP receptor is essential for signal transduction but not for ligand binding or cell surface expression. FEBS Lett 562**:** 111-117.

Zhou Q, Yang D, Wu M, Guo Y, Guo W, Zhong L*, et al.* (2019). Common activation mechanism of class A GPCRs. Elife 8.

Zhu H, Yu Y, Zheng L, Wang L, Li C, Yu J*, et al.* (2015). Chronic inflammatory pain upregulates expression of P2Y2 receptor in small-diameter sensory neurons. Metab Brain Dis 30**:** 1349-1358.

Zhu Y, Meszaros J, Walle R, Fan R, Sun Z, Dwork AJ*, et al.* (2019). Detecting G protein-coupled receptor complexes in postmortem human brain with proximity ligation assay and a Bayesian classifier. Biotechniques 68**:** 122-129.

Zimmermann H, Zebisch M, & Strater N (2012). Cellular function and molecular structure of ecto-nucleotidases. Purinergic Signal 8**:** 437-502.